The conserved coiled-coil protein CCCP1 and the endosomal complex EARP regulate dense-core vesicle cargo sorting

Jerome Cattin

A dissertation submitted in partial fulfillment of the

requirements for the degree of

Doctor of Philosophy

University of Washington

2018

Reading Committee:

Michael Ailion, Chair

Sandra Bajjellieh

Jihong Bai

Program Authorized to Offer Degree:

Biochemistry

University of Washington

Abstract

The conserved coiled-coil protein CCCP1 and the endosomal complex EARP regulate dense-core vesicle cargo sorting

Jerome Cattin

Chair of the Supervisory Committee:

Michael Ailion

Department of Biochemistry

The regulated release of peptide hormones (e.g. insulin), neuropeptides, and monoamines depends on their being packaged into dense-core vesicles (DCVs). How these vesicles are made and how their cargo is properly selected is not well understood, especially at the molecular level. DCVs are generated at the trans-Golgi network (TGN) and go through maturation steps including peptide processing and removal of improperly loaded cargo. Screens in *C. elegans* have identified several conserved molecules that are important for DCV function. These include the small G protein RAB2, its effector the conserved coiled-coil protein 1 (CCCP1), the endosome-associated recycling complex (EARP), and the EARP interacting protein 1 (EIPR1). All these proteins function in *C. elegans* neurons in the same genetic pathway. In mutants of

these proteins, DCVs are generated normally but they contain reduced levels of cargo suggesting a role in cargo sorting. To determine whether CCCP1 and EIPR1 are important for the formation of DCVs in mammalian endocrine cells, we generated *Cccp1KO* and *Eipr1KO* insulin-secreting pancreatic beta 832/13 cells. We have observed that the KO cells have reduced insulin secretion and that insulin is retained near or at the TGN suggesting that both proteins are required for sorting insulin into DCVs. In a proximity labelling BioID screen, I found that CCCP1 is in close proximity to the transmembrane protein carboxypeptidase D (CPD). CPD localizes to the TGN and to immature DCVs (iDCVs), but gets removed from iDCVs during maturation. Interestingly, I have shown that in *Cccp1KO* and in *Eipr1KO* cells, CPD is missorted and remains in mature DCVs. In subcellular localization studies, I found that both CCCP1 and EIPR1/EARP partially colocalize with TGN and iDCV markers, while a second pool of EARP localizes to recycling endosomes. By super-resolution microscopy, I observed that CCCP1 forms circles (~200 nm diameter) that surround proinsulin; suggesting that CCCP1 localizes around immature DCV membranes, around proinsulin positive TGN subdomains, or to both. Together, these localization and functional studies suggest that CCCP1 and EIPR1 are novel regulators of DCV cargo sorting in neurons and endocrine cells. The data is consistent with a model in which CCCP1 and EIPR1 control insulin sorting into DCVs at the TGN and remove cargo not destined to the regulated secretory pathway in a post-Golgi step. To gain insights into the function of CCCP1, I have performed a detailed structure-function study of CCCP1. I have shown that its C-terminal coiled-coil CC3 domain is necessary and sufficient for its localization in vivo, while its middle coiled-coil domain CC2 is required for recruiting EARP complex (likely EARP positive membrane compartment). Finally, in biophysical studies of CCCP1, I have found that the protein has features reminiscent of golgins, a family of membrane tethers. Together, my findings are

consistent with a speculative model in which a membrane tethering step between TGN/iDCVs membranes and EARP positive membranes might be required for cargo sorting to DCVs.

TABLE OF CONTENTS

LIST OF FIGURES

LIST OF TABLES

ACKNOWLEDGEMENTS

I am grateful to my thesis advisor, Michael Ailion, for his mentoring and guidance. I would also like to thank my committee member Alexey Merz for his support; I consider him as my thesis co-advisor. I am immensely fortunate to have received invaluable training and guidance from my colleague, friend, and collaborator Irini Topalidou. We have worked together for the last few years, publishing several manuscripts as co-authors. Chapters 3 and 4 of my thesis are the result of our combined effort. I would like to dedicate a special thanks to Suzanne Hoppins for help with experiments and for her encouragement. Thanks to each of those mentioned, I learned research methods from different fields including *C. elegans* genetics, biochemistry and cell biology. I additionally acknowledge my committee members Jihong Bai, Sandra Bajjellieh, and Shao-En Ong for their helpful insights developing my thesis work. I also would like to thank my colleagues from the Ailion and Merz labs past and present, including Jill Hoyt, Piero Lamelza, Brantley Coleman, Rachael Plemel, and Tom (Mengtong) Duan. Finally, I would like to thank my collaborators Shao-En Ong and Ho-Tak Lau for their help with the critical mass spectrometry experiments. I am very grateful to have worked alongside you all.

DEDICATION

I would like to thank my mother Marie-Sol Ortolá Querol, my father Philippe Cattin, and my sister Laure Cattin Ortolá for your continuous support, encouragement, and good words. I dedicate this work to my grandmother Victoria Querol Tiñena, with whom I was very close, and who I know would be very proud of me today. Another warm thank you to my friend, Irini Topalidou. To my mother- and father-in-law Andrea Jensen and Robert Young, thanks for your support, encouragement, and fashion advice. A special thanks to my life partner and future wife Margaret Elizabeth Young for her humor and her strength that helped me get through all this. GJPS.

Para mi Yaya

Chapter 1. GENERAL INTRODUCTION

1.1 PEPTIDE HORMONES, NEUROPEPTIDES, AND BIOGENIC AMINES ARE PACKAGED INTO DENSE-CORE VESICLES

All eukaryotic cells contain a constitutive secretory pathway, where soluble proteins are released at the plasma membrane (PM) in the absence of external stimulus. Neurons and endocrine cells have an additional secretory pathway: the regulated secretory pathway, which releases chemical signals in response to external stimuli, and which constitutes one of the major means of communication between cells in an organism. Some of these signals, like neurotransmitters, neuropeptides, biogenic amines, peptide hormones, growth factors, and digestive enzymes are stored in a particular type of secretory vesicle called a dense-core vesicle (DCV). This term is derived from how dense they appear on electron micrographs as they contain aggregated cargo and a high content of calcium ions (c.f. Figure 1. 1). Endocrine cells have morphologically similar secretory vesicles that are often called secretory granules; we will refer to all of these vesicles as dense-core vesicles or DCVs.

Across multiple cell types, DCVs contain hundreds of different molecules, small molecules such as biogenic amines (e.g. serotonin), and peptides of up to 100 amino acids long (e.g. the peptide hormone insulin in pancreatic beta-cells, or the neuropeptide neuropeptide Y in the central nervous system). Along with DCVs, neurons have a second class of secretory vesicles that undergo regulated secretion called synaptic vesicles (Figure 1. 1), that store and release classical neurotransmitters (e.g. acetylcholine, glutamate or GABA). While neurotransmitters released by synaptic vesicles usually bind receptors at the surface of the neighboring neurons or muscle cells, DCV cargos travel long distances through the blood stream and can have modulatory effects on

faraway cells and organs. DCV cargos have modulatory roles; they usually bind to G protein coupled receptors or receptor tyrosine kinases, mediating a slower form of signaling via second messengers. Altogether, DCV cargos regulate fundamental physiological processes such as development, behavior, and metabolism; deregulation in signaling pathways controlled by DCV cargo can lead to numerous neurological, developmental, and metabolic diseases. As a consequence, it is critical to understand how DCVs are generated and how the proper cargo is selected.

1.2 DENSE-CORE VESICLES: BIOGENESIS, MATURATION, AND RELEASE

Secretory proteins are synthesized at the endoplasmic reticulum (ER) and transported to the Golgi apparatus, where they traverse the Golgi stacks from the cis-stack to the trans-Golgi network (TGN) (Caro and Palade, 1964). At the TGN, secretory cargos can be directed to distinct routes: the constitutive secretory pathway, the endolysosomal pathway, and the regulated secretory pathway (Griffiths and Simons, 1986). Constitutive cargo is packaged into constitutive vesicles that are directly transported to the PM. Cargo destined to the endolysosomal pathway is sorted into a different class of vesicular carriers that will fuse with endosomes to eventually reach lysosomes. Cargo destined to the regulated secretory pathway are sorted into dense-core vesicles (DCVs, see below).

DCV biogenesis starts at the TGN, where neuropeptide precursors, along with their processing enzymes, SNAREs, and vacuolar ATPases, are packaged into DCVs (Borgonovo et al., 2006; Gondré-Lewis et al., 2012; Morvan and Tooze, 2008). DCVs bud off from the TGN as immature DCVs (iDCVs) and undergo an extensive maturation process (Figure 1. 2) (Borgonovo et al., 2006; Gondré-Lewis et al., 2012; Morvan and Tooze, 2008). Mature DCVs (mDCVs),

capable of regulated secretion, are transported to their sites of release (Borgonovo et al., 2006; Gondré-Lewis et al., 2012; Morvan and Tooze, 2008). Immature DCVs differ from mDCVs in their protein composition, in their biophysical properties, and in their appearance on electron micrographs (Smith and Farquhar 1966 and Tooze 1991). Most of what is known about DCV biogenesis and maturation has resulted from work done in neuroendocrine cell lines. While neuronal DCVs are likely to have differences in their transport pathway due to the different cellular architecture of these cells, it is believed that the core mechanisms of biogenesis are likely to be similar to those in neuroendocrine cells.

1.2.1 *Mechanisms of cargo sorting into the regulated secretory pathway*

The mechanisms of cargo sorting into the regulated secretory pathways are largely unknown. Two general models of dense-core vesicle cargo sorting have been debated for more than twenty years: the "sorting by entry" and "sorting by retention" models (Arvan and Halban, 2004; Gondré-Lewis et al., 2012; Morvan and Tooze, 2008). The sorting by entry model proposes that sorting occurs in the TGN as dense-core vesicles are generated (Arvan and Halban, 2004; Gondré-Lewis et al., 2012; Morvan and Tooze, 2008). Sorting by retention models posit that sorting happens at post-Golgi steps, where non-dense-core vesicle cargos are removed (see section 1.2.2.) (Arvan and Halban, 2004; Gondré-Lewis et al., 2012; Morvan and Tooze, 2008).

Some studies have suggested that luminal dense-core vesicle cargos sort via their ability to aggregate in the low pH/high Ca2+ milieu of the TGN (Chanat and Huttner, 1991), while other studies suggest that aggregation is not sufficient and that sorting relies on poorly defined sequences and/or structural motifs. Two conserved sorting signals in the cytosolic domain of the vesicular monoamine transporter 2 (VMAT2), a DCV transmembrane protein, were found to be critical to

its sorting into DCVs in PC12 cells, a cell line derived from a pheochromocytoma of the rat adrenal medulla (Li et al., 2005; Waites et al., 2001). VMAT2 contains a cluster of acidic residues that include two serines that get phosphorylated by casein kinase 2 (CK2) and a dileucine-like signal motif (Li et al., 2005; Waites et al., 2001). Both signals are required to sort VMAT2 into DCVs (Li et al., 2005; Waites et al., 2001); however, it remains unclear if this sorting step happens at the TGN when the DCVs bud off, or if it happens post-Golgi, where it is important for retaining VMAT2 into maturing DCVs. VMAT2 sorting/retention into DCVs was later shown to require the adaptor protein 3 (AP-3) and the vacuolar sorting protein VPS41 (Asensio et al., 2010, 2013). The DCV specific transmembrane protein of unknown function phogrin has a leucine-based sorting signal in its cytosolic domain, which is important for the localization of the protein into DCVs in the pancreatic beta-cell line, MIN6, and in the anterior pituitary cell line, AtT-20 (Torii et al., 2005). This same domain can bind the clathrin adaptor protein AP-1 in vitro (Torii et al., 2005), suggesting that AP-1 and clathrin are important to sort phogrin into DCVs. The prohormone convertase PC1/3, a luminal DCV cargo that can bind to membranes, was proposed to act as a sorting receptor for soluble cargo. An alpha-helical domain of PC1/3 is sufficient to sort constitutive cargo into the regulated secretory pathway in AtT-20 cells (Dikeakos and Reudelhuber, 2007; Dikeakos et al., 2009). Finally, a disulfide-bonded loop in the DCV luminal cargo chromogranin B, a DCV soluble cargo, was found to mediate membrane binding and to direct its sorting into the regulated secretory pathway in PC12 cells (Glombik et al., 1999). These different sorting signals are, in combination, required for the proper cargo selection into DCVs, however, given that DCVs across cell types contain hundreds of neuropeptide cargos, additional mechanisms of sorting are likely required. More research is needed to reveal the precise molecular mechanism of cargo sorting to the regulated secretory pathway.

1.2.2 *Membrane remodeling events and removal of cargo*

During maturation, iDCVs undergo homotypic fusion events that are critical to their conversion into mDCVs. iDCV-iDCV fusion has been observed in PC12 cells and in mouse beta-cells; it was shown to require NSF (Urbé et al., 1998), alpha-SNAP, the SNARE protein Syntaxin 6 (Wendler et al., 2001), the synaptotagmin Syt4 (Ahras et al., 2006), and the protein of unknown function HID-1 (Du et al., 2016). In a post-Golgi step, several transmembrane cargo not destined to the regulated secretory pathway are removed from iDCVs. Such cargo include the cation dependent and independent mannose-6 phosphate receptor proteins (i.e. CD-MPR, CI-MPR), which sort lysosomal hydrolases to lysosomes, the endopeptidase furin, the Carboxypeptidase D (CPD) and the SNARE proteins Syntaxin 6 and Vamp4 (Dittié et al., 1997; Gondré-Lewis et al., 2012; Klumperman et al., 1998; Varlamov et al., 1999, Hinners et al 2003). Furin, CD-MPR, and CI-MPR are well-defined cargos that cycle between the TGN, the plasma membrane, and the endosome. Their fate once they are removed from iDCVs is unknown, but has been proposed to follow the endosomal route (Arvan and Halban, 2004; Feng and Arvan, 2003). Clathrin coats can be observed at the surface of iDCVs by electron microscopy, and EM and biochemical cell-free studies have shown that the removal of furin, CD-MPR, and CI-MPR from iDCV happens via a mechanism dependent on the small GTPase Arf1, the adaptor protein AP-1 and the coat protein clathrin (Austin et al., 2000; Dittie et al., 1996, 1999; Dittié et al., 1997; Kakhlon et al., 2006). Furin contains a similar acidic cluster to VMAT2 with two serine residues that are phosphorylated by CK2 (Dittié et al., 1997). Interestingly, phosphorylation of this motif increases furin removal from DCVs while the similar motif on VMAT2 promotes its retention into DCVs (Dittié et al., 1997; Waites et al., 2001). These findings suggest that additional sorting mechanisms are yet to be described.

1.2.3 *Acidification of the vesicular lumen and propeptide processing*

Along with peptide precursors (or propeptides), peptide processing enzymes and the vacuolar ATPase are packaged into immature DCVs (Borgonovo et al., 2006; Gondré-Lewis et al., 2012; Morvan and Tooze, 2008). After iDCVs bud off the TGN, the pH of its lumen decreases; this leads to the activation of the catalytic activity of peptide processing enzymes. In beta-cells, the prohormone convertases PC1/3, PC2, and carboxypeptidase E (CPE) process the insulin precursor proinsulin into mature bioactive insulin (Davidson, 2004; Hutton, 1994). Processed peptides are believed to aggregate in the high calcium and low pH environment to form the dense core (Borgonovo et al., 2006; Gondré-Lewis et al., 2012; Kim et al., 2006).

1.2.4 *Dense-core vesicle transport and release*

DCVs fuse with the plasma membrane in a SNARE-dependent manner; their sensitivity to calcium is given by the members of the synaptotagmin family of proteins (Borgonovo et al., 2006; Gondré-Lewis et al., 2012; Hammarlund et al., 2008). Work in mammalian cells has shown that docking and tethering of DCVs at the plasma membrane is believed to involve Rab3a, Rab27a, granuphilin and Noc2 (Cheviet et al., 2004, 2004; Fukuda, 2008; Matsunaga et al., 2017; Yi et al., 2002). Another factor critical to DCV release is CAPS (or UNC-31), the calcium-dependent activator protein for secretion, which was shown in *C. elegans* to dock DCVs, to promote formation of the open form of the SNARE protein syntaxin, and to trigger fusion of DCVs (Hammarlund et al., 2008).

1.3 NEW PROTEINS THAT CONTROL DENSE-CORE VESICLE BIOGENESIS

Molecular mechanisms of dense-core vesicle biogenesis are poorly understood, largely because few proteins have been identified that function in this process. In recent years, a large number of new players have been identified to regulate the biogenesis of DCVs in mammalian endocrine cells, *C. elegans* neurons, and Drosophila salivary gland.

1.3.1 *Genetic screen in C. elegans: new proteins that control cargo sorting to dense-core vesicles*

In *C. elegans*, the small GTPase Rab2 has emerged as a major regulator of dense-core vesicle cargo trafficking (Edwards et al., 2009; Sumakovic et al., 2009). Rab GTPases control various steps of vesicular transport such as budding, tethering, and fusion (Stenmark, 2009). The activity state of Rab GTPases is regulated by proteins called guanine nucleotide exchange factors (GEFs) that activate the Rab by facilitating the GTP-bound state and GTPase-activating proteins (GAPs) that inactivate the Rab by facilitating the hydrolysis of GTP into GDP (Stenmark, 2009). GTP-bound Rab proteins bind to effectors to mediate their function. RAB-2, its effector RIC-19/ICA69, the putative RAB-2 GAP TBC-8/SGSM1,2,3, and the putative GEF GOP-1/CLEC16A have each been shown to be important for early steps in dense-core vesicle biogenesis (Edwards et al., 2009; Hannemann et al., 2012; Sumakovic et al., 2009; Yin et al., 2017). Our lab used a forward genetic screen to isolate mutants that affect dense-core vesicle function. The RUN domain containing protein 1 (RUND-1/RUNDC1) and the coiled-coil containing protein 1 (CCCP-1/CCDC186) were identified together with RAB-2 in the screen (Ailion et al., 2014). RUND-1 and CCCP1 are RAB-2 effectors that control dense-core vesicle biogenesis (Ailion et al., 2014).

In mutants of *rab-2, rund-1 and tbc-8,* morphologically normal dense-core vesicles are generated which are transported to their release sites, but these dense-core vesicles have reduced levels of both luminal neuropeptide cargo and transmembrane cargos (Ailion et al., 2014; Edwards et al., 2009; Hannemann et al., 2012; Sumakovic et al., 2009). In *C. elegans* neurons, RAB-2 and its effectors colocalize near the trans-Golgi, suggesting that they act in the neuron cell body to mediate early steps of DCV biogenesis to regulate proper cargo sorting (Ailion et al., 2014; Hannemann et al., 2012; Sumakovic et al., 2009).

Several additional molecules were identified by our lab's genetic screen for mutants in DCV function. Namely, the conserved WD40 domain protein EIPR-1/TSSC1, and the VPS-52 and VPS-53 proteins, which are shared subunits of the Golgi-associated retrograde protein (GARP) and endosome-associated recycling protein (EARP) complexes (Topalidou et al., 2016). GARP is a multisubunit tethering complex (MTC) that localizes to the TGN and is important for retrieval of retrograde cargo from endosomes in yeast, *C. elegans,* and mammalian cell lines (Conibear et al., 2000, 2003; Pérez-Victoria et al., 2008). EARP is a recently discovered multisubunit tethering complex that localizes to Rab4-positive recycling endosomes (Gillingham et al., 2014; Schindler et al., 2015) and regulates the recycling of transferrin to the plasma membrane in mammalian cell lines (Schindler et al., 2015). GARP and EARP are both composed of 4 subunits with three subunits in common; VPS-51, VPS-52, and VPS-53. GARP's fourth subunit is VPS-54, and EARP's fourth subunit is VPS-50 (Pérez-Victoria et al., 2008; Schindler et al., 2015). Using biochemical methods, we and others have shown that EIPR1 (also called TSSC1) binds to both EARP and GARP complex subunits (Gershlick et al., 2016; Topalidou et al., 2016).

Mutants that lack EIPR-1, VPS-51, VPS-52, VPS-53, and VPS-50 have defects in dense-core vesicle cargo sorting similar to those of mutants that lack RAB-2, RUND-1 or CCCP-1

(Ailion et al., 2014; Paquin et al., 2016; Topalidou et al., 2016). Interestingly, we found that mutants that lack VPS-54 don't have any of these phenotypes, suggesting that EARP --and not GARP-- regulates cargo sorting to DCVs (Topalidou et al., 2016). In mammalian cell lines, EIPR1 was found to function with both EARP and GARP in endosomal recycling and in retrograde traffic respectively (Gershlick et al., 2016).

Genetic epistasis from our lab and other labs indicates that RAB-2, RUND-1, CCCP-1, EIPR1, and EARP (comprised of VPS-51, VPS-52, VPS-53 and VPS-50) all function in the same genetic pathway (Ailion et al., 2014; Paquin et al., 2016; Topalidou et al., 2016). RAB-2 and CCCP-1 co-localize near the TGN in *C. elegans* neurons and in mammalian cell lines (Ailion et al., 2014; Gillingham et al., 2014). EARP and EIPR1 were shown to localize to recycling endosomes in mammalian cell lines, and EARP subunits localize to *C. elegans* neuronal cell bodies (Gershlick et al., 2016; Gillingham et al., 2014; Schindler et al., 2015). RAB2 and CCCP1 interact with each other and EIPR1 interacts with the EARP complex (Ailion et al., 2014; Gershlick et al., 2016; Topalidou et al., 2016). However, no interaction was detected between RAB2/CCCP1 and EIPR1/EARP, suggesting that these proteins form two independent complexes that function in the same genetic pathway to control cargo sorting to DCVs (Figure 1. 3).

1.3.2 *A growing number of proteins that control dense-core vesicle biogenesis*

In the last few years, the list of proteins that have been identified for their role in DCV biogenesis has grown; most of these are factors belonging to protein families implicated in various aspects of membrane trafficking. In *C. elegans*, we and others have identified the small GTPase RAB-2; its GAP, its GEF, its effectors, the EARP complex and its interactor EIPR-1 as described above. An additional protein was found in *C. elegans* to function in the RAB-2 genetic pathway:

the membrane-associated Golgi-localized protein HID-1 (Ailion et al., 2014; Edwards et al., 2009; Hannemann et al., 2012; Mesa et al., 2011; Paquin et al., 2016; Sumakovic et al., 2009; Topalidou et al., 2016; Yin et al., 2017).

AP-1 and clathrin have multiple roles in trafficking; together, they are involved in trafficking between the trans-Golgi and endosomes (Hirst et al., 2012; Robinson, 2004). Clathrin and AP-1 have an established role to aid the removal of transmembrane proteins not destined to DCVs (Austin et al., 2000; Molinete et al., 2001) but a more fundamental role in DCV biogenesis has been proposed recently. In PC12 cells, clathrin knockdown resulted in a near-absence of DCVs and a near-complete block of DCV cargo secretion (Sahu et al., 2017). In Drosophila, removal of AP-1 resulted in loss of glue granule formation in the salivary gland (Burgess et al., 2011). These results indicate that clathrin and AP-1 have a function in DCV biogenesis beyond their known role in removing unwanted proteins from the immature vesicle, and are likely involved in the budding of iDCVs at the TGN.

In mammals, Drosophila and *Tetrahymena thermophila*, a number of factors have been recently identified as having roles in DCV biogenesis. These include:

- The BAR domain proteins PICK1, ICA69 (the mammalian ortholog of RIC-19), and arfaptin-1 (Buffa et al., 2008; Cao et al., 2013; Gehart et al., 2012; Holst et al., 2013).
- Several small G proteins: Arl1, Rab2a and Rab3d (Buffa et al., 2008; Kögel et al., 2013; Matsunaga et al., 2017; Torres et al., 2014).
- Coat proteins and adaptor protein complexes: the coat protein clathrin (Sahu et al., 2017), and the clathrin adaptor complexes AP-1 and AP-3 (Asensio et al., 2010; Bonnemaison et al., 2014; Burgess et al., 2011).
- The SNARE protein Vti1A (Walter et al., 2014).

- Multisubunits tethering complexes: HOPS, known to be required for late endosomal function) (Asensio et al., 2013) and BLOC-1, important for the biogenesis of lysosome-related organelles) (Hao et al., 2015).
- The endosome-localized C2-domain containing Munc13-4 related protein BAIAP3 (Zhang et al., 2017).
- VPS10 domain containing proteins Sorcs1 and Sortilin (Briguglio et al., 2013; Kebede et al., 2014).

1.3.3 *Endosomal traffic and dense-core vesicle biogenesis*

Recently, several proteins known for their function at endosomes and recycling endosomes have been identified as regulators of DCV biogenesis. These include the EARP complex, EIPR1, BAIAP3, the G protein Rab2, and the VPS10 domain proteins Sortilin and Sorcs1 (Gershlick et al., 2016; Lőrincz et al., 2017; Sasidharan et al., 2012; Schindler et al., 2015; Zhang et al., 2017; Briguglio et al., 2013; Kebede et al., 2014).

- EARP and EIPR1's functions in mammals are described in section 1.3.1.
- The Munc13-4 protein BAIAP3 localizes to endosomes, and is also required for retrieval of cargo from endosomes to the TGN (Zhang et al., 2017). BAIAP3 knockdown in neuroendocrine cells causes the accumulation of defective DCVs that are fusion incompetent, and the increased lysosomal degradation of insulin containing DCVs (Zhang et al., 2017).
- Studies in *C. elegans*, Drosophila, and mammalian cell lines have demonstrated that Rab2 [and its GEF Gop1/Clec16 in *C. elegans*] are both required for endosomes and autophagosome maturation (Lőrincz et al., 2017; Yin et al., 2017). Interestingly, a study in

Drosophila has shown that Rab2 was required for developmentally programmed degradation of glue granule (a DCV-like organelle) in the fly's salivary gland (Csizmadia et al., 2018).

- VPS10 domain containing proteins are sorting receptors that are required for targeting lysosomal proteins to the regulated secretory pathway. Recent work in mouse beta-cells and in *tetrahymena thermophila* have shown that the VPS10 domain containing proteins Sorcs1 and Sortilin are also required for DCV biogenesis (Briguglio et al., 2013; Kebede et al., 2014).

All together, these findings suggest that trafficking through endosomes is required for DCV biogenesis.

1.3.4 *How could endosomal trafficking affect DCV biogenesis?*

Previous studies have shown that there exists a route where DCV cargo traffics through endosomes. Following dense-core vesicle exocytosis, the dense-core vesicle transmembrane proteins peptidylglycine α -amidating monooxygenase (PAM) and phogrin have been shown to be recycled back to dense-core vesicles via endosomal compartments (Bäck et al., 2010; Vo et al., 2004; Wasmeier et al., 2005). Even though the impact on DCV biogenesis hasn't been demonstrated, one can speculate that providing a constant pool of recycled proteins like SNAREs, processing enzymes, or yet unknown DCV cargo sorting receptors is important for the biogenesis of DCVs and for the maintenance of DCV protein homeostasis.

It has been shown that during maturation cargo is removed from iDCVs (Gondré-Lewis et al., 2012). While the fate of the cargo removed from iDCVs is unclear; it includes proteins like

Syn6 and Syt4 that are required for homotypic fusion of iDCVs, a critical step for maturation (Ahras et al., 2006; Wendler et al., 2001). These proteins must be made available for reuse into a nascent DCV and one can speculate that Syn6 and Syt4 need to be recycled back to the TGN, and this could happen via an endosomal compartment, thus endosomal trafficking would be critical for DCV biogenesis.

1.4 FIGURES

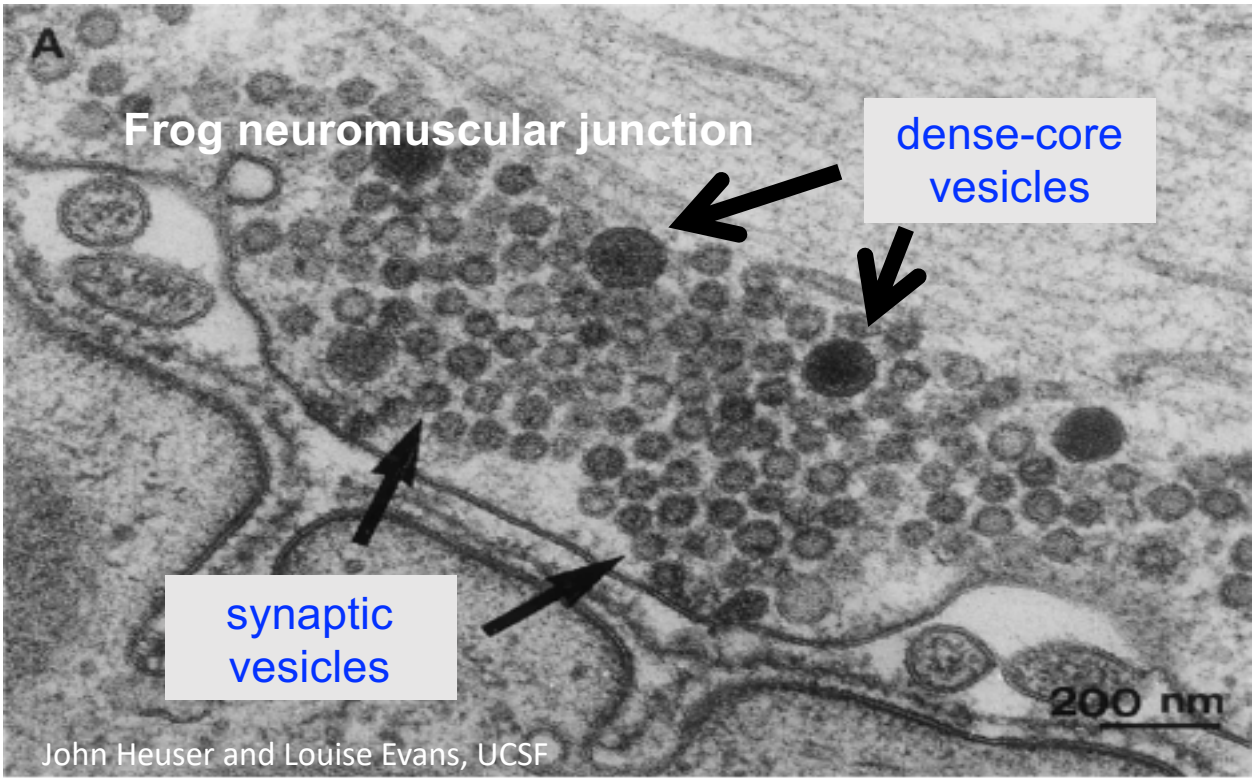

Figure 1. 1 Electron micrograph showing the active zone of a frog neuromuscular junction

The presynaptic cell on the top part contains two classes of vesicles: the clear, numerous and small are synaptic vesicles that store and release small molecule classical neurotransmitters (i.e. acetylcholine or GABA). The fewer, bigger and dense-looking vesicles are the dense-core vesicles that carry modulatory neurotransmitters such as neuropeptides or biogenic amines.

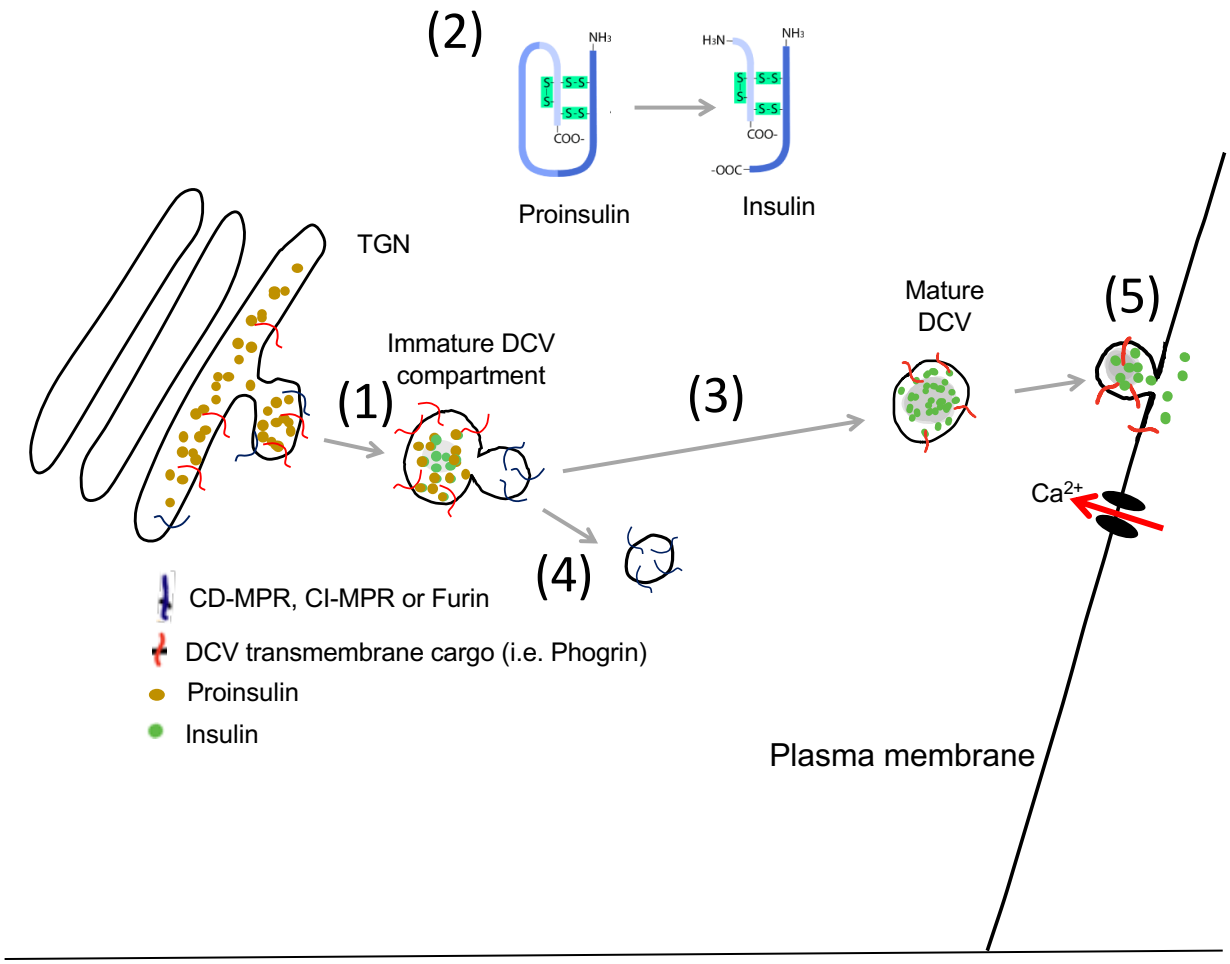

Figure 1. 2 . DCV maturation: peptide processing, membrane remodeling and removal of cargo

(1) DCVs are generated at the trans-Golgi network (TGN) as immature DCV (iDCVs) and go through a maturation process. (2) Along with peptide precursors (or propeptides), processing enzymes are sorted into iDCVs and process the propeptides into bioactive peptides. (3) iDCVs go through membrane remodeling events including homotypic fusion of iDCV and (4) removal of cargo not destined to the regulated secretory pathway (i.e. furin, CPD, CD-MPR, CI-MPR). Mature DCVs are transported to the plasma membrane and (5) are released in response to an increase in the concentration of intracellular calcium.

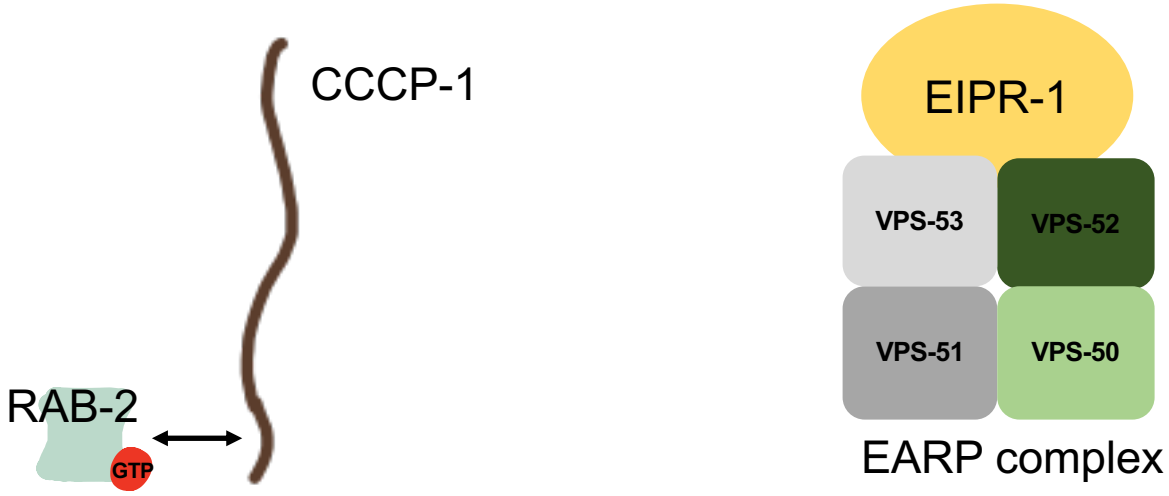

Figure 1. 3. Two groups of cytosolic factors that control luminal DCV cargo sorting in *C. elegans*

All these proteins function in the same pathway in *C. elegans* neurons, but while CCCP-1 binds activated GTP-bound RAB-2 and EIPR-1 binds to the EARP complex, no physical interaction has been detected between RAB-2/CCCP-1 and EIPR-1/EARP.

Chapter 2. THE DENSE-CORE VESICLE MATURATION PROTEIN CCCP-1 BINDS RAB-2 AND MEMBRANES THROUGH ITS C-TERMINAL DOMAIN

2.1 ABSTRACT

Dense-core vesicles (DCVs) are secretory organelles that store and release modulatory neurotransmitters from neurons and endocrine cells. Recently, the conserved coiled-coil protein CCCP-1 was identified as a component of the DCV biogenesis pathway in the nematode *C. elegans*. CCCP-1 binds the small GTPase RAB-2 and colocalizes with it at the trans-Golgi. Here we report a structure-function analysis of CCCP-1 to identify domains of the protein important for its localization, binding to RAB-2, and its function in DCV biogenesis. We find that the CCCP-1 C-terminal domain (CC3) has multiple activities. CC3 is necessary and sufficient for CCCP-1 localization and for binding to RAB-2 and is required for the function of CCCP-1 in DCV biogenesis. Additionally, CCCP-1 binds membranes directly through its CC3 domain, indicating that CC3 may comprise a previously uncharacterized lipid-binding motif. We conclude that CCCP-1 is a coiled-coil protein that binds an activated Rab and localizes to the Golgi via its C-terminus; it therefore has properties similar to members of the golgin family of proteins. CCCP-1 also shares biophysical features with golgins; it has an elongated shape and forms oligomers.

2.2 INTRODUCTION

Dense-core vesicles (DCVs) are specialized organelles of neurons and endocrine cells. DCVs store and release modulatory peptides and biogenic amines, signaling molecules that control a multitude of processes including synaptic plasticity, feeding behavior, and glucose homeostasis (Borgonovo et al., 2006; Gondré-Lewis et al., 2012; Morvan and Tooze, 2008; Tooze et al., 2001). However, DCV biogenesis is not well understood, especially at the molecular level. Immature DCVs bud off from the trans-Golgi and undergo several maturation steps, including homotypic fusion with other immature DCVs, vesicle acidification, peptide processing, and sorting of cargos (Borgonovo et al., 2006; Gondré-Lewis et al., 2012; Morvan and Tooze, 2008; Tooze et al., 2001)

In recent years, a small but growing number of proteins have been identified as playing roles in DCV biogenesis, beginning to shed some light on the molecular mechanisms underlying the steps in DCV maturation (Ahras et al., 2006; Asensio et al., 2010, 2013; Bonnemaison et al., 2014; Buffa et al., 2008; Burgess et al., 2011; Cao et al., 2013; Hao et al., 2015; Holst et al., 2013; Kebede et al., 2014; Pinheiro et al., 2014; Torres et al., 2014; Walter et al., 2014; Wendler et al., 2001). In one approach to identifying proteins important for DCV biogenesis, genetic screens were performed in *Caenorhabditis elegans* (Ailion et al., 2014; Edwards et al., 2009; Hannemann et al., 2012; Mesa et al., 2011; Sasidharan et al., 2012; Sumakovic et al., 2009; Topalidou et al., 2016). These screens identified several molecules important for early stages of DCV biogenesis and maturation, including the small G protein RAB-2 and several RAB-2 effectors, including the conserved coiled-coil protein CCCP-1 (Ailion et al., 2014). Here we perform a structure-function analysis of CCCP-1 to better understand its biochemical activities and role in DCV biogenesis.

RAB-2 is a highly-conserved member of the Rab family of small G proteins. Rabs are membrane-associated proteins that function as molecular switches that alternate between a GTP-

bound active state and a GDP-bound inactive state (Stenmark, 2009). Activated Rabs recruit effectors that execute many aspects of membrane trafficking including vesicle transport and vesicle tethering (Stenmark, 2009). CCCP-1 was recently identified as a potential RAB-2 effector (Ailion et al., 2014; Gillingham et al., 2014). In *C. elegans*, RAB-2 and CCCP-1 colocalize near the trans-Golgi and function in the same genetic pathway to regulate locomotion and DCV cargo sorting in neurons (Ailion et al., 2014). Though CCCP-1 is critical for proper DCV biogenesis, its specific molecular functions remain unclear. Here we conduct a structure-function analysis to determine which domains of CCCP-1 are important for its localization, binding to RAB-2, and its function in DCV biogenesis. Our analysis shows that CCCP-1 has structural and functional features in common with the golgins, a family of tethers that also bind activated Rabs and regulate vesicular trafficking at the Golgi (Gillingham and Munro, 2003, 2016; Sztul and Lupashin, 2009; Witkos and Lowe, 2016; Yu and Hughson, 2010). These findings suggest that CCCP-1 may act as a membrane tether.

2.3 RESULTS

2.3.1 *CCCP-1 is localized near immature DCVs and the trans-Golgi via its C-terminal domain CC3*

To assess the localization of full length CCCP-1 in *C. elegans* neurons, we generated transgenic worms expressing GFP-tagged CCCP-1. CCCP-1::GFP expressed under its own promoter as a single-copy integrated transgene was not detectable, and even when expressed as multiple copies in an extrachromosomal array, CCCP-1::GFP levels were too low to be detected in most transgenic lines. However, these single-copy and overexpressed CCCP-1::GFP constructs are functional since they rescue the locomotion defects of a *cccp-1* mutant (see below). Because CCCP-1 is expressed

predominantly in *C. elegans* neurons (Ailion et al., 2014), we expressed CCCP-1::GFP under the stronger pan-neuronal *rab-3* promoter. CCCP-1 localized mainly to perinuclear puncta in the cell body of ventral cord motor neurons (Figure 2. 1 A, top) but also localized to puncta in axons in the dorsal nerve cord (Figure 2. 1 A, bottom), suggesting that some CCCP-1 is transported out of the cell body.

To determine which domain of CCCP-1 mediates its localization, we generated transgenic worm lines carrying different GFP-tagged CCCP-1 fragments (Figure 2. 1 B) expressed under the pan-neuronal *rab-3* promoter. Like full-length CCCP-1::GFP, a fragment containing the 193 C-terminal amino acids (CC3::GFP) localized to large perinuclear puncta (Figure 2. 1 C) and had puncta in the dorsal nerve cord as well (data not shown). In contrast, CC1+2::GFP was localized diffusely in the cytoplasm (Figure 2. 1 C) as well as in the dorsal nerve cord (data not shown). These results are consistent with data showing that the N-terminal half of human CCCP1/CCDC186 localized to the cytosol and a C-terminal fragment larger than CC3 localized to perinuclear structures in COS cells (Gillingham et al., 2014).

To test whether CC3 is sufficient for proper localization of CCCP-1, we performed colocalization experiments. We previously reported that CCCP-1 colocalized with the small GTPase RAB-2 near the trans-Golgi in *C. elegans* neurons (Ailion et al., 2014). Similar to full length CCCP-1::GFP, CC3::GFP colocalized with RFP::RAB-2 in *C. elegans* neurons (Figure 2. 1 D). Thus, the C-terminal domain CC3 is both necessary and sufficient for CCCP-1 localization.

To determine the localization of the mammalian ortholog of CCCP-1, CCCP1/CCDC186, we imaged endogenous or GFP-tagged CCCP1/CCDC186 in rat insulinoma 832/13 cells (Hohmeier et al., 2000). These cells have insulin secretory granules similar to neuronal DCVs and

express CCCP1/CCDC186 (Topalidou et al., 2016). Moreover, they are larger cells than *C. elegans* neurons and have a more easily visualized separation of different organelles.

In 832/13 cells, we found that endogenous CCCP1 localizes to perinuclear structures that overlapped with chromogranin A (CgA), a DCV cargo expected to localize to the trans-Golgi, immature DCVs, and mature DCVs (Figure 2. 2 A and B). CCCP1 localization was restricted to a perinuclear area adjacent to the cis-Golgi marker GM130 (Figure 2. 2 A). However, the CCCP1 signal overlaps more with CgA than with GM130 (Figure 2. 2 B). CCCP1::GFP had a localization pattern similar to endogenous CCCP1. Like endogenous CCCP1, CCCP1::GFP overlapped with CgA and was adjacent to GM130 (Figure 2. 2 C and D). CCCP1::GFP also partially colocalized with the trans-Golgi marker TGN38. Thus, as in *C. elegans* neurons and COS cells (Ailion et al., 2014; Gillingham et al., 2014), CCCP1 localizes near the trans-Golgi in 832/13 cells (Figure 2. 2 A and D). Because no CCCP1 signal could be observed near the cell periphery and because CCCP1 localizes more closely with the DCV marker CgA than with TGN38 (Figure 2. 2 D), our results suggest that CCCP1 localizes near immature DCVs.

We tested the localization of CC3::GFP and found it similar to endogenous CCCP1 and CCCP1::GFP (Figure 2. 2 E and F). Finally, we found that, CC1+2::GFP localizes to the cytoplasm, as it does in *C. elegans* neurons (Figure 2. 2 G). Thus, CC3 is both necessary and sufficient for CCCP1/CCDC186 localization near immature DCVs and the trans-Golgi.

We then tested the localization of fragments of the CC3 domain of CCCP1. Using the PSIPRED Protein Sequence Analysis Workbench (http://bioinf.cs.ucl.ac.uk/psipred/), we determined that rat CCCP1 contains four predicted alpha-helical regions (Figure 2. 3 A in red) surrounded by sequences predicted to be unstructured (Figure 2. 3 A, in grey). The helical regions are highly conserved (Appendix A). The CC3 domain has three short predicted alpha-helical

regions (amino acids 780-830, 870-890 and 894-922) while amino acids 750-780 and 830-870 are predicted to be unstructured. We generated a large number of truncations either N-terminally Myc-tagged or C-terminally GFP-tagged. The list of constructs and the description of their localization can be found in Table 2. 1. The relevant fluorescent micrographs are shown in Figure 2. 3 A-G. We found that, like CCCP1::GFP, Myc::CCCP1 localizes near the TGN marker TGN38. Fragments missing the unstructured region (aa 750-780, Figure 2. 3 C and F) and the second half of the third alpha-helical region (aa 912-922, Figure 2. 3 F) remained TGN-localized. Interestingly, these regions are not well conserved (Appendix A). Moreover, a fragment expressing amino acids 1-867 or any fragment splitting the CC3 domain within the unstructured region (between aa 830-870) resulted in the loss of TGN-localization (Table 2. 1). The data demonstrate that amino acids 778-912 are both necessary and sufficient for CCCP1 localization and that the C-terminal conserved helical regions are required for TGN localization.

2.3.2 *CCCP-1 binds to RAB-2 via its C-terminal CC3 domain*

Multiple lines of evidence suggest that CCCP-1 is an effector of the small GTPase RAB-2. CCCP-1 and RAB-2 act in the same genetic pathway in *C. elegans* and they colocalize in worm neurons and in COS cells (Ailion et al., 2014; Gillingham et al., 2014). In addition, yeast two-hybrid experiments suggested that CCCP-1 and RAB-2, from either worm or human, interact in a GTP-dependent manner (Ailion et al., 2014; Gillingham et al., 2014). The interaction of human CCCP1/CCDC186 with RAB2A was mapped to a C-terminal fragment of CCCP1/CCDC186 (Gillingham et al., 2014). To assess the RAB-2 interaction with CCCP-1 using purified *C. elegans* proteins, we performed GST pull-downs and found that CCCP-1 binds to RAB-2 loaded with the non-hydrolysable GTP analog guanosine 5'-O-[gamma-thio]-triphosphate (GTPγS, Figure 2. 4 A,

lane 1), but not to RAB-2 loaded with GDP (Figure 2. 4 A, lane 2). The interaction of CCCP-1 with RAB-2 was detected using an antibody to the His_6 epitope tag and could not be detected on Coomassie-stained gels, suggesting that the interaction is likely of moderate affinity.

We also performed GST pull-down experiments using the CCCP-1 fragments. CC2+3 and CC3 bound to RAB-2 in a GTP-dependent manner but CC1+2 did not bind (Figure 2. 4 A), demonstrating that CC3 is necessary and sufficient for RAB-2 binding.

In *C. elegans*, CCCP-1 localizes to perinuclear puncta in the absence of RAB-2 (Ailion et al., 2014). This indicates that RAB-2 is not the sole determinant of CCCP-1 localization. We found that the localization of CC3 is also unaltered in the absence of RAB-2 (Figure 2. 1 E). Thus, the CC3 domain has at least two independent activities: RAB-2 binding and subcellular targeting.

We then performed GST pull-down experiments using the CC3 sub-fragments. Above we found that the highly conserved amino acids 778-912 of the rat protein were both necessary and sufficient for TGN localization and that amino acids 750-778 and 912-922 were not required for TGN localization (Figure 2. 3). Using the sequence alignment (Appendix A), we expressed and purified the equivalent His6 tagged *C. elegans* CCCP-1 fragments and performed GST-RAB-2 pulldowns (Figure 2. 4 B). Removal of amino acids 551-584 from CC3 (equivalent to aa 750-778 for the rat protein) had no effect on RAB-2 binding (Figure 2. 4 B). Interestingly, removal of the 14 C-terminal amino acids 729-743 from CC3 (equivalent to aa 912-922 for the rat protein) resulted in decreased binding affinity and loss of nucleotide specificity (Figure 2. 4 B). This result was surprising given that these amino acids are not conserved (Appendix A) and had no effect on the localization of the rat protein near the TGN. It is possible that in the absence of 729-743, the protein gets misfolded. Because it appeared soluble and ran as a single peak near its expected molecular weight on Size-exclusion chromatography (Data not shown), misfolding is unlikely.

Taken together, these results suggest that the 14 amino acids at the C-terminus of CCCP1 are required for RAB-2 binding and nucleotide specificity. Moreover, these residues are not required for TGN localization, a finding consistent with the results from *C. elegans* that RAB-2 is not required for CCCP1's TGN localization (Figure 2. 1 E).

2.3.3 *CC3 is necessary for CCCP-1 function*

To test whether CC3 is sufficient for the in vivo neuronal function of CCCP-1, we assayed CCCP-1 function in *C. elegans*. *cccp-1* mutant worms have a slow locomotion phenotype (Ailion et al., 2014). Because overexpression of CCCP-1 also causes slow locomotion, we instead made single-copy integrants of transgenes expressing the different CCCP-1 fragments under the endogenous *cccp-1* promoter and tested for rescue of the *cccp-1* mutant slow locomotion phenotype. Expression of full-length CCCP-1 rescued the locomotion defect of *cccp-1* mutants (Figure 2. 5 A), but neither CC1+2 nor CC3 rescued (Figure 2. 5 B). Thus, CC3 is necessary but not sufficient for CCCP-1 function.

2.3.4 *CCCP-1 binds membranes directly*

The colocalization of CCCP-1 puncta with RAB-2 and trans-Golgi markers suggests that CCCP-1 may be localized to a membrane compartment, but CCCP-1 does not have a predicted transmembrane domain. To test whether CCCP-1 is a cytosolic protein associated with membranes, we used the rat insulinoma 832/13 cell line (Hohmeier et al., 2000). We transfected cells with a GFP-tagged rat CCCP1/CCDC186 construct and performed membrane fractionation assays (Figure 2. 6 A). Most of the CCCP1/CCDC186 protein associated with membranes (Figure

2. 6 A, P90 membrane pellet versus S90 soluble fraction). In the presence of either 1 M NaCl or 1% Triton X-100, CCCP1/CCDC186 was soluble. CCCP1/CCDC186 therefore behaves as a peripheral membrane protein.

Membrane association of CCCP-1 could occur via binding an additional protein or through its direct interaction with the phospholipid bilayer. We assayed whether the purified CCCP-1 protein binds lipids directly in blot overlay and liposome flotation experiments. We generated liposomes containing cholesterol and lipids with neutral and charged head groups that mimic the lipid composition of the Golgi (Bigay et al., 2005). The liposomes were doped with a fluorescent lipid, rhodamine-phosphatidylethanolamine (Rh-PE). We incubated liposomes and protein at the bottom of a stepped sucrose density gradient (Figure 2. 6 B). When centrifuged, most of the Rh-PE-labeled liposomes floated to near the top of the gradient, and most of the CCCP-1 protein migrated with the liposomes (Figure 2. 6 C, lanes 4 and 5). In the absence of liposomes, CCCP-1 remained at the bottom of the gradient. Thus, CCCP-1 binds membranes directly.

Because CC3 is necessary and sufficient for CCCP-1 localization in vivo, we tested whether CCCP-1 binds membranes through CC3. In flotation assays, fragments containing CC3 (that is, CC3 or CC2+3) floated with the liposomes (Figure 2. 6 D, lanes 5 and 6). Other CCCP-1 fragments remained mostly at the bottom; however, a small amount of CC1+2 migrated to the top of the tube (Figure 2. 6 D, lanes 5 and 6). Because less CC3 bound to liposomes than full-length CCCP-1, the binding affinity of CC3 to membranes may be weaker. However, the CC3 protein was less stable than the full-length CCCP-1 so the decreased liposome binding of CC3 may also be due to its decreased stability. We conclude that CCCP-1 has the capacity to bind membrane bilayers via its CC3 domain.

Domain structure prediction software does not indicate the presence of any canonical lipid-binding domain in CCCP-1, nor does CCCP-1 have a lipid-binding Amphipathic Lipid Packing Sensor (ALPS) motif (our unpublished observations). Thus, CCCP-1 may contain a previously uncharacterized lipid-binding domain or motif. To test whether CCCP-1 has affinity for phospholipids bearing specific head groups, we used a protein-lipid overlay assay (PIP strip) (Figure 2. 6 E). CCCP-1 showed a weak preference for binding to phosphatidylinositides with a single phosphate group: phosphatidylinositol 3-phosphate (PI (3)P), phosphatidylinositol 4-phosphate (PI (4)P) and phosphatidylinositol 5-phosphate (PI (5)P). In addition, CCCP-1 showed some affinity for phosphatidic acid (PA) and phosphatidylserine (PS) (lipid head groups with a negative net charge), and phosphatidylethanolamine (PE) (a neutral head group) (Figure 2. 6 E). Thus, at least in blot overlay assays, the interaction is not selective for a specific lipid and not purely electrostatic or hydrophobic. To determine whether CCCP-1 prefers binding to a specific phosphatidylinositol with a single phosphate, we performed a protein-lipid overlay assay using a membrane spotted with a range of concentrations of phosphatidylinositols (PIP array). No obvious chemical selectivity was apparent (Figure 2. 6 F).

Together, these results demonstrate that CC3 contains a RAB-2 binding site and suggest the existence of a novel membrane-association domain or motif.

2.3.5 *CCCP-1 forms oligomers and has an elongated structure*

CCCP-1 is predicted to be a coiled-coil protein with a domain structure reminiscent of the golgins, elongated proteins that act as Golgi-localized tethering factors (Gillingham and Munro, 2003, 2016; Sztul and Lupashin, 2009; Witkos and Lowe, 2016; Yu and Hughson, 2010). To test whether CCCP-1 has biophysical properties similar to golgins, we studied bacterially expressed

C. elegans His_6-tagged CCCP-1 (Figure 2. 7 A). Though CCCP-1 has a predicted monomeric molecular mass of 89 kDa, it eluted from a Superose 6 size-exclusion column in two peaks, both with an apparent mass larger than a 670 kDa globular protein standard (Figure 2. 7 B, top). This result suggests that CCCP-1 may have an elongated non-globular shape, form oligomers, or be aggregated. Golgins are elongated and generally form oligomer

To test whether the CCCP-1 protein contains mostly coiled-coils as predicted, we performed circular dichroism (CD) spectroscopy. The CD scans of the protein eluting in the pooled SEC fractions 11-12 exhibit the typical profile of a predominantly α-helical protein with minima at 208 nm and 222 nm (Figure 2. 7 C, top left), confirming that CCCP-1 is composed of the expected secondary structure. The melting curve shows a single sharp transition (Figure 2. 7 C, top right), implying that the protein is homogeneously folded. Moreover, the CD scans and melting curves of the protein eluting in the SEC void peak (fractions 8-9) are highly similar to those of the protein in fractions 11-12 (Figure 2. 7 C, middle). These results confirm that CCCP-1 is folded and suggest that the protein exist as at least two populations of conformers or of oligomeric states.

Interestingly, lowering the pH from pH 7.6 to 6.5 resulted in a shift in the size exclusion chromatography profile towards the smaller peak (Figure 2. 7 B, bottom). Moreover, the CD scan and melting curve of the protein eluting in the single peak at pH 6.5 are very similar to the CD data at pH 7.6 (Figure 2. 7 C, bottom). These data suggest that CCCP-1 undergoes a pH dependent change in conformation, in oligomerization state, or in both.

To study the biophysical properties of the protein further, we subjected His_6-CCCP-1 to velocity sedimentation through a 5-25% linear sucrose gradient. At pH 7.6, His_6-CCCP-1 sedimented in a broad peak with most of the protein migrating between the 44 kDa and 157 kDa standards (Figure 2. 8 A, top, lanes 3 and 4). Very little protein was found in the pellet (Figure 2.

8 A, top, lane 7), indicating that the protein is not aggregated. The combination of large apparent molecular weight by size-exclusion chromatography (SEC) and slow sedimentation suggests that CCCP-1 has an elongated shape. To test whether CCCP-1 exists in multiple populations of oligomeric states or conformations, we subjected SEC fractions 10 and 12 to velocity sedimentation in a sucrose gradient (Figure 2. 8, B). Fraction 10 sedimented faster than fraction 12 suggesting that the protein exists in multiple conformations or oligomeric states (Figure 2. 8, B). At pH 6.5, the protein sedimented in the same peak as the protein eluting by SEC in fraction 12 at pH 7.6 (Figure 2. 8 A, bottom, lane 3 and 4). These results suggest that the conformation or the oligomeric status of pH 6.5 and SEC fraction 12 at pH 7.6 is identical. These data are suggestive that at pH 7.6, the protein exists in at least two populations of conformers or of oligomeric states, and that the population distribution is sensitive to pH.

To determine the oligomeric state, we analyzed His_6-CCCP1 by SEC-Multiple Angle Light Scattering (SEC-MALS). Protein from SEC fraction 12 (Figure 2. 7 B, top) eluted as a monodisperse peak (polydispersity was 1±16.8%) with a molar mass of 219 kDa (±11.9%) (Figure 2. 8 C). Thus, the smaller form of CCCP-1 is a dimer. Consistent with this, we found that CCCP-1 interacts with itself in yeast two-hybrid experiments (data not shown). We could not analyze the larger forms of the protein by SEC-MALS because they eluted in the column's void.

We further examined CCCP-1 structure by negative-stain electron microscopy (EM). At pH 7.6, SEC fraction 11-12 of CCCP-1 formed elongated filaments of varying shapes and sizes (Figure 2. 8 D, left), explaining why the protein runs large on SEC and sediments slowly. This result further suggests that CCCP-1 may exist as polymorphic oligomers with multiple flexible forms. Similar biophysical features have been observed for other golgins (Cheung et al., 2015; Ishida et al., 2015; Sapperstein et al., 1995). Strikingly, lowering the pH to 6.5 resulted in a

dramatic change (Figure 2. 8 D, right) as CCCP-1 went from an elongated conformation to a globular conformation. The oligomeric state of the globular-looking structure at pH 6.5 is unknown. Taken together, these data suggest that CCCP-1 undergoes a pH-dependent change in conformation, in oligomerization state, or in both.

To determine which domain of the protein is responsible for its large apparent molecular mass, we analyzed purified CCCP-1 fragments by SEC. Fragments containing the CC2 middle domain (CC2, CC1+2, and CC2+3) ran at a very large apparent molecular weight (Figure 2. 9). Furthermore, we observed that CC1 and CC3 ran closer to but still larger than their predicted globular monomeric masses (Figure 2. 9).

Together, these results indicate that CCCP-1 likely forms extended oligomers and that the CC2 middle domain mediates the formation of higher-order oligomeric states, the formation of elongated structures, or both.

2.3.6 *CC3 is highly conserved among metazoans and beyond*

In Basic Local Alignment Search Tool (BLAST) analyses, we found a single clear CCCP-1 ortholog in most metazoans, including primitive metazoans like sponges and cnidarians (Appendix A), though it is not apparent in other primitive metazoans including ctenophores and placozoans. Interestingly, we also found a likely CCCP-1 ortholog in two single-celled organisms closely related to metazoans: the choanoflagellate *M. brevicollis* and the snail symbiont *C. owczarzaki*. This suggests that CCCP-1 originated shortly before the origin of metazoans and was perhaps lost in some early metazoan lineages. An alignment of CCCP-1 and its orthologs shows that the C-terminal domain of CCCP-1 that includes the third coiled-coil domain and sequence downstream is the most highly conserved region of the protein (Appendix A). The middle part of the protein shows moderate conservation and the N-terminal region is the most diverged

(Appendix A). Thus, the proposed lipid-binding and localization domain of CCCP-1 is the most highly conserved part of the protein, suggesting that it has been selected to maintain these functions and that the ancestral function of CCCP-1 may have been in membrane trafficking.

2.4 DISCUSSION

Here we performed a structure-function analysis of CCCP-1 to identify the important domains of the protein and assign activities to these domains. We found that the ~200 amino acid C-terminal domain (CC3) has multiple activities. First, CC3 is necessary and sufficient for localization near immature DCVs and the trans-Golgi. Second, CC3 is necessary and sufficient for binding RAB-2. Third, CC3 mediates direct physical interaction with synthetic membrane bilayers. Furthermore, CC3 is required for CCCP-1 function in *C. elegans* neurons. We propose that CC3 is a novel membrane-binding domain that targets CCCP-1 to membranes and is necessary for CCCP-1 function in DCV biogenesis. Interestingly, RAB-2 is not required for the localization of either CCCP-1 or its CC3 domain in vivo. Thus, the CC3 domain appears to contain the information to target CCCP-1, even in the absence of RAB-2. Though CCCP-1 localization could theoretically be determined by its binding to membranes with specific physical or chemical properties, we found a relative lack of specificity in the interaction of CCCP-1 with lipids. Thus, CCCP-1 must also depend on additional factors for localization, perhaps through a combination of protein and lipid-binding activities.

2.4.1 *CC3 directs CCCP-1 to immature DCVs near the trans-Golgi, potentially via a novel membrane-binding domain*

Our data indicate that CC3 contains a membrane-binding domain and that direct membrane association may be important for the function of CCCP-1. Unlike other long coiled-coil trafficking proteins, CCCP-1 does not contain a recognizable membrane targeting domain such as the GRIP domain found in golgins (GRIP = "Golgi targeting domain golgin-97, RanBP2alpha, Imh1p and p230/golgin-245") (Ailion et al., 2014; Gillingham and Munro, 2003, 2016; Munro and Nichols, 1999). The blot overlay experiments suggest that CCCP-1 does not have chemical selectivity for a specific lipid and that it binds to both negatively-charged and neutral lipid head groups. These data raise the possibility that the interaction of CCCP-1 with membranes may depend on a combination of physical and chemical factors such as membrane curvature, electrostatics, hydrophobicity, or lipid packing. Protein-membrane interactions are often mediated by amphipathic helices such as the ALPS motif (Antonny et al., 1997; Drin and Antonny, 2010; Miller et al., 2015). We found that CC3 contains several potential amphipathic helices in and downstream of its predicted coiled-coil domain (Appendix A, HeliQuest (Gautier et al., 2008)), but none of them have the properties of the lipid-binding ALPS motif which contains bulky aromatic residues on the hydrophobic side of the helix and mostly noncharged residues on its polar side (Bigay et al., 2005; Drin and Antonny, 2010; Drin et al., 2007).

2.4.2 *Is CCCP-1 a golgin?*

Several features of CCCP-1 suggest that it should be included as a member of the golgin family. First, CCCP-1 has a domain structure predicted to be largely coiled-coil, and golgins belong to a family of conserved proteins that are composed of extended coiled-coil domains

(Gillingham and Munro, 2003, 2016). Second, like other golgins, CCCP-1 is localized to the Golgi. Third, CCCP-1 localization is mediated by its C-terminal domain, in part through direct membrane association. Similarly, golgins are often anchored by their C-termini to specific regions of the Golgi (Gillingham and Munro, 2003, 2016), either through a C-terminal transmembrane anchor or a lipid-binding domain (Gillingham and Munro, 2003, 2016). Fourth, both CCCP-1 and golgins form oligomers (Brown et al., 2011; Gillingham and Munro, 2016; Ishida et al., 2015; Sapperstein et al., 1995). Fifth, CCCP-1 forms elongated structures like golgins (Brown et al., 2011; Gillingham and Munro, 2016; Ishida et al., 2015; Sapperstein et al., 1995). Sixth, both CCCP-1 and golgins bind activated Rab proteins. Moreover, we found that CCCP-1 undergoes a striking pH dependent change in conformation, in oligomerization state, or in both. The physiological significance of this conformational change remains to be investigated. Conformational changes in golgin have been observed before, and proposed to be required for their function (Cheung et al., 2015; Murray et al., 2016).

What do these similarities suggest about the molecular function of CCCP-1? Golgins often function as molecular tethers, capturing incoming vesicles at the Golgi to help mediate fusion (Gillingham and Munro, 2003, 2016; Wong and Munro, 2014), with different golgins tethering vesicles that emerge from different compartments (Wong and Munro, 2014). Perhaps CCCP-1 also functions as a molecular tether to help facilitate membrane fusion events that occur during early steps in DCV biogenesis. Given that CCCP-1 is anchored at its C-terminus, interactions with other membrane compartments might be mediated by its N-terminal domains that may be extended away from the trans-Golgi.

2.4.3 *What is the function of CCCP-1 in DCV biogenesis?*

Why might a long coiled-coil tether be important in DCV biogenesis? There are several steps in DCV maturation that involve membrane fusion reactions that may require tethering molecules. One is the homotypic fusion of immature DCVs (Gondré-Lewis et al., 2012; Urbé et al., 1998; Wendler et al., 2001), a process recently shown to involve the HID-1 protein (Du et al., 2016). Interestingly, *hid-1* mutants in *C. elegans* have defects in locomotion and DCV cargo sorting similar to *cccp-1* and *rab-2* mutants (Ailion and Thomas, 2003; Mesa et al., 2011; Yu et al., 2011), suggesting that RAB-2 and CCCP-1 may also be important for homotypic fusion of immature DCVs. Also, a recent human exome sequencing project identified likely causative mutations in the human orthologs of *hid-1* and *cccp-1* in two people with a range of similar neurological symptoms (Monies et al., 2017). A second step of DCV maturation that may involve membrane fusion reactions is the post-Golgi "sorting by exit" of non-DCV cargos from immature DCVs (Arvan and Halban, 2004; Borgonovo et al., 2006; Gondré-Lewis et al., 2012; Klumperman et al., 1998; Morvan and Tooze, 2008). In *rab-2* mutants, DCV cargos are inappropriately lost to the endosomal/lysosomal system (Edwards et al., 2009; Sumakovic et al., 2009), possibly due to overactivation of the sorting by exit pathway. Consistent with this possibility, we recently discovered that the endosomal-associated retrograde protein (EARP) complex functions in the RAB-2-CCCP-1 genetic pathway to mediate cargo sorting to DCVs (Topalidou et al., 2016). EARP is a member of the family of multisubunit tethering complexes (Schindler et al., 2015; Topalidou et al., 2016). Perhaps CCCP-1 interacts with EARP to mediate the tethering of endosomally-derived vesicles that contain DCV cargo or recycled sorting factors.

2.5 MATERIAL AND METHODS

2.5.1 *Strains*

Worm strains were cultured and maintained using standard methods (Brenner, 1974). A complete list of strains and mutations used is provided in the Strain List (Table 2. 2)

2.5.2 *Molecular biology and transgenes*

A complete list of constructs used in this study is provided in the Plasmid List (Table 2. 3 and Table 2. 4). Using the multisite Gateway system, we cloned the full-length *cccp-1b* cDNA tagged at the C-terminal with eGFP under the expression of the *rab-3* and *cccp-1* promoters into the pCFJ150 destination vector used for Mos1-mediated single copy insertion (MosSCI) (Frøkjær-Jensen et al., 2008, 2012). For the different CCCP-1 truncations, vector backbones and *cccp-1* cDNA fragments containing 20-30 bp overlapping ends were PCR amplified and combined by Gibson cloning (Gibson et al., 2009). All single copy integrations were made by the direct injection MosSCI method at the *ttTi5605* insertion site (Frøkjær-Jensen et al., 2008, 2012). Extrachromosomal arrays were made by standard transformation methods (Mello et al., 1991). For most constructs, we isolated two or more independent lines that behaved similarly. We generated only one line for the constructs overexpressing CC3::GFP under the *rab-3* promoter, coexpressing tagRFP::RAB-2 and CCCP1::GFP, and coexpressing tagRFP::RAB-2 and CC3::GFP.

For bacterial protein expression, *C. elegans* cDNAs coding for RAB-2, CCCP-1, and CCCP-1 fragments (as shown in

B) were inserted in pGST or pHIS parallel vectors (Sheffield et al., 1999) by Gibson cloning between the vector BamHI and XhoI restriction sites for RAB-2, and between the BamHI and EcoRI restriction sites for the other constructs.

For cloning the rat CCCP1 cDNA, rat cDNA was generated from PC12 cells using QuantiTect Reverse transcription kit (Qiagen) and an anchored Oligo (dT) primer. The CCCP1 cDNA was PCR amplified using gene specific primers and sequenced. The sequence had a few variations compared to the reported sequence and was submitted to Genbank (accession # KX954625). Rat CCCP1 and its fragments CC1+2 (amino acids 1-743) and CC3 (amino acids 750-922) were cloned into the pEGFP-N1 vector at the EcoRI and BamH1 restriction sites using either classical restriction digest and ligation for the full length protein or Gibson cloning with PCR amplified vector and inserts for the fragments.

2.5.3 *C. elegans fluorescence imaging*

Worms were mounted on 2% agarose pads and anesthetized with 100 mM sodium azide. To image the dorsal nerve cords, young adult animals were oriented with dorsal side up by exposure to the anesthetic for ten minutes before placing the cover slip. Images were obtained using a Nikon Eclipse 80i wide-field compound microscope with 40x or 60x oil objectives (numerical apertures of 1.30 and 1.40 respectively). Images were acquired at room temperature using an Andor Technology Neo sCMOS camera, model number DC152Q-C00-FI. The acquisition software used was NIS Elements AR 4.10.01. Raw images were then cropped with FIJI. Strains were imaged multiple times.

2.5.4 *Cell culture and immunostaining of 832/13 cells*

The insulinoma INS-1-derived 832/13 rat cell line was obtained from Dr. Christopher Newgard (Duke University School of Medicine) via Dr. Ian Sweet and Dr. Duk-Su Koh (University of Washington). 832/13 cells were routinely grown at 5% CO2 at 37°C in RPMI-1640, GlutaMAXTM (GIBCO), supplemented with 10% FBS, 1 mM Sodium pyruvate, 10 mM HEPES, 50 μM 2-mercaptoethanol, and 1X Pen/Strep (GIBCO). Cells were passaged biweekly after trypsin-EDTA detachment. All studies were performed on 832/13 passages between 70 and 90.

832/13 cells were plated on a coverslip at 80-90% confluency. After 24 to 48h hours, cells were transfected with a construct expressing C-terminally EGFP-tagged rat CCCP1, CC1+2 (amino acids 1-743) or CC3 (amino acids 750-922) using Lipofectamine 2000 (Thermo Fisher) according to the manufacturer's instructions. Cells were immunostained as described (Topalidou et al., 2016). Primary antibodies were the rabbit polyclonal anti-CCCP1 (1:150, NovusBio, human C10orf118 antibody NBP1-90440), mouse monoclonal anti-GM130 (1:200, BD biosciences, #610822), mouse monoclonal anti-Chromogranin A (1:50, Santa Cruz, #sc-393941), rabbit polyclonal anti-TGN38 (1:350, Sigma #T9826) rabbit polyclonal anti-GFP (1:200, Santa Cruz, #sc-8334), mouse monoclonal anti-GFP (1:200, Santa Cruz #sc-9996) and mouse monoclonal anti-Myc (1:200, Santa Cruz #sc-40) . The CCCP1 antibody was validated by showing that this antibody labeled the same structures as the GFP antibody in 832/13 cells expressing CCCP1::GFP (data not shown). Secondary antibodies were the Rhodamine (TRITC)-conjugated anti-rabbit secondary antibody (1:1000, Jackson Immunoresearch #111-025-144), Alexa Fluor 488-conjugated anti-rabbit (1:1000, Jackson Immunoresearch #111-545-003), Rhodamine Red-X-conjugated anti-mouse (1:1000, Jackson Immunoresearch #715-295-150) and Alexa Fluor 488-conjugated anti-mouse (1:1000, Jackson Immunoresearch #115-545-146). Images were obtained

using an Olympus FLUOVIEW FV1200 confocal microscope with a 60x UPlanSApo oil objective with a numerical aperture of 1.35. The acquisition software used was Fluoview v4.2. Pearson's correlation coefficients were determined using FIJI and the JaCOP plugin by drawing a rectangle around the perinuclear structure for each cell.

2.5.5 *Locomotion assays*

To measure worm locomotion, first-day adults were picked to thin lawns of OP50 bacteria (2-3 day-old plates) and body bends were counted for one minute immediately after picking. A body bend was defined as the movement of the worm from maximum to minimum amplitude of the sine wave. Worms mutant for *cccp-1*, like other mutants affecting DCV function, have a stereotypical "unmotivated" phenotype in which worms are slow when placed on food (Ailion et al., 2014). In our assay conditions in which the worm was stimulated by transfer to a new plate, expression of full length CCCP-1 fully rescued the locomotion defect of *cccp-1* mutants (Figure 2. 5 A). However, we observed that the transgene only partially rescued the locomotion defect of a *cccp-1* mutant when worms were not stimulated. This incomplete rescue could be due to the GFP tag, differences in expression levels, or the use of cDNA in the transgenes. This result further suggests that worm locomotion is sensitive to CCCP-1 expression levels. The locomotion assays were repeated twice or more.

2.5.6 *Protein expression in bacteria and purification*

GST-RAB-2, His_6-CCCP-1, GST-CCCP-1, GST, and all His_6-CCCP-1 fragments were transformed into *E. coli* BL21 (DE3), pLys Rosetta cells (Invitrogen). His_6-CCCP-1 was grown in

LB medium containing ampicillin and chloramphenicol to OD600 = 0.4-0.6. Protein expression was induced with 0.4 mM Isopropyl β-D-1-thiogalactopyranoside (IPTG) at 20°C overnight. Bacteria were harvested by a 5,000g spin at 4°C and cells were resuspended in ice-cold lysis buffer containing 50 mM Tris, pH 7.6, 200 mM NaCl, 10% glycerol, 5 mM 2-mercaptoethanol, 1-2 mM $MgCl_2$, 0.5-1% Triton-X100, up to 1 μL of benzonase nuclease (Sigma) per 10 mL of lysis buffer, and supplemented with protease inhibitor cocktail (Pierce, according to manufacturer's instructions) and 1 mM PMSF. 10-25 mM imidazole was added to the lysis buffer to decrease nonspecific binding to the nickel resin. Cells were lysed by sonication. An additional 1 mM PMSF was added to the lysate during sonication. Lysates were clarified by a 20,000g spin at 4°C. The supernatant was incubated with PerfectPro Ni-NTA Agarose (5 Prime) by either gravity flow using a disposable column or batch purification. The resin was washed with buffer containing 50 mM Tris, pH 7.6, 25-35 mM imidazole, 200 mM NaCl, 10% glycerol, and 5 mM 2-mercaptoethanol. The resin was eluted with the same buffer containing 250 to 400 mM imidazole.

For the His_6-CCCP-1 used for SEC, CD and EM, the protein eluted from the Nickel-NTA beads was concentrated using an Amicon-Ultra centrifugal filter, and buffer exchanged to 50 mM Tris pH 7.6, 200 mM NaCl, 5 mM 2-mercaptoethanol using a PD-10 column (GE Healthcare). Protein aliquots were flash-frozen in liquid nitrogen and stored at –80°C.

The His_6 tag of full length CCCP-1 was cleaved off using TEV protease, which was expressed and purified as described (Tropea et al., 2009). An estimated 1:10 molar amount of His_6-TEV protease was added to the eluted CCCP-1 protein and incubated overnight at 4°C with gentle rotation. The protein was buffer exchanged (20 mM Tris pH 7.6, 200 mM NaCl, 2 mM 2-mercaptoethanol) by dialysis. The cleaved tag and the protease were removed by incubation with

PerfectPro Ni-NTA resin for 1 hour at 4°C. Cleaved protein was concentrated, supplemented with 10% glycerol, aliquoted and flash frozen in liquid nitrogen.

His_6-CCCP-1 fragments were grown in TB medium containing ampicillin and chloramphenicol to OD600 = 0.8-1 and protein expression was induced with 1 mM IPTG. The protein was handled like His_6-CCCP-1 full length except that the lysis buffer lacked benzonase and $MgCl_2$. The eluted protein was dialyzed with 20 mM Tris pH 7.6, 200 mM NaCl, 2 mM 2-mercaptoethanol, concentrated, supplemented with 10% glycerol, aliquoted and flash frozen in liquid nitrogen.

For the GST-CCCP-1 and GST used for the protein-lipid overlay assays, cells were grown in TB medium containing ampicillin and chloramphenicol to OD600 = 0.5-0.8 and protein expression was induced with 0.5 mM IPTG. After induction, bacteria were then incubated at 20°C overnight. Harvested cells were resuspended in the same ice-cold lysis buffer described above for His_6-tagged proteins except lacking imidazole, benzonase and $MgCl_2$ and lysed by sonication. The clarified lysate was incubated with GST-Sepharose resin (GE Healthcare). The resin was then washed with 50 mM Tris, pH 7.6, 200 mM NaCl, 10% glycerol, 5 mM 2-mercaptoethanol and eluted with the same buffer containing 20 mM reduced glutathione. The eluted protein was dialyzed (20 mM Tris pH 7.6, 200 mM NaCl, 2 mM 2-mercaptoethanol, supplemented with 10% glycerol), aliquoted and flash frozen in liquid nitrogen.

GST-RAB-2 and GST used for the GST-RAB-2 pull downs were grown in LB medium containing ampicillin and chloramphenicol to OD600 = 0.4-0.6. Protein expression was induced with 1 mM IPTG at 18°C overnight. Bacteria were harvested and resuspended in ice-cold lysis buffer containing 50 mM Tris, pH 7.6, 200 mM NaCl, 10% glycerol, 5 mM 2-mercaptoethanol, 2 mM $MgCl_2$, 0.2% Triton-X100, up to 1 μL of benzonase nuclease (Sigma) per 10 mL of lysis

buffer and supplemented with protease inhibitor cocktail (Pierce, according to manufacturer's instructions) and 1 mM PMSF. Cells were lysed as above and stored as a clarified lysate at -80°C. The concentration of GST or GST-RAB-2 in the lysate was estimated by a small-scale affinity purification.

Protein expression and purification conditions typically yielded more than 1 mg of protein per liter of culture media. The protein concentration was measured with Bradford reagent and purity was assessed by Coomassie-stained SDS-PAGE. GST-tagged proteins were estimated to be over 95% pure. CCCP-1 fragments containing CC3, especially CC3 alone, yielded less protein and the measured concentration of protein was adjusted by comparing the band intensity with purer His_6-tagged fragments on a Western blot. All proteins migrated on SDS-PAGE to their expected molecular weight, except for GST-RAB-2 (predicted 50 kDa) that migrated between the 37 kDa marker and the 50 kDa marker, and the His_6-CC1 fragment (predicated 19 kDa) that migrated above the 20 kDa marker.

For the experiments at pH 6.5: the protocol was identical, except that the buffer used had 50mM PIPES pH 6.5 instead of 50 mM Tris pH 7.6.

2.5.7 *Western blotting*

Protein samples were solubilized in SDS loading dye and resolved on 8%, 10% or 12% SDS-PAGE gels. Proteins were then transferred to PVDF or nitrocellulose membranes using a semi-dry transfer apparatus (Biorad) system. The membranes were blocked with 3% dry milk in TBST (10 mM Tris pH 7.4, 150 mM NaCl, 0.05% Tween-20) for 1 hour at room temperature or overnight at 4°C. Primary and secondary antibodies were diluted in TBST + 3% dry milk and incubated 1 hour at room temperature or overnight at 4°C. The following primary antibodies were

used: mouse monoclonal anti-His_6 (1:1000, Thermo Scientific HIS.H8 #MA1-21315), mouse monoclonal anti-GFP (1:1000, Roche #11814460001), mouse monoclonal anti-beta-tubulin antibody (1:1000, Thermo Scientific #MA5-16308) and rabbit polyclonal anti-Rab2 (1:200, Santa Cruz Biotechnology (FL-212) sc-28567, produced from a human RAB2A antigen). The secondary antibodies were: Alexa Fluor 680-conjugated affinity pure goat anti-mouse antibody (1:20,000, Jackson Immunoresearch #115-625-166) and Alexa Fluor 680-conjugated affinity pure goat anti-rabbit antibody (1:20,000 Jackson Immunoresearch #111-625-144). A Li-COR processor was used to develop images.

2.5.8 *GST-RAB-2 pulldowns*

To decrease nonspecific binding, we used LoBind microcentrifuge tubes (Eppendorf). 25 µL of glutathione sepharose resin (GE Healthcare) was blocked for 1 hour at room temperature or overnight at 4°C with 5% bovine serum albumin (BSA) in reaction buffer (50 mM Tris pH 7.6, 150 mM NaCl, 10% glycerol, 5 mM 2-mercaptoethanol, 5 mM $MgCl_2$ and 1% Triton-X100). The resin was washed with reaction buffer and incubated with clarified bacterial lysates containing about 50 µg of GST-RAB-2 or 25 µg of GST for 1 hour at 4°C with gentle agitation. Beads were washed with nucleotide loading buffer (50 mM Tris pH 7.6, 150 mM NaCl, 10% glycerol, 5 mM 2-mercaptoethanol, 5 mM EDTA and 1% Triton-X100) and incubated with either 60X molar ratio of GTPγS or 300X of GDP on a rotator at room temperature for 2 hours. 20 mM $MgCl_2$ was added to the reaction and incubated for another 15 minutes at room temperature. Nucleotides were washed off with reaction buffer and the beads were incubated with CCCP-1 or its fragments (at 1:2 molar ratio with GST-RAB-2) for 2 hours at 4°C on a rotator. Beads were washed three times with low volumes of reaction buffer (3 x 200 µL) and the resin was eluted with 20 mM reduced

glutathione in reaction buffer. Half of the eluent was loaded on SDS-PAGE gels and analyzed by Western blotting against the His_6-tag. The pulldown was repeated four times with the full-length CCCP-1 protein and twice with the fragments with identical results.

2.5.9 *Cell fractionation*

We used a similar method to the one described (Schindler et al., 2015). Specifically, 832/13 cells were grown on a 15 cm dish to 90% confluence and transfected with CCCP1::eGFP using Lipofectamine 2000 (Thermo Fisher) according to the manufacturer's instructions. After 24 h, cells were washed twice with ice cold PBS and detached using a cell scraper. Cells were then transferred to a microcentrifuge tube and pelleted for 5 min at 300g in a tabletop centrifuge at 4°C. Cells were resuspended in 500 µL sucrose buffer (20 mM HEPES, pH 7.4, 250 mM sucrose supplemented with protease inhibitors (Pierce) and 1 mM PMSF) and were homogenized on ice by a Dounce homogenizer (20 strokes). The cell lysate was then centrifuged at 1,000g for 5 minutes at 4°C to remove unbroken cells and nuclear debris. The post-nuclear supernatant was further clarified by centrifugation at 13,000g for 10 min at 4°C. The supernatant was divided into four samples, one of which was supplemented with SDS loading buffer (supernatant, S13). Membranes in the other three samples were pelleted using a Beckman TLA100 rotor (45 minutes, 90,000g, 4°C). The supernatant from one of the samples was supplemented with SDS page loading buffer (supernatant, S90) and its pellet was resuspended in an equal volume of sucrose buffer and supplemented with SDS loading buffer (pellet, P90). The pellets of the two last samples were resuspended in either high-salt buffer (50 mM Tris, pH 7.4, 1 M NaCl, 1 mM EDTA supplemented with 10% glycerol and protease inhibitors) or detergent buffer (50 mM Tris, pH 7.4, 150 mM NaCl, 1% Triton X-100, 1 mM EDTA supplemented with 10% glycerol and protease inhibitors).

After incubation for 1 hour on ice the samples were centrifuged at 90,000g for 45 min at 4°C. The collected membrane fractions, either salt-extracted (S90, 1 M NaCl) or detergent-extracted (S90, 1% Triton X-100), were then supplemented with SDS loading buffer. Their pellets were resuspended in equal volumes of high salt or detergent buffer and then supplemented with SDS loading buffer (P90, 1 M NaCl and P90, 1% Triton X-100). Samples were analyzed by Western blot.

2.5.10 *Golgi-mix liposome preparation*

The following lipids were used: 1-palmitoyl-2-oleoyl-sn-glycero-3-phosphocholine (POPC), 1,2-dipalmitoyl-sn-glycero-3-phosphoethanolamine (DPPE), and 1,2-di-oleoyl-sn-glycero-3-phospho-l-serine (DOPS) were purchased from NOF America Corporation. Cholesterol, L-α-phosphatidylinositol from soy (PI) and 1,2-dioleoyl-sn-glycero-3-phosphoethanolamine-N-(lissamine rhodamine B sulfonyl) (Rh-PE) were purchased from Avanti Polar Lipids. The composition of Golgi-mix liposomes was as described (Bigay et al., 2005) with the following fractions given as molar percent: POPC (49%), DPPE (19%), DOPS (5%), Soy-PI (10 %), cholesterol (16%) and Rhodamine-PE (1%). The lipids dissolved in chloroform were mixed together and chloroform was dried under compressed nitrogen for 3 hours to overnight and then lyophilized in a Labconco Free Zone 2.5 lyophilizer for 1 hour to remove residual chloroform. The dried lipid mixture was resuspended in 50 mM Tris pH 7.6 and 50 mM NaCl. To generate the liposomes, the mixture was sonicated for 5 minutes in a 50°C water bath. Liposomes were stored at room temperature and used within 2-3 days.

2.5.11 *Flotation experiments*

Proteins (1 μM) and Golgi-mix liposomes (1 mM) were incubated in 50 mM Tris pH 7.6, 50 mM NaCl buffer at room temperature for 30 minutes. The suspension was adjusted to 40% sucrose by adding 75% w/v sucrose solution in the same buffer for a total volume of 200 μL and transferred to a polycarbonate ultracentrifuge tube (Beckman Coulter, 343778). Three layers were overlaid on top of the high sucrose suspension: 500 μL of 30% sucrose, 300 μL of 10% sucrose and 200 μL of 0% sucrose in 50 mM Tris pH 7.6, 50 mM NaCl. The sample was centrifuged at 200,000g in a Beckman Coulter swinging bucket rotor (TLS 55) for 2 hours at 25°C. Most of the fluorescently labeled liposomes migrated to the top of the tube in three layers close to the 0%-10% sucrose interface. Six fractions of 200 μL each were collected from the top. The second fraction contained most of the pink color coming from rhodamine, with some in the third fraction as well. Experiments with full-length untagged CCCP-1 were analyzed by SDS-PAGE and Coomassie blue staining. Experiments with the His_6-tagged CCCP-1 fragments were analyzed by Western blot using an antibody to the His_6 epitope tag. Experiments with the full-length CCCP-1 protein were performed three times with two independent liposome preparations. The key experiments with CC3 and CC1+2 were performed side by side twice with independent liposome preparations and both found CC3 to be a much stronger liposome binder.

2.5.12 *PIP Strips and PIP arrays*

The PIP strips and PIP arrays were purchased from Echelon and used as recommended by the manufacturer. The membranes were blocked for 1 hour at room temperature with PBST (0.1% v/v Tween-20) + 3% fatty acid-free BSA (Sigma). The membranes were incubated for 1 hour at room temperature with GST or GST-CCCP-1. For the PIP strip, equimolar amounts of GST and

GST-CCCP-1 were used (around 100 nM in PBST + 3% fatty acid-free BSA). For the PIP array, 70 nM of GST-CCCP-1 and 150 nM of GST were used. The membranes were washed with PBST and incubated with the anti-GST antibody Horseradish Peroxidase (HRP) conjugate (K-SEC2 from Echelon) in PBST + 3% fatty acid-free BSA. Lipid binding was detected by adding 3,3',5,5'-tetramethylbenzidine (TMB) precipitating solution (K-TMB from Echelon). The positive control PI (4,5)P2 Grip (PLC-δ1-PH) was obtained from Echelon (Catalog #G-4501) and used as recommended by the manufacturer. The membranes were imaged with a conventional digital camera. The experiments were performed once each.

2.5.13 *Size-exclusion chromatography (SEC)*

Aliquots of His_6-CCCP-1 expressed and purified as described above were loaded on a Superose 6 column (GE Healthcare) at 4°C. His_6-CCCP-1 was eluted with 50 mM Tris pH 7.6, 200 mM NaCl and 5 mM 2-mercaptoethanol. Given that CCCP-1 does not contain any tryptophan residues, its extinction coefficient is very low. Since the size-exclusion chromatogram was very sensitive to more optically absorbent contaminants, we collected 1 mL fractions and analyzed them by Coomassie-stained SDS-PAGE gels. Recombinant His_6-CCCP-1 fragments were loaded on a Superose 6 (or Superdex 200) column and eluted with 50 mM Tris pH 7.6 and 200 mM NaCl. Fractions were analyzed by Western blot to the His_6 tag. For the experiments at pH 6.5: the protocol was identical, except that the buffer used had 50mM PIPES pH 6.5 instead of 50 mM Tris pH 7.6.

2.5.14 *Velocity Sedimentation*

5-25% linear sucrose gradients were made in 50 mM Tris pH 7.6, 200 mM NaCl, 5 mM 2-mercaptoethanol in polycarbonate ultracentrifuge tubes (Beckman Coulter, 349622). Aliquots of His_6-CCCP-1 SEC fractions 10 or 12 were loaded at the top of the gradient and tubes were centrifuged at 100,000g for 16 hours at 4°C in a Beckman Coulter swinging bucket rotor (SW 50). Fractions were collected from top to bottom and analyzed by SDS-PAGE and Coomassie blue staining.

2.5.15 *SEC–MALS*

SEC–MALS was performed by injecting fraction 12 from SEC (Figure 2. 8 C) of purified recombinant His_6-CCCP-1 on a Superose 6 Increase 3.2/100 column (GE Healthcare) that was equilibrated in 50 mM Tris pH 7.6, 200 mM NaCl, 5 mM 2-mercaptoethanol. The eluted sample was monitored by ultraviolet absorption at 280 nm, light scattering at 658 nm (Wyatt Technology) and differential refractometry (Wyatt Technology). The data was analyzed using ASTRA software (Wyatt Technology). The protein absolute molecular mass was calculated assuming a dn/dc value of 0.185.

2.5.16 *Circular dichroism spectroscopy*

Samples were analyzed using a Jasco J-1500 circular dichroism (CD) spectrometer. Protein in 50 mM Tris pH 7.6, 200 mM NaCl and 5 mM 2-mercaptoethanol was used to collect the CD data. Fractions from SEC (pooled fractions 8-9 and 11-12 at pH 7.6 and pooled fractions 11-12 at pH 6.5, Figure 2. 7 B) were concentrated around 10-fold using an Amicon Ultra centrifugal unit

and flash frozen in liquid nitrogen before use. The signal was blanked with buffer only. For the CD scan, the samples were kept at 4°C and the ellipticity (in mdeg) was measured at wavelengths between 195 nm and 260 nm. For the melting curve, the ellipticity (mdeg) was measured at 222 nm as the temperature was increased from 4°C to 100°C. For the experiments at pH 6.5: the protocol was identical, except that the buffer used had 50mM PIPES pH 6.5 instead of 50 mM Tris pH 7.6.

2.5.17 *Negative-stain electron microscopy*

Frozen aliquots of pooled and concentrated SEC fractions 11-12 were diluted to 0.01 mg/mL in 50 mM Tris pH 7.6, 200 mM NaCl and 5 mM 2-mercaptoethanol. Samples were prepared by negative stain, using a 0.7% uranyl formate solution, and spotted onto a 400-mesh copper-coated grid. Electron micrographs were acquired on a Tecnai T12 microscope (FEI co.), operating at 120 kV, at 52,000X magnification, with images taken by a Gatan US4000 CCD camera. Similar results were observed using protein from an independent protein preparation and imaged using a Morgagni M268 electron microscope. For the experiments at pH 6.5: the protocol was identical, except that the buffer used had 50mM PIPES pH 6.5 instead of 50 mM Tris pH 7.6.

2.5.18 *Statistics*

For the *C. elegans* locomotion assay, data were tested for normality by a Shapiro-Wilk test. We used the Kruskal-Wallis test followed by Dunn's test to investigate whether there was statistical significance between groups. For the 832/13 cells, data were tested for normality by a

Shapiro-Wilk test followed by a one-way Anova test with Bonferroni correction to investigate whether there was statistical significance between groups.

2.6 ACKNOWLEDGMENTS

We thank Kumud Raj Poudel and Jihong Bai for sharing purified phospholipids and for help with generating liposomes; Amanda Clouser for help with CD spectroscopy; Amanda Clouser and Mengtong Duan for help with SEC-MALS; Christopher Newgard, Ian Sweet, and Duk-Su Koh for the 832/13 and PC12 cell lines; Suzanne Hoppins for sharing equipment and experimental guidance; Maximillian Greenwald for assistance with *C. elegans* locomotion assays; Andrew Borst for help with electron microscopy; and Jihong Bai for comments on the manuscript. JC was supported in part by an NIH Institutional Training Grant for Neurobiology (T32 GM007108). This work was supported by a University of Washington Diabetes Research Center Pilot and Feasibility Award to MA (NIH grant P30 DK017047), by NIH grant R01 GM077349 to AJM, and by NIH grant R00 MH082109 and an Ellison Medical Foundation New Scholar

2.7 FIGURES

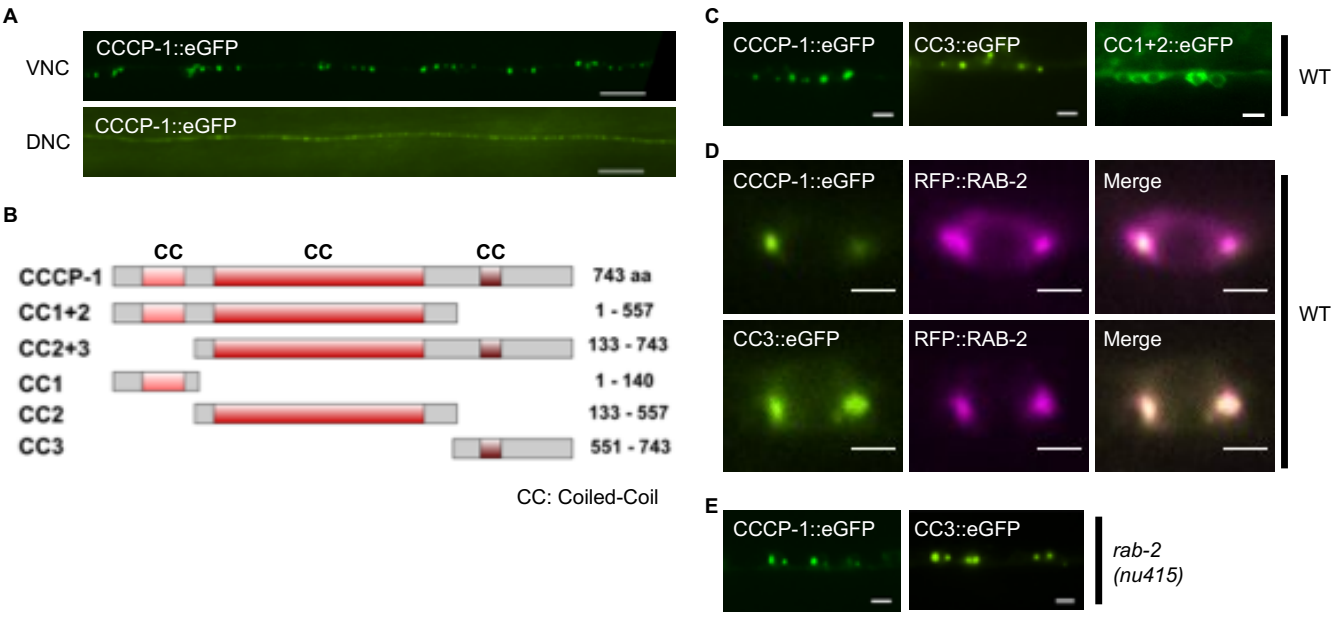

Figure 2. 1 The CC3 C-terminal domain of CCCP-1 localizes the protein

A, CCCP-1 localizes to perinuclear and axonal puncta. Representative images of CCCP-1::eGFP expressed under the pan-neuronal rab-3 promoter, showing cell bodies of *C. elegans* ventral cord motor neurons (VNC) and axons of the dorsal nerve cord (DNC). Scale bar: 20 µm.

B, Domain structure of worm CCCP-1 and its different fragments. The CC1, CC2 and CC3 fragments carry the predicted coiled-coil domains.

C, CC3 is necessary and sufficient for CCCP-1 localization. Representative images of the cell bodies of multiple adjacent ventral cord motor neurons expressing CCCP-1::eGFP, CC3::eGFP or CC1+2::eGFP, in wild-type animals. Scale bar: 5 µm.

D, CC3 is necessary and sufficient for localization of the protein to RAB-2 positive membrane structures. Representative images of a single ventral cord motor neuron cell body coexpressing CCCP-1::eGFP or CC3::eGFP and tagRFP::RAB-2 in neurons of wild-type animals. Scale bar: 2 µm.

E, CCCP-1 and CC3 localization does not require RAB- 2. Representative images of ventral cord motor neuron cell bodies expressing CCCP-1::eGFP or CC3::eGFP in a *rab-2*(*nu415*) mutant background. Scale bar: 5 µm.

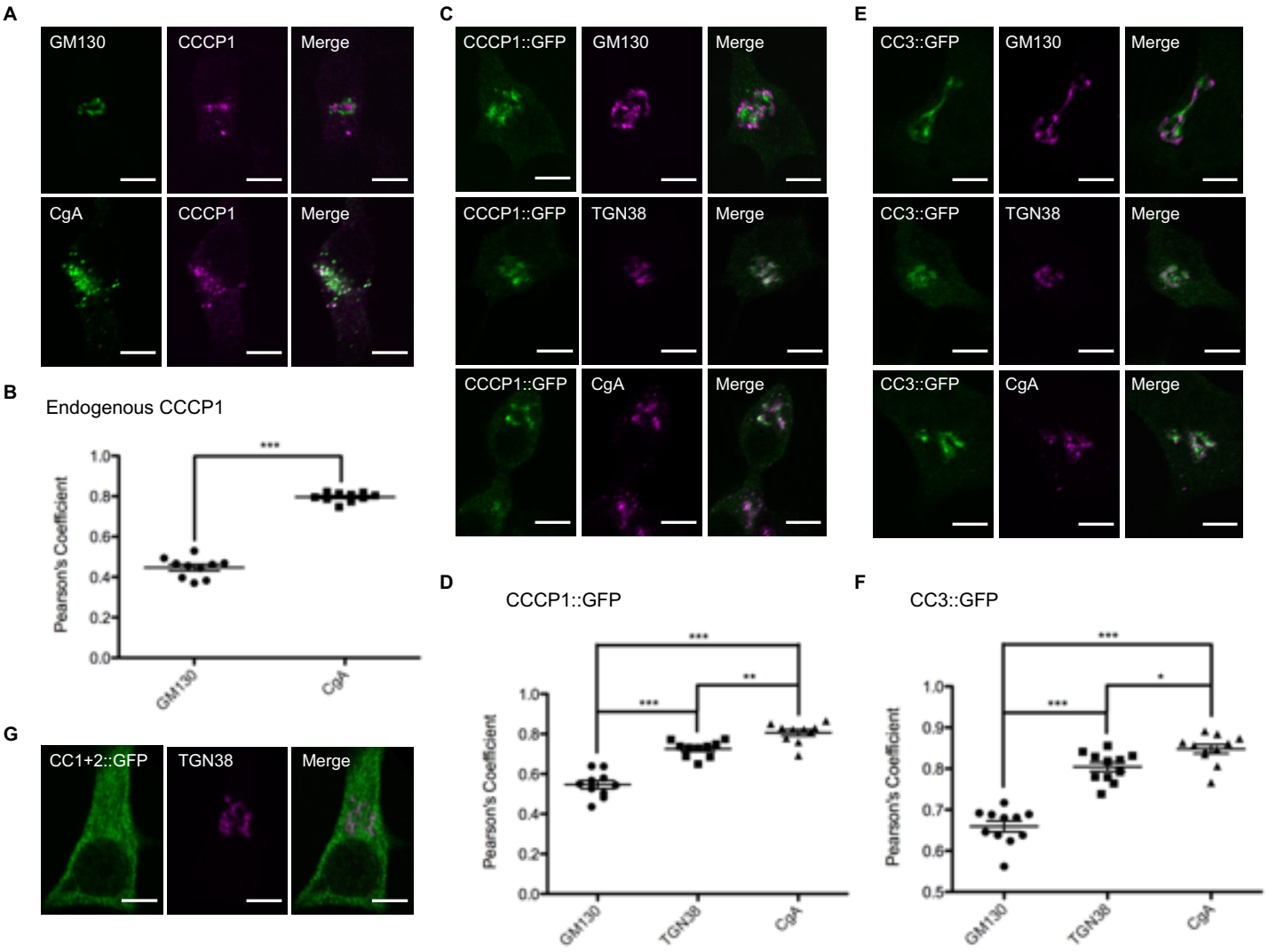

Figure 2. 2 CC3 (amino acids 750-922) is necessary and sufficient for localization of rat CCCP1/CCDC186 near the trans-Golgi

A, Endogenous rat CCCP1 localizes to a perinuclear structure near a marker for DCV cargo, Chromogranin A (CgA). Representative images of 832/13 cells co-stained for endogenous CCCP1 and for the cis-Golgi marker GM130 (upper panel) and for the DCV marker CgA (lower panel). Scale bar: 5 µm.

B, Quantification of endogenous CCCP1 colocalization with GM130 and CgA. ***P < .001, n = 10 each.

C, CCCP1::GFP localizes to a perinuclear structure near the trans-Golgi marker TGN38 and the DCV marker CgA. Representative images of 832/13 cells co-stained for CCCP1::GFP and for the cis-Golgi marker GM130 (upper panel), the trans-Golgi marker TGN38 (middle panel) and for the DCV marker CgA (lower panel). Scale bar: 5 µm.

D, Quantification of CCCP1::GFP co-localization with GM130, TGN38 and CgA. ***P < .001, **P < .01, n = 10 each.

E, CC3::GFP localizes to a perinuclear structure near the trans-Golgi marker TGN38 and the DCV marker CgA. Representative images of 832/13 cells co-stained for CC3:: GFP and for the cis-Golgi marker GM130 (upper panel), the trans-Golgi marker TGN38 (middle panel) and for the DCV marker CgA (lower panel). Scale bar: 5 μm.

F, Quantification of CC3::GFP co-localization with GM130, TGN38 and CgA. ***P < .001, *P < .05, n = 11 each. G, CC1 +2::GFP localizes to the cytoplasm. Representative images of 832/13 cells co-stained for CC1+2::GFP and for the trans Golgi marker TGN38. Scale bar: 5 μm.

A, rat CCCP1, amino acids (aa) 1-922

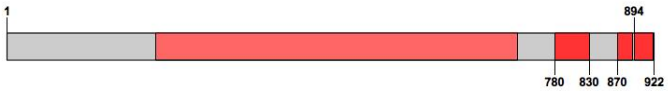

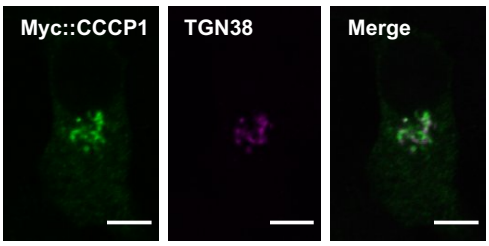

B,

750-922

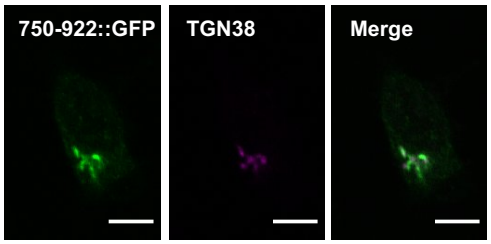

C

778-922

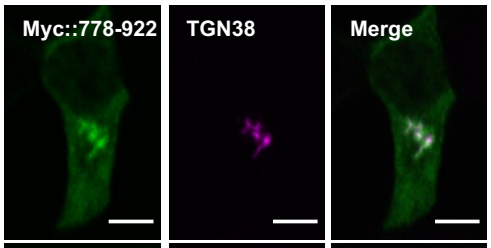

D

804-922

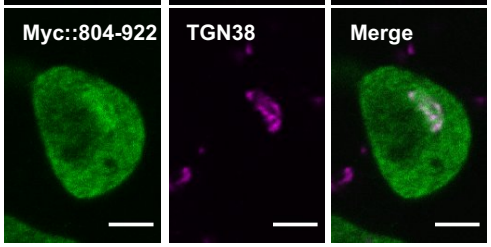

E

832-922

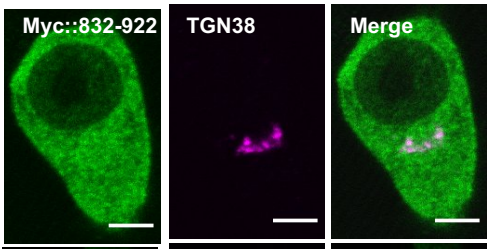

F

778-912

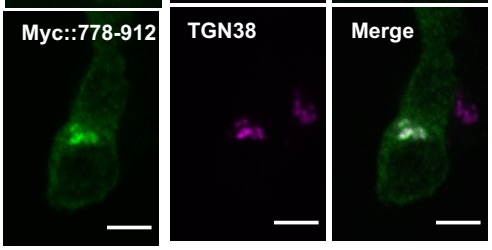

G

778-893

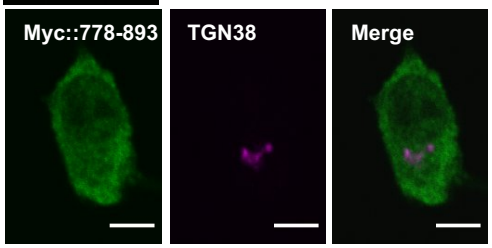

Figure 2. 3 Amino-acids 778-912 of rat CCCP1 are sufficient for localization near the trans-Golgi

A-G, At left: domain structure of CCCP1 shown in grey are regions predicted to not have a secondary structure while shown in red are regions predicted to be alpha-helical. The CC3 domain has 3 short predicted alpha-helical regions (amino acids 780-830, 870-890 and 894-922). Amino acids 750-780 and 830-870 are predicted to be unstructured. At right: Representative images 832/13 cells transfected with a construct expressing Myc::CCCP1 of CCCP1 truncations and co-stained for Myc tag and the TGN marker TGN38. Scale bar: 5 μm.

A, Myc-tagged CCCP1 localizes near the TGN marker TGN38, like the CCCP1::GFP construct in Figure 4.

B-G, analysis of the domain of CCCP1 sufficient for localization near the TGN suggests that amino-acids 778-912 are sufficient for localization of CCCP1 to the TGN.

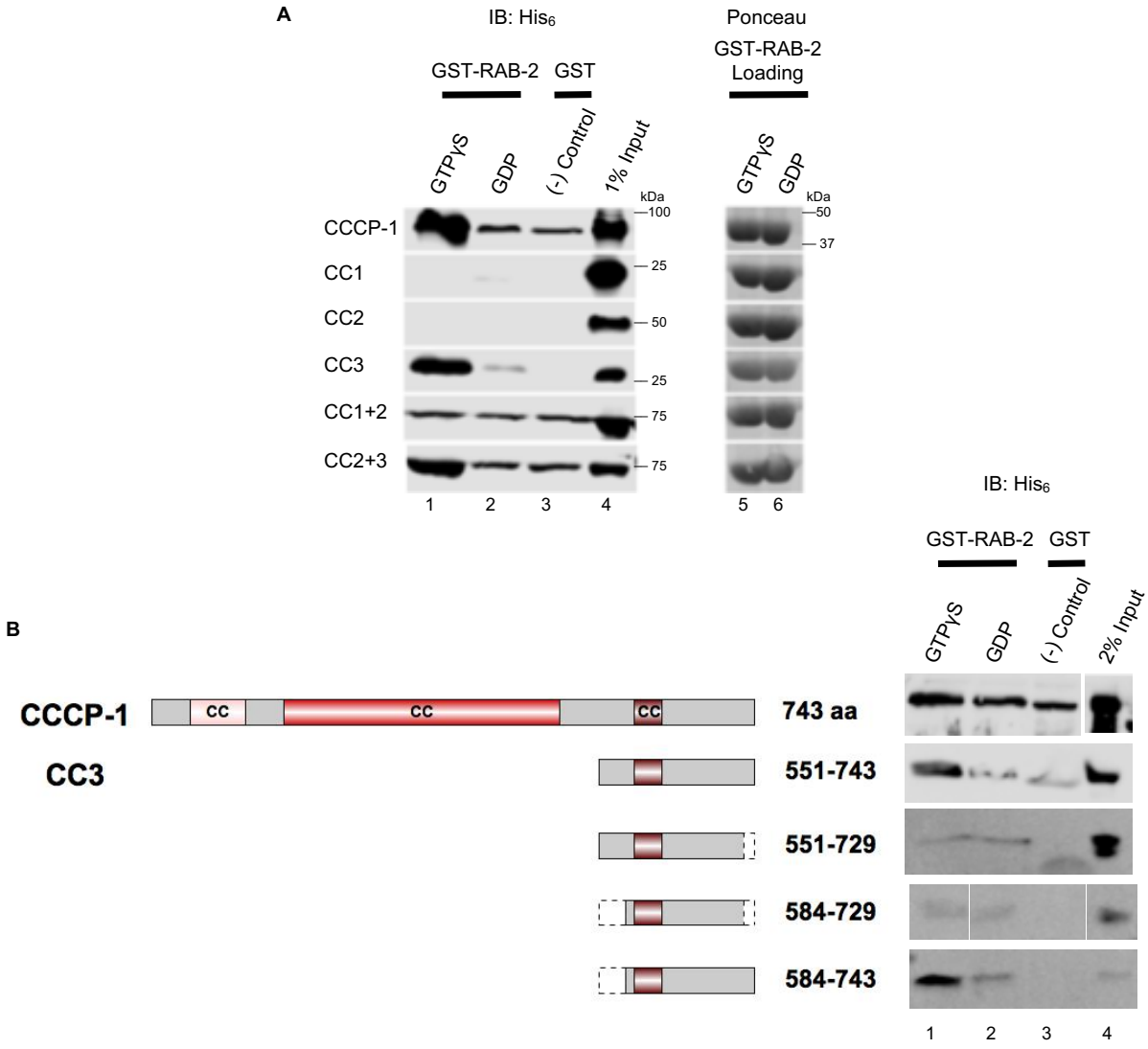

Figure 2. 4 The C-terminal domain of CCCP1 is necessary and sufficient for RAB-2 binding

A, The CC3 domain of *C. elegans* CCCP-1 binds directly to RAB-2. (Left) GST-pulldowns were performed using purified recombinant His6-CCCP-1 or its fragments and GST-RAB-2 loaded with either GTPγS (lane 1) or GDP (lane 2). GST on its own was used as a negative control (lane 3); 1% of the protein input is shown in lane 4. Samples were analyzed by Western blot against the His6 tag. (Right) GST-RAB-2 loading controls visualized by Ponceau staining show that approximately equal amounts of GST-RAB-2 were used (lanes 5 and 6). IB: immunoblot.

B, Amino-acids 730-743 domain of *C. elegans* CCCP-1 (equivalent of amino acids 912-922 of the rat protein) are necessary for nucleotide specificity of RAB-2 binding, while amino acids 551-583 are not required for binding to RAB-2. GST-pulldowns were performed using purified recombinant His6-CCCP-1 or its fragments and GST-RAB-2 loaded with either GTPγS (lane 1) or GDP (lane 2). GST on its own was used as a negative control (lane 3); 2% of the protein input is shown in lane 4. Samples were analyzed by Western blot against the His6 tag. IB: immunoblot.

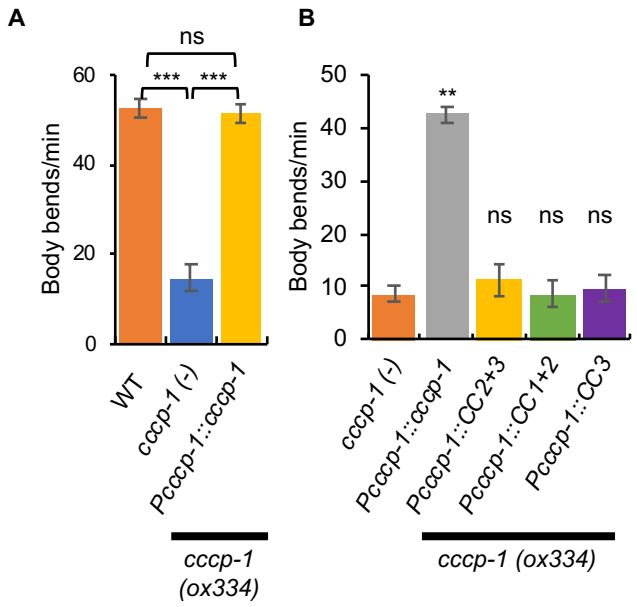

Figure 2. 5 CC3 is necessary but not sufficient for CCCP-1 function in *C. elegans*

A, *cccp-1* mutant animals have slow locomotion which is rescued by a single-copy transgene of GFP-tagged CCCP-1 cDNA expressed under the *cccp-1* promoter. ***P < .001, ns: P > .05,n = 10 each.

B, the slow locomotion of *cccp-1* mutants is not rescued by expression of CC3 or other CCCP-1 fragments. **P < .01, ns: P > .05 compared to *cccp-1* mutant, n = 10 each.

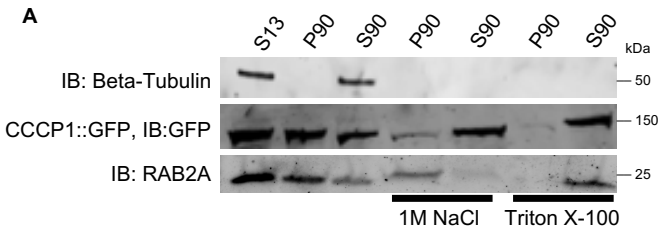
A
S13
P90
S90
P90
S90
P90
S90
kDa
IB: Beta-Tubulin
CCCP1::GFP, IB:GFP
IB: RAB2A
50
150
25
1M NaCl
Triton X-100

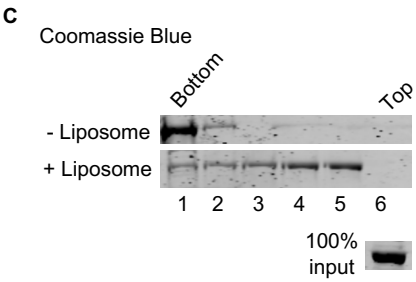
C
Coomassie Blue
Bottom
Top
- Liposome
+ Liposome
1 2 3 4 5 6
100% input

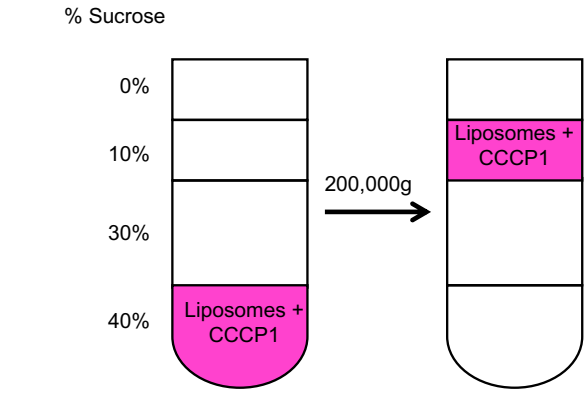
B
% Sucrose
0%
10%
30%
40%
Liposomes + CCCP1
200,000g
Liposomes + CCCP1

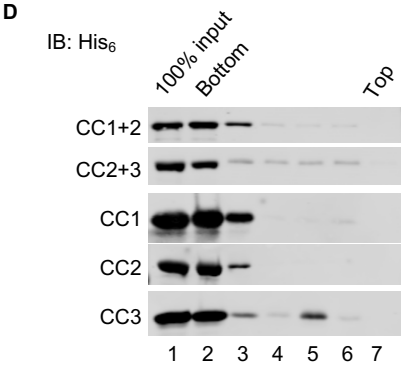
D
IB: His6
100% input
Bottom
Top
CC1+2
CC2+3
CC1
CC2
CC3
1 2 3 4 5 6 7

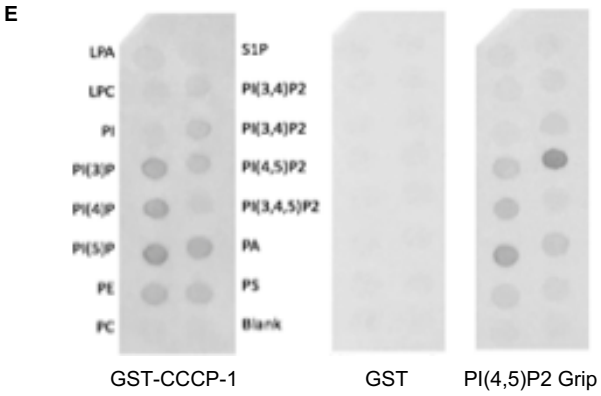
E
LPA
LPC
PI
PI(3)P
PI(4)P
PI(5)P
PE
PC
S1P
PI(3,4)P2
PI(3,4)P2
PI(4,5)P2
PI(3,4,5)P2
PA
PS
Blank
GST-CCCP-1
GST
PI(4,5)P2 Grip

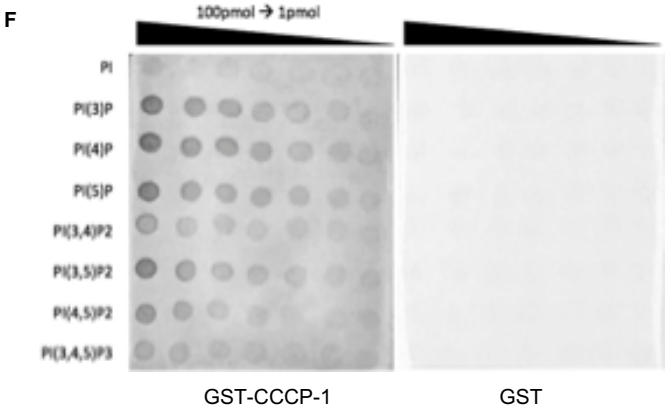
F
100pmol → 1pmol
PI
PI(3)P
PI(4)P
PI(5)P
PI(3,4)P2
PI(3,5)P2
PI(4,5)P2
PI(3,4,5)P3
GST-CCCP-1
GST

Figure 2. 6 CC3 binds membranes directly.

A, Rat CCCP1/CCDC186 is a peripheral membrane protein. In insulinoma 832/13 cell fractions, rat CCCP1/CCDC186 was found primarily in the post-nuclear P90 membrane fraction and could be extracted by 1 M NaCl or Triton X-100. RAB2A associates with membranes via a lipid anchor and could be extracted by Triton X-100 but not by 1 M NaCl. Tubulin served as a control soluble protein. S13: the supernatant obtained by a 13 000 g spin of the post-nuclear supernatant, containing the cytosolic proteins and proteins associated with small membrane compartments. S90, P90: supernatant and pellet fractions obtained by a 90 000 g spin of the S13 fraction, containing cytosolic and membrane-associated proteins respectively.

B, Schematic of the liposome flotation assay. The CCCP-1 protein (1 μM) was incubated with Golgi-mix liposomes (1 mM lipids) containing a rhodamine-labeled lipid. The suspension was adjusted to 40% w/v sucrose and overlaid with 3 cushions of decreasing sucrose concentration. The tube was centrifuged for 2 hours at 200 000 g. The efficiency of the flotation is demonstrated by observing the rhodamine-labeled lipid near the top of the tube.

C, CCCP-1 binds to membranes directly. CCCP-1 membrane-binding activity was assayed by liposome flotation. Untagged recombinant CCCP-1 was assayed in the absence (top) or presence (bottom) of Golgi-mix liposomes. After centrifugation, fractions were collected from the top (lane 6) to the bottom (lane 1) and analyzed by Coomassie-stained SDS-PAGE. The protein input shown here was part of the same Coomassie gel.

D, CC3 is necessary and sufficient for CCCP-1 membrane association. Representative blots from flotation assays using Golgi-mix liposomes and His6-tagged recombinant CCCP-1 fragments. After centrifugation, fractions were collected from the top (lane 7) to the bottom (lane 2) and analyzed by Western blot against the His6 tag.

E, CCCP-1 binds to phosphatidylinositol lipids with a single phosphate group. Equimolar amounts of GST-CCCP-1 or GST were incubated with membranes coated with different membrane phospholipids (PIP strips). Binding activity was detected using an antibody to the GST tag. PI(4,5)P2 Grip, a GST-tagged PLC-δ1-PH domain protein, was used as a positive control. LPA: lysophosphatidic acid, LPC: lysophosphocholine, PI: phosphatidylinositol, PI(3)P: phosphatidylinositol (3) phosphate, PI(4)P: phosphatidylinositol (4) phosphate, PI(5)P: phosphatidylinositol (5) phosphate, PE: phosphatidylethanolamine, PC: phosphatidylcholine, S1P: sphingosine 1-phosphate, PI(3,4)P2: phosphatidylinositol (3,4) bisphosphate, PI(3,5)P2: phosphatidylinositol (3,5) bisphosphate, PI(4,5)P2: phosphatidylinositol (4,5) bisphosphate, PI(3,4,5)P3: phosphatidylinositol (3,4,5) trisphosphate, PA: phosphatidic acid, and PS: phosphatidylserine.

F, CCCP-1 does not show obvious binding selectivity between phosphatidylinositol lipids. Equimolar amounts of GST-CCCP-1 or GST were incubated with membranes coated with different phosphatidylinositols of decreasing concentration (PIP arrays). Binding activity was detected using an antibody to the GST tag.

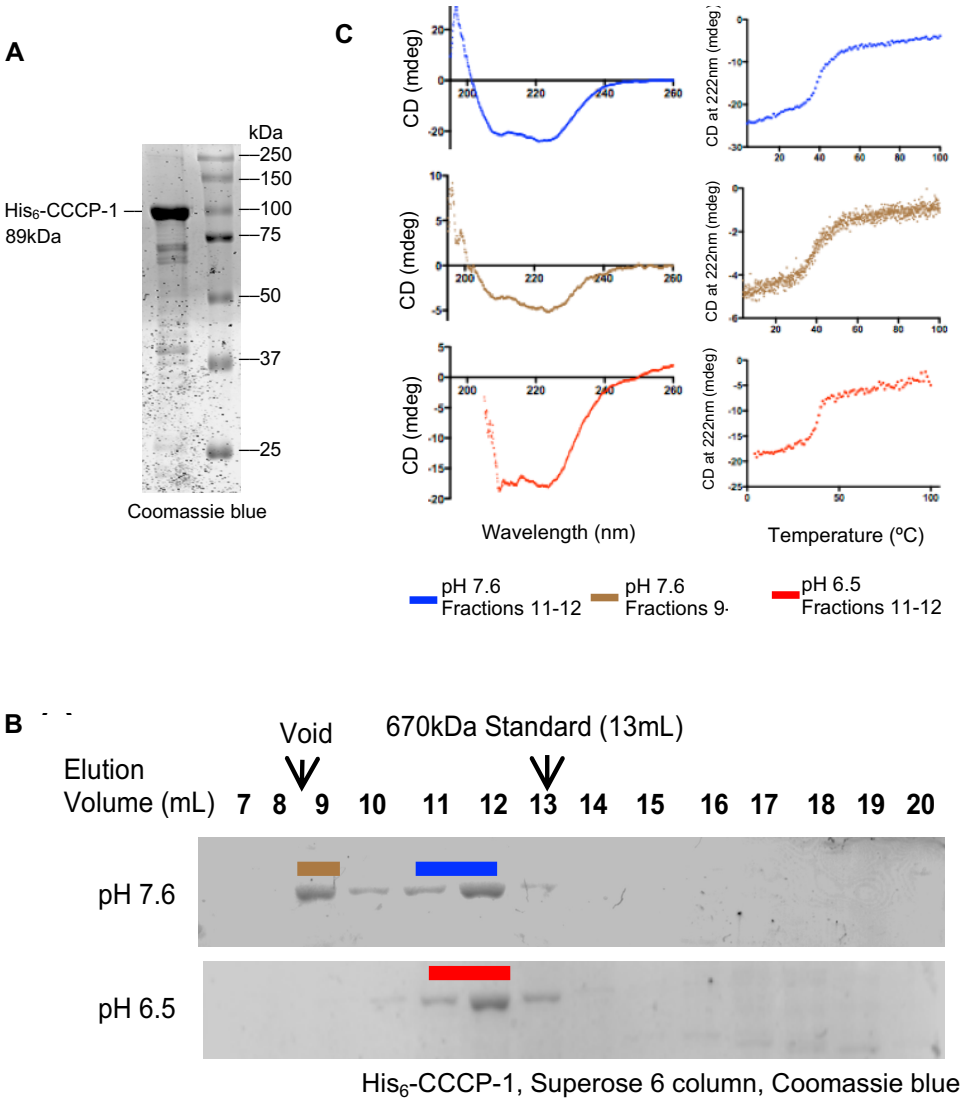

Figure 2. 7 The CCCP-1 is mostly alpha-helical and on size-exclusion chromatography, it runs larger than its predicted molecular weight

A, Coomassie blue stained gel showing bacterially expressed His6-CCCP-1.

B, recombinant His6-CCCP-1 protein runs larger by gel filtration than its predicted molecular weight and goes through a pH dependent change conformation and/or oligomerization state. At pH7.6, His6-CCCP-1 eluted in 2 peaks larger than the 670 kDa thyroglobulin standard. Interestingly, at pH 6.5 His6-CCCP-1 elutes in a single smaller peak, but still larger than the 670kDa standard.

C, CCCP-1 is folded and composed mostly of alpha helices. Fractions eluting off the Superose 6 column (panel B) were analyzed by circular dichroism (CD) spectroscopy. (Left) Far-UV CD spectra of His6-CCCP-1. Ellipticity (mdeg) was plotted as a function of wavelength (nm). (Right) Melting curve spectra. Ellipticity (mdeg) was measured as a function of increasing temperature.

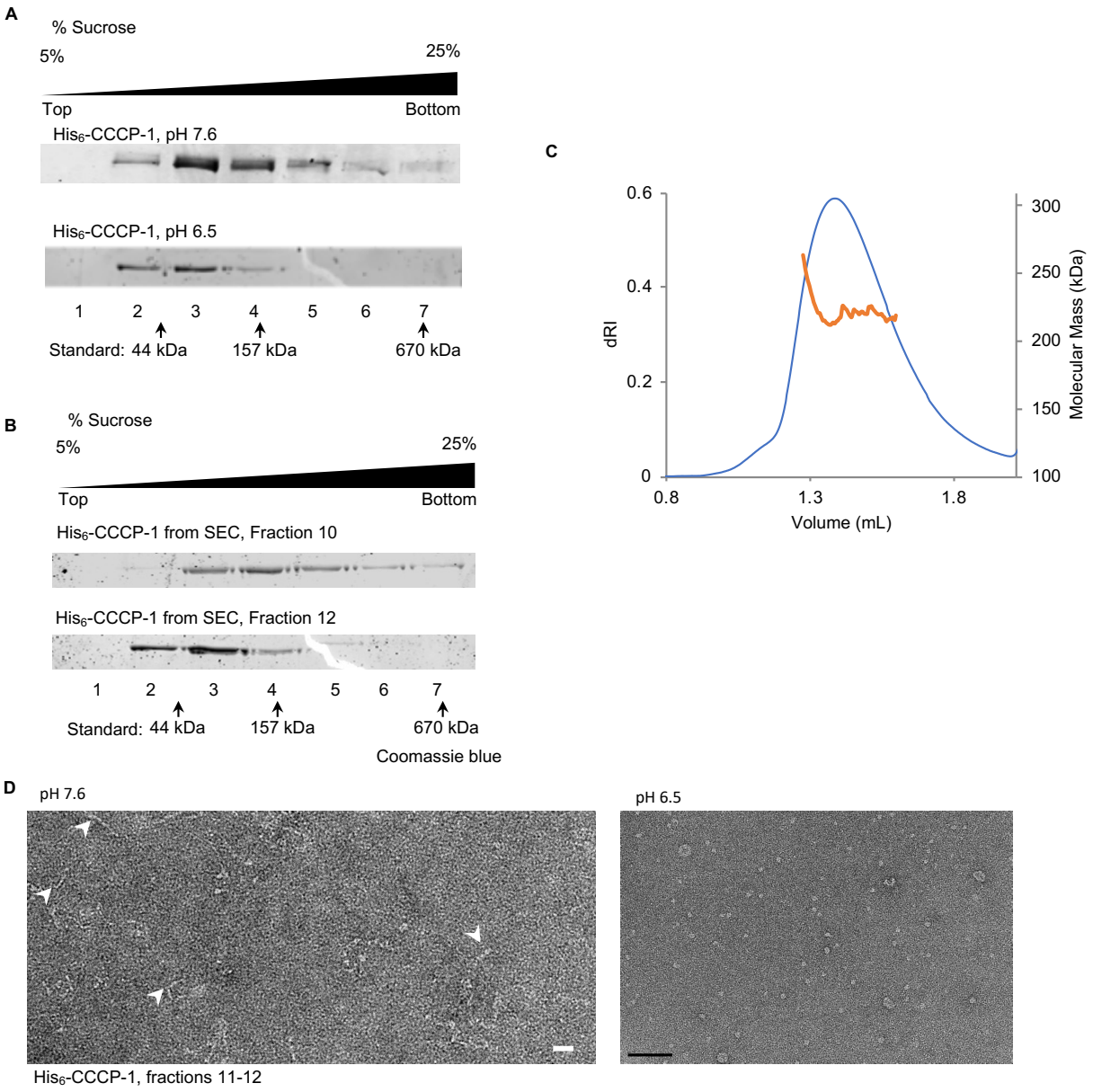

Figure 2. 8. The CCCP-1 protein is elongated, alpha-helical and forms oligomers, and undergoes a pH dependent change in conformation and/or in oligomeric state

A, Velocity sedimentation using a 5%-25% linear sucrose gradient shows that at pH 7.6, His6-CCCP-1 sediments as a broad peak near its expected molecular weight, mainly between the 44 kDa ovalbumin and the 157 kDa gamma-globulin standards. At pH 6.5, CCCP1 elutes as a single peak. After centrifugation, fractions were collected from top to bottom and analyzed by SDS-PAGE.

B, the 2 peaks seen on SEC at pH 7.6 have different velocity sedimentation profiles, suggesting a change in shape or a change in oligomeric state. Velocity sedimentation analysis of fractions 10 and 12 from size exclusion chromatography (see Figure 2.7 panel B) on a sucrose gradient identical to panel A.

C, SEC-MALS analysis suggests that the smaller form of CCCP-1 is dimeric. The oligomeric state of His6-CCCP-1 SEC fraction 12 was determined by SEC-MALS. The measured molar mass is 219 kDa (11.9%).

D, at pH7,6, His6-CCCP-1 forms elongated and floppy filaments while at pH 6.5 it forms globular structures. Negative-stain electron microscopy of His6 CCCP-1. Protein eluting off a Superose 6 column (fractions 11 and 12) was imaged by electron microscopy. White arrowheads point to the elongated flexible structures. Scale bar: 20 nm for pH 7.6 and 100nm for pH 6.5.

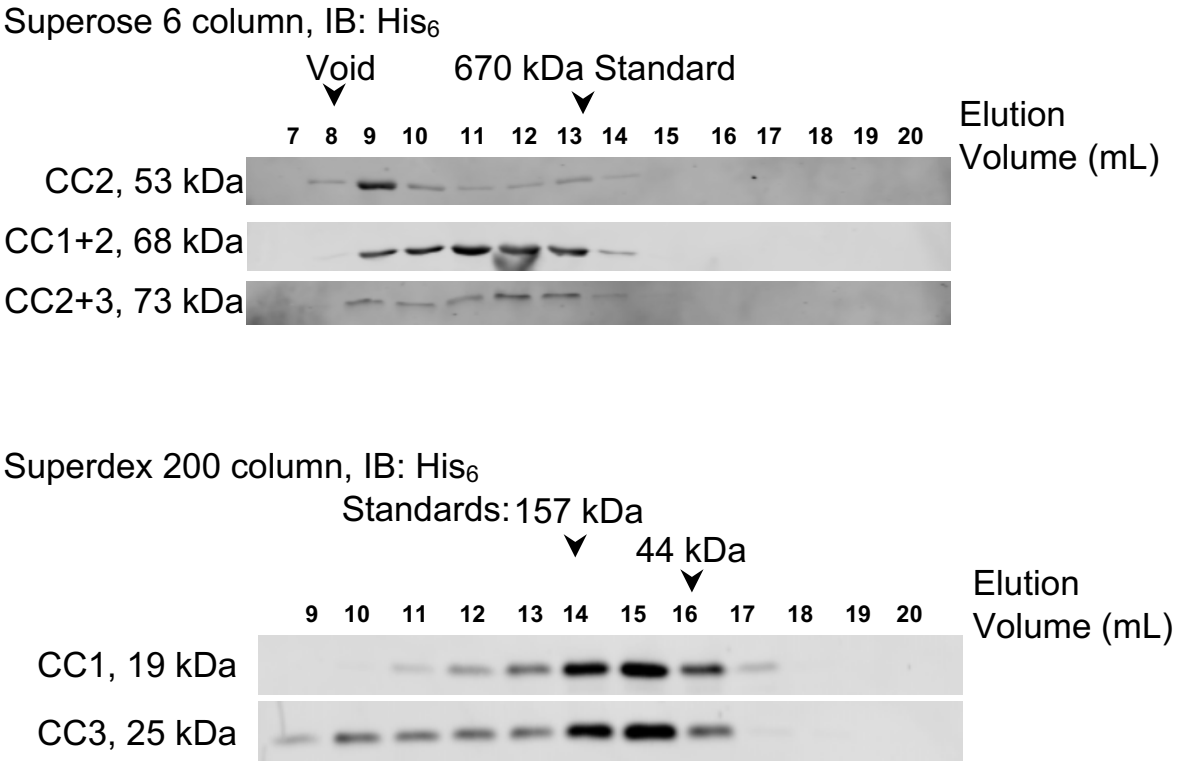

Figure 2. 9 The central CC2 domain is responsible for the large apparent molecular mass of CCCP-1

Fractionation of CCCP-1 fragments by gel filtration on a Superose 6 column for large fragments (top) or Superdex 200 column for smaller fragments (bottom). 1 mL fractions were collected and analyzed by Western blot against the His6 tag. IB: immunoblot.

Construct	Description	Comment	Localization in double stains anti-Myc and anti-TGN38
pET50	CCCP1::GFP	FL	Golgi-like
pET158	CCCP1(1-743)::GFP	Also called CC1+2	Diffuse, cytosolic looking
pJC218	CCCP1(750-922)-GFP	Also called CC3	Golgi-like
pJC239	Myc-CCCP1(FL, 1-922)		Golgi-like
pJC240	Myc-CCCP1(Δ789-833)		Diffuse, cytosolic looking
pJC241	Myc-CCCP1(Δ755-872)		Diffuse, cytosolic looking. Occasional partial Golgi-looking cell
pJC238	Myc-CCCP1(1-867)		Diffuse, cytosolic looking
pJC237	Myc-CCCP1(1-743)	also called CC1+2	Diffuse, cytosolic looking
pJC235	Myc-CCCP1(Δ741-769)	Eliminates the serine rich domain	Golgi-like
pJC247	Myc-CCCP1(10894)		
pJC248	Myc-CCCP1(Δ869-893)		Diffuse, occasional Golgi-like structures in low expressing cells
pJC249	Myc-CCCP1(Δ779-832)		Diffuse, cytosolic looking
pJC250	Myc-CCCP1(Δ833-868)		Golgi-like, many vacuoles
pJC246	Myc-CCCP1(Δ751-779)		Golgi-like
pJC245	Myc-CCCP1(Δ804-832)		Diffuse, cytosolic looking
pJC244	Myc-CCCP1(Δ778-803)		Golgi-like
pJC251	Myc-CCCP1(778-922)		Golgi-like
pJC252	Myc-CCCP1(778-912)		Golgi-like, additional bright puncta
pJC253	Myc-CCCP1(778-893)		Diffuse, cytosolic looking. It still forms large vacuoles like many of the localized constructs
pJC254	Myc-CCCP1(804-922)		Diffuse, cytosolic looking. Weak Golgi-looking presence
pJC255	Myc-CCCP1(832-922)		Diffuse, cytosolic looking

pJC256	Myc-CCCP1(778-868)		Diffuse, cytosolic looking
pJC257	Myc-CCCP1(804-893)		?
pJC258	Myc-CCCP1(778-832)		Diffuse, cytosolic looking
pJC259	Myc-CCCP1(778-893)		Diffuse, cytosolic looking
pJC260	Myc-CCCP1(831-893)		Diffuse, cytosolic looking
pJC225	CCCP1(1-867)-EGFP		Diffuse
pJC226	CCCP1(867-922)-EGFP		Diffuse
pJC227	CCCP1(750-867)-EGFP		Diffuse

Table 2. 1 Truncation constructs of the rat protein for expression in 832/13 cells

EG334 *cccp-1(ox334) III*
EG5627 *rab-2(nu415) I*
XZ1804 *yakEx101*[*Prab-3::cccp-1* cDNA::eGFP, *Pmyo-3::mcherry*]
XZ1808 *yakEx99*[*Prab-3::CC2+3* cDNA::eGFP, *Pmyo-3::mcherry*]
XZ1803 *yakEx100*[*Prab-3::CC3* cDNA::eGFP, *Pmyo-3::mcherry*]
XZ1801 *yakEx98*[*Prab-3::CC1+2* cDNA::eGFP, *Pmyo-3::mcherry*]
XZ1813 *rab-2(nu415) I; yakEx101*[*Prab-3::cccp-1* cDNA::eGFP, *Pmyo-3::mcherry*]
XZ1812 *rab-2(nu415) I; yakEx99*[*Prab-3::CC2+3* cDNA::eGFP, *Pmyo-3::mcherry*]
XZ1810 *rab-2(nu415) I; yakEx100*[*Prab-3::CC3* cDNA::eGFP , *Pmyo-3::mcherry*]
XZ1809 *rab-2(nu415) I; yakEx98*[*Prab-3::CC1+2* cDNA::eGFP, *Pmyo-3::mcherry*]
XZ1877 *oxIs602*[*cb-unc-119(+), Pcccp-1::cccp-1* cDNA::eGFP] II ; *cccp-1(ox334)* III
XZ1807 *yakSi21*[*Pcccp-1::CC1+2* cDNA::eGFP, *cb-unc-119(+)]* II ; *cccp-1(ox334)* III
XZ1893 *yakSi23*[*Pcccp-1::CC2+3* cDNA::eGFP, *cb-unc-119(+)]* II ; *cccp-1(ox334)* III
XZ1897 *yakSi25*[*Pcccp-1::CC3* cDNA::eGFP, *cb-unc-119(+)]* II ; *cccp-1(ox334)* III
XZ2068 *yakEx132*[*Prab-3::cccp-1* cDNA::eGFP, *Punc-129*::tagRFP::*rab-2*, *Pmyo-2::mcherry*]
XZ2070 *yakEx134*[*Prab-3::CC3* cDNA::eGFP, *Punc-129*::tagRFP::*rab-2*, *Pmyo-2::mcherry*]

Table 2. 2 *C. elegans* strain list

pMA59 *Prab-3::cccp-1* cDNA::eGFP in pCFJ150
pJC200 *Prab-3::CC2+3* cDNA::eGFP in pCFJ150
pJC201 *Prab-3::CC1+2* cDNA::eGFP in pCFJ150
pJC198 *Prab-3::CC3* cDNA::eGFP in pCFJ150
pMA58 *Pcccp-1::cccp-1* cDNA::eGFP in pCFJ150
pJC187 *Pcccp-1::CC2+3* cDNA::eGFP in pCFJ150
pJC188 *Pcccp-1::CC1+2* cDNA::eGFP in pCFJ150
pJC193 *Pcccp-1::CC3* cDNA::eGFP in pCFJ150
pMA160 *Punc-129*::tagRFP::*rab-2* in pCFJ150

Table 2. 3 *C. elegans* vector list

Construct	Description	Predicted MW	Binding to GST-RAB-2
pJC116	GST-RAB-2 on pGST//		
pJC121	6xHis-CCCP-1 on pHis //	89kDa	Binds GTPγS loaded RAB2
pJC160	6xHis-CC3 on pHis //	25kDa	Binds GTPγS loaded RAB2
pJC158	6xHis-CC1 on pHis //	19kDa	No binding
pJC159	6xHis-CC1+2 on pHis //	73kDa	No binding
pJC161	6xHis-CC2+3 on pHis //	68kDa	Binds GTPγS loaded RAB2
pJC190	6xHis-CC2 on pHis //	53kDa	No binding
pJC164	GST-CCCP-1 on pGST//	110kDa	?
pJC261	6xHis-CCCP-1(551-729) on pHis //	23.5kDa	Binds weakly to both GTPγS and GDP loaded RAB2. Lost its nucleotide selectivity
pJC262	6xHis-CCCP-1(584-729) on pHis //	20kDa	Binds weakly to both GTPγS and GDP loaded RAB2. Lost its nucleotide selectivity
pJC263	6xHis-CCCP-1(584-743) on pHis //	21.6kDa	Binds GTPγS loaded RAB2

Table 2. 4 Truncation constructs of the *C. elegans* protein for GST-RAB-2 pulldown experiment

Chapter 3. EIPR1 CONTROLS DENSE-CORE VESICLE CARGO SORTING AND EARP COMPLEX LOCALIZATION IN INSULINOMA CELLS

3.1 ABSTRACT

Dense core vesicles are secretory vesicles of the regulated secretory pathway that are found in neurons and endocrine cells and that transfer and release several types of cargos such as neuropeptides, biogenic amines, and peptide hormones. These cargo modulate a variety of physiological processes from development to mental state. DCVs are generated at the trans-Golgi network as immature dense core vesicles and go through a poorly understood maturation process. Recently, we identified the endosome-associated recycling protein (EARP) complex and the WD40-domain protein EARP-interacting protein EIPR-1, as regulators of the dense core vesicle biogenesis pathway, in *C. elegans* neurons. Here, we describe the role of EIPR1 in insulin-secreting insulinoma cells. Using *Eipr1* knockout and rescue experiments we find that EIPR1 controls proper insulin secretion and localization of mature DCV cargo, suggesting that neurons and endocrine cells have conserved pathways for DCV biogenesis. In *Eipr1KO* cells mature dense core vesicle cargo is accumulated in the TGN region resulting in the secretion of less insulin. In addition, we find that EIPR1 is required for the stability of the EARP complex subunits and for the localization and association of EARP with membranes. These data, suggest that EIPR1 is an essential regulator of EARP localization and that together with EARP it regulates DCV biogenesis probably through controlling the trafficking of DCV cargo into or out of endosomes.

3.2 INTRODUCTION

Dense-core vesicles (DCVs) are regulated secretory vesicles found in neurons and endocrine cells, where they are also called secretory granules. DCVs package several types of cargos, including neuropeptides and hormones, for release at the cell membrane. The secreted cargos modulate a variety of processes including development, growth, glucose metabolism, and mental state. DCVs are generated at the trans-Golgi network (TGN) in a process that includes correct sorting of cargos and acquisition of proper compartmental identity. Because DCVs are not regenerated locally at release sites, the DCV pool needs to be continuously supplied by the TGN (Borgonovo et al., 2006; Gondré-Lewis et al., 2012; Tooze et al., 2001).

Genetic studies in the nematode *C. elegans* have identified several new molecules that function in DCV biogenesis, including the endosome-associated recycling protein (EARP) complex and the WD40-domain protein EARP-interacting protein EIPR-1, which interacts with EARP (Paquin et al., 2016; Topalidou et al., 2016). The EARP complex is structurally similar to the Golgi-associated retrograde protein (GARP) complex. EARP shares the VPS51, VPS52, and VPS53 subunits with the GARP complex, but uses VPS50 instead of VPS54 as the fourth subunit (Gillingham et al., 2014; Schindler et al., 2015). Whereas GARP functions in retrograde transport or cargo from endosomes to the TGN (Conibear et al., 2000, 2003; Pérez-Victoria and Bonifacino, 2009; Pérez-Victoria et al., 2008, 2010), EARP was proposed to act in recycling cargos from endosomes back to the plasma membrane (Schindler et al., 2015). In *C. elegans*, the EARP complex and EIPR1 were shown to be required for cargo sorting to DCVs (Topalidou et al., 2016). The VPS50 subunit of the EARP complex was also shown to be required for the maturation of

DCV cargos and DCV acidification (Paquin et al., 2016). It is unclear whether the EARP function in DCV biogenesis is independent of its function in recycling cargo out of endosomes.

In this study we investigate the role of mammalian EIPR1 in DCV function and EARP complex formation using insulin-secreting insulinoma cells. We used insulinoma cells previously to demonstrate that EIPR1 physically interacts with the EARP complex (Topalidou et al., 2016). An independent study also identified EIPR1 (also named TSSC1) as a direct interactor and functional partner of both the GARP and EARP complexes (Gershlick et al., 2016). WD40 domain-containing proteins like EIPR1 often act as scaffolds for the assembly of protein complexes (Stirnimann et al., 2010). Although EIPR1 interacts with EARP, it has not been determined whether EIPR1 is required for the localization or stability of the EARP complex. Fluorescence recovery after photobleaching in Eipr1 knockdown cells showed that EIPR1 is required for efficient recruitment of GARP to the TGN (Gershlick et al., 2016).

Here we use Eipr1 knockout and rescue experiments in insulin-secreting cells to demonstrate that EIPR1 is required for the stability of the EARP complex subunits and for proper localization and association of EARP with membranes, but it does not appear to be required for the interactions between the EARP complex subunits. In addition, we show that EIPR1 controls proper insulin secretion and distribution of mature DCV cargo, suggesting that neurons and endocrine cells have conserved pathways for DCV biogenesis. These data, together with the observation that EARP localizes to endosomal compartments (Gershlick et al., 2016; Gillingham et al., 2014; Schindler et al., 2015), suggest a role for the EARP complex and its interactor EIPR-1 in controlling the trafficking of DCV cargo into or out of endosome (Topalidou et al., 2016). Such a model suggests that the biogenesis of DCVs involves trafficking through endosomes,

supporting other studies (Bäck et al., 2010; Edwards et al., 2009; Sumakovic et al., 2009; Vo et al., 2004; Wasmeier et al., 2005; Zhang et al., 2017).

3.3 RESULTS

3.3.1 *EIPR1 is required for insulin secretion*

We recently showed that the *C. elegans* WD40-domain containing protein EIPR-1 is needed for dense-core vesicle (DCV) cargo trafficking in *C. elegans* neurons (Topalidou et al., 2016). To investigate a possible role for EIPR1 in the trafficking of mammalian DCV cargo, we generated EIPR1 knockout (KO) insulinoma 832/13 cells using the CRISPR (Ran et al., 2013) by inserting a puromycin cassette in the first exon of Eipr1 (Figure S3. 1A) We identified positive clones by PCR (Figure S3. 1B and C). To confirm that EIPR1 was missing in the *Eipr1KO* line, we analyzed our cells for EIPR1 expression by Western blot. Wild-type (WT) cells displayed a band at around 45 kD, the approximate molecular weight of EIPR1, which was missing from *Eipr1KO* cells (Figure 3. 1A).

To examine whether EIPR1 is needed for cargo sorting to DCVs in insulinoma cells, we measured the insulin secretion of WT and *Eipr1KO* cells under resting (5 mM KCl, 0 mM glucose) and stimulating (55 mM KCl, 25 mM glucose) conditions (see Materials and Methods). Insulin secretion under both resting and stimulating conditions from *Eipr1KO* cells was lower than that from WT cells (stimulated secretion was reduced to ~ 25% of WT, Figure 3. 1B, left panel). To verify that the effects were due to loss of EIPR1, we introduced a wild type Eipr1 cDNA back into the *Eipr1KO* cells by lentiviral transduction (Figure 3. 1A). Expression of wild type EIPR1 in

Eipr1KO cells (Eipr1(+)) rescued the stimulated insulin secretion defect of the *Eipr1KO* line, confirming that this defect is due to loss of EIPR1 (Figure 3. 1B, left panel).

Defective insulin secretion can be due to reduced insulin content. Thus, we measured total insulin and found that total insulin is reduced in *Eipr1KO* cells (reduced to ~ 63% of WT, Figure 3. 1B, middle panel), and this reduction is only partially rescued in Eipr1(+) cells. After normalizing insulin secretion to the total insulin levels, we found that insulin secretion under stimulating conditions is still significantly reduced in the *Eipr1KO* line (~49% of WT, Figure 3. 1B , right panel), suggesting that the reduced insulin secretion cannot be fully explained by reduced total insulin levels. This result in in agreement with our studies in *C. elegans* neurons, showing that in *eipr-1* null mutants secretion of DCV cargo is reduced (Topalidou et al., 2016).

The observed decrease in insulin secretion and total insulin content in the *Eipr1KO* could be due to a defect in the processing of proinsulin to insulin. Therefore, we measured the total and secreted levels of proinsulin. Surprisingly, although secretion of proinsulin was not altered in *Eipr1KO* (Figure 3. 1C, left panel), total proinsulin content seems to be reduced (43% of WT, Figure 3. 1C, middle panel). Also, secretion of proinsulin was similar in resting and stimulating conditions, suggesting that its release is independent of the regulated secretory pathway. Despite an observed increase in normalized proinsulin secretion in the *Eipr1KO* (Figure 3. 1C, right panel), the ratio of total cellular proinsulin/insulin remains unchanged (Figure 3. 1D), suggesting that proinsulin processing is not significantly affected in the absence of EIPR1.

We next examined the levels of other known DCV cargos, such as the proprotein convertase 1/3 (PC1/3) and proprotein convertase 2 (PC2) in *Eipr1KO* cells. As shown in Figure 3. 1E, loss of Eipr1 resulted in reduced levels of PC1/3 but normal levels of PC2. Expression of wild type EIPR1 in *Eipr1KO* cells rescued the PC1/3 defect. However, this decrease in PC1/3 has

no obvious effect on proinsulin processing (Figure 3. 1D). These data suggest a role for EIPR1 in regulating levels of DCV cargos in insulinoma cells.

3.3.2 *EIPR1 is required for the localization of mature DCV cargos in insulin-secreting cells*

To investigate whether EIPR1 is required for DCV cargo sorting, we first examined the subcellular localization of insulin via immunostaining. In wild type cells, insulin was detected as puncta spread throughout the cytoplasm (Figure 3. 2A). In contrast, in *Eipr1KO* cells insulin accumulated in a perinuclear region that partially overlapped with the trans-Golgi (TGN) marker TGN38 (Figure 3. 2A,B). This phenotype was rescued in *Eipr1KO* cells that stably expressed wild type EIPR1 (Figure 3. 2A,B). We also examined the localization of additional cargo such as chromogranin A (CgA), a cargo of mature DCVs, and proinsulin, a cargo of immature DCVs. In wild type cells, most CgA staining displayed a punctate pattern throughout the cytoplasm, similar to that of insulin (Figure 3. 3A). In contrast, *Eipr1KO* cells showed accumulation of CgA in the perinuclear region around the TGN (Figure 3. 3A). Proinsulin, the unprocessed form of insulin, was localized in a similar perinuclear region both in wild type and *Eipr1KO* cells (Figure 3. 3B). These data suggest that EIPR1 affects the distribution of mature DCV cargos in insulin-secreting cells. This reduction of the level of cytoplasmic DCV cargo could also explain the reduction in insulin secretion in *Eipr1KO* cells under stimulating conditions (Figure 3. 1B, right panel).

To investigate whether the mature DCV cargo is permanently stuck at the TGN in *Eipr1KO* cells, we used a pulse-chase method to monitor cargo exit from the TGN. We transiently transfected the DCV cargo ANF::GFP into WT and *Eipr1KO* 832/13 cells and blocked cargo exit from the Golgi by incubating for 2 hours at 20° (Kögel et al., 2013; Kögel Tanja et al., 2010).We first verified that at steady state (before the temperature block), in *Eipr1KO* cells, ANF::GFP

accumulated at a perinuclear region (Figure S3. 2A), similarly to insulin and CgA. After the temperature block (pulse), cells were returned to 37°C and incubated for different times (chase). They were then processed for GFP immunostaining and imaging (Figure S3. 2B). Cells were scored based on whether ANF::GFP was (1) predominantly at the TGN-region ("Golgi-like" in Figure S3. 2C), (2) found both at the TGN-region and at the cell periphery ("Intermediate" in Figure S3. 2C), or (3) excluded from the Golgi ("Periphery" in Figure S3. 2C). We observed that the accumulation of ANF::GFP at the TGN was significantly different between WT and *Eipr1KO* cells at all time points (Figure S3. 2D), confirming that EIPR1 affects the distribution of DCV cargo. Interestingly, the accumulation of ANF::GFP significantly changed in *Eipr1KO* cells during the chase period, with most of the cells having ANF::GFP at the Golgi at t = 0, and most of the cells having ANF::GFP at both the TGN and the periphery at t = 80 min (Figure S3. 2D). This indicates that the DCV cargo is not permanently stuck at the TGN region in *Eipr1KO* cells but is able to reach the cell periphery, although probably at a slower rate or less efficiently than in WT cells.

3.3.3 *EIPR1 is needed for the localization of EARP subunits in insulin-secreting cells*

It was recently shown that mammalian EIPR1 interacts with the EARP and GARP complex subunits and functions with EARP in endosomal recycling and with GARP in endosome-Golgi retrograde trafficking (Gershlick et al., 2016; Topalidou et al., 2016). However, *eipr-1* mutants in *C. elegans* have behavioral and cellular phenotypes similar to EARP-specific mutants, but not GARP-specific mutants (Topalidou et al., 2016). EIPR1 is a WD40-domain containing protein, and WD40 domains often act as scaffolds for mediating protein interactions and multi-protein complex assembly (Stirnimann et al., 2010). To investigate whether EIPR1 is required for the

localization of EARP or GARP complex subunits in insulin-secreting cells, we examined the localization of transiently transfected Myc-tagged VPS50 (the sole EARP-specific subunit), GFP-tagged VPS54 (the sole GARP-specific subunit), and Myc-tagged VPS51 and VPS53 that are present in both GARP and EARP complexes. We also examined the localization of endogenous VPS50 using a commercial antibody, the only antibody we have for EARP or GARP subunits that is suitable for immunofluorescence. In wild type cells, VPS50, VPS51, VPS53, and VPS54 all showed a punctate pattern of localization. The GARP-specific VPS54 subunit was localized mostly to a perinuclear region overlapping TGN38, but the other subunits were more dispersed throughout the cytoplasm (Figure 3. 4 A-D, Figure S3. 3A-B). Interestingly, the punctate localization of the EARP-specific subunit VPS50 and of the EARP/GARP common subunits VPS51 and VPS53 was disrupted in *Eipr1KO* cells, with fluorescence being largely diffuse throughout the cytoplasm. In contrast, the GARP-specific subunit VPS54 was still punctate and localized near the TGN in *Eipr1KO* cells, and could not be distinguished from wild type in blind experiments. We conclude that EIPR1 is needed for the localization of the EARP complex subunits, but not GARP complex subunits.

Depletion of GARP leads to redistribution of TGN38 to cytoplasmic vesicles thought to correspond to retrograde transport intermediates (Pérez-Victoria et al., 2008). We too found that siRNA knockdown of the VPS51 subunit of the GARP complex caused redistribution of TGN38 to cytoplasmic puncta (Figure S3. 4), but the *Eipr1KO* had no obvious change in the distribution of TGN38 (Figure 3. 2A and Figure S3. 4). This result suggests that EIPR1 does not function with GARP in the retrograde trafficking of TGN38.

3.3.4 *The EARP complex localizes in at least two distinct pools*

Gershlick et al. (2016) recently showed that EIPR1 is needed for endocytic recycling in HELA cells. To examine whether EIRP1 also participates in endocytic recycling in insulin-secreting 832/13 cells we examined the recycling of Alexa 488–labeled transferrin in WT and *Eipr1KO* 832/13 cells . Cells were incubated for 25 min with Alexa 488- labeled transferrin, washed, and then chased for specific time points. Similar to Gershlick et al (2016) we found that *Eipr1KO* cells retained more transferrin then WT cells, suggesting that EIPR1 also plays a role in endocytic recycling in insulin-secreting cells (Figure 3. 5).

Our observations and those of Gershlick et al. (2016) suggest that EIPR1 and EARP participate in endocytic recycling but also in dense core vesicle cargo sorting (Topalidou 20016 and this study). To examine whether the EARP complex localizes in different pools in the cell to mediate these functions we immunostained 832/13 cells, transfected with CCCP1::GFP and incubated with Alexa 568-labelled transferrin, with an antibody against VPS50. The coiled-coil protein CCCP1 is localized near immature dense core vesicles and the TGN (Cattin-Ortolá et al., 2017) while transferrin is found at early and recycling endosomes. We observed that VPS50 was predominantly found in two distinct pools; in the one pool VPS50 colocalized with CCCP1::GFP and in the other with transferrin (Figure 3. 5B). This result suggests that VPS50 localizes in at least two distinct compartments that are related to its function: an endocytic recycling compartment and a dense core vesicle-related compartment.

3.3.5 *EIPR1 is not required for the physical interactions between EARP complex subunits*

Because EIPR1 is needed for the proper localization of EARP complex subunits and WD40 domains often serve as scaffolds for complex assembly, we reasoned that EIPR1 might be needed

for the formation of the EARP complex. To investigate this, we first compared the endogenous levels of VPS50 and VPS51 in wild type and *Eipr1KO* 832/13 cells. As shown in Figure 3. 6A, *Eipr1KO* cells had reduced levels of VPS50 and VPS51, and this defect was rescued by expression of wild type EIPR1. This result suggests that EIPR1 is required for either expression or stability of the individual subunits. To test whether these reduced protein levels were due to reduced transcription, we examined the levels of the VPS50 and VPS51 mRNAs in WT and *Eipr1KO* cells. Quantitative PCR using total cDNA from WT and *Eipr1KO* cells showed no difference in the mRNA levels of these EARP complex subunits (Figure S3. 5A).

Second, we expressed GFP-tagged VPS50 with Myc-tagged VPS51 or Myc-tagged VPS53 in wild type and *Eipr1KO* 832/13 cells and performed coimmunoprecipitation experiments to determine whether EIPR1 is required for physical interactions between the individual EARP subunits. GFP-tagged VPS50 coimmunoprecipitated with either Myc-tagged VPS51 or Myc-tagged VPS53, but these interactions were not disrupted by loss of EIPR1 (Figure 3. 6B,C). To test whether EIPR1 is required for the interactions between GARP complex subunits we expressed GFP-tagged VPS54 with Myc-tagged VPS51 in wild type and *Eipr1KO* 832/13 cells. GFP-tagged VPS54 coimmunoprecipitated with Myc-tagged VPS51 as expected, but this interaction was not changed in *Eipr1KO* cells (Figure 3. 6D). These data show that EIPR1 is not required for interactions between the individual subunits of the EARP or GARP complexes, suggesting that EIPR1 is not required for the formation of these complexes, at least under these conditions where some subunits are overexpressed.

Finally, to further examine whether the EARP complex is disrupted in the absence of EIPR1, we subjected detergent cell lysates from wild type and *Eipr1KO* 832/13 cells to velocity sedimentation through an 8%-30% linear sucrose gradient and blotted for VPS50. VPS50

sedimented in a broad peak between the 158 and 670 kDa standards, indicating that the protein is part of a complex (Figure 3. 7A) and cosedimented with VPS51. Interestingly, EIPR1 sedimentation from the same cell lysate showed a similar peak to VPS50, suggesting that EIPR1 and VPS50 might be part of the same complex (Figure 3. 7A). However, sedimentation of VPS50 did not appear to be affected by loss of EIPR1 (Figure 3. 7B), suggesting that the EARP complex still forms in the absence of EIPR1.

3.3.6 *EIPR1 is required for the normal association of EARP complex subunits with membranes*

Our results suggest that the EARP complex forms in the absence of EIPR1 but is not properly localized. To test whether the diffuse localization of EARP subunits in the *Eipr1KO* is due to a requirement of EIPR1 for the association of EARP with membranes, we fractionated 832/13 cell lysates and probed for VPS50. VPS50 was found primarily in the membrane fraction (P100) in wild-type cells (Figure 3. 7C), but the association of VPS50 with membranes was partially lost in *Eipr1KO* cells (Figure 3. 7C). Similarly, VPS51 was found in the membrane fraction in wild-type cells (Figure 3. 7D) and this association was reduced in the *Eipr1KO*. We conclude that EIPR1 is partially required for the proper association of EARP complex subunits with membranes.

3.4 DISCUSSION

In this study, we demonstrate that the EARP complex interacting-protein EIPR1 is required for localization and association of the EARP complex with membranes and regulates proper insulin

secretion and distribution of mature DCV cargo. These data , together with the fact that EIPR1 and EARP have been reported to localize to endosomal compartments and to act in endosomal recycling (Gershlick et al., 2016; Schindler et al., 2015), suggest that DCV cargo trafficking involves the recycling of cargo or sorting factors from endosomal compartments via EIPR1 and EARP (Topalidou et al., 2016).

3.4.1 *EIPR1 regulates the localization of the EARP complex and its association with membranes*

The WD40-domain containing protein EIPR1 was identified by two independent studies as an interactor of the EARP (Topalidou et al., 2016) and GARP/EARP (Gershlick et al., 2016) complexes in rat insulin-secreting cells and human neuroglioma cells, respectively. Additionally, two mass spectrometry interactome data sets found that EIPR1 interacts with EARP subunits in human HEK293T or HeLa cells (Hein et al., 2015; Huttlin et al,. 2015). In one of these studies (Hein et al., 2015), VPS50 was shown to pull down VPS51, VPS52, VPS53 and EIPR1, but not VPS54, as a stoichiometric complex, indicating that EIPR1 may form a stable complex with EARP but not GARP. Although WD40-domain containing proteins are reported to play roles as scaffolds for the assembly of large protein complexes (Stirnimann et al., 2010) our data suggest that EIPR1 is not needed for the formation of the EARP (or GARP) complex. First, EIPR1 is not required for interactions between individual subunits of the EARP and GARP complexes as shown by coimmunoprecipitation experiments. Second, sedimentation of VPS50 was not affected by loss of EIPR1, suggesting that the EARP complex does not collapse in the absence of EIPR1. By contrast, we find that EIPR1 is needed for the stability of the individual subunits, the localization of the EARP complex subunits, and association of EARP with membranes, supporting the model that EIPR1 acts as a recruiter or stabilizer of the EARP complex to its site of action.

Although localization of the EARP subunits was disrupted in the absence of EIPR1, localization of the GARP-specific VPS54 subunit was not obviously affected, suggesting that EIPR1 is not required for the localization of GARP in insulinoma cells. A recent study showed that VPS54::GFP stably expressed in H4 cells is localized at the TGN region in both wild type and EIPR1 knockdown (KD) cells (Gershlick et al., 2016) but detailed FRAP analysis showed that EIPR1 contributes to GARP recruitment to the TGN. Although our data support an involvement of EIPR1 in the proper localization of EARP but not GARP in insulinoma cells, it is possible that EIPR1 is important for the recruitment of GARP in other cell types or under different experimental conditions.

3.4.2 *EIPR1 participates in EARP- specific functions*

EARP and EIPR1 were recently shown to participate in the endocytic recycling of the transferrin receptor (Gershlick et al., 2016; Schindler et al., 2015). In this study we also showed that EIPR1 is needed for endocytic recycling of the transferrin receptor in insulin-secreting cells. To investigate whether EIPR1 might act together with GARP as well as EARP, we examined the distribution of TGN38 in *Eipr1KO* and Vps51 KD cells. In the absence of GARP, TGN38 is misdistributed to cytoplasmic vesicles (Pérez-Victoria et al., 2008 and this study) but *Eipr1KO* had no obvious effect on the distribution of TGN38. Additionally, *C. elegans* GARP mutants were shown to have enlarged lysosomes in coelomocytes but our previous work showed that *eipr-1* and *vps-50* mutants do not have enlarged lysosomes (Topalidou et al., 2016). These results suggest that EIPR1 does not participate in GARP-specific functions, which agrees with our model that EIPR1 is required for the localization of EARP but not GARP. However, EIPR1 was reported to be required for the retrograde traffic of STxB, whose trafficking also depends on GARP (Gershlick

et al., 2016). We were unable to examine the trafficking of STxB in insulin-secreting cells since we found that these cells do not uptake STxB. These observations suggest that if EIPR1 functions together with GARP, it only mediates a subset of GARP functions.

3.4.3 *EARP localizes in two distinct pools*

The dual functionality of EIPR1/EARP in endocytic recycling and DCV cargo sorting prompted us to examine the cellular distribution of EARP. We observed that EARP resides in at least two distinct pools, one that is associated to endosomes and one associated to the TGN and/or immature DCVs. At this point we are not able to say whether the endosomal recycling and DCV cargo sorting features of EARP and EIPR1 reflect two independent functions or whether they are interconnected. One possibility would be that the EARP complex moves from the one location to the other to participate in the sorting/removal or DCV cargo through an endocytic compartment. Another alternative is that DCV-bound EARP performs an independent function not related to endocytic recycling. It would be interesting to see whether blockage of the EARP- driven endocytic recycling pathway affects DCV biogenesis.

3.4.4 *EIPR1 regulates DCV cargo levels and distribution*

Our *C. elegans* studies support a role for EIPR1 in cargo sorting to dense-core vesicles (Topalidou et al., 2016). To determine whether EIPR1 plays a similar role in insulin-secreting cells, we examined the total and secreted levels of DCV cargos. Interestingly, the total levels of insulin, proinsulin and proprotein convertase 1/3 (PC1/3) were reduced in *Eipr1KO* cells. To examine whether these reduced levels were due to a transcription defect we examined the mRNA

levels of proinsulin and PC1/3 by performing quantitative RT-PCR using total cDNA from WT and *Eipr1KO* cells. No difference was observed at the mRNA levels of these DCV cargos in *Eipr1KO* cells (Figure S3. 5B), suggesting that EIPR1 plays a role at a post-transcriptional level in controlling the level s of cargos destined to the DCVs.

Our insulin secretion data showing that *Eipr1KO* cells secrete less insulin suggest that either DCVs from *Eipr1KO* cells contain less insulin or that EIPR1 is required for exocytosis. The data showing that (1) DCVs from *C. elegans eipr-1* null animals have less cargo and that (2) EIPR1 was shown to localize to recycling endosomes (Gershlick et al., 2016) and to interact with the EARP complex (Gershlick et al., 2016; Hein et al., 2015; Topalidou et al., 2016) do not support a role for EIPR1 in exocytosis. Also, the fact that we find less insulin in cytoplasmic puncta of *Eipr1KO* cells and most insulin is accumulated in the TGN region fits together with the fact that less insulin is secreted from these cells. Both these observations support that insulin in *Eipr1KO* cells is retained in a TGN region. Similarly, we observed that chromogranin A is accumulated in the region around the TGN, also supporting a role of EIPR1 in cargo sorting from the TGN to DCVs. Alternatively, EIPR1 could be needed for the actual budding of DCVs from the TGN.

3.4.5 *A growing numbers of reports suggest a role of endosomal recycling in DCV biogenesis*

The demonstration that EARP, an endosomal-recycling complex, and the EARP-interacting protein EIPR1 are involved in DCV trafficking (Topalidou et al., 2016) suggests that dense-core vesicle cargo trafficking involves not only the trafficking of cargo into nascent dense-core vesicles as they bud off from the trans-Golgi, but also the retrieval or recycling of cargo or sorting factors from endosomal compartments. Such a model would suggest that the biogenesis of DCVs involves trafficking through endosomes.

Several studies have implied or supported a role of endosomes in DCV maturation (Bäck et al., 2010; Cattin-Ortolá et al., 2017; Edwards et al., 2009; Sumakovic et al., 2009; Vo et al., 2004; Wasmeier et al., 2005; Zhang et al., 2017). The AP-1 adaptor that is involved mainly in trafficking between the trans-Golgi and endosomes has been shown to associate with immature dense-core vesicles and to mediate the removal of syntaxin 6 and mannose 6-phosphate receptors from immature DCVs (Klumperman et al., 1998). In a recent study the secretory cell-specific Munc13-4 paralog BAIAP3, which was shown to localize to late and recycling endosomes and to be needed for endosome recycling to the TGN, was also shown to affect DCV maturation (Zhang et al., 2017). Two studies on the role of *C. elegans* RAB-2 in DCV biogenesis supported that RAB-2 acts at a maturation step by preventing DCV soluble cargo from getting lost through the endosomal-lysosomal system (Edwards et al., 2009; Sumakovic et al., 2009). Given that *C. elegans* EIPR-1 is shown to act in the same genetic pathway as RAB-2, the role of EIPR-1 might also be to prevent cargo loss through the lysosomal system.

Another study examined the recycling of dense-core vesicle membrane protein peptidylglycine amidating α-monooxygenase (PAM), an enzyme that catalyzes the final step in peptide processing (Bäck et al., 2010). PAM reaches the cytoplasmic membrane following exocytosis while plasma membrane PAM was shown to return to dense-core vesicles through early endosomes and multivesicular bodies (Bäck et al., 2010). This suggests a critical role of endosomal recycling in the recycling of DCV membrane proteins following exocytosis. Given that EARP and EIPR1 are proposed to act in endosomal recycling (Gershlick et al., 2016; Schindler et al., 2015) we could envision a model where EARP and EIPR1 are needed for the recycling of DCV membrane cargo from the plasma membrane to endosomes and the TGN. It will be interesting to

determine whether DCV membrane cargo is recycled from the plasma membrane to the TGN through endosomes in an EIPR1 and EARP-dependent manner .

3.5 MATERIAL AND METHODS

3.5.1 *Cell culture*

The 832/13 cell line is an INS-1-derived clone that was isolated by Dr. Christopher Newgard (Duke University School of Medicine) (Hohmeier et al., 2000) and obtained by Dr. Duk-Su Koh via Dr. Ian Sweet (University of Washington). Cell lines were grown in RPMI 1640-GlutaMAX™ (GIBCO) medium supplemented with 10% FBS (RMBIO), 1 mM sodium pyruvate (GIBCO), 10 mM HEPES (GIBCO), 1X Pen/Strep (GIBCO), and 0.0005% 2-beta-mercaptoethanol at 5% CO2 and 37°C. Cells were transfected using Lipofectamine 2000 (Thermo Fisher) according to the manufacturer's instructions.

3.5.2 *Constructs*

The plasmids Vps51::13Myc, VPS53::13Myc, VPS50::13Myc, VPS54::GFP, and VPS50::GFP were a gift from Juan Bonifacino (Pérez-Victoria et al., 2008; Schindler et al., 2015) The EIPR1_pBabe-hygro construct used for making Eipr1(+) stable lines was constructed by amplifying rat EIPR1 cDNA from an 832/13 cDNA library using primers:

oET513: 5'- ccatggatccatggaagacgacgccccg-3' and

oET514: 5'- ctgagaattctcagagcagtatgtggtacttcagtgc-3'

The PCR product was digested by EcoRI/BamHI and cloned into EcoRI/BamHI-digested pBabe-hygro (a gift from Suzanne Hoppins).

3.5.3 *Eipr1 knock out using CRISPR editing*

To knock out EIPR1 we performed Cas9-mediated genome editing via homology-directed repair (HDR) in 832/13 cells using the protocol described (Ran et al., 2013).

For designing guide RNAs we used the online CRISPR design tool (Ran et al., 2013) and selected three guide RNAs that recognize sequences in or near the first exon of rat Eipr1:

guide 1: 5'-gacgacgccccggtgatctacggg-3'

guide 2: 5'-gagcccgagtcccgcctcaccagg-3'

guide 3: 5'-gtatcatggaagacgacgccccgg-3'

The guide RNAs were cloned into pSpCas9(BB)-2A-GFP vector using the indicated protocol (Ran et al., 2013). The efficiency of the cloned guide RNAs was tested using the SURVEYOR nuclease assay (Figure S3. 1A) according to the manufacturer's instructions (Surveyor Mutation Detection kit, Transgenomic). guide RNA #1 was selected for all subsequent experiments.

To design the homology-directed repair (HDR) template we used the pPUR (Clontech) vector as a backbone and cloned approximately 1.5 kb Eipr1 homology arms upstream and downstream of the puromycin selection cassette. The HDR template was assembled using Gibson.

To cotransfect the CRISPR plasmid and HDR template into 832/13 cells, cells were grown in two 10-cm petri dishes to near confluency. Cells were cotransfected with 7 μg CRISPR plasmid and 7 μg non-linearized HDR template using Lipofectamine 3000 according to the instructions (Thermo Fisher). 48 hours after transfection, the media was removed and replaced with new media together with 1 μg/ml puromycin. The puromycin selection was kept until individual clones could be picked, grown in individual dishes, and tested for CRISPR editing.

Individual puromycin-resistant clones were tested for proper CRISPR editing of the Eipr1 gene using genomic DNA extraction and PCR (Figure S3. 1B). The primers used for the PCR screening of positive clones were the following:

oET236: 5'-gaggtccgttcacccacag-3' (hybridizes just upstream of the left homology arm).

oET237: 5'-gcctggggactttccacac-3' (hybridizes in the SV40 promoter that drives the expression of the puromycin resistance gene).

5 out of 16 of the puromycin-resistant clones showed the band indicative of insertion of the puromycin cassette into Eipr1. To test for homozygosity, we performed PCR using primers that amplify the wild-type Eipr1 locus:

oET236: 5'-gaggtccgttcacccacag-3' (hybridizes just upstream of the left homology arm).

oET200: 5'- gagcagtatccaacacacacctc-3' (hybridizes just downstream of the Cas9 cleavage site and in the first Eipr1 intron).

Out of the 16 clones tested, three did not show the wild-type band with primers oET236 and oET200 and were subsequently tested for EIPR1 expression by Western blot. Clone #3 (Figure 3. 1A and Figure S3. 1) showed no EIPR1 expression by Western.

3.5.4 *Insulin and proinsulin secretion*

Cells were grown in 24-well plates to near confluency, washed twice with PBS, and incubated for 1 hour in 200 µl per well resting buffer (5 mM KCl, 120 mM NaCl, 24 mM $NaHCO_3$, 1 mM $MgCl_2$, 15 mM HEPES pH 7.4). The medium was collected, cleared by centrifugation, and stored at -80°C. The cells were incubated for 1 hour in 200 µl per well stimulating buffer (55 mM KCl, 25 mM glucose, 70 mM NaCl, 24 mM $NaHCO_3$, 1 mM $MgCl_2$, 2 mM $CaCl_2$, 15 mM HEPES pH 7.4). After stimulation, the medium was cleared by centrifugation and stored at -80°C. The

cells were washed once with PBS, harvested in PBS, and extracted in 100 µl per well acid-ethanol solution (absolute ethanol:H20:HCl, 150:47:3). The pH of the acid-ethanol solution was neutralized by addition of 20 µl of 1M Tris Base per 100 µl of acid ethanol and the samples were stored at -80°C.

Samples were assayed for insulin or proinsulin content using ELISA according to the instructions of the manufacturers (Rat/Mouse insulin ELISA, Millipore, #EZRMI-13K. Rat/Mouse proinsulin ELISA, Mercodia, #10-1232-01). Secreted insulin and proinsulin levels were normalized against total cellular protein concentration and were presented as % of the wild type under stimulating conditions (Figure 3. 1 B,C left panels). These values were then normalized against total cellular insulin or proinsulin levels (Figure 3. 1 B,C middle panels) to give the "normalized" secretion data (Figure 3. 1 B,C right panels).

3.5.5 *ANF-GFP pulse-chase*

To monitor the exit of DCV cargo from the TGN, we used a protocol similar to the one described (Kögel et al., 2013; Kögel Tanja et al., 2010). WT and *Eipr1KO* 832/13 cells were seeded on glass coverslips and grown for 24 hours. We then transfected 100 ng of ANF::GFP (Hummer et al, 2017) with Lipofectamine 2000 for 12-16 hours at 37°C in complete growth medium. Cells were then incubated at 20°C in PBS for 2 h in a conventional incubator (pulse) to block the formation of DCVs. 30 minutes before the end of the low temperature block, 10 µg/ml of cycloheximide was added to the PBS to block the synthesis of new ANF::GFP. Cells were then transferred in growth medium to 37°C (chase) for the indicated times and then were fixed with 4% PFA, stained, and imaged as described (see immunostaining section). Cells were scored in three categories: those that had most of the ANF::GFP concentrated at the TGN ("Golgi-like"),

those that had ANF::GFP both at the TGN-region and at the cell periphery ("Intermediate"), and those where the ANF::GFP was excluded from the TGN ("Periphery"). 50 to 100 cells per time point and per genotype were counted. The experimenter was blind to the genotypes of the cell lines used and the time point. The experiment was repeated three times with similar results.

3.5.6 *Lentiviral production, infection of cells, and selection of stable lines*

Platinum-E (Plat-E) retroviral packaging cells (a gift from Suzanne Hoppins) were grown for a couple of generations in DMEM-GlutaMAX™ (GIBCO) medium supplemented with 10% FBS (RMBIO), 1X Pen/Strep (GIBCO), 1 µg/ml puromycin, and 10 µg/ml blastocidin at 5% CO2 and 37°C. On day one, approximately 3.6 x 105 Plat-E cells per well were plated in a six-well dish in DMEM-GlutaMAX™ medium supplemented with 10% FBS and 1X Pen/Strep. On day two, a mix of 152 µl Opti-MEM (Thermo Fisher), 3 µg EIPR1_pBabe-hygro DNA, and 9 µl Fugene HD transfection reagent (Promega) was incubated for 10 minutes at room temperature and transfected into each well. On day three, the media was removed and replaced with new Plat-E media. On day four, approximately 1.5 x 105 *Eipr1KO* 832/13 cells per well were plated in a six-well dish in RPMI 1640-GlutaMAX, supplemented with 10% FBS, 1 mM sodium pyruvate, 10 mM HEPES, 1X Pen/Strep, and 0.0005% 2-beta-mercaptoethanol. 3 µl of 8 mg/ml hexadimethrine bromide (Sigma) was added in each well. The supernatant of the Plat-E cells (48 hours viral supernatant) was collected with a sterile syringe, passed through a 0.45 micron filter, and added to the *Eipr1KO* cells. The *Eipr1KO* cells were incubated for 5-8 hours at 5% CO2 and 37°C, then the media was changed and replaced with new media. The cells were incubated overnight at 5% CO2 and 37°C. On day five, the supernatant was removed from the *Eipr1KO* cells and replaced with the supernatant from the Plat-E cells (72 hours viral supernatant) after passing through a 0.45 micron

filter. 3 µl of 8 mg/mL hexadimethrine bromide was added in each well and the cells were incubated for 5-8 hours. The media was replaced with new 832/13 cell media. On day six, the *Eipr1KO* cells were collected, transferred into a 10-cm petri dish, and 200 µg/ml hygromycin was added. The cells were grown under hygromycin selection until individual clones could be picked and tested for EIPR1 expression.

3.5.7 *Protein extraction and coimmunoprecipitation*

The anti-GFP nanobody was expressed and purified as described (Topalidou 2016). For protein extraction or coimmunoprecipitation, approximately 4 X 106 832/13 cells were plated onto 10-cm plates. Twenty-four hours later cells were transfected with 8 µg each of the relevant plasmids, if transfection was required. After 24 to 48 hours the cells were washed with cold PBS twice and harvested in lysis buffer containing 50 mM Tris, pH 7.5, 150 mM NaCl, 1% NP40 and protease inhibitor cocktail (Pierce). Lysates were transferred to microcentrifuge tubes and passed 10 times through a 20G needle followed by incubation for 30 min at 4°. Lysates were centrifuged at 20,000g for 15 min at 4°. Approximately 1/10th of the supernatant was kept as input control for subsequent immunoblot analysis. The remaining lysate was incubated with 20 µg anti-GFP nanobody bound to magnetic beads, for two to four hours at 4°C. The beads were washed three times with lysis buffer and resuspended in Laemmli loading buffer. The input and immunoprecipitated samples were resolved on 8% SDS-polyacrylamide gels and blotted onto PVDF membranes.

3.5.8 *Immunoblotting*

PVDF membranes were incubated in 3% milk in TBST (50 mM Tris pH 7.4, 150 mM NaCl, 0.1% Tween 20) for 1 hour at room temperature and stained with the relevant antibodies in 3% milk in TBST overnight, followed by three 5-minute washes in TBST. For the membrane fractionation, membranes were blocked with Odyssey® Blocking Buffer (PBS, 927-10100) to reduce background signal. Antibodies were incubated in the same buffer and washed with PBST (137 mM NaCl, 2.7 mM KCl, 10mM Na2HPO4, 1.8mM KH2PO4, pH 7.4 supplemented with 0.1% Tween-20). The following primary antibodies were used: rabbit polyclonal anti-GFP (1:1000, a gift from Dr. Alexey Merz), mouse monoclonal anti-c-Myc (1:1000, Santa Cruz, sc-40), mouse monoclonal anti-beta-tubulin (1:1000, ThermoFisher, BT7R, #MA5-16308), mouse monoclonal anti-beta-tubulin (1:1,000, DHSB, E7), rabbit polyclonal anti-PCSK1 (PC1/3) (1:1000, Sigma, #SAB1100415), rabbit polyclonal anti-TSSC1/EIPR1 (1:1000, Thermo Scientific, #PA5-22360), rabbit polyclonal anti-CCDC132/VPS50 (1:1000, Sigma, #HPA026679), rabbit polyclonal anti-VPS51 (1:1000, Atlas antibodies, #HPA061447), rabbit polyclonal PC2 (1:1000, #13/4, a gift from Sharon Tooze; Dittie and Tooze, 1995). Membranes were stained with the relevant secondary antibodies in 3% milk in TBST, followed by three 5-minute washes in TBST. The secondary antibodies used were an Alexa Fluor 680-conjugated goat anti-mouse antibody (1:20,000, Jackson Laboratory, #115-625-166), Alexa Fluor 790-conjugated donkey anti-mouse antibody (1:20,000, Jackson Laboratory, #715-655-150), or Alexa Fluor 680-conjugated goat anti-rabbit antibody (1:20,000, Jackson Laboratory, #115-625-144). A LI-COR processor was used to develop images.

3.5.9 *Immunostaining*

Approximately 105 to 2 X 105 cells per well were plated onto cover slips (Thomas Scientific #121N79) placed in 24-well cell culture plates. Cells were transfected with Lipofectamine 2000, according to manufacturer's instruction, at least 24h after seeding. After 24 to 48 hours, the cells were rinsed twice with PBS and fixed with 4% paraformaldehyde (made in PBS) for 20 minutes at room temperature. The cells were rinsed twice with PBS and permeabilized with 0.5% Triton X-100 in PBS for 5 minutes at room temperature. The cells were rinsed twice with PBS and placed in 5% milk in PBS for 1 hour at room temperature. Cells were stained with primary antibodies in 0.5% milk in PBS at room temperature for 1 hour. The following primary antibodies were used: mouse monoclonal anti-c-Myc (1:1000, Santa Cruz, sc-40), rabbit polyclonal anti-CCDC132/VPS50 (1:50, Sigma #HPA026679), mouse monoclonal anti-GFP (1:200 to 1:350, Santa Cruz, #sc-9996), mouse monoclonal anti-insulin (1:350, Sigma, #K36AC10), mouse monoclonal anti-proinsulin (1:100, Abcam, #ab8301), rabbit polyclonal anti-TGN38 (1:350, Sigma, #T9826), mouse monoclonal anti-CgA (1:350, Santa Cruz, #sc-13090). The cells were then washed with PBS three times for 5 minutes each and incubated with rhodamine anti-rabbit secondary antibody (1:1000, Jackson Immunoresearch #111-025-144), Alexa Fluor 488 anti-rabbit secondary antibody (1:1000, Jackson Immunoresearch, #115-545-152), Alexa Fluor 488 anti-mouse secondary antibody (1:1000, Jackson Immunoresearch, #115-545-146), and Rhodamine Ret-X anti mouse secondary antibody (1:1000, Jackson Immunoresearch #715-295-150) at room temperature for 1 hour. The cells were washed with PBS three times for 5 min each, mounted onto glass slides using Vectashield (Vector laboratories H1000) or Prolong Diamond (Life Technologies P36965) and examined by fluorescence microscopy. Images were obtained using a Nikon 80i wide-field compound microscope with a 60X oil objective or an Olympus

FLUOVIEW FV1200 confocal microscope with a 60X UPlanSApo oil objective. The acquisition software used for the Nikon was NIH elements and for the Olympus it was Fluoview v4.2. Pearson's correlation coefficients were determined using Fiji and the coloc-2 plugin by taking maximum intensity projections of z-stacks and drawing a line around each individual cell.

3.5.10 *VPS51 knockdown by RNAi*

VPS51 knockdown was performed using stealth siRNA from Life Technologies (# 10620312-353281 D10, 5'-GAUGGACAGUGAGAcGGACAUGGUG-3'). Transfection of oligonucleotides (20 nM) was done using Lipofectamine 2000 as follows: cells were seeded on cover slips placed in 24-well cell culture plates until they reached approximately 50% confluence. On days one and three, cells were transfected with 1 µl of oligonucleotides and 1 µl Lipofectamine according to the manufacturer's instructions. On day five, cells were stained with the relevant antibodies following standard immunostaining procedure.

3.5.11 *Cofractionation on sucrose velocity gradients*

WT or *Eipr1KO* 832/13 cells were grown to confluence in 15-cm tissue culture plates. Cells were washed twice with ice cold PBS, transferred into microcentrifuge tubes in PBS, and centrifuged at 500g for 10 minutes at 4°C. Cells were resuspended in lysis buffer (50 mM Tris-Cl [pH 7.6], 150 mM NaCl, 1% NP-40, 1 mM EDTA, protease inhibitor cocktail from Pierce), kept on ice for 20 minutes and centrifuged at 20,000g for 10 minutes at 4°C. The clarified lysate was loaded on top of a linear 8%-30% (or linear 8%-25% as indicated) sucrose gradient prepared in an ultracentrifuge tube (Beckman Coulter, #349222) in lysis buffer. Tubes were centrifuged at

100,000g for 16h at 4°C in a SW50 rotor. Fractions were collected from top to bottom and supplemented with 6X SDS loading sample buffer. EARP complex subunits were analyzed by immunoblotting using antibodies to the endogenous proteins. Sizing standards (Bio-Rad #151-1901) were analyzed by Coomassie-stained SDS-PAGE gels.

3.5.12 *Cell fractionation*

WT 832/13 or *Eipr1KO* 832/13 cells were seeded on a 24-well cell culture plate and grown until sub-confluence. Where indicated, cells were transfected with VPS51::13Myc for 48 hours before fractionation using lipofectamine 2000, according to the manufacturer's instructions. Cells were washed twice with ice cold PBS, transferred into microcentrifuge tubes in PBS, and centrifuged at 500g for 10 minutes at 4oC. Cells were resuspended in lysis buffer (20 mM HEPES pH 7.4, 250 mM sucrose supplemented with protease inhibitors from Pierce) and disrupted by repeated passage through a 30-gauge needle. Cell lysates were centrifuged twice at 1,000g for 10 minutes at 4°C. The post nuclear supernatant was transferred into an ultracentrifuge tube (Beckman Coulter #343775) and centrifuged at 100,0000g for 1h at 4oC in a TLA100 rotor. The supernatant was removed and supplemented with 6x SDS loading dye. The pellet was washed once with lysis buffer, resuspended in equal volume of lysis buffer, and supplemented with SDS loading dye. Samples were analyzed by immunoblotting as described.

3.5.13 *Transferrin recycling and immunostaining assay s*

For the transferrin recycling assay WT and *Eipr1KO* 832/13 cells were seeded onto 24-wells plate and grown in complete media until they reached confluence. Cells were placed in warm

uptake medium for a 25 minutes pulse (Serum free RPMI + 1% BSA + 25 mM HEPES + 50 µg/mL Alexa 488-Transferrin (Invitrogen #T13342)). Medium was then exchanged for complete RPMI medium and cells were chased for the indicated times, washed, and transferred onto ice. Cells were washed 2X with ice-cold PBS and detached on ice with 10mM EDTA in PBS for 30 minutes to 1 hour with manual agitation and gentle pipetting. Detached single cells were transferred into a microcentrifuge tube and fixed at 4°C with 4% PFA (final concentration ~ 3.5%) for 10 minutes on a nutator to avoid clumping. Fixed cells were washed with PBS and analyzed by FACS using a LSRII (BD Biosciences). Data were analyzed using FlowJo.

For transferrin immunostaining cells were seeded onto cover slips in 24-well plates for 24 to 48 hours. Cells were then placed in warm uptake medium for a 25 minutes pulse (Serum free RPMI + 1% BSA + 25 mM HEPES + 50 µg/mL Alexa 568-Transferrin (Invitrogen #T23365)), washed 2X with ice-cold PBS , and fixed with 4% PFA as already described.

3.5.14 *Quantitative RT-PCR*

WT or *Eipr1KO* cells were grown in 10 cm plates, harvested in 1 ml of TRIzol (Invitrogen), and frozen at -80°. Total RNA was isolated following the manufacturer's protocol and cDNA was synthesized from 1 µg RNA using the QuantiTekt Reverse Transcription kit (Qiagen) according to the manufacturer's instructions. Each 10 µl qPCR reaction contained 1 µl of cDNA and 5 µl of 2× Sybr Green Master Mix (Kappa Biosystems). Absorbance was measured over 40 cycles using a CFX Connect Real-Time System (Biorad). The cycle quantification value (Cq) for each sample was measured using the provided software and normalized to actin control.

3.5.15 *Statistics*

Data were tested for normality by a Shapiro-Wilk test. When the data did not pass the normality test, we used the Kruskal-Wallis test followed by Dunn's test to investigate whether there was statistical significance between groups. When data passed the normality test, we used a 1-way ANOVA test with Bonferroni correction.

3.6 ACKNOWLEDGEMENTS

We thank Christopher Newgard, Ian Sweet and Duk-Su Koh for the 832/13 cell line, with the support of the UW DRC Cell Function and Analysis Core (DK17047); Suzanne Hoppins for the pBabe vector, plat-E cells, and protocol for lentiviral production and infection; Juan Bonifacino for the EARP and GARP subunit plasmids; Cedric Asensio for the ANF::GFP plasmid; Alex Merz and Sharon Tooze for antibodies. This work was supported by a University of Washington Diabetes Research Center Pilot and Feasibility Award (NIH grant P30 DK017047) and by NIH grant R01 GM121481.

3.7 FIGURES

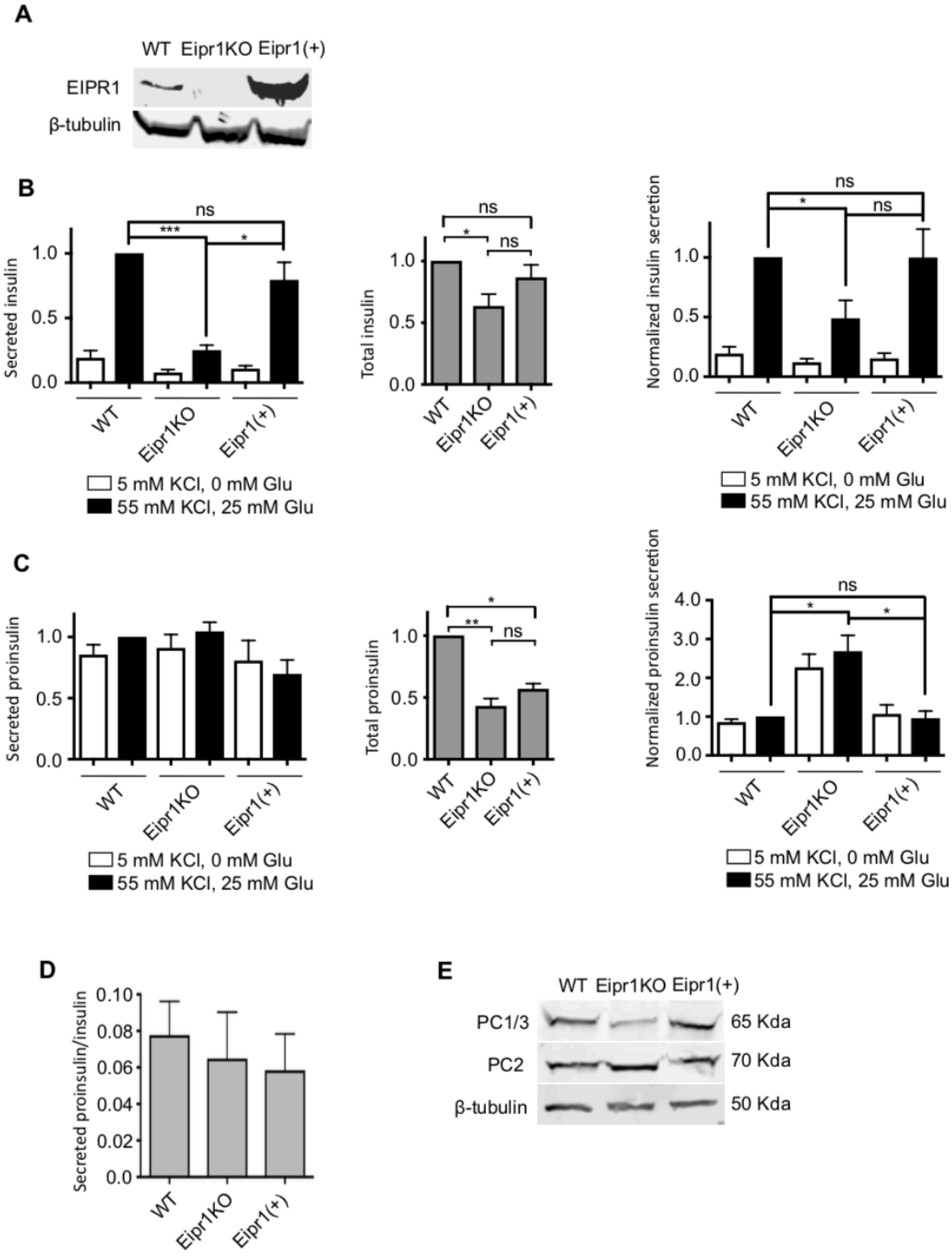
A
WT Eipr1KO Eipr1(+)
EIPR1
β-tubulin
B
Secreted insulin
Total insulin
Normalized insulin secretion
ns
*
***
WT
Eipr1KO
Eipr1(+)
5 mM KCl, 0 mM Glu
55 mM KCl, 25 mM Glu
C
Secreted proinsulin
Total proinsulin
Normalized proinsulin secretion
**
D
Secreted proinsulin/insulin
E
PC1/3
PC2
β-tubulin
65 Kda
70 Kda
50 Kda

Figure 3. 1 Insulin secretion is reduced in *Eipr1KO* cells

A, *Eipr1KO* cells do not express wild type EIPR1. Protein extracts from WT, *Eipr1KO*, and *Eipr1KO* 832/13 cells expressing a wild type Eipr1 cDNA (Eipr1(+)) were blotted with an EIPR1 antibody. β-tubulin served as a loading control.

B, (Left panel) Insulin secretion under resting (5 mM KCl, 0 mM glucose) and stimulating conditions (55 mM KCl, 25 mM glucose) from WT, *Eipr1KO,* and Eipr1(+) 832/13 cells. All values were normalized to the value of the WT under stimulating conditions. (n= 7; *$p<0.05$, ***$p<0.001$, error bars are +/- SEM). (Middle panel) Total insulin content in WT, *Eipr1KO*, and Eipr1(+) cells. All values were normalized to the WT. (n= 7; *$p<0.05$, ns $p>0.05$, error bars are +/- SEM). (Right panel) Insulin secretion normalized to insulin content under resting (5 mM KCl, 0 mM glucose) and stimulating conditions (55 mM KCl, 25 mM glucose) from WT, *Eipr1KO*, and Eipr1(+) cells. All values were normalized to the WT under stimulating conditions. (n= 7; *$p<0.05$, ns $p>0.05$, error bars are +/- SEM).

C, (Left panel) Proinsulin secretion under resting (5 mM KCl, 0 mM glucose) and stimulating conditions (55 mM KCl, 25 mM glucose) from WT, *Eipr1KO*, and Eipr1(+) cells. All values were normalized to the value of the WT under stimulating conditions. (n= 6). (Middle panel) Total proinsulin content in WT, *Eipr1KO*, and Eipr1(+) cells. All values were normalized to the WT. (n= 6; *$p<0.05$, **$p<0.01$, ns $p>0.05$, error bars are +/- SEM) (Right panel) Normalized proinsulin secretion under resting (5 mM KCl, 0 mM glucose) and stimulating conditions (55 mM KCl, 25 mM glucose) from WT, *Eipr1KO*, and Eipr1(+) cells. All values were normalized to the WT under stimulating conditions. (n= 6; *$p<0.05$, ns, $p>0.05$, error bars are +/- SEM).

D, Ratio total cellular proinsulin vs total insulin.

E, PC1/3 processed levels are reduced in *Eipr1KO* 832/13 cells but PC2 processed levels remain unaffected. Protein extracts from WT, *Eipr1KO,* and Eipr1(+) 832/13 cells were blotted with antibodies against PC1/3 and PC2. β-tubulin served as a loading control.

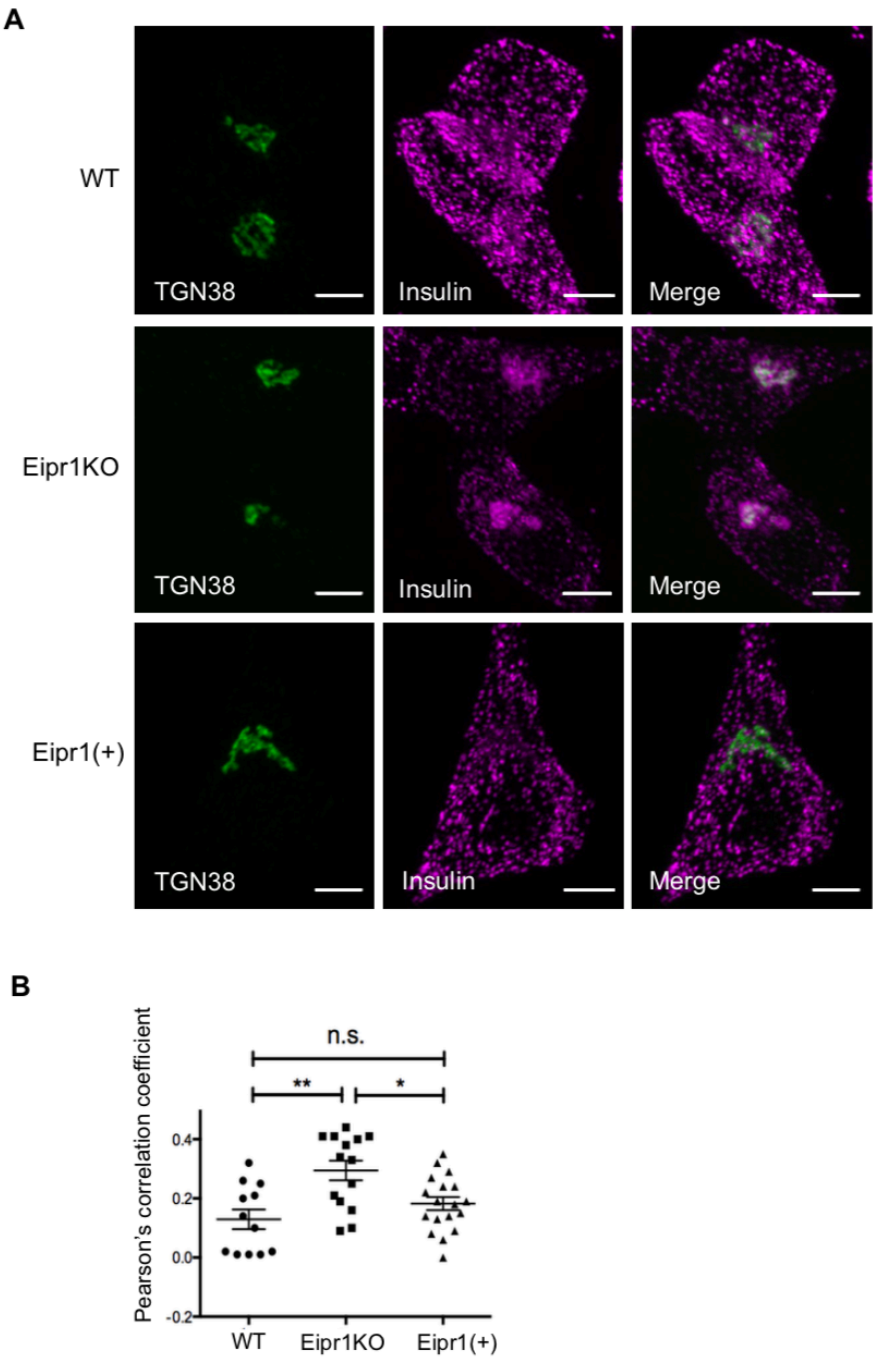

Figure 3. 2 Localization of insulin is disrupted in *Eipr1KO* cells

A, Representative images of WT, *Eipr1KO,* and Eipr1(+) 832/13 cells costained for endogenous insulin and TGN38. Scale bar: 5 µm. In wild type and Eipr1(+) cells, insulin is spread throughout the cytoplasm, but in *Eipr1KO* cells insulin accumulates in a perinuclear region that partially overlaps with TGN38. The experiment was repeated at least three times and the experimenter was blinded for the genotypes of the stained cells.

B, Pearson's correlation coefficient was measured to quantify the localization between insulin and the TGN marker TGN38 (see Material and Methods, n=12 for WT, n=14 for *Eipr1KO* and n=18 with Eipr1(+), **p<0.01, *p<0.05, ns, p>0.05). The experiment was repeated three or more times.

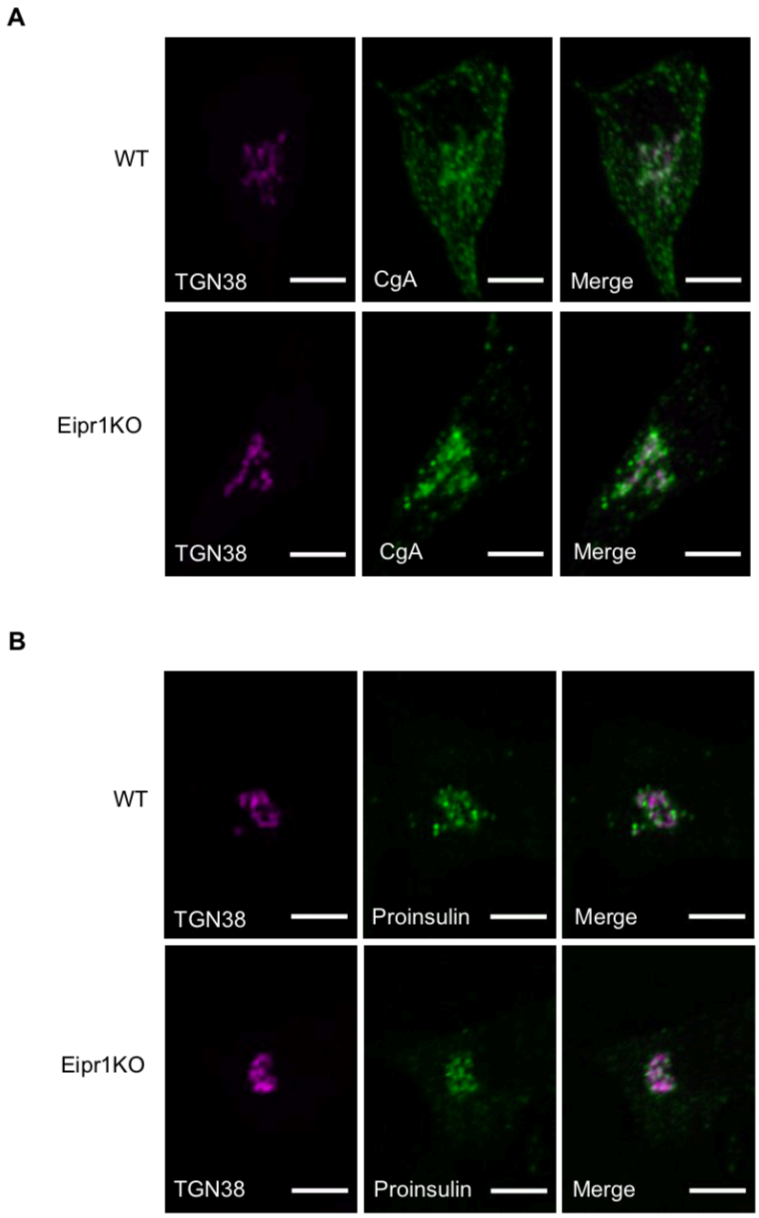

Figure 3. 3 Localization of chromogranin A and proinsulin in *Eipr1KO* cells

A, Representative images of WT and *Eipr1KO* 832/13 cells costained for endogenous chromogranin A (CgA) and TGN38. Scale bar: 5 μm. In wild type cells CgA is spread throughout the cytoplasm, but in *Eipr1KO* cells CgA accumulates in a perinuclear region that partially overlaps with TGN38.

B, Representative images of WT and *Eipr1KO* 832/13 cells costained for endogenous proinsulin and TGN38. Scale bar: 5 μm. In both WT and *Eipr1KO* cells, proinsulin is localized in a perinuclear region that partially overlaps with TGN38.

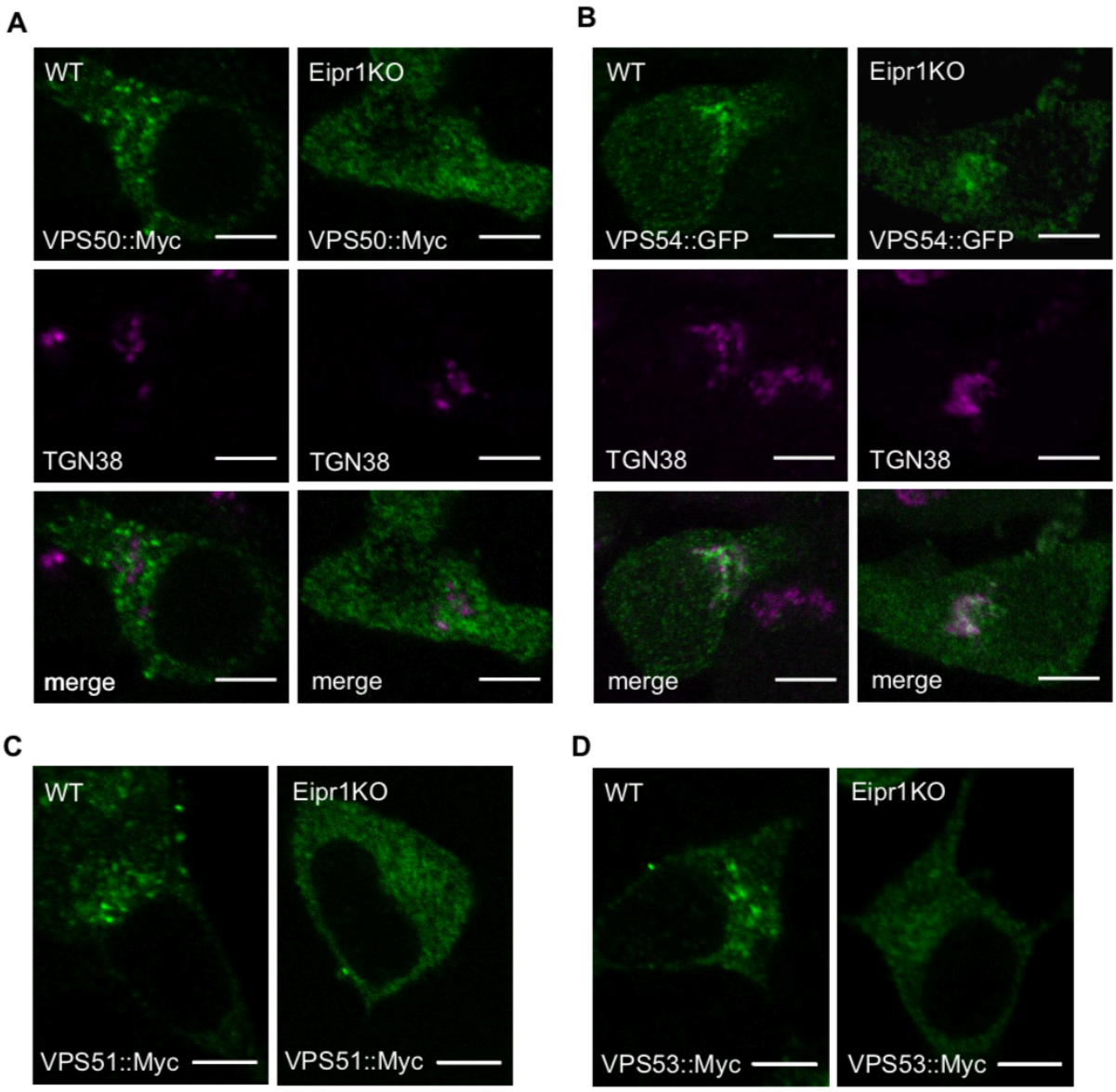

Figure 3. 4 Localization of GARP and EARP subunits is disrupted in *Eipr1KO* cells

A, Representative images of WT and *Eipr1KO* 832/13 cells transfected with VPS50::13Myc (VPS50::Myc) and costained with anti-Myc and anti-TGN38 antibodies. Scale bar: 5 µm. In wild type cells, VPS50::13Myc is localized in puncta but in *Eipr1KO* cells fluorescence is diffuse throughout the cytoplasm. Note that the punctate pattern of localization of VPS50::13Myc overlaps only partially with TGN38.

B, Representative images of WT and *Eipr1KO* 832/13 cells transfected with VPS54::GFP (VPS54::GFP) and costained with anti-GFP and anti-TGN38 antibodies. Scale bar: 5 µm. Both in wild type and *Eipr1KO* cells VPS54::GFP is localized in perinuclear puncta that largely overlap with TGN38.

C, Representative images of WT and *Eipr1KO* 832/13 cells transfected with VPS51::13Myc (VPS51::Myc) and stained with anti-Myc antibody. Scale bar: 5 μm. In wild type cells VPS51::13Myc is localized in puncta but in *Eipr1KO* cells fluorescence is diffuse throughout the cytoplasm.

D, Representative images of WT and *Eipr1KO* 832/13 cells transfected with VPS53::13Myc (VPS53::Myc) and stained with anti-Myc antibody. Scale bar: 5 μm. In wild type cells VPS53::13Myc is localized in puncta but in *Eipr1KO* cells fluorescence is diffuse throughout the cytoplasm.

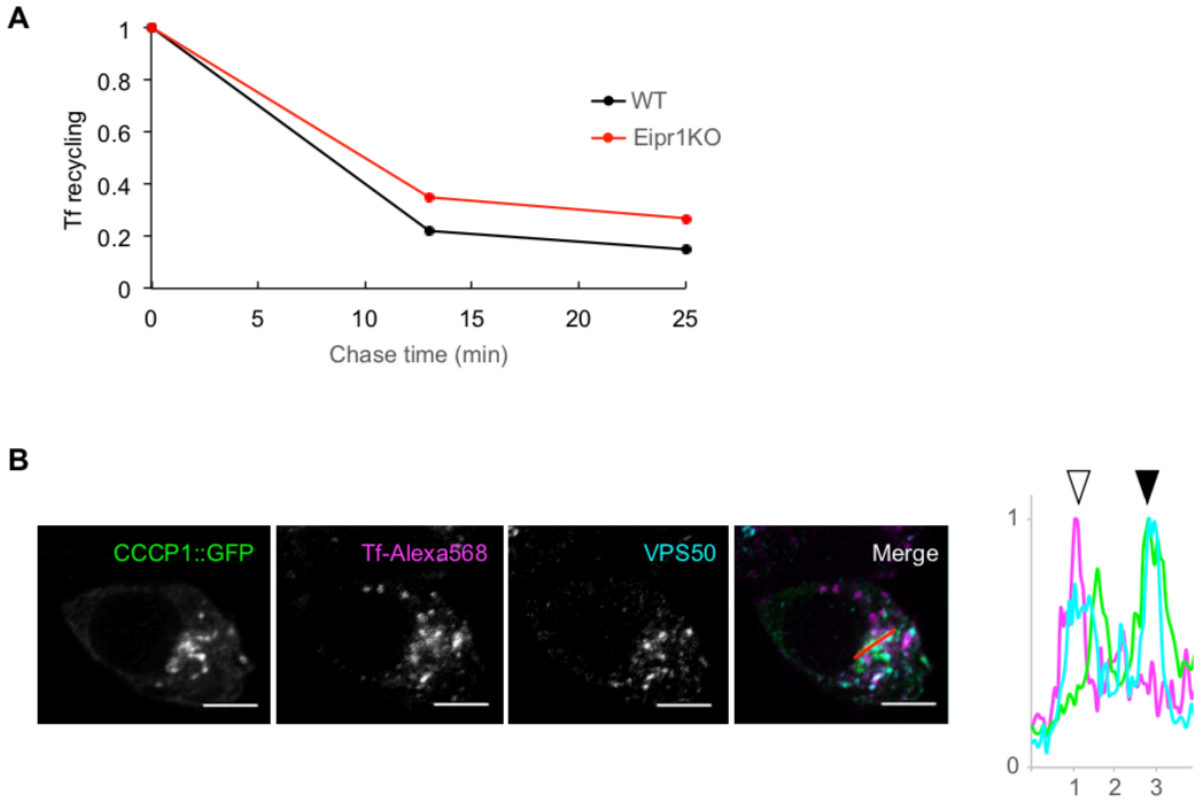

Figure 3. 5 EIPR1 is needed for transferrin recycling and EARP localizes in two distinct pools in the cell

A, EIPR1 is needed for transferrin recycling. FACS analysis of Alexa 488- labeled transferrin in WT and *Eipr1KO* 832/13 cells following a chase experiment after 25 min uptake.

B, EARP localizes in at least two distinct pools; a CCCP1-positive pool and an endosomal transferrin- positive pool. 832/13 cells were transiently transfected with GFP-tagged CCCP1, incubated with Alexa 568-labeled transferrin and immunostained for VPS50 and GFP. (Left) Representative confocal images of cells co-stained for endogenous VPS50 and GFP. Scale bar: 5 µm. (Right) The graph shows a representative intensity plot of normalized signal intensity versus distance in µm for each channel (Green: GFP, Magenta: Tf and Cyan: VPS50). White arrowhead: Overlap between VPS50 and Tf. Black arrowhead: Overlap between VPS50 and CCCP1.

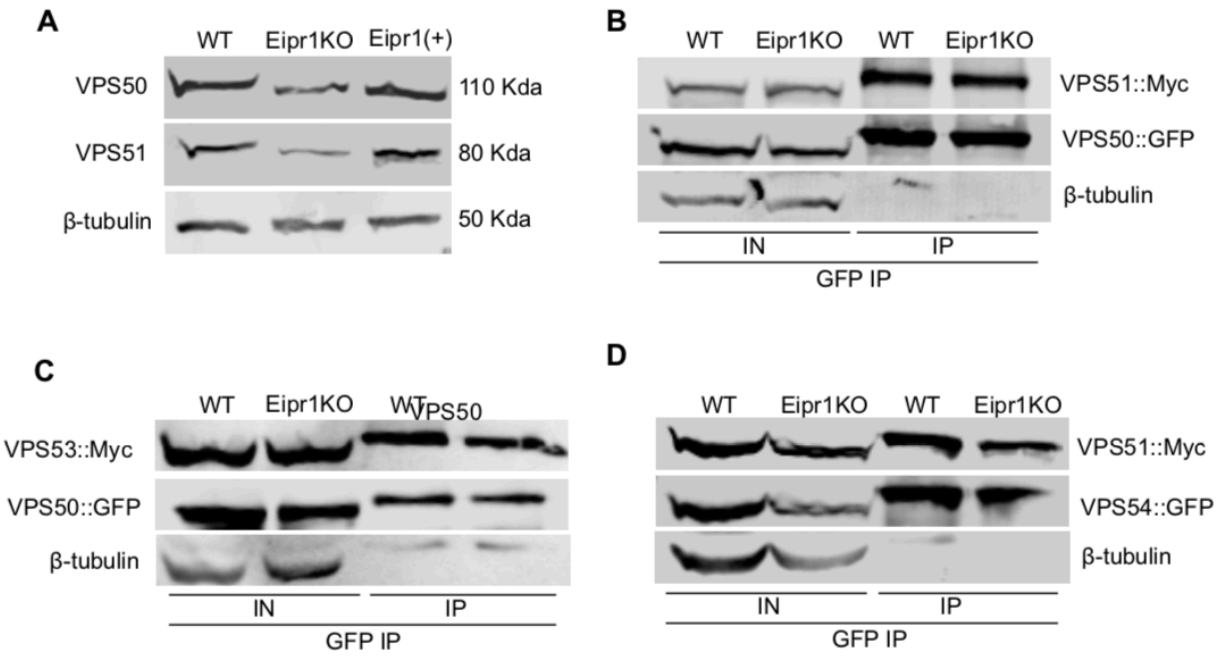

Figure 3. 6 Stability and interactions of EARP and GARP subunits in the absence of Eipr1

A, VPS50 and VPS51 levels are reduced in *Eipr1KO* cells. Protein extracts from WT, *Eipr1KO* and Eipr1(+) 832/13 cells were blotted with antibodies against VPS50 and VPS51. β-tubulin served as a loading control.

B, VPS50 interacts with VPS51 in an EIPR1-independent way. EGFP-tagged VPS50 was coexpressed with 13Myc-tagged VPS51 in WT and *Eipr1KO* 832/13 cells. Immunoprecipitation of VPS50::GFP pulled down VPS51::Myc, but not β-tubulin, independent of EIPR1. IN: input. IP: immunoprecipitated.

C, VPS50 interacts with VPS53 in an EIPR1-independent way. EGFP-tagged VPS50 was coexpressed with 13Myc-tagged VPS53 in WT and *Eipr1KO* 832/13 cells. Immunoprecipitation of VPS50::GFP pulled down VPS53::Myc, but not β-tubulin, independent of EIPR1. IN: input. IP: immunoprecipitated.

D, VPS51 interacts with VPS54 in an EIPR1-independent way. EGFP-tagged VPS54 was coexpressed with 13Myc-tagged VPS51 in WT and *Eipr1KO* 832/13 cells. Immunoprecipitation of VPS54::GFP pulled down VPS51::Myc, but not β-tubulin, independent of EIPR1. IN: input. IP: immunoprecipitated

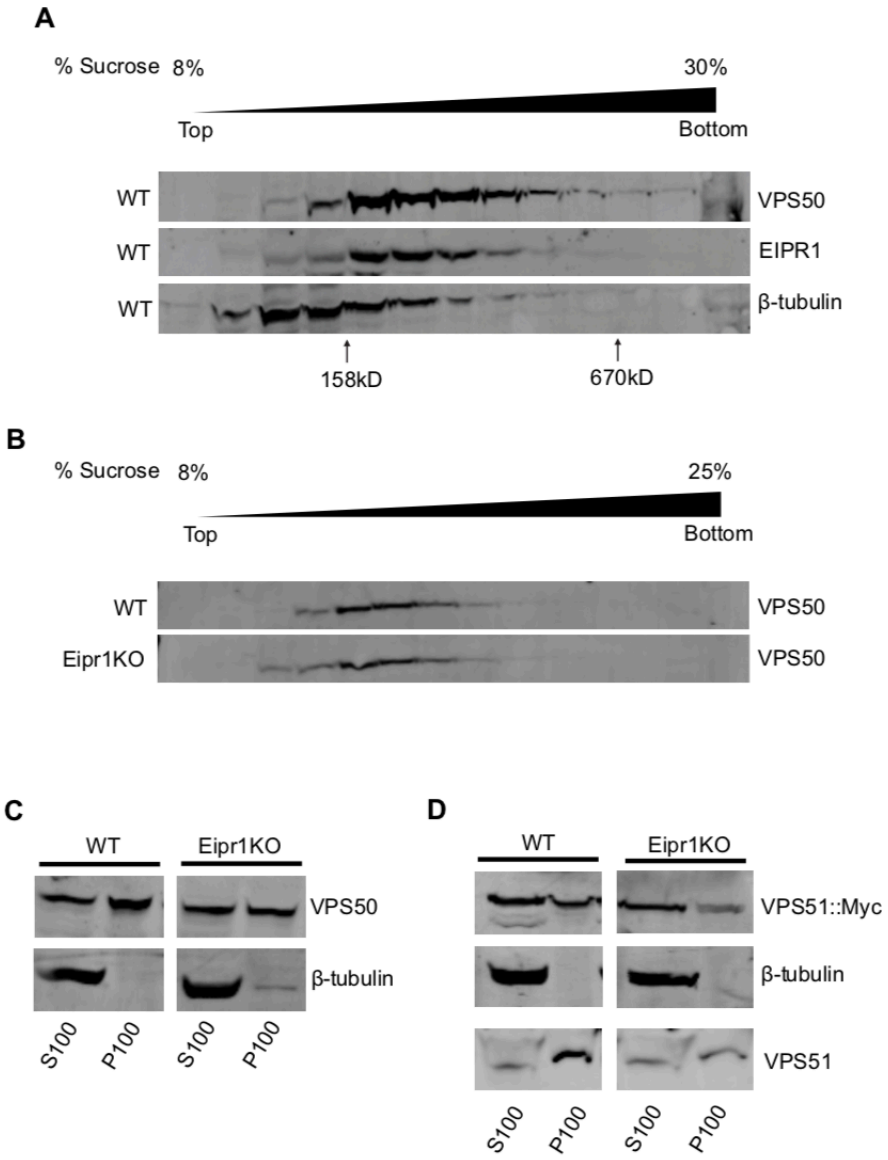

Figure 3. 7 Stability of the EARP complex and association of the EARP and GARP complex with membranes in *Eipr1KO* cells

A, VPS50 and EIPR1 cofractionate on a linear 8%-30% sucrose velocity gradient. Fractions from WT 831/13 cell lysate were blotted with antibodies against VPS50 and EIPR1. β-tubulin served as a control soluble protein.
B, VPS50 fractionates similarly from cell lysates of WT and *Eipr1KO* 832/13 cells on a linear 8%-25% sucrose velocity gradient. Fractions from WT and *Eipr1KO* 832/13 cell lysates were blotted with antibodies against VPS50.
C, VPS50 associates with membranes in a manner partially dependent on EIPR1. In 832/13 cell fractions, endogenous VPS50 was found primarily in the post-nuclear P100 membrane fraction. In *Eipr1KO* 832/13 cells, VPS50 was equally distributed between the post-nuclear P100 membrane fraction and the S100 cytosolic fraction. β-tubulin served as a control soluble protein. S100, P100:

supernatant and pellet fractions obtained by a 100,000g spin of the cell lysate, containing cytosolic and membrane-associated proteins respectively.
D, VPS51 associates with membranes in an EIPR1-dependent manner. In 832/13 cell fractions, VPS51::13Myc (VPS51::Myc) was roughly equally distributed between the post-nuclear P100 membrane fraction and the S100 cytosolic fraction and endogenous VPS51 was found primarily in the post-nuclear P100 membrane fraction. In *Eipr1KO* 832/13 cells, VPS51::Myc was mostly found in the S100 soluble fraction and endogenous VPS50 was equally distributed between the post-nuclear P100 membrane fraction and the S100 cytosolic fraction . β-tubulin served as a control soluble protein. S100, P100: supernatant and pellet fractions obtained by a 100,000g spin of the cell lysate, containing cytosolic and membrane-associated proteins respectively.

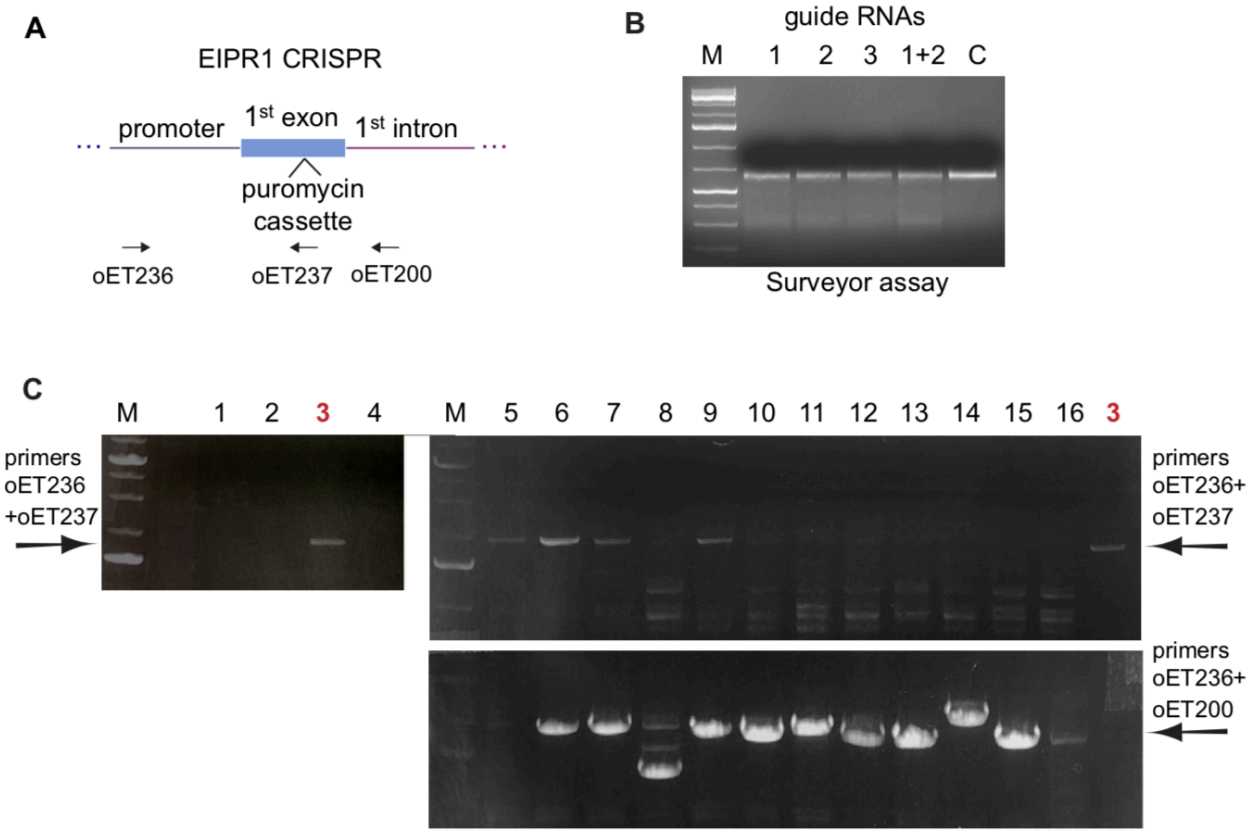

Figure S3. 1 . *Eipr1KO* strategy using the CRISPR technology

A, Surveyor nuclease assay testing the efficiency of three different guide RNAs (1, 2, 3) and the combination of guide RNAs #1 and #2 (1+2). All three guide RNAs recognize sequences at or around the 1st exon of rat Eipr1 (see Materials and Methods). Guide RNA #1 was used for all subsequent experiments. C: control.

B, To make the *Eipr1KO* 832/13 cell line, Cas9-induced DNA cleavage was used to insert a puromycin cassette in the first exon of Eipr1. oET236, oET237 and oET200 are the primers used in (C) for detecting the positive clones.

C, PCR detection of the Eipr1 CRISPR positive clones using the indicated primers. Primers oET236 and oET237 detect clones positive for the puromycin insertion. Primers oET236 and oET200 detect clones that contain the wild type product. Clones #3 and #5 were selected as candidate *Eipr1KO*s. A Western blot showed that clone #3 lacked EIPR1 expression (Figure 1A), but that #5 still expressed the wild type EIPR1 product. Clone #3 was used for all the *Eipr1KO* experiments in this study.

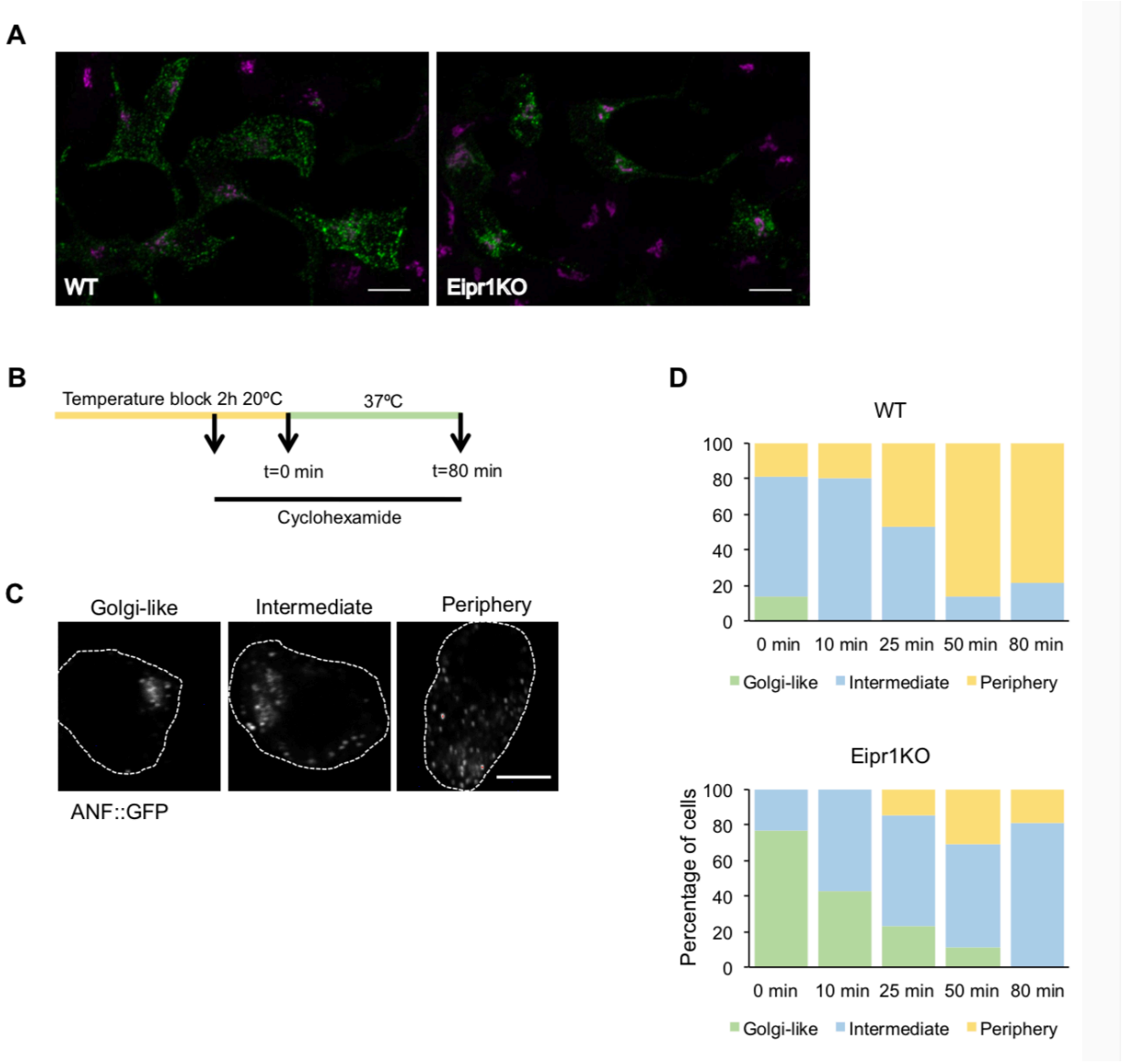

Figure S3. 2 Monitoring the exit of ANF::GFP from the TGN using a pulse-chase method

A, The exogenous DCV cargo ANF::GFP accumulates near the TGN in *Eipr1KO* cells. Representative images of WT and *Eipr1KO* 832/13 cells transfected with ANF::GFP and costained for GFP and TGN38. Maximum intensity projection. Scale bar: 10 µm.

B, Schematic of the pulse-chase experiment. Cells transiently transfected with ANF::GFP were incubated at 20°C for 2 h to cause the accumulation of DCV cargos at the TGN (pulse). 30 minutes before the end of the temperature block, cycloheximide was added to block protein translation. At the end of the temperature block, cells were returned to 37°C and incubated for various times (chase) before fixation and immunostaining.

C, Representative images of the cell categories used for qualitative assessment of TGN exit depending on whether ANF::GFP was (1) concentrated at the TGN region (Golgi-like), (2) distributed both at the TGN and at the cell periphery (Intermediate), or (3) excluded from the TGN (Periphery). Scale bar: 5 µm.

D, Percentage of WT or *Eipr1KO* 832/13 cells with the indicated ANF::GFP distribution at the indicated time points. The data from one representative experiment is plotted as percentage of each phenotype. For each data point and each genotype, 50 to100 cells were counted blindly. The experiment was repeated three times with similar results.

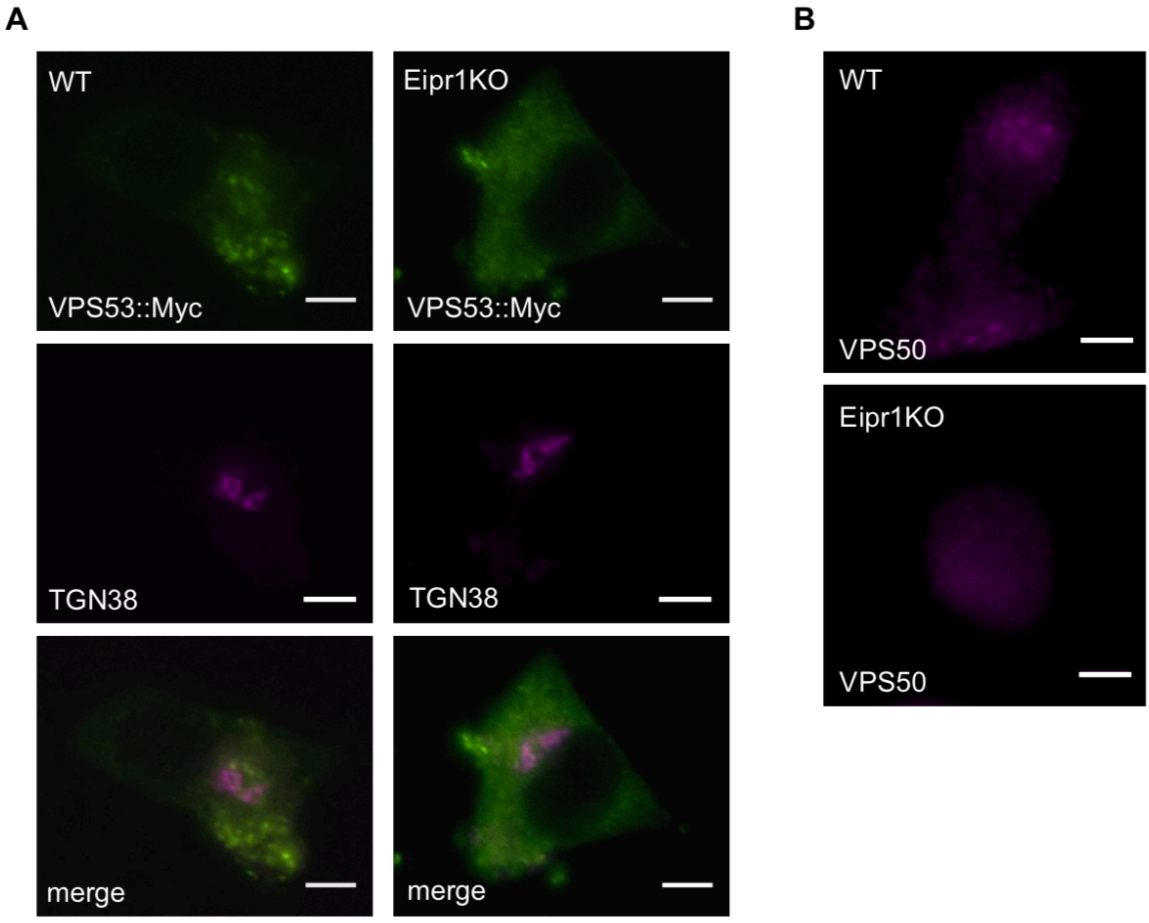

Figure S3. 3 Localization of VPS53::Myc and endogenous VPS50 is disrupted in *Eipr1KO* cells

A, Representative images of WT and *Eipr1KO* 832/13 cells transfected with VPS53::13Myc (VPS53::Myc) and costained with anti-Myc and anti-TGN38 antibodies. Scale bar: 5 μm. VPS53::13Myc is punctate in wild type cells but diffuse throughout the cytoplasm in *Eipr1KO* cells. Note that the punctate pattern of localization of VPS53::13Myc does not overlap with TGN38.

B, Representative images of WT and *Eipr1KO* 832/13 cells stained with anti-VPS50 antibody. Scale bar: 5 μm. Endogenous VPS50 is punctate in wild type cells, but diffuse throughout the cytoplasm in *Eipr1KO* cells.

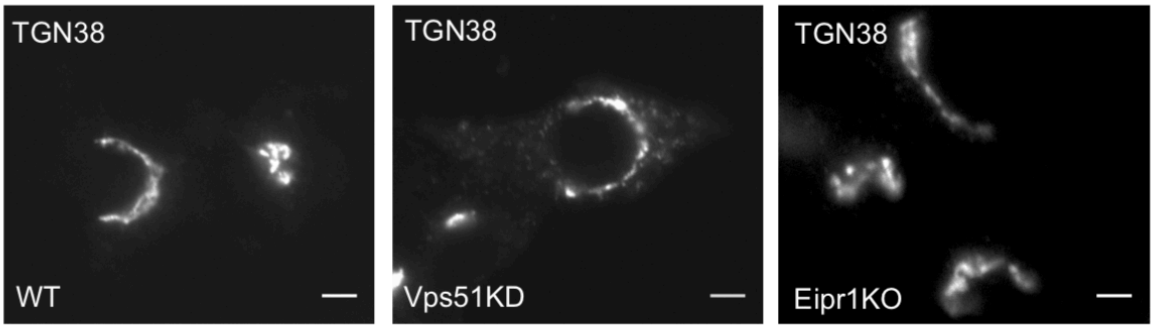

Figure S3. 4 TGN38 is redistributed in Vps51 knockdown but not *Eipr1KO* cells

Representative images of WT, Vps51 knockdown 832/13 cells (Vps51KD), and *Eipr1KO* 832/13 cells stained with TGN38. Note that TGN38 is partially redistributed to cytoplasmic puncta in VPS51 knockdown cells, but is still localized to the Golgi in *Eipr1KO* cells.

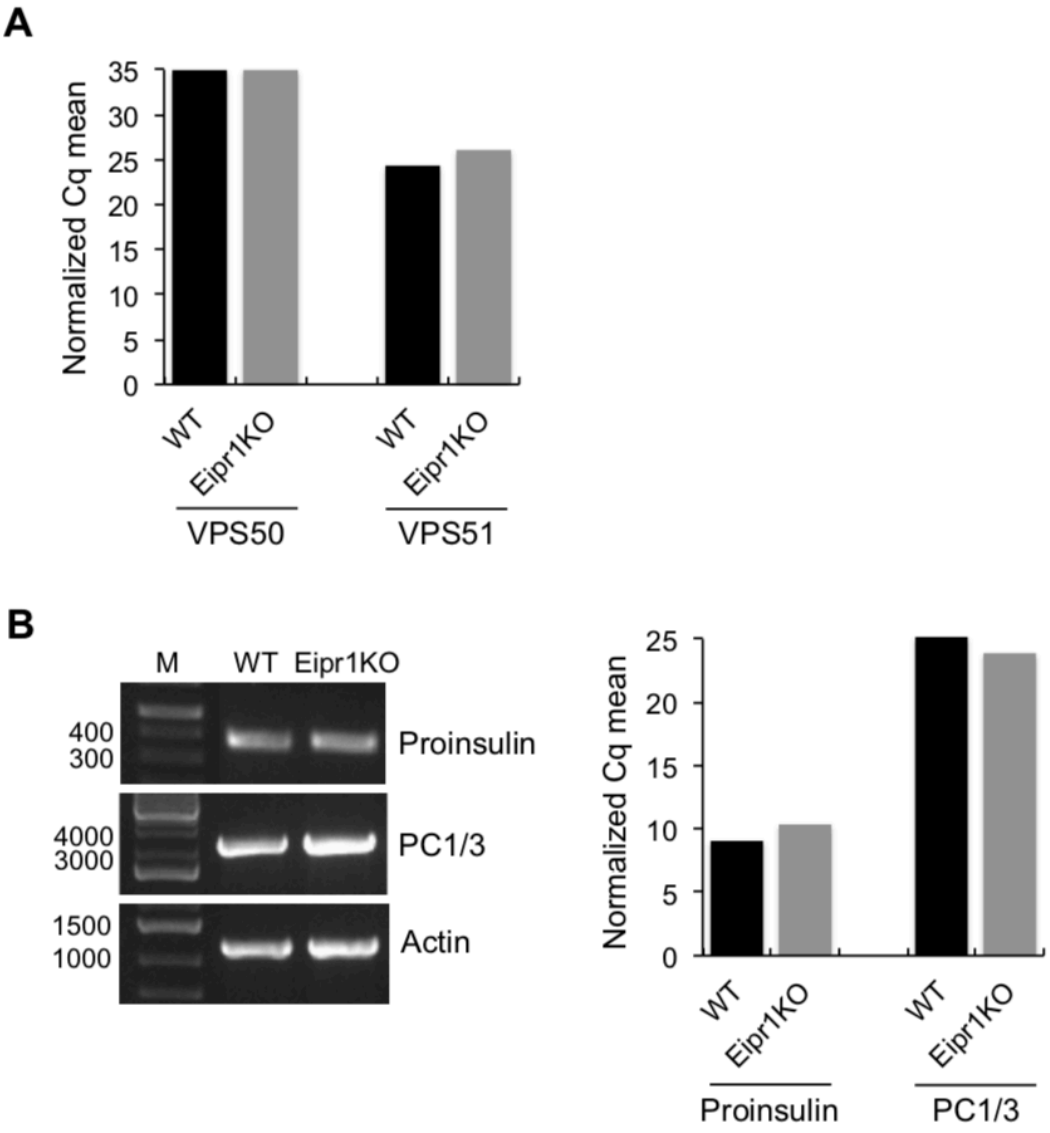

Figure S3. 5 EIPR1 knock out doesn't affect the transcript abundance of DCV cargos and EARP or GARP subunits

No change in transcript abundance of (A) VPS50 and VPS51, (B) proinsulin and PC1/3 in *Eipr1KO* cells as measured by qRT-PCR. Actin served as an internal control. The Cq mean for the target genes was normalized against the Gq mean for the actin control.

Chapter 4. CCCP1 IS A REGULATOR OF CARGO SORTING TO THE REGULATED SECRETORY PATHWAY

4.1 ABSTRACT

The regulated release of peptide hormones, neuropeptides and monoamines depends on their being packaged into dense-core vesicles (DCVs). How these vesicles are made and how their cargo is properly selected is not well understood, especially at the molecular level. DCVs are generated at the trans-Golgi network (TGN) and go through post-Golgi maturation steps, including peptide processing and removal of cargo such carboxypeptidase D (CPD), that are not destined to the regulated secretory pathway. In screens for mutants that affect DCV function, we identified several conserved molecules; including the coiled-coil containing protein CCCP1, the endosome-associated recycling complex (EARP), and the EARP-interacting protein EIPR1. We generated *Cccp1KO* insulin-secreting pancreatic beta 832/13 cells. We found that the KO cells have reduced secretion of insulin, and that mature insulin is retained near or at the TGN; similar to what we have reported in *Eipr1KO* cells. In a proximity labelling BioID screen, we found that CCCP1 is in close proximity to the transmembrane protein CPD. CPD localizes to the TGN, but in *Cccp1KO* cells (and in *Eipr1KO* cells), CPD is missorted to mature DCVs. Both CCCP1 and EARP colocalize near TGN and immature DCV markers, while there is a second pool of EARP at recycling endosomes. Interestingly, we find that overexpression of CCCP1 recruits the EARP complex or interacts with an EARP-positive membrane compartment. Thus, CCCP1 controls luminal cargo

sorting to DCVs at the TGN, removal of cargo not destined to the regulated secretory pathway in a post-Golgi step and localization of the EARP complex.

4.2 INTRODUCTION

Dense-core vesicles (DCVs) are secretory vesicles found in neurons and endocrine cells that store and release neuropeptides, growth factors, biogenic amines, digestive enzymes, and peptide hormones. These cargos are released in a regulated manner in response to external stimuli, and modulate a variety of physiological processes; including development, growth, metabolism, and mental state. DCVs are generated at the trans-Golgi network (TGN) as immature DCV (iDCVs) and go through a maturation process, which includes cargo sorting into and out of iDCVs, and acquisition of proper compartmental identity and release competency (Borgonovo et al., 2006; Gondré-Lewis et al., 2012; Kim et al., 2006; Tooze et al., 2001). Despite the importance of DCV cargos in physiology, how DCVs are made and how their proper cargo is selected is poorly understood-- especially at the molecular level.

Genetic studies in the nematode *C. elegans* have identified several new molecules that function in neuronal DCV biogenesis, including the small G protein RAB-2, its effector, the coiled-coil containing protein 1 (CCCP-1), the endosome-associated recycling protein (EARP) complex composed of four subunits (VPS50, VPS51, VPS52 and VPS53), and its interactor EIPR-1 (Ailion et al., 2014; Cattin-Ortolá et al., 2017; Edwards et al., 2009; Paquin et al., 2016; Sumakovic et al., 2009). These proteins act in the same genetic pathway. In mutants of *rab-2*, normal DCVs in number and morphology are made, but they have reduced transmembrane and luminal cargo (Ailion et al., 2014; Edwards et al., 2009; Sumakovic et al., 2009; Topalidou et al., 2016). In *C.*

elegans and in insulin secreting insulinoma cells (832/12 cell line an INS-1 derivative (Hohmeier et al., 2000)), RAB2 and CCCP1 localize near the TGN, where the early steps of DCV biogenesis take place (Ailion et al., 2014; Cattin-Ortolá et al., 2017). Together, these data suggest that RAB2 and CCCP1 control cargo sorting to DCVs.

In this study we use *Cccp1* knock out (*Cccp1KO*) and rescue experiments in 832/13 cells to investigate the role of CCCP1 in DCV biogenesis, maturation, and cargo selection. We find that in the absence of CCCP1, insulin secretion is reduced and that insulin accumulates at or around the Golgi. In a proximity biotinylation BioID screen (Roux et al., 2012; Shin et al., 2017), we find that CCCP1 is in close proximity to the transmembrane protein carboxypeptidase D (CPD). CPD localizes to the TGN and to immature DCVs (iDCVs), but gets removed from iDCVs during maturation (Bonnemaison et al., 2014; Varlamov and Fricker, 1998; Varlamov et al., 1999b, 1999a). Interestingly, in the absence of CCCP1 or EIPR1, CPD gets missorted to mature DCVs. In subcellular localization studies, we find that CCCP1 and EIPR1/EARP colocalize near the TGN and to iDCVs, while EIPR1/EARP also localizes to recycling endosomes. Interestingly, we find that overexpression of CCCP1 relocates EARP to CCCP1-positive compartments, indicating that CCCP1 recruits EARP or interacts with an EARP-positive membrane compartment. By super-resolution microscopy, we show that CCCP1 forms ~200 nm diameter circles around proinsulin, suggesting that CCCP1 localizes around iDCVs, proinsulin-positive TGN subdomains, or both. Together, these localization and functional studies suggest that CCCP1 controls: (1) cargo sorting to DCVs at the TGN, (2) removal of CPD from iDCVs in a post-Golgi step, and (3) recruitment of the EARP complex. We propose that CCCP-1 is a major sorting factor for the regulated secretory pathway.

4.3 RESULTS

4.3.1 *CCCP-1 and EIPR-1/EARP act in the same genetic pathway in C. elegans to control locomotion and dense-core vesicle cargo sorting*

C. elegans mutants in *rab-2, cccp-1, eipr-1,* and in all four subunits of the EARP complex (*vps-50, vps-51, vps-52, vps-53*) have slow locomotion rates and reduced axonal levels of DCV cargos (Ailion et al., 2014; Cattin-Ortolá et al., 2017; Edwards et al., 2009; Paquin et al., 2016; Sumakovic et al., 2009). We have previously shown that CCCP-1, EIPR-1, and EARP act in the RAB-2 genetic pathway (Ailion et al., 2014; Cattin-Ortolá et al., 2017; Edwards et al., 2009; Paquin et al., 2016; Sumakovic et al., 2009). While EIPR-1 and EARP complex subunits act in the same pathway, it is unknown whether CCCP-1 and EIPR-1/EARP act in the same pathway, or if they act in parallel pathways that converge with RAB-2. To test this, we built double mutants between *cccp-1* and either *eipr-1* or *vps-50* and assayed their locomotion rate (Figure 4. 1 A) and the axonal levels of the DCV soluble cargo NLP-21 tagged to Venus (Figure 4. 1 B). In both cases, their double mutants have similar phenotypes to the single mutants (Figure 4. 1 A,B), suggesting that CCCP-1 and EIPR-1/EARP act in the same genetic pathway to control locomotion behavior and cargo sorting to DCVs.

4.3.2 *CCCP1 is required for insulin secretion*

The mammalian CCCP1 homolog is known as CCDC186 or C10orf118. We will use the name CCCP1 throughout this study. Using a commercially available antibody to human CCCP1 (C10orf118), we found that CCCP1 is expressed in multiple tissues in mice, including brain, heart, kidney, and spleen (Figure 4. 2 A). To investigate a possible role for mammalian CCCP1 in DCV

cargo-sorting, we generated *Cccp1* knock out (KO) rat insulinoma 832-13 cells using the CRISPR technology. To confirm that CCCP1 was missing in the *Cccp1KO* line, we analyzed the cells for CCCP1 expression by immunofluorescence and immunoblotting (Figure 4. 2 B,C).

To examine whether CCCP1 is needed for DCV cargo sorting in 832/13 cells, we measured the insulin secretion of WT and *Cccp1KO* cells under resting (5 mM KCl, no glucose) and stimulating (55 mM KCl, 25 mM glucose) conditions. While insulin secretion under resting conditions was not noticeably impacted by the absence of CCCP1, stimulated insulin secretion was significantly reduced (to ~ 49% of WT, Figure 4. 3 A). To verify that the effects were specifically due to loss of CCCP1, we introduced a wild type CCCP1 cDNA back into the *Cccp1KO* cells by lentiviral transduction (Figure 4. 2 B,C). Expression of wild type CCCP1 in *Cccp1KO* cells (Cccp1(+)) rescued the insulin secretion defect of the *Cccp1KO* line, indicating that the insulin secretion defect is due to loss of CCCP1 (Figure 4. 3 A).

The defective insulin secretion observed could be due to reduced insulin content. Thus, we measured the total cellular amount of insulin and found that it was slightly but not significantly increased in *Cccp1KO* cells (Figure 4. 3 B). After normalizing resting and stimulated secreted insulin against total insulin, we found that the stimulated secreted insulin is still significantly reduced in the *Cccp1KO* line (~ 41% of WT, Figure 4. 3 C) but only partially rescued in Cccp1(+) cells (Figure 4. 3 C). Thus, in *Cccp1KO* cells, insulin doesn't get released properly.

Next, we examined the levels of the prohormone convertase 1/3 (PC1/3 or PCSK1), which is required for the processing of proinsulin into insulin (Davidson, 2004; Hutton, 1994). We found that loss of CCCP1 resulted in reduced levels of PC1/3, that was partially rescued in Cccp1(+) cells (Figure 4. 3 D). The decrease in PC1/3 could result in impaired proinsulin processing into insulin. Therefore, we measured secreted and cellular levels of proinsulin. We found that secretion

slightly increased in *Cccp1KO* cells, but the difference didn't reach statistical significance. The cellular levels of proinsulin were slightly but significantly increased (~ 138% of WT) (Figure 4. 4 B). However, the ratio of total proinsulin to insulin was unchanged (Figure 4. 4 D). Altogether, our data suggest that CCCP1 is not required for proinsulin processing, but is rather required for the release of the mature form of insulin.

4.3.3 *CCCP1 is required for the localization of mature DCV cargos*

To investigate whether CCCP1 is needed for sorting insulin into DCVs, we examined the subcellular localization of insulin by immunostaining. In wild type cells, insulin was detected as puncta spread throughout the cytoplasm and accumulated at the cell periphery (Figure 4. 5 A, B). In contrast, in *Cccp1KO* cells, insulin seemed to accumulate in a perinuclear region that partially colocalized with the trans-Golgi (TGN) marker TGN38 (Figure 4. 5 A,B) and colocalized with beta-galactoside alpha-2,6-sialyltransferase tagged to GFP (ST6Gal1::GFP), a protein that localizes to the lumen of the trans-Golgi and the TGN (Roth et al., 1985) (Figure 4. 5 C). The insulin localization phenotype was fully rescued in *Cccp1KO* cells that stably expressed wild type CCCP1 (Figure 4. 5 A, B). Because our anti-insulin antibody also likely detects insulin's precursor form, proinsulin, we investigated whether it is insulin or proinsulin form that accumulates at the Golgi. We used an anti-proinsulin antibody specific to proinsulin that only stains a TGN-like perinuclear area and not the cell periphery (Figure 4. 6A). By immunofluorescence, we found that in *Cccp1KO* cells, the localization of proinsulin was unchanged (Figure 4. 6A). Given that the localization of proinsulin, the levels of both insulin and proinsulin, and the ratio of proinsulin/insulin are not largely affected by the absence of CCCP1, we propose that the mature form of insulin makes up the majority of that accumulating at a late Golgi-compartment of

Cccp1KO cells. To test whether the change in localization of insulin is specific to this particular DCV cargo, we also examined the localization of another luminal DCV cargo, chromogranin A (CgA), and found that its distribution was similarly defective in *Cccp1KO* cells (Figure 4. 6B,C). These results suggest that the reduced secretion of insulin is due to the reduced accumulation of mature insulin in DCVs localized at the cell periphery.

To investigate whether DCV cargo is stuck at the TGN in *Cccp1KO* cells, we used a pulse chase method to monitor the exit of the exogenous DCV cargo ANF::GFP from the TGN (Kögel et al., 2013; Kögel Tanja et al., 2010). At steady state, ANF::GFP was distributed throughout the cytoplasm in WT cells but it was accumulated near the TGN in *Cccp1KO* cells, like insulin (Figure 4. 7 A). ANF::GFP exit from the TGN was blocked with incubation at 20°C (pulse) and the synthesis of new proteins was inhibited by incubation with cycloheximide (Figure 4. 7 B) (Kögel et al., 2013; Kögel Tanja et al., 2010). After the temperature block, cells were brought back to 37ºC and incubated for the indicated time points (chase) (Figure 4. 7 B). Cells were then counted blindly based on whether ANF::GFP was (1) predominantly accumulated at the TGN-region ("Golgi-like" in Figure 4. 7 C, top), (2) found both at the TGN-region and at the cell periphery ("Intermediate" in Figure 4. 7 C middle), or (3) excluded from the Golgi ("Periphery") (Figure 4. 7 C, bottom). At every time point, the accumulation of ANF::GFP appeared to be more Golgi-like in *Cccp1KO* cells than in WT cells, but in both cell types the localization of ANF::GFP clearly went from mostly "Golgi-like" at t=0min to mostly "periphery" at the end of the chase period (t=50min) (Figure 4. 7 D). This indicates that DCV cargo eventually exits the TGN in *Cccp1KO* cells and reaches the cell periphery, even though it does so less efficiently than in WT cells.

4.3.4 *CCCP1 localizes to membranes positive for iDCV markers*

We previously reported that in *C. elegans* neurons, CCCP1 colocalizes with RAB-2 near the TGN and that in 832/13 cells it localizes at or close to the TGN and iDCVs (Ailion et al., 2014; Cattin-Ortolá et al., 2017). Here, we present a more detailed subcellular localization study in 832/13 cells. Endogenous CCCP1 localized to a perinuclear area, and co-labelling experiments revealed that it did not colocalize with markers of the ERGIC (ERGIC53, Figure 4. 8 A), cis-Golgi (GM130, Figure 4. 8 A), early endosome (EEA1, GFP::RAB5A and Alexa568-transferrin Figure 4. 8 and 9A), late endosome (GFP::RAB7A, Figure 4. 9 A), or recycling endosome (GFP::RAB4A and Alexa568-transferrin, Figure 4. 9 A). Interestingly, endogenous CCCP1 localized to an area adjacent to, but not overlapping with, the TGN marker TGN38 (Figure 4. 8 A). Neither did CCCP1 colocalize with TGN subdomains marked by Vti1a and Golgin-97 (Figure 4. 10 A). In contrast, CCCP1 colocalized with the SNARE protein Syntaxin6, and the DCV cargos Chromogranin A (CgA), insulin, and proinsulin (Figure 4. 8 A and 10A). Syntaxin6 and proinsulin localize to the TGN, but also to iDCVs, and are excluded from mDCVs (Klumperman et al., 1998; Wendler et al., 2001). The anti-CgA and anti-insulin antibodies stained a perinuclear area, and largely localized to puncta throughout the cytoplasm and the cell periphery, suggesting that it marks TGN, iDCVs and mDCVs. Quantification of those colocalization experiments confirmed our observations (Figure 4. 8 A). Furthermore, we found that endogenous CCCP1 colocalized with both rat RAB2 paralogs GFP::RAB2A and GFP::RAB2B (Figure 4. 9 B); which is consistent with results in *C. elegans* neurons, Drosophila, and COS cells (Ailion et al., 2014; Gillingham et al., 2014). We propose that CCCP1 likely localizes to iDCVs or a TGN subdomain positive for iDCV cargo.

If CCCP1 localizes to structures that bud off the TGN, treatment with brefeldin A (BFA) would increase the association of CCCP1 with the TGN. BFA is an inhibitor of Arf1 that blocks the formation of vesicular carriers at the Golgi (Klausner et al., 1992; Lippincott-Schwartz et al., 1991). We found that a 5 minute treatment with BFA increased partially but significantly the colocalization between TGN38 and CCCP1 (Figure 4. 10 B,C). Thus CCCP1, at least partially, localizes to Golgi-derived structures.

To study CCCP1's localization at higher resolution, we used structured illumination microscopy (SIM) (Figure 4. 11 A) and stimulated emission depletion (STED) microscopy (Figure 4. 11 B). With both techniques, we observed CCCP1 forming circular structures of variable sizes (ca. 200-500 nm diameter). Interestingly, several of these circular structures surrounded proinsulin. These results confirm that CCCP1 localizes either to iDCV membranes, to a subdomain of the TGN through which DCV cargo transits, or to both.

4.3.5 *CCCP1 localizes specifically to a pool of EARP that is negative for recycling endosome marker*

In *C. elegans*, CCCP-1 functions in the same genetic pathway as EIPR-1 and the EARP complex subunit VPS-50. Furthermore, *Cccp1KO* and *Eipr1KO* 832/12 cells have similar defects in insulin secretion and localization. These data suggest that CCCP1 and EIPR1/EARP may function at the same location in the cell. We decided to test this possibility using immunofluorescence in 832/13 cells. No antibody is available to EIPR1 that works in IF; furthermore, we found that overexpression of epitope tagged EIPR1 results in a diffuse cytoplasmic-like localization (Topalidou et al., 2016). Overexpressed epitope-tagged VPS50 has been reported to localize to RAB4-positive recycling endosomes (Gillingham et al., 2014;

Schindler et al., 2015). Using an antibody to VPS50 (Paquin et al., 2016), we observed that endogenous VPS50 was mostly perinuclear but less compact than the localization of CCCP1. In co-labelling experiments, we showed that endogenous VPS50 partially localized to transferrin-positive endosomes (Figure 4. 12 A). Interestingly, we found that CCCP1 colocalized with the EARP complex subunits VPS50 and VPS51 (Figure 4. 12 B). CCCP1 didn't colocalize with recycling endosome markers (Figure 4. 9 A), suggesting that EARP localizes in at least two distinct pools: CCCP1 positive compartments and recycling endosomes. We verified that this was the case with triple-labelling experiments between Alexa568-labeled transferrin, endogenous CCCP1, and Myc-tagged VPS50 or VPS51 (Figure 4. 12 C). Thus, EARP localizes to at least two distinct compartments: recycling endosomes and CCCP1-positive compartments.

4.3.6 *CCCP1 overexpression recruits VPS50*

While endogenous VPS50 localizes in perinuclear puncta that are spread throughout the cytoplasm, we found that in cells that overexpress CCCP1, VPS50 localization is concentrated to CCCP1 positive structures (Figure 4. 13 A). Additionally, in cells overexpressing CCCP1, endogenous VPS50 appeared as brighter puncta; this is likely due to its concentration in a smaller region, given that CCCP1 overexpression did not increase the levels of VPS50 (Figure 4. 13 B). Thus, overexpressed CCCP1 relocates VPS50. The absence of CCCP1 didn't noticeably affect the VPS50 protein levels or localization (Figure 4. 13 B and data not shown). Interestingly, we found that in *Eipr1KO* cells, CCCP1 overexpression didn't recruit VPS50 (Figure 4. 14 C). Thus, recruitment of VPS50 is dependent on EIPR1. The obvious explanation of CCCP1 overexpression recruiting VPS50 would be that VPS50 and CCCP1 bind each other via EIPR1. However, in multiple co-IP experiments, we were unable to detect any interaction between CCCP1 and either

VPS50 or EIPR1 (data not shown). These negative results indicate that they either don't interact, or that their interaction is of low affinity or too transient to be detected. One other alternative would be that overexpressed CCCP1 recruits membrane compartments positive for VPS50. In Chapter 3, we describe that EIPR1 is critical for the localization of EARP to the correct membrane compartment. As in the absence of EIPR1, CCCP1 overexpression no longer recruits VPS50, our data is consistent with a model where CCCP1 overexpression recruits EARP-positive membranes.

Given that a subset of VPS50 localizes to recycling endosomes, we reasoned that CCCP1 overexpression could recruit such endosomes. To test this possibility, we performed co-labelling experiments between overexpressed CCCP1 and recycling endosomal markers (Figure 4. 9 B). We found that there was no detectable impact on the localization or GFP::RAB4 and Alexa568-labelled transferrin, suggesting that overexpressed CCCP1 doesn't recruit endosomes positive for these markers. CCCP1 overexpression has no detectable impact on any other markers of cell compartments tested (iDCVs, TGN, early- and late-endosome Figure 4. 9 B and (Cattin-Ortolá et al., 2017)). Thus, overexpression of CCCP1 specifically recruits VPS50 or membranes positive for VPS50.

To map down which domain of CCCP1 is important to recruit VPS50, we generated GFP-tagged truncations of CCCP1 (Figure 4. 14 A), expressed them transiently in 832/13 cells, and co-stained for GFP and endogenous VPS50 (Figure 4. 14 B). We have reported previously that CC3 is both necessary and sufficient for localization to TGN/iDCV membranes (Cattin-Ortolá et al., 2017). Interestingly, no apparent change in the localization of endogenous VPS50 was observed in cells overexpressing CC3 (Figure 4. 14 B). Overexpression of a fragment missing the N-terminal domain CC1 (CC2+3::GFP) resulted in recruitment of VPS50 (Figure 4. 14 B). Thus, CC3 and the middle domain CC2 are together required for recruiting VPS50.

4.3.7 *Mitochondrial relocation strategy to gain insight into CCCP1's function*

To gain insight into the identity of the membranes bound by CCCP1, we used a relocation strategy; CCCP1 was ectopically expressed and localized at the mitochondria through attachment to the mitochondrial transmembrane domain of monoamine oxidase (MAO) (Wong and Munro, 2014) (Figure 4. 15 A). We generated constructs where full length CCCP1, the CC3, or the CC1+2 domain of CCCP1 were fused at their C-terminus to a HA tag and to MAO (Figure 4. 15 B). Experiments using the full-length protein fused to MAO resulted in low expression of the construct and high toxicity in 832/13 cells and thus were not used. We showed by immunofluorescence that both CC3::HA::MAO and CC1+2::HA::MAO fully colocalized with the mitochondrial marker Mitotracker and that neither construct colocalized with the TGN marker TGN38 (Figure 4. 15 C). Of note, we observed that overexpression of CC3::HA::MAO caused mitochondria clustering to perinuclear structures adjacent to TGN markers, while CC1+2::HA::MAO had no apparent effect on mitochondrial distribution/structure (Figure 4. 15 C).

We next tested whether we could recapitulate the relocation of VPS50 by CCCP1 using the mitochondria-relocation method. We found that expression of CC1+2::HA::MAO but not of CC3::HA::MAO relocated Myc-tagged VPS50 to the mitochondria (Figure 4. 16 B). Detection of relocated endogenous VPS50 was inconclusive, likely due to the low levels of endogenous VPS50. We also found that CC1+2::HA::MAO relocated VPS51 to the mitochondria, suggesting that CCCP1 recruits the entire EARP complex (Figure 4. 16 C). Finally, we found that relocation of VPS50 to the mitochondria by CC1+2::HA::MAO was dependent on EIPR1 (Figure 4. 16 C). We previously reported that CC3 was both necessary and sufficient for binding to RAB2 (Cattin-Ortolá et al., 2017). According to this result, we observed that CC3::HA::MAO but not

CC1+2::HA::MAO relocated the constitutively active forms of both RAB2A and RAB2B (data not shown). Thus, our mitochondrial relocation experiment recapitulates relocation of EARP and interaction with RAB2.

We reasoned that if CC3 binds to iDCV membranes, relocation of CC3 to the mitochondria might result in at least partial relocation of iDCVs. However, co-labelling experiments with proinsulin and relocated CC3::HA::MAO did not have any obvious effect on proinsulin localization (data not shown). Thus, either CCCP1 does not bind iDCV membranes, or its interaction with iDCVs is too weak or transient to be detected by the mitochondria relocation strategy.

4.3.8 *Proximity labelling screen identifies carboxypeptidase D as being in close proximity to CCCP1*

To discover new interactors of CCCP1, we performed several proteomic experiments. First, we immunoprecipitated CCCP1::GFP from 832/13 cells and performed mass spectrometry which didn't reveal any interactors. Second, we did GST-CCCP-1 pulldowns. We passed *C. elegans* cell lysates through a column containing bacterially expressed recombinant GST-CCCP-1 and performed mass spectrometry; again we found no interactors. As an alternative strategy, we decided to use the proximity biotinylation BioID approach. This method allows us to discover new interactors, but also to investigate the protein composition of the membranes with which CCCP1 associates. To increase the specificity of labelling of the membranes relocated by CC3 or CC1+2, we used the mitochondrial relocation strategy, as it would likely give a very different unspecific background composed of mitochondrial proteins that we could easily discard (Roux et al., 2012; Shin et al., 2017).

We fused the promiscuous biotin ligase BirA* to the C termini of CC1+2 or CC3 (CC1+2::BirA*::HA::MAO and CC3::BirA*::HA::MAO). BirA*::HA::MAO was used as a negative BioID control. Instead of using 832/13 cells, we generated PC12 cell lines that stably expressed these three constructs for technical reaction (see Material and Methods). Inspection of the mass spectrometry data revealed that peptides for CCCP1 were found in the CC3 and CC1+2 samples but not the negative control, demonstrating the efficacy of the labelling (Figure 4. 17 C and Table 4. 1). Comparison of CC1+2::HA::MAO with the negative control didn't lead to any highly promising candidates, while comparison of CC3::HA::MAO with the negative control gave carboxypeptidase D (CPD) as a specific hit (Figure 4. 17 C, Tables 4. 1 and 4. 2). Immunoblotting streptavidin-purified biotinylated proteins from cells expressing the different BirA* constructs using an anti-CPD antibody validated the MS results (Figure 4. 17 D). Finally, we observed that expression of CC3::HA::MAO but not CC1+2::HA::MAO resulted in partial relocation of CPD to the mitochondria (Figure 4. 17 E). Thus, CCCP1 interacts with CPD or is in close proximity to CPD in vivo.

4.3.9 *CCCP1 is required for carboxypeptidase D trafficking*

CPD belongs to the family of metallocarboxypeptidases and removes arginine or lysine residues from the C-terminus of proteins and peptides (Fricker, 2013). CPD is a transmembrane protein with three carboxypeptidase domains at its N-terminus and a short cytosolic tail at its C-terminus (Kuroki et al., 1995; Xin et al., 1997). Immunofluorescence in 832/13 cells showed that CCCP1 and CPD partially colocalized in a perinuclear area (Figure 4. 18 A). CPD localizes to the TG and has been reported to traffic between the cell surface, endosomes, and the TGN (Varlamov and Fricker, 1998). We reasoned that CCCP1 could be important for CPD trafficking; therefore,

we used immunofluorescence to test whether the steady state localization of CPD was affected by the absence of CCCP1. We found that in WT cells CPD tightly localized to a perinuclear region and largely colocalized with the TGN marker TGN38 (Figure 4. 18 B, top). Strikingly, we found that in *Cccp1KO* cells, CPD was localized to the TGN, but also largely to puncta distributed all throughout the cytoplasm (Figure 4. 18 B). This phenotype was specific to the absence of CCCP1 since in Cccp1(+) cells, the localization of CPD was similar to WT cells. Given that both EIPR1 and CCCP1 function in the same pathway in DCV biogenesis, we tested whether CPD localization was affected by the absence of EIPR1 as well. We found that in *EiprKO* cells, CPD also localized to puncta distributed into the cytoplasm, but that the phenotype was weaker than in *Cccp1KO* cells (Figure 4. 18 B). Thus, CCCP1 --and to a lesser extent EIPR1-- are required for CPD localization.

What are the CPD positive cytoplasmic puncta in *Cccp1KO* and in *Eipr1KO* cells? Studies in AtT-20 cells have shown that CPD localizes to the TGN and to iDCVs but it is mostly absent from mDCVs, indicating that the protein gets removed from iDCVs during maturation (Varlamov et al., 1999a). We reasoned that the punctate cytoplasmic pattern in *Cccp1KO* cells and *Eipr1KO* cells could be the result of defective CPD removal from iDCVs. Therefore, we tested whether the CPD puncta were also positive for insulin and found this to be the case. In *Cccp1KO,* most CPD-positive cytoplasmic puncta colocalized with insulin. This was also true to a lesser extent in *Eipr1KO* cells (Figure 4. 18 C). We also showed that in *Cccp1KO* cells, the CPD cytoplasmic puncta are mostly negative for proinsulin (data not shown). Thus, in *Cccp1KO* and in *Eipr1KO* cells, CPD gets mislocalized to mature DCVs.

Like CPD, the cation-dependent mannose-6-phosphate receptor (CD-MPR) is a transmembrane protein that also cycles between the cell surface, endosomes, the TGN, and iDCVs and gets removed from iDCVs during maturation (Dittie et al., 1999; Ghosh et al., 2003; Johnson

and Kornfeld, 1992; Kirchhausen et al., 1997). Both proteins have similar signal motifs in their short cytosolic domain that are important for their trafficking (Dittie et al., 1999; Ghosh et al., 2003; Johnson and Kornfeld, 1992; Kirchhausen et al., 1997). Given the large number of specificities between these proteins, we tested whether CD-MPR was similarly affected by the absence of CCCP1 or EIPR1. In WT and KO cells, CD-MPR localized to both perinuclear Golgi-like structures and cytoplasmic puncta; in *Cccp1KO* and *Eipr1KO* cells, we didn't observe any obvious changes in its localization (data not shown). Strikingly, the CD-MPR positive cytoplasmic puncta were negative for both insulin (data not shown) and CPD (data not shown). Thus, CCCP1 and EIPR1 are specifically involved in the removal of CPD from iDCVs. Because EIPR1 has been proposed to be required for retrograde transport of cargo from endosomes to the Golgi (Gershlick et al., 2016), we tested whether CPD cytoplasmic puncta are positive for the endosomal marker transferrin. Co-labelling between alexa488-transferrin and CPD in *Cccp1KO* and *Eipr1KO* cells demonstrated no colocalization (data not shown). Together, our data suggest that CCCP1 and EIPR1 are required for removal of CPD from iDCVs during DCV maturation.

4.3.10 *Unlike EIPR1, CCCP1 is not required for endocytic recycling*

It has been reported that EARP and EIPR1 are required for endocytic recycling, and that knock-down experiments of VPS50 or EIPR1 result in defects in the recycling of transferrin from endosomes to the plasma membrane (Gershlick et al., 2016; Schindler et al., 2015). CCCP1, EIPR1, and EARP share many phenotypic specificities, however it is not known whether CCCP1 is important for endocytic recycling. Using transferrin recycling assays, we found that unlike *Eipr1KO* cells, *Cccp1KO* cells had no defects in transferrin recycling (Figure 4. 19). Thus, unlike EIPR1 and EARP, CCCP1 is not required for endocytic recycling.

4.4 DISCUSSION

In this study, we investigated the role of CCCP1 in DCV function in the rat insulin secreting pancreatic beta-cell line 832/13. We showed that *Cccp1KO* cells have reduced secretion of insulin due to its retention near the Golgi, similarly to *Eipr1KO* cells (Chapter 3). In a proximity biotinylation BioID screen, we found that CCCP1 is in close proximity to the transmembrane protein CPD. CPD localizes to the TGN and to immature DCVs (iDCVs), but gets removed from iDCVs during maturation (Varlamov et al., 1999a). In *Cccp1KO* cells and to a lesser extent in *Eipr1KO* cells, CPD localized to mature DCVs, highlighting a role for CCCP1 (and EIPR1) in the cargo removal pathway. In subcellular localization studies, we found that CCCP1 and EIPR1/EARP colocalize near the TGN and iDCV markers, while EARP also localizes at recycling endosomes. By super-resolution microscopy, we found that CCCP1 forms circles (~200 nm diameter) that surround proinsulin, suggesting that CCCP1 localizes around immature DCV membranes, around proinsulin-positive TGN subdomains, or around both. Interestingly, we observed that CCCP1 overexpression recruits EARP in an EIPR1 dependent manner; in WT cells but not in *Eipr1KO* cells, overexpression of CCCP1 relocated EARP from its recycling endosomal pool to the CCCP1 TGN/iDCV pool. Moreover, relocation of CCCP1 to the mitochondria recruits EARP to the mitochondria. These data indicate CCCP1 recruits EIPR1/EARP protein or interacts with an EARP positive membrane compartment. Together, these localization and functional studies suggest that CCCP1 has multiple functions in DCV biogenesis: CCCP1 controls (1) cargo selection into DCVs at the TGN, (2) removed of CPD from iDCVs in a post-Golgi step, and (3) recruitment of the EARP complex. Therefore, we propose that CCCP1 is a regulator of DCV cargo

selection. In addition to describing the role of a novel protein in DCV biogenesis, our study highlights that the same molecules are important for DCV biogenesis in both neurons and endocrine cells.

4.4.1 *CCCP1 drives DCV cargo selection into DCVs*

C. elegans mutants in *rab-2, cccp-1, eipr-1,* and the EARP complex subunits have reduced levels of DCV cargo (Ailion et al., 2014; Edwards et al., 2009; Sumakovic et al., 2009; Topalidou et al., 2016). However, these observations were based on exogenous DCV cargos overexpressed in neurons. In this study, we use the rat insulin secreting insulinoma cell line 832/13 and investigate the secretion, localization, and processing of endogenous DCV cargo. We have shown that, in the absence of CCCP1, the cells remain responsive to stimulated secretion, but secrete reduced levels of insulin due its retention in the Golgi. Noting that in *C. elegans*, mutants in *rab-2* and its effectors produce normal DCVs in number and morphology (Ailion et al., 2014; Edwards et al., 2009; Hannemann et al., 2012; Sumakovic et al., 2009), our data is consistent with a model in which CCCP1's role is to drive the selection of DCV cargo into DCVs as they bud off the TGN (Figure 4. 20). Proinsulin processing into mature insulin requires acidification to activate the prohormone convertases 1/3 (PC1/3), PC2, and carboxypeptidase E (CPE), a step believed to happen after iDCVs bud off the TGN membranes (Arvan and Castle, 1998; Arvan and Halban, 2004; Huang and Arvan, 1994). In *Cccp1KO* cells, processing is not impaired and mature insulin accumulates at the Golgi. This suggests that in the Golgi of *Cccp1KO* cells, the processing enzymes and the vacuolar ATPase are also retained and mediate acidification of the Golgi lumen, leading to peptide processing in the wrong compartment.

4.4.2 *CCCP1 functions in the removal of CPD from immature DCVs*

In our proximity biotinylation screen, we identified CPD as being in close proximity to the C-terminal CC3 domain of CCCP1 in vivo. CPD belongs to the family of metallocarboxypeptidases; it functions in the processing of proteins that transit the secretory pathway (Fricker, 2013). CPD is a transmembrane protein with a short (ca. 50 amino acids) cytosolic tail (Kuroki et al., 1995; Xin et al., 1997). Relocation of CC3 to the mitochondria is both necessary and sufficient to relocate a subset of CPD to the mitochondria, while it didn't noticeably relocate TGN38 and proinsulin. The basis of the interaction between CCCP1 and CPD positive membranes is unclear. In Co-IP experiments from 832/13 detergent lysates we couldn't detect any interaction between GFP-tagged CCCP1 and endogenous CPD or overexpressed mCherry-tagged CPD cytosolic tail, indicating that CCCP1 and CPD don't interact directly or that their interaction is weak or transient. CCCP1 might bind to CPD positive membranes via interaction with another protein or by direct binding to membranes. We have previously reported that CC3 domain of CCCP1 is necessary and sufficient for localization to TGN/iDCV membranes, and that it is capable of direct association with synthetic membrane liposomes; this evidence strengthens the possibility of direct interaction with membranes. The nature of the CPD-positive membranes relocated by CC3 is unknown, but they could be TGN38-negative and CPD-positive subdomains of the TGN, or CPD-positive transport vesicles.

In this study, we report that in the absence of CCCP1 (or EIPR1), CPD accumulates in insulin-positive vesicles. Work in AtT-20 cells has shown that CPD localizes to the TGN and to iDCVs, but is mostly absent from mDCVs (Varlamov et al., 1999a). Thus, we propose that CCCP1 (and EIPR1) removes CPD from iDCVs. CPD is not the only cargo known to follow a removal route from iDCVs; the same phenomenon has been described for the cation-independent mannose-6-

phosphate receptor (CI-MPR), cation-dependent mannose-6-phosphate receptor (CD-MPR), and the endoprotease furin (Dittie et al., 1999; Dittié et al., 1997; Klumperman et al., 1998). These are all transmembrane proteins with short cytosolic tails that have similar signal motifs as CPD, including a cluster of acidic residues, a putative casein kinase-2 (CK2) consensus sequence, a dileucine based motif, and a tyrosine-based motif-- all required for their trafficking (Dittie et al., 1999; Dittié et al., 1997; Johnson and Kornfeld, 1992; Kirchhausen et al.). Like CPD, these proteins are known to cycle between the cell surface, endosomes, and the TGN (Dittié et al., 1997; Johnson and Kornfeld, 1992; Varlamov and Fricker, 1998). The current model is that these proteins are improperly loaded into iDCVs and follow a removal pathway that depends on AP-1 and clathrin (Dittie et al., 1999; Dittié et al., 1997; Klumperman et al., 1998). Once removed, the fate of these proteins is unknown, but it is proposed that they follow the endosomal route (Arvan and Halban, 2004; Feng and Arvan, 2003). Strikingly, CD-MPR removal from iDCVs was not affected by the absence of CCCP1 and of EIPR1. These data are consistent with a model in which CCCP1 mediates the specific removal of CPD from iDCVs via a novel pathway (Figure 4. 20). Currently we do not know why CCCP1 removes CPD from iDCVs, nor why this is important. One possibility would be that CCCP1 removes additional unwanted cargos which are not yet identified. Therefore, the mistrafficking of CPD to iDCVs could be an indication that in the absence of CCCP1, the DCVs being made do not have their proper compartmental identities. CPD is ubiquitously expressed, but its role in the processing of peptides destined to the regulated secretory pathway remains unclear (Fricker, 2013).

4.4.3 *CCCP1 and EARP*

Our results show that CCCP1, the EARP complex, and the EARP interactor EIPR1 function in the same genetic pathway in *C. elegans* neurons to promote locomotion and cargo sorting to DCVs. Furthermore, we found that *Eipr1KO* 832/13 cells have similar DCV cargo sorting defects to *Cccp1KO* 832/13 cells. CCCP1 partially colocalizes with EARP, suggesting that they function at the same location. This was surprising since overexpressed tagged EIPR1 and VPS50 were reported to localize to Rab4-positive recycling endosomes and to regulate endosomal recycling of transferrin (Gershlick et al., 2016, 2016; Gillingham et al., 2014). We found that VPS50 localizes to two pools, a CCCP1 positive pool and a recycling endosome pool, from which CCCP1 is excluded. It is unknown whether these two pools of EARP are functionally connected or whether they have independent functions. The endosomal pool might be important for EARP's role in endocytic recycling, while the CCCP1-positive pool might mediate EARP's role in DCV function. Our finding that CCCP1, unlike EIPR1 and EARP, is not required for endocytic recycling of transferrin strengthens the hypothesis that these are two functionally independent pools of EARP. Interestingly, we discovered that CCCP1 controls the localization of EARP; (1) overexpression of CCCP1 displaces EARP from its recycling endosome pool, and (2) relocation of CCCP1 to the mitochondria relocates EARP. The interplay between these two pools suggests that they are connected and interdependent. Both CC3 and CC2 domains of CCCP1 were required for the relocation. Of note, we also observed that relocation of EARP by CCCP1 was dependent on EIPR1. The molecular basis of the relocation is unknown. Given that we could not detect protein-protein interactions between CCCP1 and EIPR1/EARP from detergent lysates, we suggest that CCCP1 recruits EARP-positive membranes in a manner dependent on EIPR1 (Figure 4. 21). Our finding that EIPR1 is important for EARP localization to membranes is consistent with this

model. We propose that CCCP1's CC3 domain localizes CCCP1 to CPD positive TGN or iDCV membranes while its CC2 domain recruits the EARP positive membranes via EIPR1.

4.4.4 *What is the role of CCCP1 (and EARP/EIPR1) in DCV biogenesis?*

Our data suggest that CCCP1 has multiple functions in DCV biogenesis in neurons and endocrine cells: CCCP1 controls (1) cargo selection into DCVs at the TGN, (2) removal of CPD from iDCVs in a post-Golgi step, and (3) the recruitment of the EARP complex or EARP positive membranes via EIPR1. CCCP1 could have a direct function in DCV cargo sorting by actively driving cargo departure from the TGN while DCVs bud off, and by actively driving CPD departure from iDCVs in a post-Golgi step. An alternative possibility is that CCCP1 has a more indirect function. It could control proper trafficking and localization of proteins that function in the sorting of insulin into DCVs and removal of CPD. The interplay between the CCCP1 and EARP complex raises the possibility of the existence of a trafficking step between EIPR1/EARP positive endosomes and CCCP1 positive TGN/IDCVs. Such trafficking step has been described: after exocytosis the DCV specific transmembrane protein phogrin is recycled and traffics through endosomes before reaching newly generated DCVs. CCCP1 and EARP/EIPR1 could mediate the recycling step of DCV proteins from endosomes to the TGN and disruption of such a step could impair the proper trafficking of sorting receptors that are required for DCV biogenesis.

4.5 MATERIAL AND METHODS

4.5.1 *Molecular Biology*

A complete list of constructs is provided in the Plasmid List (Table 4. 3). Vector backbones and PCR amplified fragments containing 20-30 bp overlapping ends were PCR amplified (or digested when restriction sites were available) and combined by Gibson cloning (Gibson et al., 2009).

4.5.2 *Cell culture*

The 832/13 cell line is an INS-1-derived clone that was isolated by Dr. Christopher Newgard (Duke University School of Medicine) and obtained by Dr. Duk-Su Koh via Dr. Ian Sweet (University of Washington). Cell lines were grown in RPMI 1640-GlutaMAX™ (GIBCO) medium supplemented with 10% FBS (RMBIO), 1 mM sodium pyruvate (GIBCO), 10 mM HEPES (GIBCO), 1X Pen/Strep (GIBCO), and 0.0005% 2-beta-mercaptoethanol at 5% CO_2 and 37°C. The PC12 cells were obtained by Dr. Duk-Su Koh (University of Washington). Cell lines were grown in DMEM-GlutaMAX™ (GIBCO) medium supplemented, 10% Horse Serum (RMBIO), 5% FBS (RMBIO), and 1X Pen/Strep (GIBCO) at 5% CO_2 and 37°C. Cell lines were kept mycoplasma-free by occasional DAPI staining and PCR test (ABM, G238).

4.5.3 *Generation of Cccp1KO by CRISPR*

To knock out CCCP1, we performed Cas9-mediated genome editing in 832/13 cells using the protocol described (Ran et al, 2013). For designing guide RNAs, we used the online

CRISPR design tool (Ren et al, 2013) and selected guide RNAs that recognize sequences in the first exon of rat *Cccp1*:

5'- GCGTGAGTCGTCCTTCAACTCGG -3'

The guide RNAs were cloned into pSpCas9(BB)-2A-GFP vector using the indicated protocol (Ren et al, 2013). The efficiency of the cloned guide RNAs was tested using the SURVEYOR nuclease assay according to the manufacturer's instructions (Surveyor Mutation Detection kit, Transgenomic). We designed a homology-directed repair (HDR) template using the pPUR (Clontech) vector as a backbone and cloned approximately 1.5 kb *Cccp1* homology arms upstream and downstream of the puromycin selection cassette. The HDR template was assembled using Gibson.

To cotransfect the CRISPR plasmid and HDR template into 832/13 cells, 832/13 cells were grown in two 10-cm petri dishes to near confluency. Cells were cotransfected with 7 μg CRISPR plasmid and 7 μg non-linearized HDR template using Lipofectamine 3000 according to the instructions (ThermoFisher). 48 hours after transfection, the media was removed and replaced with new media, together with 1 μg/ml puromycin. The puromycin selection was kept until individual clones could be picked, grown in individual dishes, and tested for *Cccp1KO*.

Individual puromycin-resistant clones were initially tested for CRISPR editing of the *Cccp1* gene using genomic DNA extraction and PCR, but for unknown reasons PCR in the region around the CCCP1 CRISPR was inefficient and therefore misconclusive. Therefore, we screened for *Cccp1*KO by immunofluorescence and subsequently by Western blot. Three independent clones were identified.

4.5.4 *Lentiviral production, infection of cells, and selection of stable lines*

Platinum-E (Plat-E) retroviral packaging cells (a gift from Suzanne Hoppins) were grown for a couple of generations in DMEM-GlutaMAX™ (GIBCO) medium supplemented with 10% FBS (RMBIO), 1X Pen/Strep (GIBCO), 1 µg/ml puromycin, and 10 µg/ml blastocidin at 5% CO2 and 37°C. On day one, approximately 3.6 x 105 Plat-E cells per well were plated in a six-well dish in DMEM-GlutaMAX™ medium, supplemented with 10% FBS and 1X Pen/Strep. On day two, a mix of 152 µl Opti-MEM (ThermoFisher), 3 µg CCCP1_pBabe-hygro DNA, and 9 µl Fugene HD transfection reagent (Promega) was incubated for 10 minutes at room temperature and transfected into each well. On day three, the media was removed and replaced with new Plat-E media. On day four, approximately 1.5 x 10^5 *Cccp1KO* 832/13 cells per well were plated in a six-well dish in RPMI 1640-GlutaMAX, supplemented with 10% FBS, 1 mM sodium pyruvate, 10 mM HEPES, 1X Pen/Strep, and 0.0005% 2-beta-mercaptoethanol. 3 µl of 8 mg/ml hexadimethrine bromide (Sigma) was added in each well. The supernatant of the Plat-E cells (48 hours viral supernatant) was collected with a sterile syringe, passed through a 0.45 micron filter, and added to the *Cccp1KO* cells. The *Cccp1KO* cells were incubated for 5-8 hours at 5% CO2 and 37°C, then the media was changed and replaced with new media. The cells were incubated overnight at 5% CO_2 and 37°C. On day five, the supernatant was removed from the *Cccp1KO* cells and replaced with the supernatant from the Plat-E cells (72 hours viral supernatant) after passing through a 0.45 micron filter. 3 µl of 8 mg/mL hexadimethrine bromide was added in each well and the cells were incubated for 5-8 hours. The media was replaced with new 832/13 cell media. On day six, the *Cccp1KO* cells were collected, transferred into a 10-cm petri dish, and 200 µg/ml hygromycin was added. The cells were grown under hygromycin selection until individual clones could be picked and tested for CCCP1 expression.

4.5.5 *Immunoblotting*

Protein extracts were loaded on 8, 10, or 12% SDS PAGE gels and transferred onto PVDF membranes. Membranes were blocked in 3% milk in TBST (50 mM Tris pH 7.4, 150 mM NaCl, 0.1% Tween 20) for 1 hour at room temperature and stained with the relevant primary and then secondary antibodies in 3% milk in TBST for 1h at RT or overnight at 4ºC, followed by three 5-minute washes in TBST. The antibodies used are listed in Tables 4. 4 and 4. 5. A LI-COR processor was used to image the membranes.

4.5.6 *Immunofluorescence*

Cells were seeded onto cover slips (Thomas Scientific #121N79) and placed in 24-well cell culture plates. At least 24h after seeding, cells were transfected with Lipofectamine 2000 (Fisher), according to manufacturer's instruction for 24 to 48 hours. When indicated, cells where incubated for 25 minutes with 50 µg/mL Alexa 488- or Alexa 568- transferrin (Invitrogen #T12242 or # T23365) dissolved in serum-free RPMI media + 25 mM HEPES + 1% BSA before fixation. For the Brefeldin A (BFA) treatment, cells were incubated for the indicated times with a 3ug/mL of BFA (provided as a 1000X solution in methanol, Invitrogen #00-4506-51) in complete medium. Where indicated, cells were incubated with mitotracker deep red FM (Thermofisher #M22426) at a final concentration of 300 nm for 15 minutes in complete medium at 37ºC.

Cells were rinsed twice with PBS and fixed with 4% paraformaldehyde (made in PBS) for 20 minutes at room temperature. The cells were rinsed twice with PBS and permeabilized with 0.1% Triton X-100 in PBS for 20 minutes at room temperature. The cells were rinsed twice with PBS and placed in 5% milk in PBS for 1 hour at room temperature. Cells were stained with primary

antibodies in 0.5% milk in PBS at room temperature for 1 hour, washed three times with PBS, and incubated in secondary antibody for 1h at room temperature. The cells were washed with PBS three times, mounted onto glass slides using Vectashield (Vector laboratories H1000) or Prolong Diamond (Life technologies P36965), sealed with transparent nail polish and examined by fluorescence microscopy. The list of primary and secondary antibodies used and their working dilution are listed in Tables 4. 4 and 4. 5. Images were obtained using an Olympus FLUOVIEW FV1200 confocal microscope with a 60X UPlanSApo oil objective. The acquisition software was Olympus Fluoview v4.2. When indicated a Nikon 80i wide-field compound microscope was used. For the quantification of the insulin or the CgA distribution phenotype in *Cccp1KO* cells, Pearson's correlation coefficients were determined from confocal images using Fiji and the coloc-2 plugin by taking maximum intensity projections of whole cells and drawing a line around each individual cell. For all other quantification of colocalization experiments, a square was drawn around the perinuclear area, and Pearson's correlation coefficients were determined using Fiji and the JACOP plugin.

For super-resolution imaging, cells were prepared as described, but specific secondary antibodies were used at higher concentration (See Tables 4. 4 and 4. 5). Coverslips were mounted in DAPI-free fresh Prolong diamond, sealed with a polymer and imaged with a Leica STED microscope. For SIM imaging, coverslips were mounted with DAPI-free Vectashield and imaged with a 3D SIM OMX microscope (GE Healthcare).

4.5.7 *Insulin and proinsulin secretion*

Cells were grown in 24 well plates to near confluency. Cells were washed twice with PBS and incubated for 1 hour in 200 µL per well resting buffer (5 mM KCl, 120 mM NaCl, 24 mM NaHCO3, 1 mM MgCl2, 15 mM HEPES pH 7.4). The medium was collected, cleared by centrifugation, and stored at -80°C. The cells were incubated for 1 hour in 200 µL per well with stimulating buffer (55 mM KCl, 25 mM glucose, 70 mM NaCl, 24 mM NaHCO3, 1 mM MgCl2, 2 mM CaCl2, 15 mM HEPES pH 7.4). After stimulation, the medium was cleared by centrifugation and stored at -80ºC. The cells were washed once with PBS, harvested in PBS, and extracted in 100 µL per well acid-ethanol solution (absolute ethanol:H20:HCl, 150:47:3). The pH of the acid-ethanol solution was neutralized by addition of 20 µL of 1 M Tris Base per 100 µL of acid ethanol and the samples were stored at -80ºC.

Samples were assayed for insulin or proinsulin content using ELISA according to the instructions of the manufacturers (Rat/Mouse insulin ELISA, Millipore, #EZRMI-13K. Rat/Mouse proinsulin ELISA, Mercodia, #10-1232-01). Secreted insulin and proinsulin levels are presented as normalized against total cellular protein concentration and as ratio of the wild type values.

4.5.8 *ANF-GFP pulse/chase-like method*

To monitor the exit of DCV cargo from the TGN, a protocol similar to the one described was used (Kögel et al., 2013; Kögel Tanja et al., 2010). WT and *Cccp1KO* 832/13 cells were seeded on glass coverslips and after at least 24 hours ANF::GFP was transfected with Lipofectamine 2000 for 12-16 hours at 37ºC in complete medium. Subsequently, cells were incubated at 20ºC in PBS for 2 h in a conventional incubator (pulse) to block protein exit from the TGN. 30 minutes before the end of the low temperature block, 10 µg/mL of cycloheximide was

added to the medium to block the synthesis of new ANF::GFP. Cells were then transferred in complete medium at 37ºC (chase) for the indicated times, fixed with 4% PFA, and stained with an anti-GFP antibody as described (see immunostaining section). Cells were separated in three categories; those that had most of the ANF::GFP concentrated at the TGN ("Golgi-like"), those that had ANF::GFP both at the TGN-region and at the cell periphery ("Intermediate") and those where the ANF::GFP was excluded from the TGN ("Periphery"). 50 to 100 cells per time point and per genotype were imaged and counted using a Nikon 80i wide-field compound microscope. The experimenter was blind to the genotypes of the cell lines used and to the time point. The experiment was repeated twice with similar results.

4.5.9 *Generation of PC12 stable lines for BioID*

PC12 cells were used instead of 832/13 cells for selection drug compatibility reasons. Moreover, apparent toxicity of the mitochondria relocation constructs appeared to be less of a problem in PC12 cells. A 6cm plate was transfected with the appropriate plasmid using Lipofectamine 2000 (ThermoFisher) according to the manufacturer's instructions. After 48 hours the cell culture media was replaced with selection media (DMEM-GlutaMAX™ (GIBCO) medium supplemented with 5% FBS (RMBIO), 10% Horse Serum (RMBIO), and 700 µg/mL G418). The selection media was changed every 2-3 days until large single colonies could be observed. Colonies were transferred to a 96-wells plate and expanded in selection media and then to 24-well plate and to 6cm plates before being frozen in 10% DMSO. Individual clones were screened by immunostaining using an anti-HA antibody. Highly expressing clones were used for the BioID experiment.

4.5.10 *Transferrin recycling assay*

WT, *Eipr1KO,* and *Cccp1KO* 832/13 cells were seeded onto a 24-well plate and grown in complete media until they reached confluence. Cells were placed in warm uptake medium for a 25 minute pulse (Serum free RPMI + 1% BSA + 25 mM HEPES + 50 µg/mL of Alexa488-Transferrin from Invitrogen (T13342)). Media was exchanged with complete media and cells were chased for the indicated times, washed, and transferred onto ice. Cells were washed 2x with ice-cold PBS and detached on ice with 10 mM EDTA in PBS for 30 minutes to 1 hour with manual agitation and gentle pipetting. Detached single cells were transferred into a microcentrifuge tube and fixed at 4°C with 4% PFA (final concentration ~ 3.5%) for 10 minutes on a Nutator to avoid clumping. Fixed cells were washed with PBS and analyzed by FACS sorting using an LSRII instrument (BD Biosciences). Data were analyzed using FlowJo software.

4.5.11 *BioID experiment and sample preparation for mass spectrometry*

The protocol for isolating proteins biotinylated by BirA* was adapted from Shin et al., 2017. PC12 cells stably expressing the BirA* constructs (BirA*::HA::MAO, CC1+2::BirA*::HA::MAO and CC3::BirA*::HA::MAO) were grown to confluence in three 175 cm2 flasks in complete DMEM medium. 24hours before harvest, cells were incubated with 50 µm Biotin (10 mg/mL stock in DMSO). Cells were transferred on ice, washed 2x with ice-cold PBS and harvested by gentle pipetting. Cells were pelleted by centrifugation (10 minutes, 3,000rpm) and resuspended in lysis buffer (50 mM Tris pH 7.4, 0.1M NaCl, 1 mM EDTA, 1% Triton X-100, 1 mM PMSF, protease inhibitor cocktail (Pierce)),vortexed briefly, incubated on ice for 20 min and vortexed again. Lysates were clarified by centrifugation at 20,000g for 10 minutes at 4ºC and supernatants were mixed with equal volume of 50 mM Tris pH 7.4. The total protein content was

about 30 mg as revealed by BCA assay. The supernatant was incubated with 250 ulu Dynabeads MyOne Streptavidin C1 beads (Invitrogen) that had been pre-washed twice in the same buffer. The beads were incubated at 4ºC overnight on a nutator, washed 2x8 minutes in 2% SDS–PAGE + protease inhibitor cocktail (Pierce), 3x8 min in 1% Triton X-100, 0.1% deoxycholate, 500 mM NaCl, 1 mM EDTA, 50 mM HEPES, protease inhibitor cocktail (Pierce) pH 7.5 and 3x 8minutes in 50 mM Tris pH 7.4, 50 mM NaCl, protease inhibitor cocktail (Pierce). Finally, the beads were incubated for 5 minutes at 98ºC with 50 µL 1X LDS sample buffer containing 10% β-mercaptoethanol and 3 mM biotin and the beads were discarded.

The samples were then prepared for mass spectrometry: the eluted proteins in 1xLDS were reduced with 1 mM TCEP at 37ºC for 20 minutes on a shaker and alkylated with 2 mM chloroacetamide for 20 minutes at 37ºC. The reaction was quenched by incubation with 1 mM TCEP for 20 minutes at 37ºC and 60% of the eluent was ran onto an SDS PAGE gel. The gel was stained with colloidal Coomassie (Biorad #1610803) overnight at room temperature and distained with milliQ water. Gel slices (4 slices per lane) were excised and destained with 2x10 minutes washes with 50/50 solution of high grade ethanol/100 mM Triethylammonium Bicarbonate (TEAB). The gel was dehydrated with 2 washes of high grade ethanol. Gel slices were rehydrated with a solution of 12.5ng/µL trypsin (Promega Trypsin Gold, Mass Spectrometry Grade #PRV5280) diluted in 100 mM TEAB. Once rehydrated, 2-3 volumes of 100 mM TEAB was added and the sample was digested overnight at 37ºC in a shaking thermomixer at 1,400 rpm. The reaction was quenched by addition of 1/5 10% TFA and digested peptides were purified by StageTips (homemade, 2 punches of C18 matrix). StageTips were washed with 50 µL methanol, 50 µL reaction buffer B (0.1% TFA, 80% Acetonitrile (ACN)), and equilibrated with 50 µL of buffer A (5% ACN, 0.1% TFA in water) by centrifugation at 2,000 g at room temperature. The

sample was loaded onto StageTips that were then washed once with 50 µL buffer A and kept at 4ºC for several days until mass spectrometry analysis.

4.5.12 *Liquid chromatography / mass spectrometry (LC/MS) analysis.*

Peptides were eluted from StageTips using elution buffer (50% acetonitrile, 0.1% TFA) and then loaded to self-pulled 360 µm OD x 100 µm ID 20 cm column with a 7 µm tip packed with 3 µm Reprosil C18 resin (Dr. Maisch, Germany). Peptides were analyzed in a 120 minutes, 5% to 35% acetonitrile gradient in 0.1% acetic acid at 300 nL/min nanoLC-MS (Thermo Dionex RSLCnano) on an Orbitrap Elite. Orbitrap FTMS spectra (R = 30 000 at 400 m/z; m/z 350–1600; 3e6 target; max 500ms ion injection time) and Top15 data dependent CID MS/MS spectra (1e4 target; max 100ms injection time) were collected with dynamic exclusion for 20s and an exclusion list size of 500. The normalized collision energy applied for CID was 35% for 10ms.

Mass spectra were searched against Uniprot rat reference proteome downloaded on February 12th, 2018 using MaxQuant v1.5.7.4. Detail MaxQuant settings were: Under “Group-specific parameters” tab, “Label-free quantification”, “LFQ” was chosen in the drop-down box, “Fast LFQ” box was checked; in “Global parameters” tab, under “General”, “Match between run” box was checked. Other settings were kept as default.

4.5.13 *Statistics*

Data were tested for normality by a Shapiro-Wilk test. When the data did not pass the normality test, we used the Kruskal-Wallis test followed by Dunn's test to investigate whether

there was statistical significance between groups. When data passed the normality test, we used a one-way ANOVA test with Bonferroni correction.

4.6 ACKNOWLEDGEMENTS

I would like to thank Alex Merz for his mentorship and advice. I also thank Christopher Newgard, Ian Sweet, and Duk-Su Koh for the 832/13 cell line; Suzanne Hoppins for the pBabe vector, plat-E cells, and protocol for lentiviral production and infection and help with cell cultures; Juan Bonifacino for the EARP subunit plasmids; Cedric Asensio for the ANF::GFP plasmid; Sean Munro and John Shin for the mito-relocation and BirA* plasmids, advice, and experimental protocols for the BioID; Lloyd Fricker for the anti-CPD antibodies; Joshua C. Vaughan and Aaron Halpern for secondary antibodies used in STED microscopy. This work was supported by a University of Washington Diabetes Research Center Pilot and Feasibility Award (NIH Grant P30 DK017047) and by NIH Grant R01 GM121481.

4.7 FIGURES

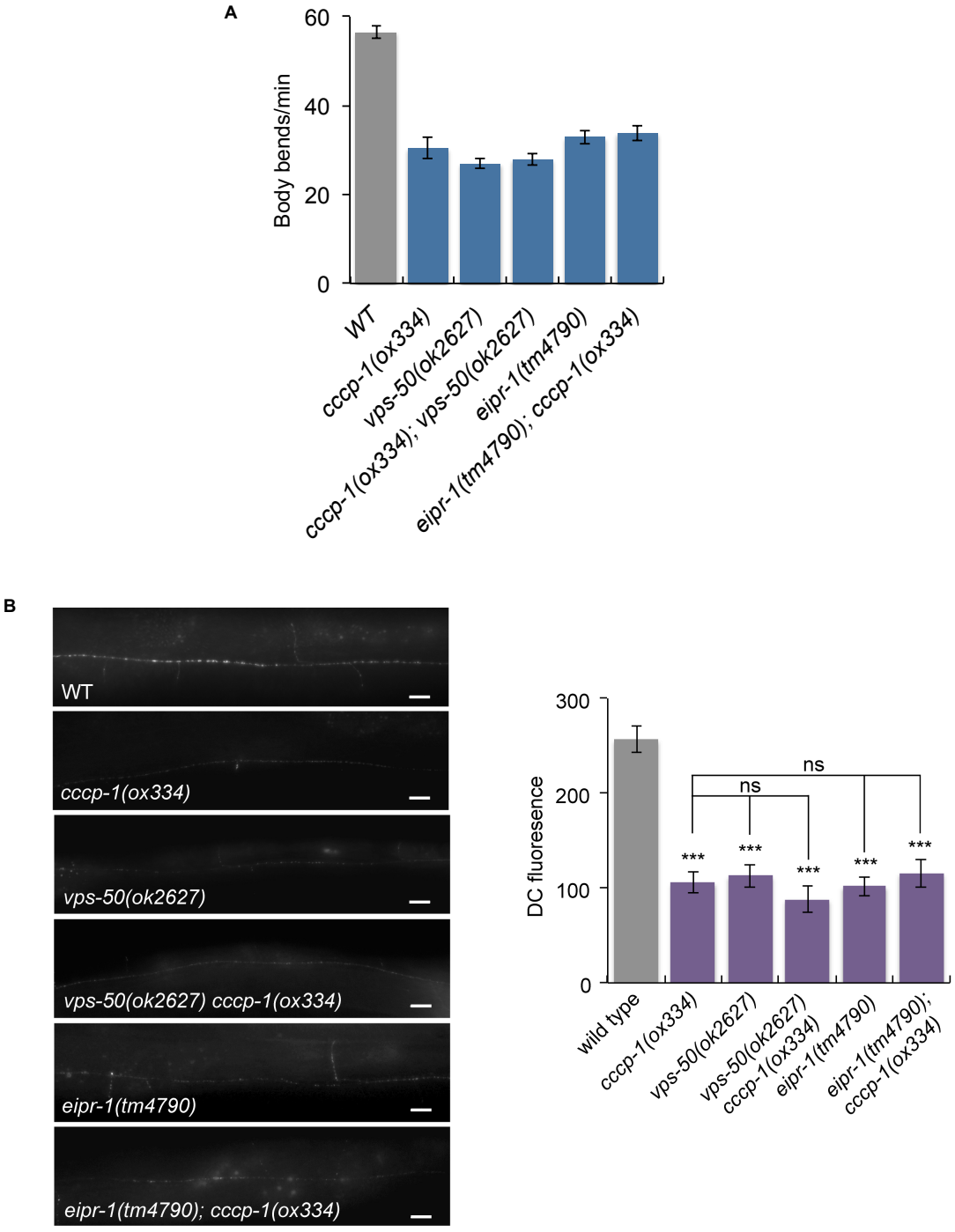

Figure 4. 1 *cccp-1* functions in the same genetic pathway as *eipr-1* and *vps-50* to control locomotion and dense-core vesicle cargo sorting

A, *cccp-1* acts in the same genetic pathway as *eipr-1* and *vps-50* to control locomotion. *cccp-1*(*ox334*) doesn't enhance the slow locomotion phenotype of either *eipr-1*(*tm4790*) or *vps-50*

(*ox2627*) mutants (***, P<0.001 compared to wild type; ns, not significant, P>0.05). Error bars = SEM; n = 10, scale bar: 10 μm.

B, *cccp-1* acts in the same genetic pathway as *eipr-1* and *vps-50* to control DCV cargo trafficking. (Left) Representative images of NLP- 21::Venus (*nuIs183* transgene) fluorescence in motor neuron axons of the dorsal nerve cord. Scale bar: 10 μm. (Right) Quantification of NLP-21::Venus fluorescence levels in the dorsal nerve cord (DC). Double mutants of *cccp-1*(*ox334*) with *eipr-1*(*tm4790*) or *vps-50*(*ox2627*) are not significantly different than the single mutants (***, P<0.001 ns, P>0.05). Error bars = SEM; n = 10.

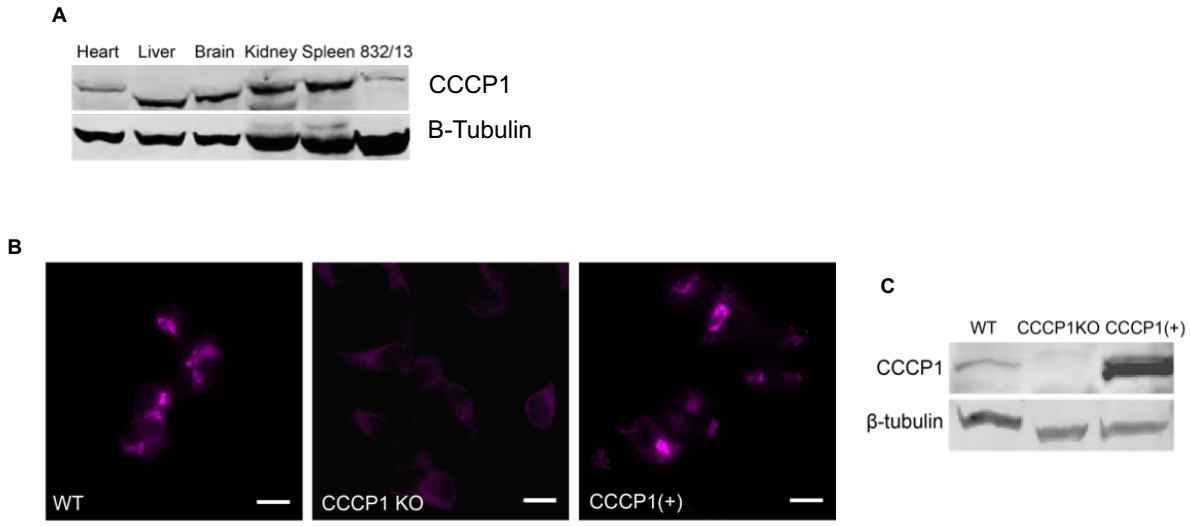

Figure 4. 2 Generation of a *Cccp1KO* insulin secreting beta-cell line 832/13

A, CCCP1 is expressed in multiple mouse tissues. Protein extracts from different mouse tissues were blotted for CCCP1 using a commercial antibody. β-tubulin is used as a loading control.

B, *Cccp1KO* cells do not express CCCP1. WT, *Cccp1KO*, and *Cccp1KO* 832/13 cells expressing wild type CCCP1 (Cccp1(+)) were stained with anti-CCCP1 antibody. Bright field microscopy, scale bar: 10 μm.

C, Protein extracts from WT, *Cccp1KO* and Cccp1(+) 832/13 cells blotted with anti-CCCP1 antibody. β-tubulin is used as a loading control.

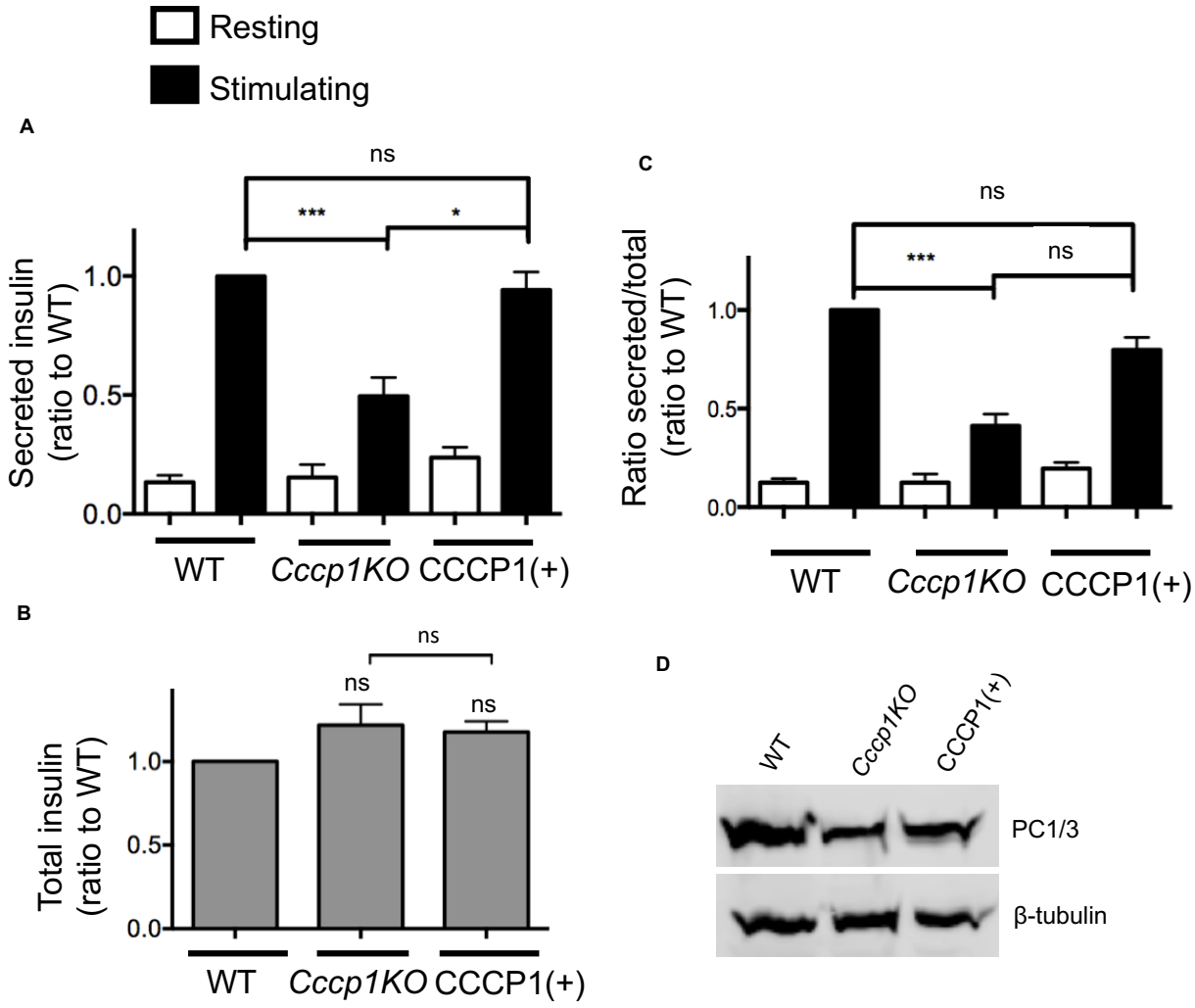

Figure 4. 3 : *Cccp1*KO cells secrete less insulin under stimulating conditions

A, Insulin secretion from 832/13 cells under resting (no glucose, 5 mM KCl, white bars) and stimulating (25 mM glucose, 55 mM KCl, black bars) conditions in WT, *Cccp1KO*, and Cccp1(+) cells. All values were normalized to the WT value in stimulating conditions. (n = 8; *p<0.05, ***p<0.001, ns p>0.05, error bars = SEM).

B, Total insulin content in WT, *Cccp1KO*, and Cccp1(+) 832/13 cells. All values were normalized to WT. (n = 8; *p<0.05, ns p>0.05, error bars = SEM)

C, Insulin secretion normalized to insulin content in WT, *Cccp1KO*, and Cccp1(+) 832/13 cells. All values were normalized to the WT value in stimulating conditions. (n = 8; *** p<0.001, ns p>0.05, error bars = SEM).

D, *Cccp1KO* cells have reduced levels of the prohormone convertase PC1/3. Detergent lysates from WT, *Cccp1KO* and Cccp1(+) 832/13 cells blotted with antibodies to PC1/3. β-tubulin is used as a loading control.

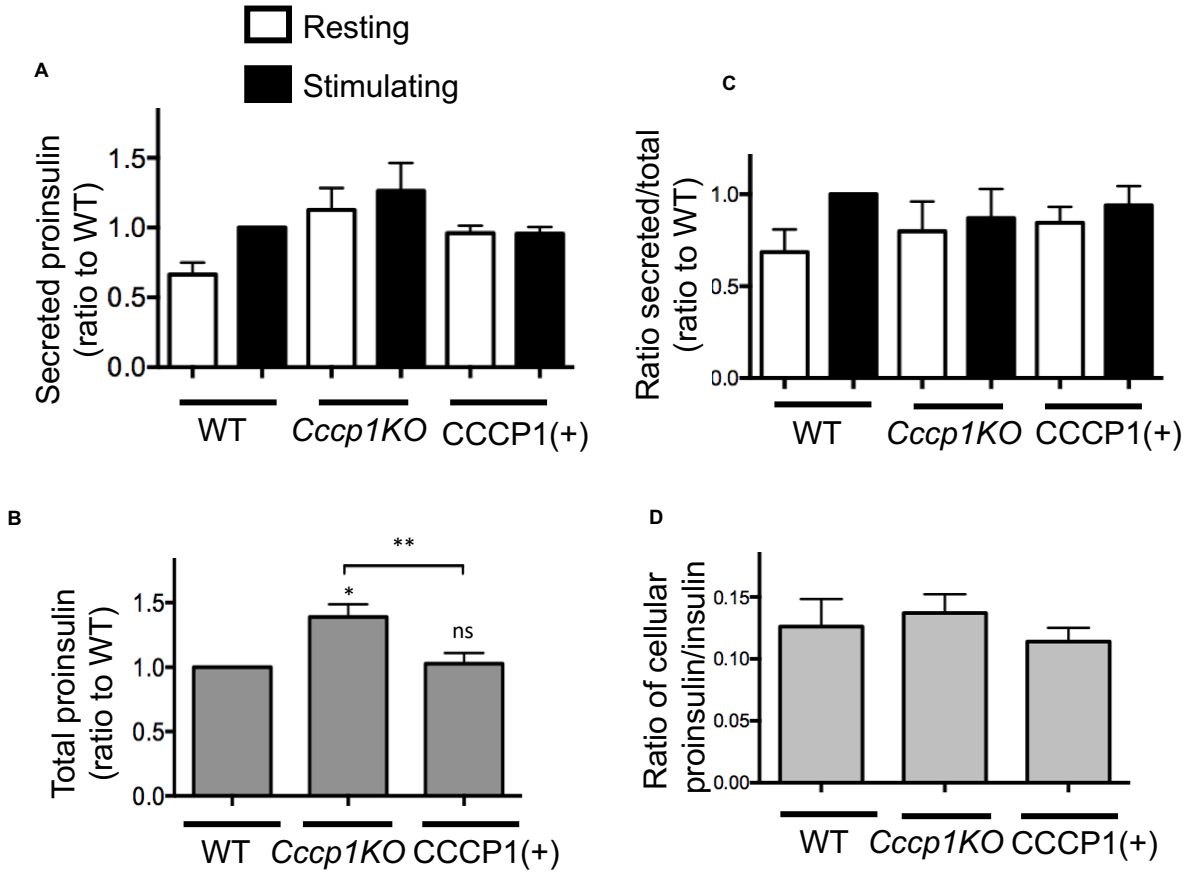

Figure 4. 4 *Cccp1KO* cells have normal secretion but increased cellular levels of proinsulin

A, Proinsulin secretion under resting and stimulating conditions from WT, *Cccp1KO* and Cccp1(+) 832/13 cells. All values were normalized to WT value in stimulating conditions. (n = 6, error bars = SEM)

B, Total proinsulin content in WT, *Cccp1KO*, and Cccp1(+) 832/13 cells. All values were normalized to WT. (n = 6; **$p<0.01$, *$p<0.05$, ns $p>0.05$, error bars are = SEM).

C; Proinsulin secretion normalized to proinsulin content under resting and stimulating conditions from WT, *Cccp1KO*, and Cccp1(+) 832/13 cells. All values were normalized to WT value in stimulating conditions. (n = 5; error bars are = SEM).

D, CCCP1 is not required for proinsulin processing. Ratio of the total cellular proinsulin content over the total cellular insulin content in WT, *Cccp1KO*, and Cccp1(+) 832/13 cells.

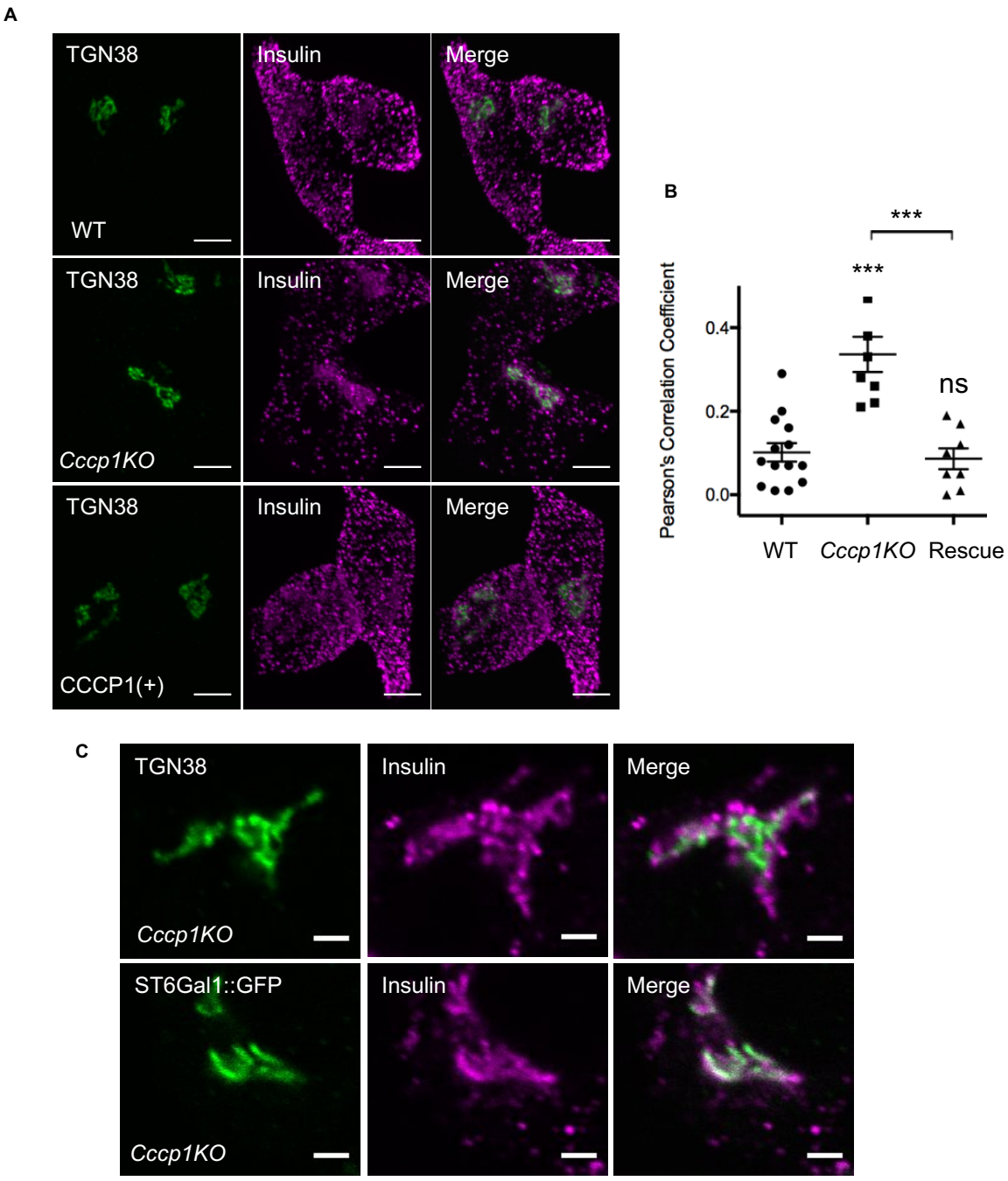

Figure 4. 5 : In *Cccp1KO* cells, insulin is retained at a late Golgi compartment

A, Insulin is accumulated at or around the TGN in *Cccp1KO* cells. Representative confocal images of WT, *Cccp1KO* and Cccp1(+) 832/13 cells costained for insulin and TGN38. Maximum intensity projection. Scale bar: 5 μm.

B, Pearson's correlation coefficient was measured to quantify the localization between insulin and the TGN marker TGN38. (Error bars = SEM, ***$p<0.001$, ns $p>0.05$).

C, In *Cccp1KO* cells, insulin is retained in late Golgi compartments. (Top) Representative confocal images of *Cccp1KO* 832/13 cells costained for insulin and the TGN marker TGN38.

(Bottom) Representative confocal images of *Cccp1KO* 832/13 cells transiently expressing GFP-tagged beta-galactoside alpha-2,6-sialyltransferase 1 (ST6Gal1::GFP), a trans-Golgi and TGN resident protein and costained for insulin and GFP. Scale bar: 2 μm.

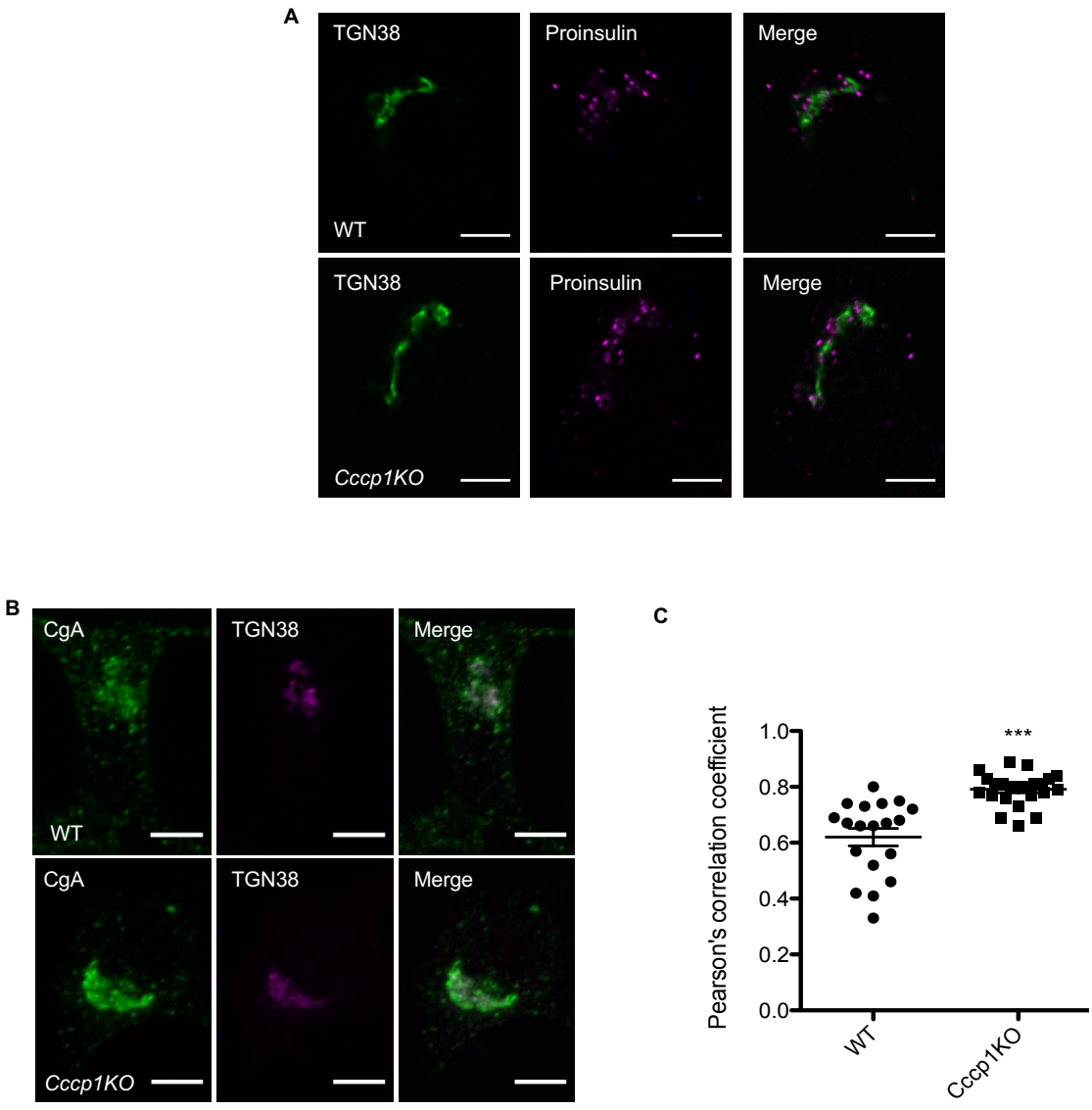

Figure 4. 6 In *Cccp1KO* cells, CgA is retained near the TGN while proinsulin localization is not affected

A, The localization of proinsulin is not affected by the absence of CCCP1. Representative images of WT and *Cccp1KO* 832/13 cells costained for endogenous proinsulin and TGN38. Scale bar: 5 μm.

B, Accumulation of the DCV luminal cargo chromogranin A (CgA) near the TGN in *Cccp1KO* cells. Representative images of WT and *Cccp1KO* 832/13 cells costained for endogenous CgA and TGN38. Maximum intensity projection. Scale bar: 5 μm.

C, Pearson's correlation coefficient was used to quantify the colocalization between CgA and the TGN marker TGN38. (Error bar = SEM, ***$p<0.001$).

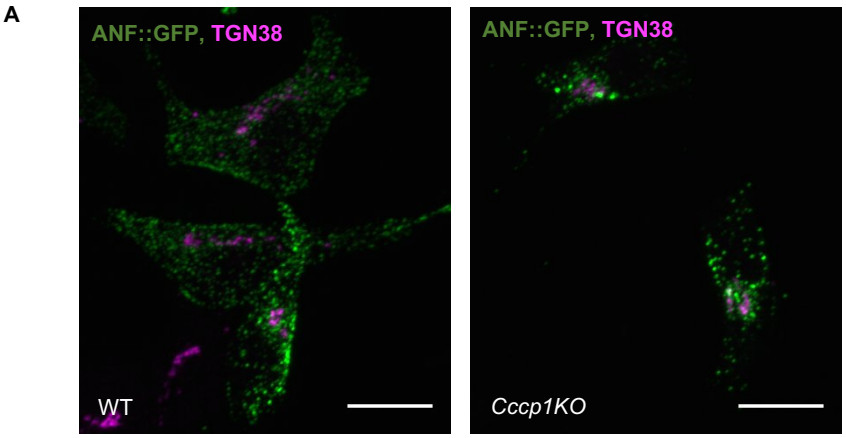
A
ANF::GFP, TGN38
WT
ANF::GFP, TGN38
Cccp1KO

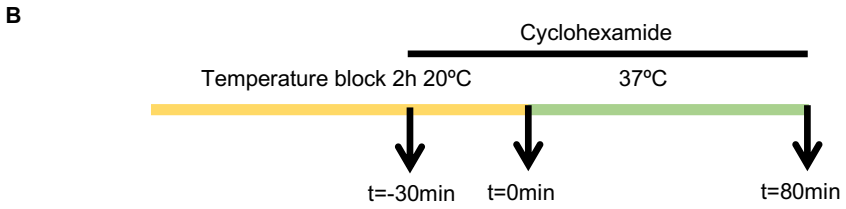
B
Cyclohexamide
Temperature block 2h 20ºC
37ºC
t=-30min
t=0min
t=80min

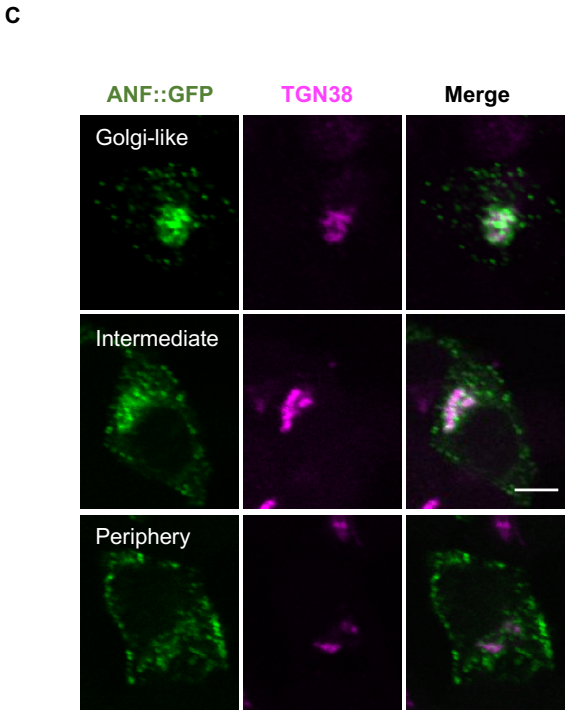
C
ANF::GFP
TGN38
Merge
Golgi-like
Intermediate
Periphery

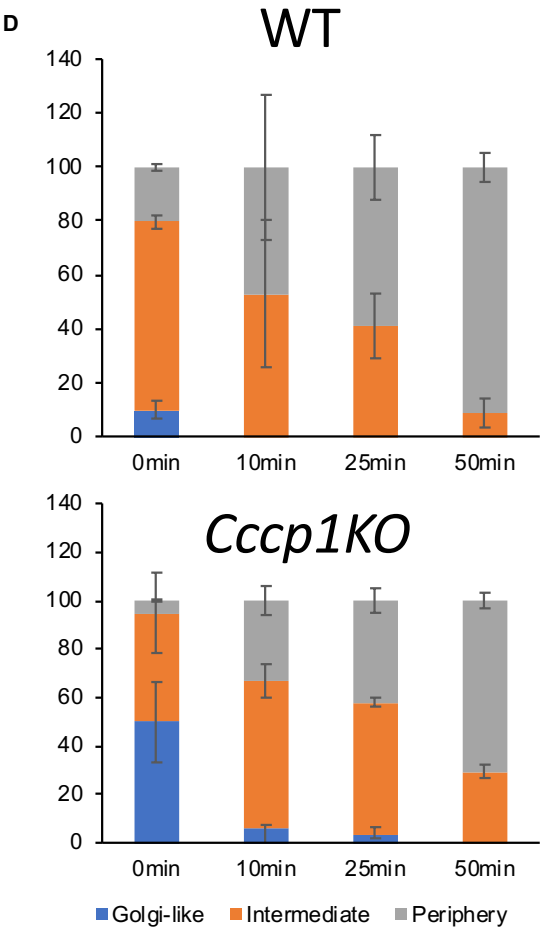
D
WT
140
120
100
80
60
40
20
0
0min
10min
25min
50min
Cccp1KO
Golgi-like
Intermediate
Periphery

Figure 4. 7 Pulse-chase like protocol monitoring exit of DCV cargo from the TGN in WT and *Cccp1KO* cells

A, The exogenous DCV cargo ANF::GFP accumulates near the TGN in *Cccp1KO* cells. Representative images of WT and *Cccp1KO* 832/13 cells transfected with ANF::GFP and costained for GFP and TGN38. Maximum intensity projection. Scale bar: 10 μm.

B, Experimental set up: cells were transiently transfected with ANF::GFP for 12-16h. Incubation at 20ºC for 2h resulted in blocking ANF::GFP from exiting the TGN (pulse). 30 minutes before the end of the low temperature incubation, cycloheximide was added to inhibit synthesis of new ANF::GFP. Following the end of the chase, cells were incubated at 37ºC for the indicated times (chase) before fixation and imaging.

C, Representative images of the three cell categories used for qualitative assessment of TGN exit: those with most of the fluorescence concentrated at the TGN (Golgi-like), those where the TGN was still apparent but a large portion of the fluorescence was at the cell periphery (Intermediate) and those were the TGN was no longer apparent (Periphery). Scale bar: 5 μm.

D, ~70 cells for each time point and genotype were imaged blindly. The data are plotted as percentage of each phenotype at each time point. n=2, Error bars=SEM.

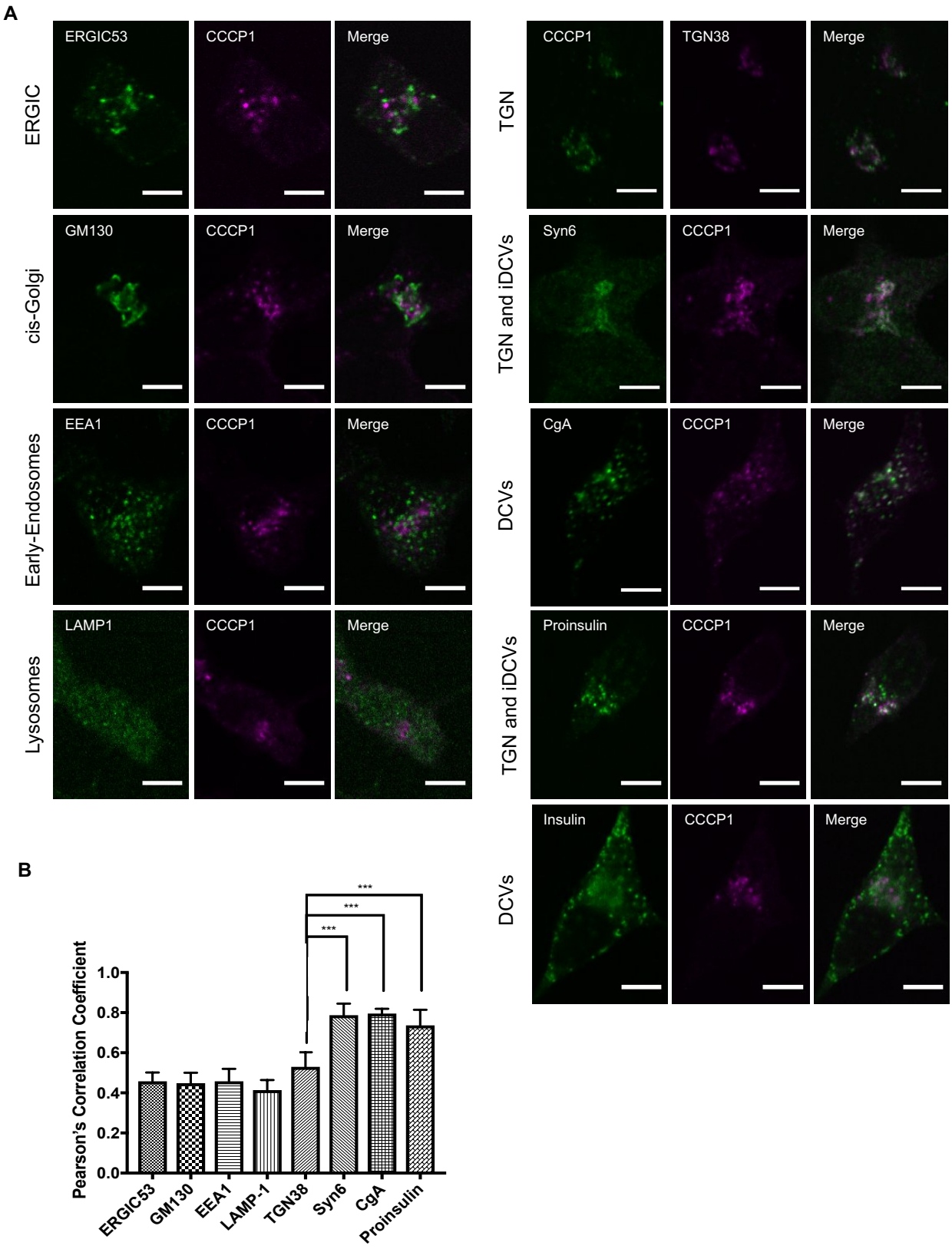
A
ERGIC
ERGIC53
CCCP1
Merge
cis-Golgi
GM130
CCCP1
Merge
Early-Endosomes
EEA1
CCCP1
Merge
Lysosomes
LAMP1
CCCP1
Merge
TGN
CCCP1
TGN38
Merge
TGN and iDCVs
Syn6
CCCP1
Merge
DCVs
CgA
CCCP1
Merge
TGN and iDCVs
Proinsulin
CCCP1
Merge
DCVs
Insulin
CCCP1
Merge
B
Pearson's Correlation Coefficient
1.0
0.8
0.6
0.4
0.2
0.0
***
***
***
ERGIC53
GM130
EEA1
LAMP-1
TGN38
Syn6
CgA
Proinsulin

Figure 4. 8 In 832/13 cells, endogenous CCCP1 localizes to a perinuclear area near markers for the TGN and immature DCVs

A, Representative confocal images of 832/13 cells costained for endogenous CCCP1 and markers for different cell compartments: the ERGIC marker ERGIC53, the cis-Golgi marker GM130, the early-endosome marker EEA1, the lysosomal marker LAMP-1, the TGN marker TGN38, the TGN/DCV markers Syntaxin6 (Syn6), chromogranin A (CgA) and proinsulin the DCV marker insulin. Scale bar: 5 μm.

B, Pearson's correlation coefficient was measured to quantify the colocalization between CCCP1 and the different markers. (Error bar = SEM, n>9, ***: p<0.001).

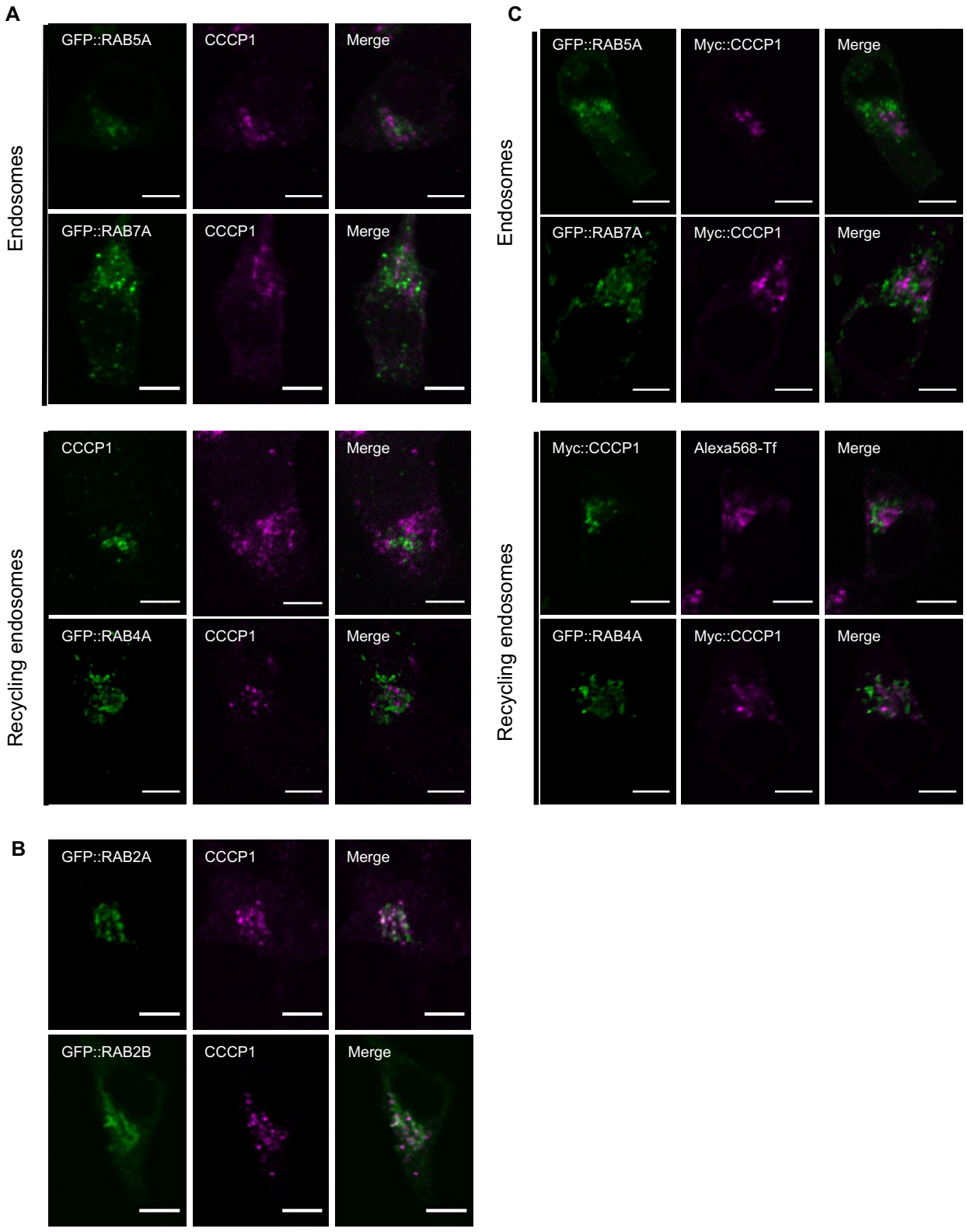

Figure 4. 9 In rat 832/13 cells, endogenous CCCP1 colocalizes with RAB2A and RAB2B but does not localize to early, late, or recycling endosomes

A, Representative confocal images of 832/13 cells transiently transfected with GFP-tagged RAB5A, RAB7A, RAB4A or incubated with Alexa-568 labelled transferrin (Tf) and costained for endogenous CCCP1 and GFP. RAB5A is a marker of early-endosomes, RAB7A is a marker of late-endosomes, transferrin is a marker of early and recycling endosomes and RAB4A is a marker of recycling endosomes. Scale bar: 5 μm.

B, Representative confocal images of 832/13 cells transiently transfected with GFP-tagged RAB2A or RAB2B and costained for endogenous CCCP1 and GFP. Scale bar: 5 μm.

C, Same as A, except than cells were transiently cotransfected with Myc::CCCP1 and indicated constructs. Scale bar: 5 μm.

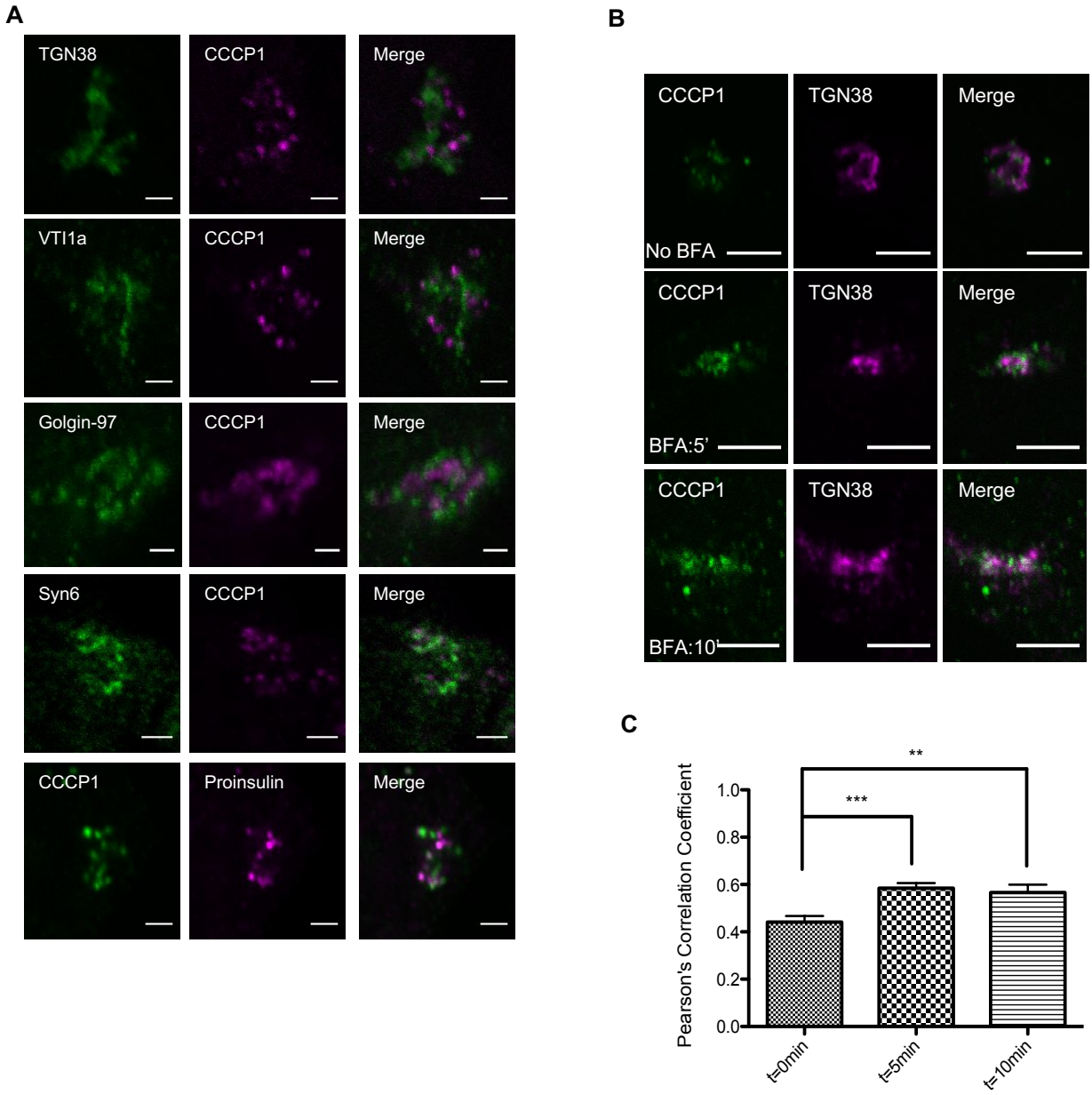

Figure 4. 10 In rat 832/13 cells, CCCP1 partially localizes to membranes derived from the TGN

A, CCCP1 localizes to a TGN subdomain or iDCVs membranes marked by Syn6 and Proinsulin but not by TGN38, Vti1A, or Golgin-97. Representative confocal images showing the perinuclear area of 832/13 cells where CCCP1 localizes. Cells were co-stained for CCCP1 and for the TGN markers TGN38, Golgin-97, Vti1a or for the TGN/iDCVs markers Syn6 and proinsulin. Scale bar: 2 μm.

B, CCCP1 is partially relocated to TGN38-positive membranes upon treatment with BFA. Representative confocal images of 832/13 cells co-stained with endogenous CCCP1 and the TGN marker TGN38 in the absence of BFA or following a 5 or 10 minute incubation with BFA. Scale bar: 5 μm. Similar results were observed in an additional independent experiment.
C, Pearson's correlation coefficient was measured to quantify the colocalization between CCCP1 and TGN38 without BFA treatment or following a 5 or 10 minute incubation with BFA. (Error bars = SEM, n>9, ***: $p<0.001$, **: $p<0.01$). Similar results were observed in an additional independent experiment.

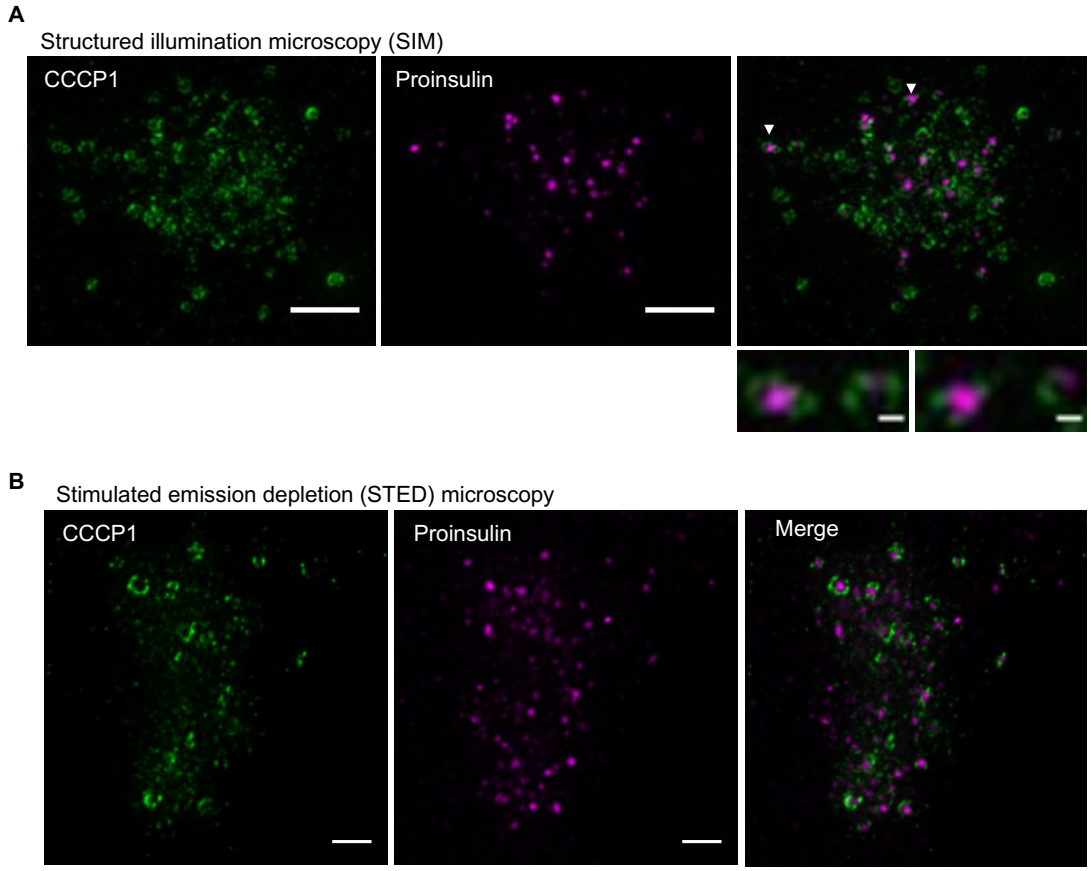

Figure 4. 11 Super resolution microscopy in 832/13 cells shows that endogenous CCCP1 localizes to circular structures around the TGN/iDCV marker proinsulin

A, Representative structured illumination microscopy (SIM) images of 832/13 cells co-stained for endogenous CCCP1 and proinsulin. Upper panels, scale bar: 2 μm. Lower panels, scale bar: 200 nm.

B, Representative stimulated emission depletion (STED) microscopy images of 832/13 cells co-stained for endogenous CCCP1 and endogenous proinsulin. Scale bar: 2 μm.

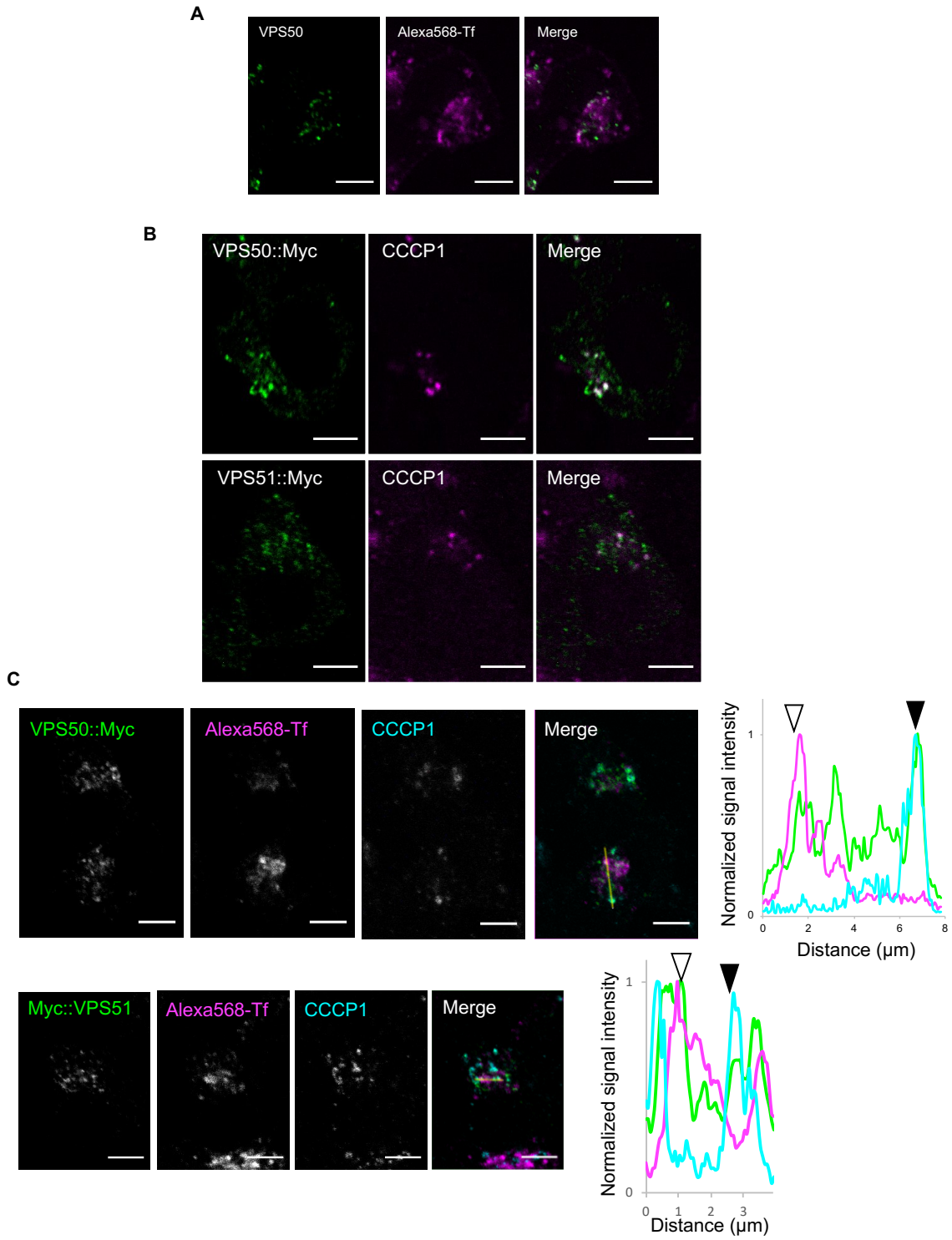

Figure 4. 12 . In rat 832/13 cells, EARP exists in at least two distinct compartments

A, VPS50 partially colocalizes with the early- and recycling- endosome marker transferrin. Upper panel: representative confocal images of 832/13 incubated with Alexa 568 labelled transferrin (Tf) and stained for VPS50. Scale bar: 5 μm.

B, CCCP1 co-localizes with the EARP complex subunits VPS50 and VPS51. Representative confocal images of 832/13 cells transiently transfected with the EARP complex subunits VPS50::Myc (upper panel) or VPS51::Myc (lower panel) and costained for Myc and endogenous CCCP1. Scale bar: 5 μm.

C, EARP localizes to at least two distinct pools; a CCCP1 TGN/iDCV pool and a recycling endosomal pool positive for transferrin (Tf). Representative confocal images of 832/13 cells transiently transfected with VPS50::Myc (upper panel) or VPS51::Myc (lower panel), incubated with Alexa 568-labelled Tf and costained for Myc and endogenous CCCP1. The graphs to the right show representative intensity plots of normalized signal intensity versus distance in μm in each channel (Green: Myc, Magenta: Tf and Cyan: CCCP1). White arrowhead: Overlap between VPS50/VPS51 and Tf. Black arrowhead: Overlap between VPS50/VPS51 and CCCP1. Scale bar: 5 μm.

A

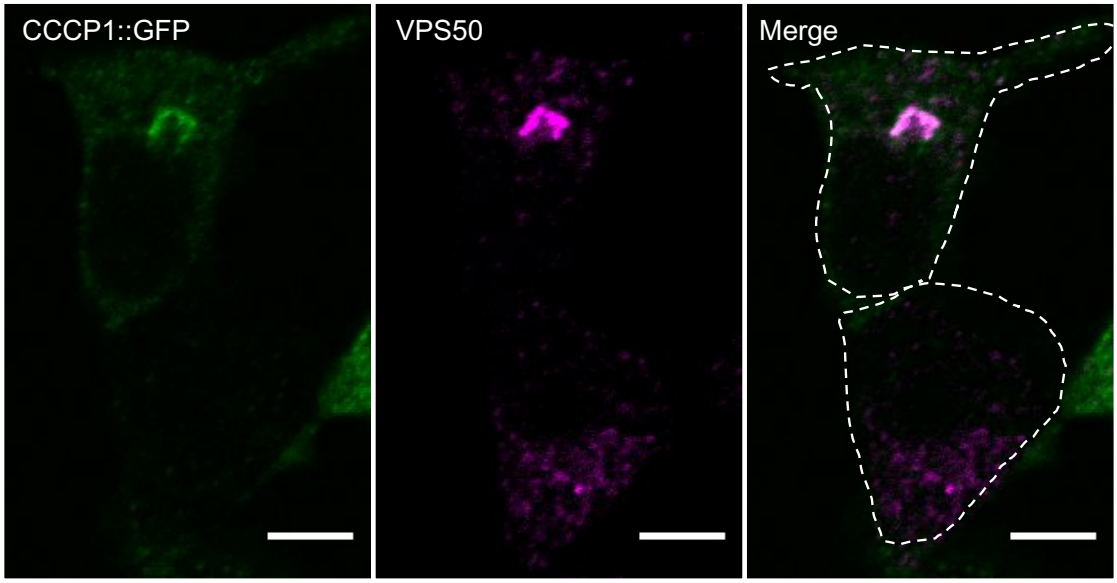
CCCP1::GFP
VPS50
Merge

B

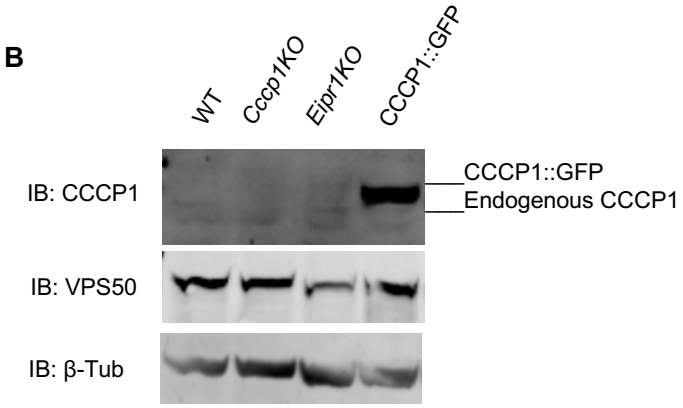
WT
Cccp1KO
Eipr1KO
CCCP1::GFP
IB: CCCP1
CCCP1::GFP
Endogenous CCCP1
IB: VPS50
IB: β-Tub

C

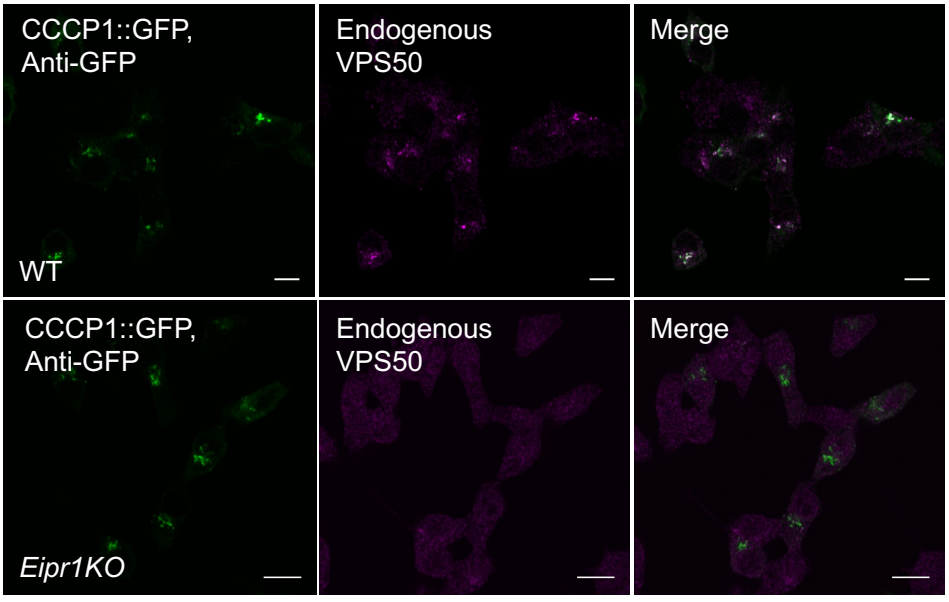
CCCP1::GFP,
Anti-GFP
Endogenous
VPS50
Merge
WT
CCCP1::GFP,
Anti-GFP
Endogenous
VPS50
Merge
Eipr1KO

Figure 4. 13 Overexpression of CCCP1 recruits EARP via EIPR1

A, CCCP1 overexpression recruits VPS50. Representative confocal images of 832/13 cells transiently transfected with CCCP1::GFP and costained for GFP and endogenous VPS50. Please notice that the top cell does not express detectable levels of CCCP1::GFP but the bottom cells do. The broken white line marks the periphery of each cell. Scale bar: 5 μm.

B, Overexpression or absence of CCCP1 has no effect on VPS50 levels. Protein extracts from WT, *Cccp1KO*, *Eipr1KO* and WT cells transiently transfected with CCCP1::GFP blotted for CCCP1 and VPS50. β-tubulin is used as a loading control.

C, EIPR1 is required for recruitment of VPS50 by CCCP1. Representative confocal images of WT (top) or *Eipr1KO* (bottom) 832/13 cells transiently transfected with CCCP1::GFP and co-stained for GFP and endogenous VPS50. Scale bar: 5 μm.

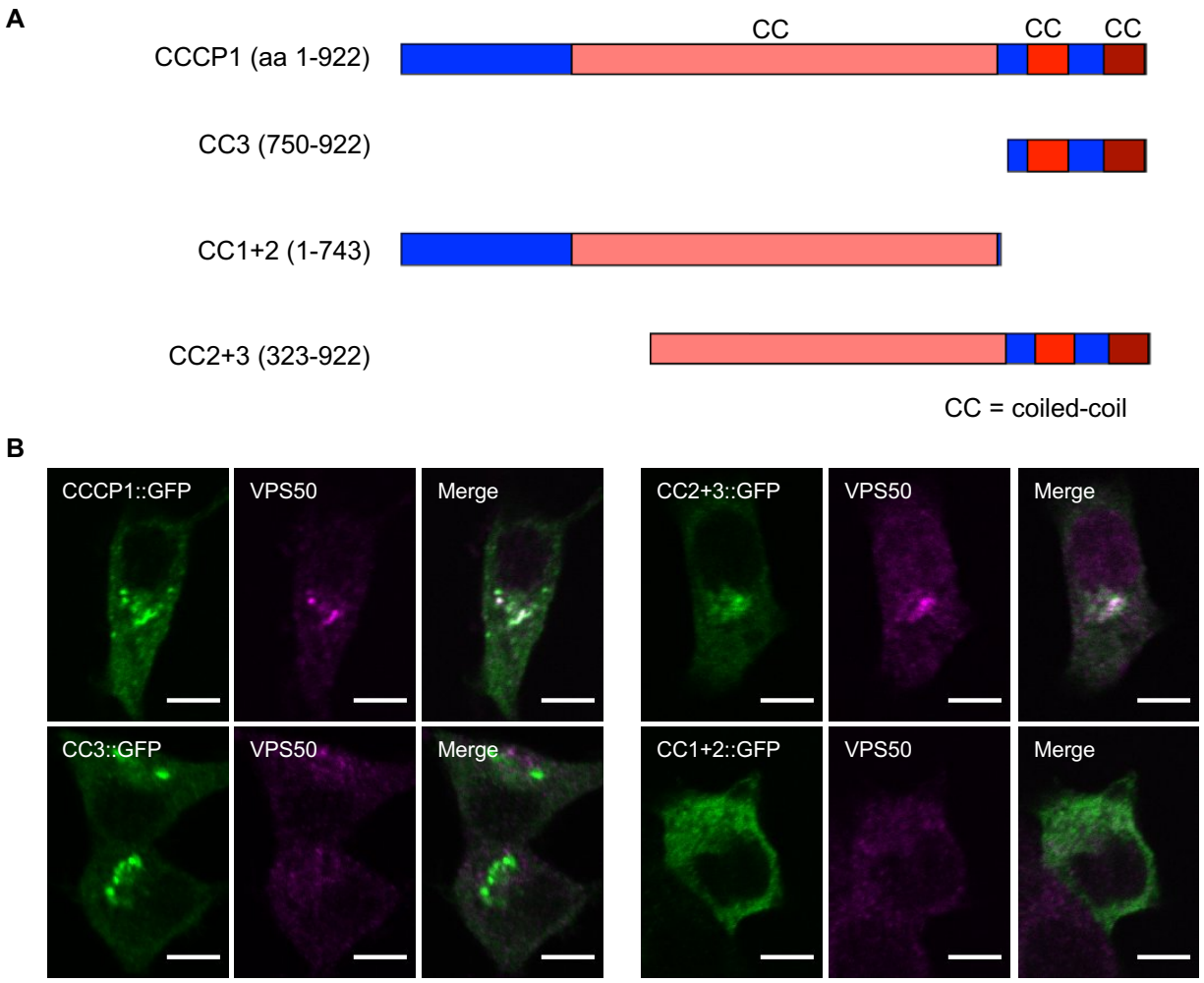

Figure 4. 14 The middle domain CC2 is necessary but not sufficient for localization of rat CCCP1/CCDC186 near the trans-Golgi

A, Domain structure of rat CCCP1 and its different fragments related to the *C. elegans* truncations (Chapter2). The domains colored with different shades of red are predicted coiled-coil domains.

B, Overexpression of full length CCCP1 or CC2+3::GFP (CCCP1(323-922)::GFP) relocates endogenous VPS50 while overexpression of CC1+2::GFP (CCCP1(1-743)::GFP) or CC3::GFP (CCCP1(750-922)::GFP) has no noticeable effect on VPS50 localization. Representative confocal image of 832/13 cells transiently transfected with CCCP1::GFP, CC2+3::GFP, CC1+2::GFP or CC3::GFP and co-stained for GFP and endogenous VPS50. Scale bar: 5 μm.

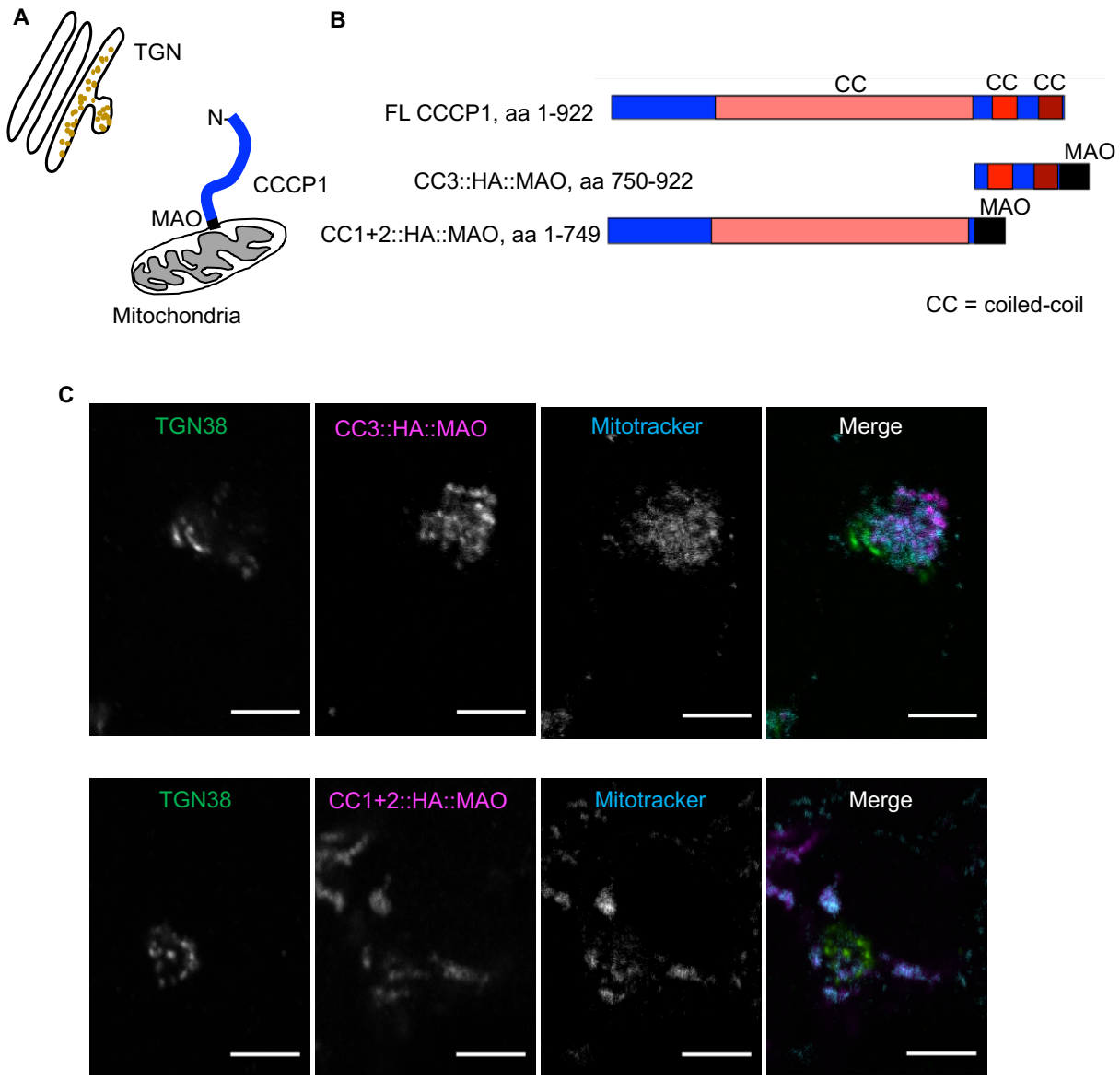

Figure 4. 15 Mitochondria relocation of CCCP1 fragments

A, Schematics of the CCCP1 mitochondria relocation experiment.

B, Domain structure of CCCP1 fragments fused to their C-terminus to the C-terminal transmembrane domain of monoamine oxidase (MOA, black). The domains marked with different shades of red are predicted coiled-coil domains.

C, CCCP1 fragments fused to MAO are relocated to the mitochondria. Representative confocal image of 832/13 cells transiently transfected with (Upper panel) CC1+2::HA::MAO or (Lower panel) CC3::HA::MAO, incubated with mitotracker and costained for HA and TGN38. Scale bar: 5 μm.

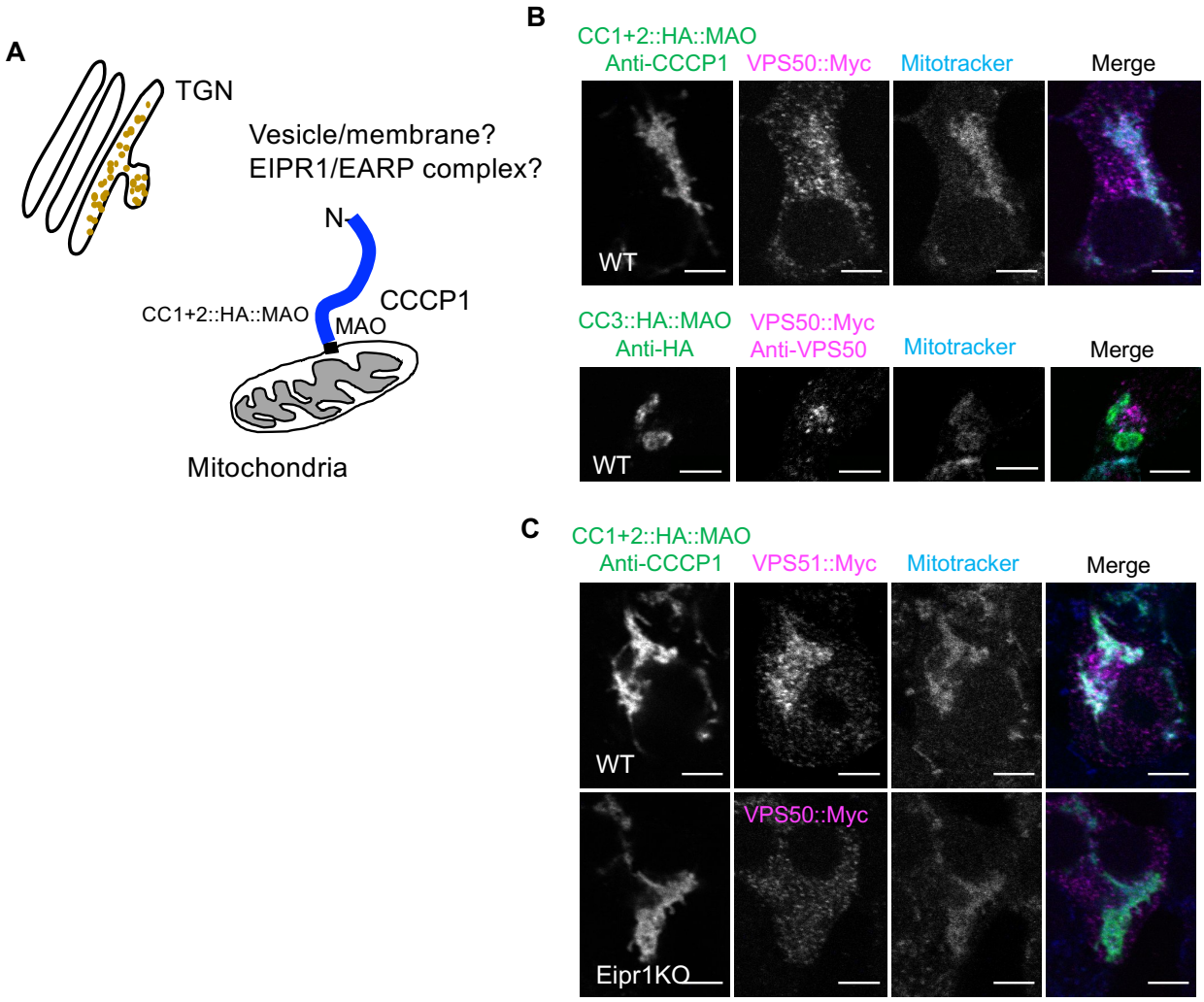

Figure 4. 16 CC1+2::HA::MAO relocates VPS50 and VPS51 to the mitochondria in an EIPR1-dependent manner

A, Schematics of the experiment where mitochondria relocated CC1+2::HA::MAO recruits either the EIPR1/EARP complex or membranes/vesicles that bind EIPR1/EARP.

B, CC1+2::HA::MAO but not CC3::HA::MAO efficiently relocates the EARP complex subunit VPS50 to the mitochondria. Representative confocal image of 832/13 cells transiently cotransfected with VPS50::Myc and CC1+2::HA::MAO or CC3::HA::MAO, incubated with mitotracker and costained for CCCP1 and Myc (Upper panel) or HA and VPS50 (Lower panel). Scale bar: 5 µm.

C, CC1+2::HA::MAO efficiently relocates VPS51 in a manner dependent on EIPR1. (Top) Representative confocal image of 832/13 cells transiently co-transfected with CC1+2::HA::MAO and VPS51::Myc, incubated with mitotracker, and costained for CCCP1 and Myc. (Bottom) Representative confocal image of *Eipr1KO* 832/13 cells transiently cotransfected with CC1+2::HA::MAO and VPS50::Myc, incubated with mitotracker and costained for CCCP1 and Myc. Scale bar: 5 µm.

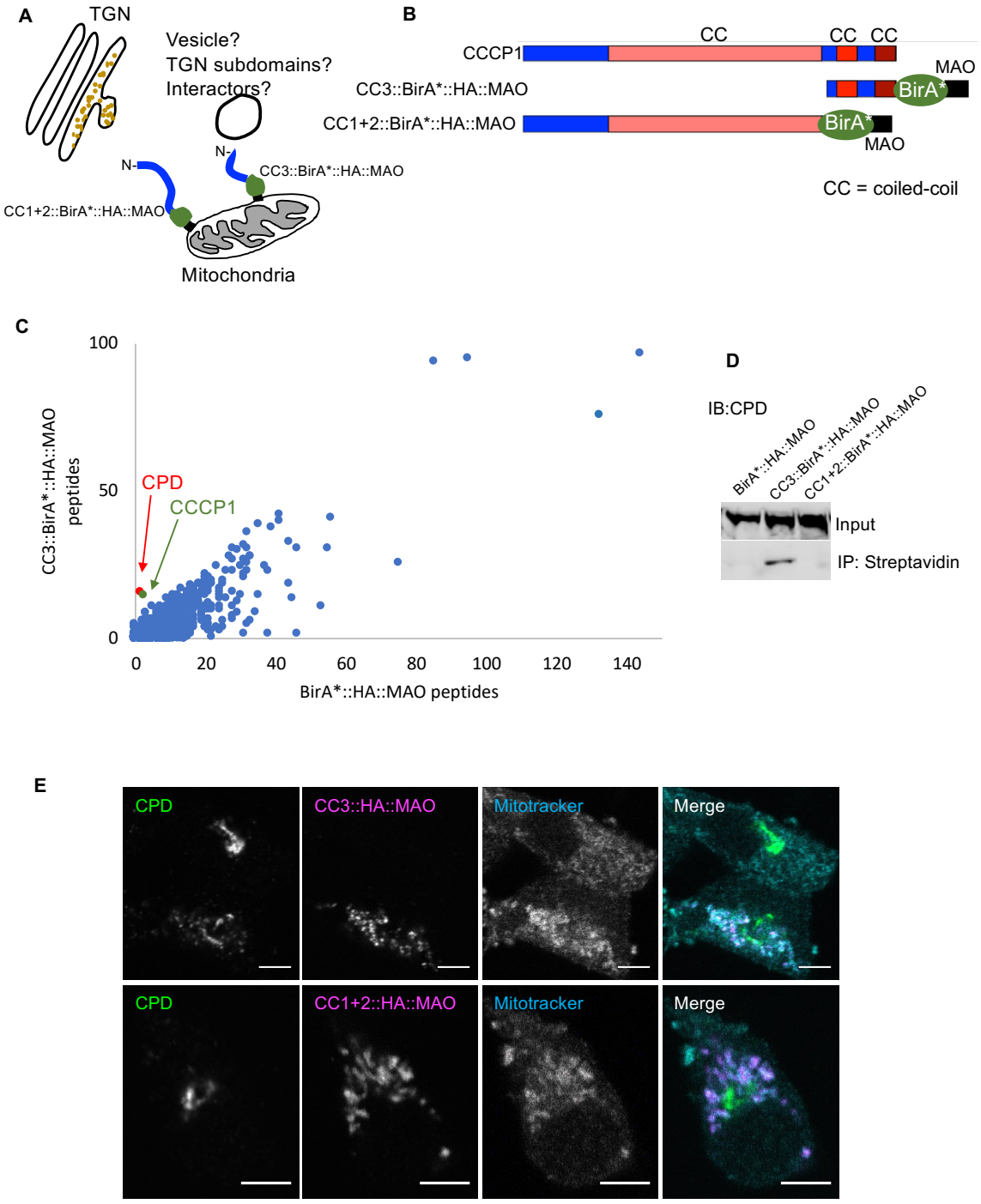

Figure 4. 17 Proximity biotinylation (BioID) screen for proteins in close proximity to CCCP1 identifies carboxypeptidase D (CPD) as a hit

A, Schematics of the proximity biotinylation BioID experiment where promiscuous biotin ligase BirA* biotinylates proteins that are in close proximity.

B, Domain structure of the CCCP1 fragments that we used for the screen. The fragments were fused to MAO (in black) and to the promiscuous biotin ligase BirA* (in green). The domains marked with different shades of red are predicted to be coiled-coil domains.

C, Mass-spectrometric analysis of biotinylated proteins from PC12 cells stably expressing CC3::BirA*::HA::MAO or the negative control BirA*::HA::MAO. The plot compares the number of unique peptides between CC3::BirA*::HA::MAO and negative control. In green: the bait CCCP1, in red: carboxypeptidase D.

D, CPD is specifically recruited by CC3::BirA*::HA::MAO. Biotinylated proteins form PC12 cell extracts stably expressing BirA*::HA::MAO, CC3::BirA*::HA::MAO or CC1+2::HA::MAO were purified with streptavidin-coated beads and immunoblotted for CPD.

E, CPD is partially relocated to the mitochondria by CC3::HA::MAO but not by CC1+2::HA::MAO. Representative confocal image of 832/13 cells transiently transfected with CC1+2::HA::MAO or CC3::HA::MAO, incubated with mitotracker and costained for HA and CPD. Scale bar: 5 μm.

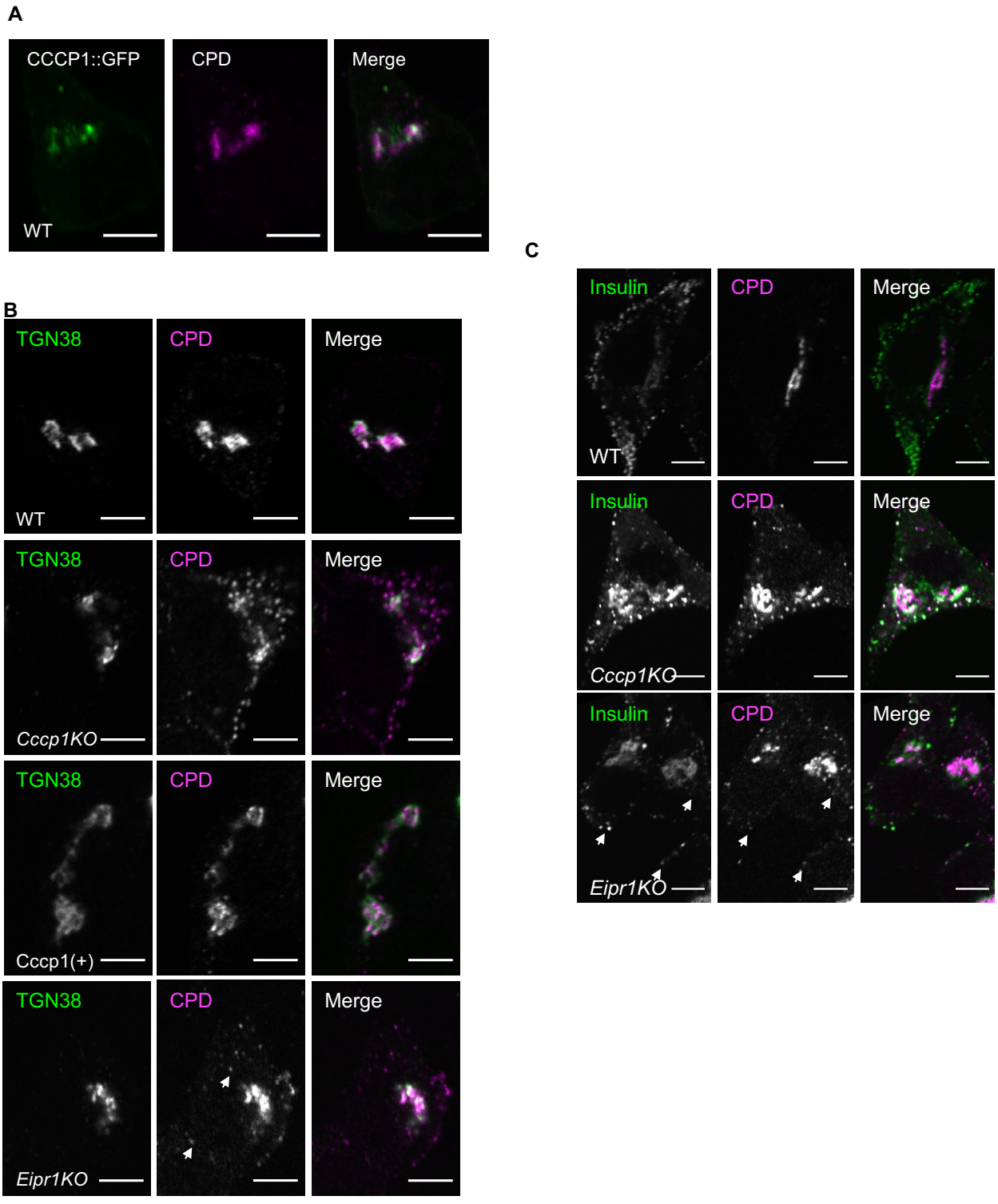
A
CCCP1::GFP
CPD
Merge
WT
B
TGN38
CPD
Merge
WT
TGN38
CPD
Merge
Cccp1KO
TGN38
CPD
Merge
Cccp1(+)
TGN38
CPD
Merge
Eipr1KO
C
Insulin
CPD
Merge
WT
Insulin
CPD
Merge
Cccp1KO
Insulin
CPD
Merge
Eipr1KO

Figure 4. 18 In *Cccp1KO* and *Eipr1KO* 832/13 cells, CPD mislocalizes to mature DCVs

A, CPD partially co-localizes with CCCP1::GFP. Representative confocal images of 832/13 cells transiently transfected with CCCP1::GFP and co-stained for endogenous CPD and GFP. Scale bar: 5 μm.

B, CCCP1 and to a lesser expend EIPR1 is required for CPD localization to the TGN. Representative confocal images of WT, *Cccp1KO*, Cccp1(+) or EIpr1KO 832/13 cells co-stained for endogenous CPD and for the TGN marker TGN38. The white arrows in the lower panel indicate the presence of unusual low intensity puncta in *Eipr1KO* cells. Scale bar: 5 μm.

C, In the absence of CCCP1 and to a lesser extent of EIPR1, CPD is mislocalized to insulin-positive vesicles. Representative confocal images of WT, *Cccp1KO,* or *Eipr1KO* 832/13 cells co-stained for endogenous CPD and insulin. The intensity of CPD signal in WT cells was increased to show the occasional presence of low intensity puncta that don't overlap with insulin. Scale bar: 5 μm.

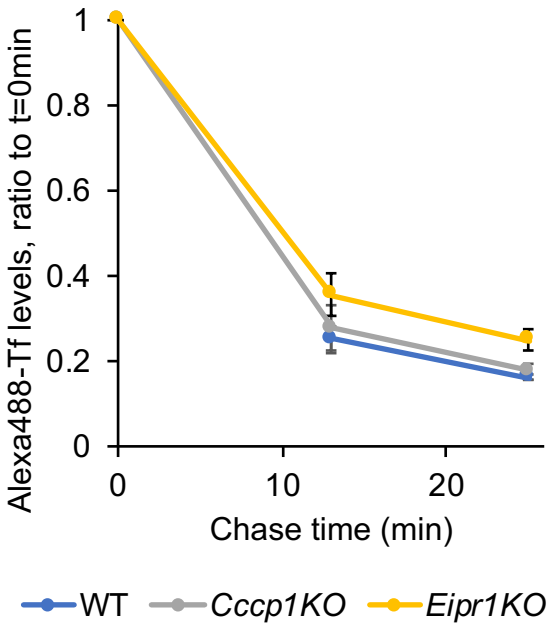

Figure 4. 19 CCCP1 is not required for endocytic recycling of transferrin (Tf).

FACS analysis of Alexa488–Tf released from 832/13 WT, *Cccp1KO,* and EIpr1KO cells after 25 minutes uptake. The plot represents the median of Alexa 488–Tf intensity of the population (~20,000 cells) as a function of time (minutes). Error bars = SEM from three independent experiments.

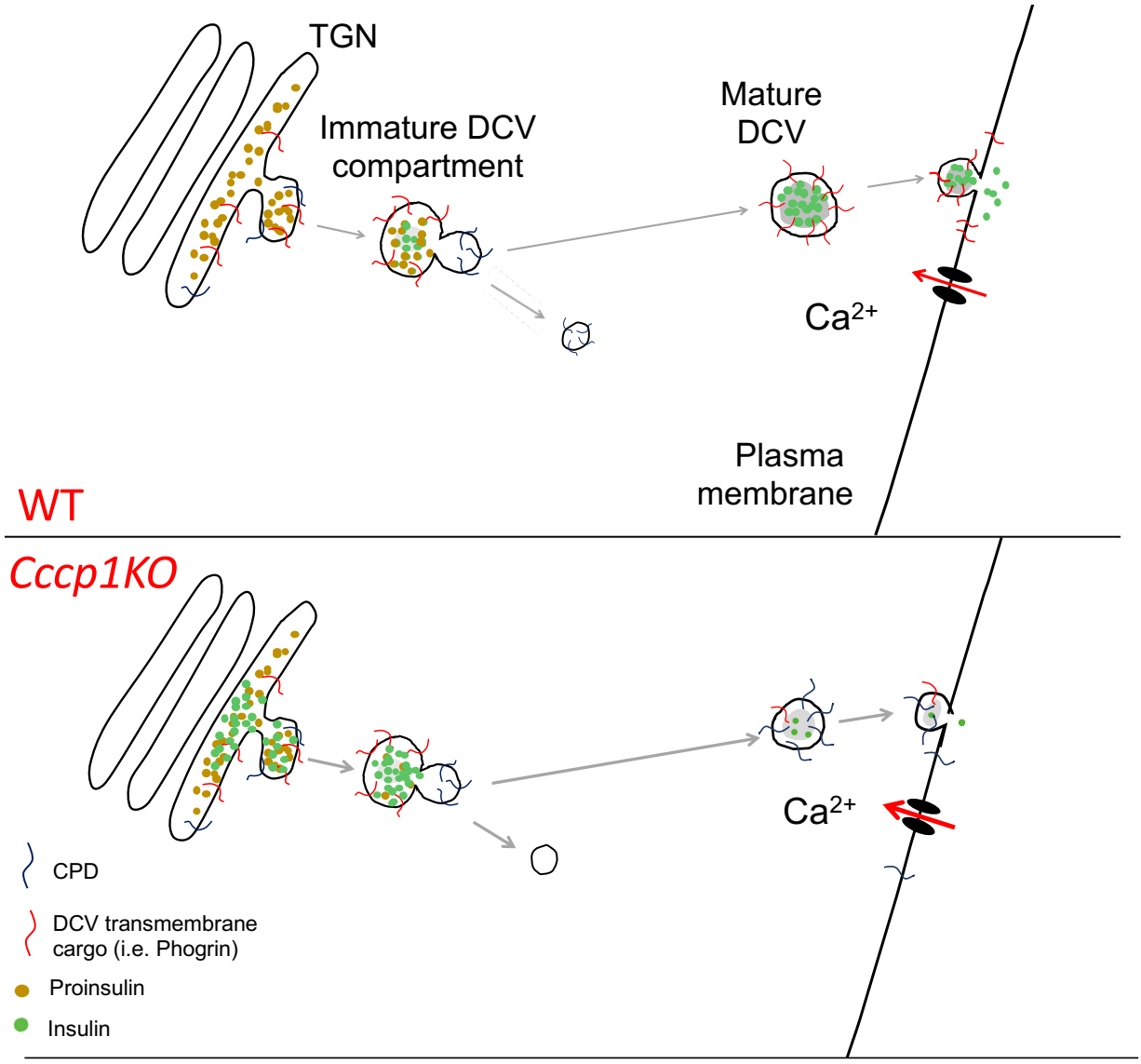

Figure 4. 20 Model figure: CCCP1 is required for the trafficking of multiple DCV cargos

(Top) CCCP1 localizes to TGN/iDCV membranes via its CC3 domain and recruits EARP/EIPR1 in an EIPR1- dependent manner through its CC2 domain. It is unknown whether CCCP1 recruits the EIPR1/EARP complex by protein-protein interaction or whether it recruits EARP- positive membranes.

(Bottom) CCCP1 is a master sorting factor for DCVs. In *Cccp1KO* cells there is retention of mature insulin and other luminal mature DCV cargo at the Golgi and of CPD in mature DCVs, suggesting that CCCP1 controls the packaging of DCV cargo into DCVs and the removal of unwanted cargo from iDCVs.

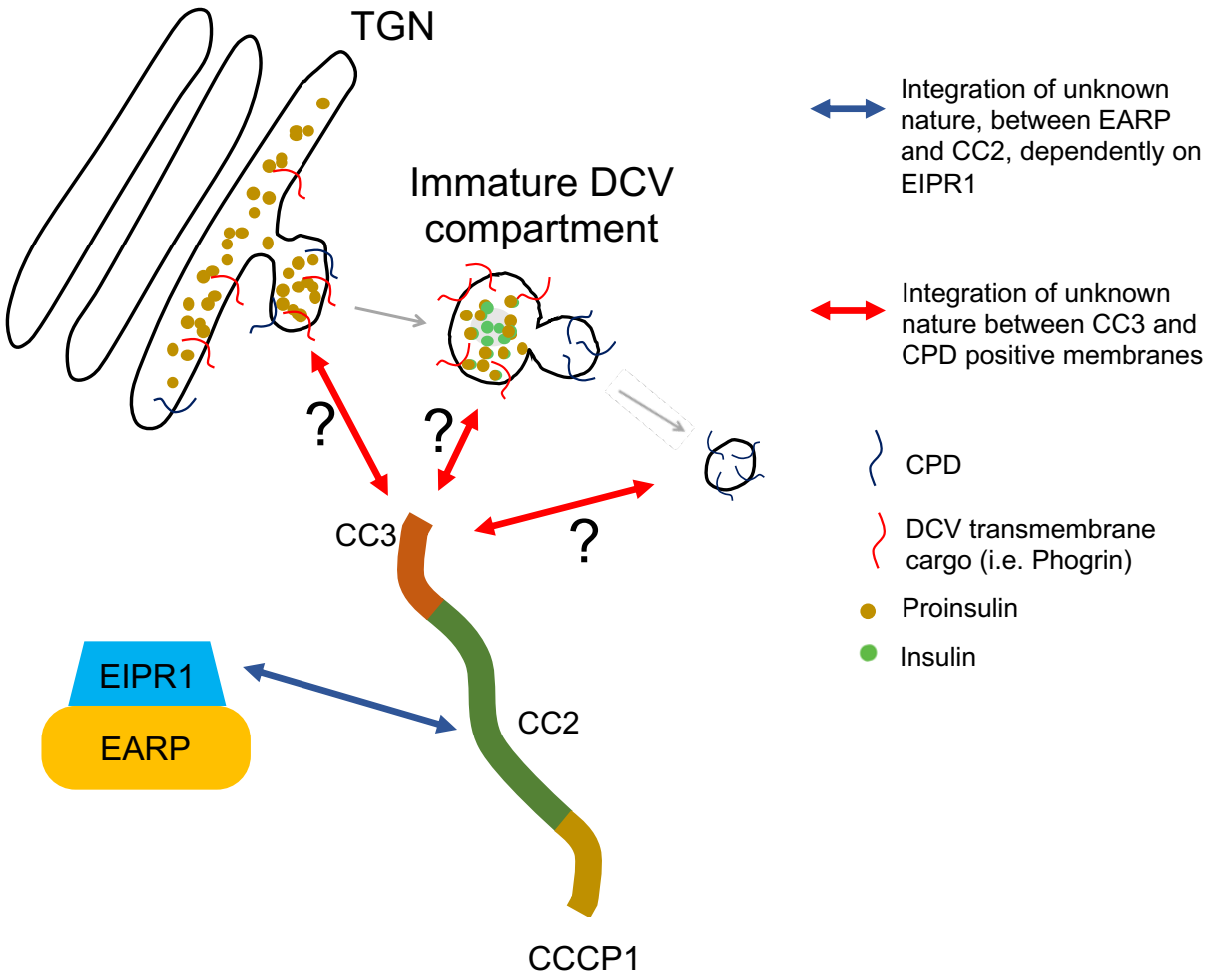

Figure 4. 21 Model figure: CCCP1 recruits EARP in an EIPR1- dependent manner

CCCP1 localizes to TGN/iDCV membranes via its CC3 domain and recruits EARP in a manner dependent on EIPR1 through its CC2 domain. It is unknown whether CCCP1 recruits the EIPR1/EARP complex by protein-protein interaction or whether it recruits EARP- positive membranes.

Protein IDs	Gene names	Peptides BirA*::HA::MAO (control)	Peprides CC1+2::BirA*::HA-MAO	Peptides CC3::BirA*::HA::MAO	Difference peptides CC3::BirA*::HA::MAO minus peptides BirA*::HA::MAO
Q9JHW1	Cpd	1	0	16	15
A0A0G2K8K1	**CCCP1**	**2**	**16**	**15**	**13**
P52873	Pc	85	93	94	9
F1M9D0;B5DF98	Map3k2	3	9	9	6
G3V6W7	Cpsf3	5	10	11	6
O08722	Unc5b	3	1	9	6
B1WBW7	Traf7	0	4	5	5
G3V6B0;F1M024	Pdxdc1	9	8	14	5
Q9QYF3;P70569; F1M111	Myo5a	35	42	39	4
P11960	Bckdha	6	11	10	4
Q5I0C3	Mccc1	32	36	36	4
Q63347	Psmc2	13	17	17	4
D3ZFX4	Pgm3	2	6	6	4
Q9EQH1	Gab2	11	14	15	4
Q62807	Syt17	3	5	7	4
F1LM47	Sucla2	7	8	11	4
B4F775	Gopc	0	1	4	4
Q62673	Plk1	2	3	6	4
D4ACS3	Mb21d2	0	1	4	4
Q99P39	Nfs1	3	8	6	3
E9PSQ0	Acacb	11	15	14	3
Q6QDP7;Q66HA2	Creb3l2	4	8	7	3
P13437	Acaa2	10	13	13	3
Q501R9	Nbr1	6	9	9	3
B5DEJ5	Eefsec	1	4	4	3
P14882	Pcca	28	30	31	3
F1LT49	Lrrc47	11	13	14	3
P68136;P68035;P 63269;P62738	Acta1;Actc1; Actg2;Acta2	12	14	15	3
D3ZJ50	Pkp3	2	3	5	3
P63045;P63025	Vamp2;Vamp 3	1	0	4	3
D4A017	Tmem87a	1	0	4	3

Table 4. 1 Mass spectrometry results from CC3::BirA*::HA::MAO

Unique peptide count organized in the descending order of the difference in number of unique peptides from CC3::BirA*::HA::MAO minus the number of peptides in the negative control BirA*::HA::MAO. The table shows the hits where the difference was 3 or greater.

Protein IDs	Gene names	Peptides BirA*::HA::MAO	Peptides CC1+2::BirA*::HA::MAO	Peptides CC3::BirA*::HA::MAO	Difference peptides CC1+2::BirA*::HA::MAO minus BirA*::HA::MAO
P11497	Acaca	95	110	95	15
A0A0G2K8K1	**CCCP1**	**2**	**16**	**15**	**14**
P11442	Cltc	28	42	16	14
D4A5A6	Polr2a	31	40	32	9
P52873	Pc	85	93	94	8
Q9QYF3;P70569;F1M111	Myo5a	35	42	39	7
P12785	Fasn	21	28	12	7
F1M9D0;B5DF98	Map3k2	3	9	9	6
D4A020	Med14	9	15	8	6
A0A0G2K9J0		34	40	9	6
G3V6W7	Cpsf3	5	10	11	5
P11960	Bckdha	6	11	10	5
Q99P39	Nfs1	3	8	6	5
F1LMV6	Dsp	7	12	5	5
F1LXF1	Bcr	6	11	2	5
M0R715	Pnpla6	13	18	7	5
G3V9S3	Ptpn13	11	16	4	5
B1WBW7	Traf7	0	4	5	4
Q5I0C3	Mccc1	32	36	36	4
Q63347	Psmc2	13	17	17	4
D3ZFX4	Pgm3	2	6	6	4
E9PSQ0	Acacb	11	15	14	4
Q6QDP7;Q66HA2	Creb3l2	4	8	7	4
B0BN64	Polr1e	6	10	8	4
P0C644	Ppip5k1	9	13	10	4
F1LT09	Wdr33	5	9	2	4
D4A2D3	Mycbp2	37	41	25	4
D4A8A0;P07756	Cad	38	42	23	4
M0RAP5	Sbf1	30	34	15	4
Q9EQH1	Gab2	11	14	15	3
P13437	Acaa2	10	13	13	3
Q501R9	Nbr1	6	9	9	3
B5DEJ5	Eefsec	1	4	4	3
Q5U2U0	Clpx	11	14	13	3
P35233	Ptpn2	2	5	2	3
Q9ERH3	Wdr7	1	4	1	3
P59215	Gnao1	3	6	2	3
F1M9W9	Trappc8	3	6	0	3
F1M801	Anapc1	7	10	2	3
D3ZL50	Ttc37	6	9	1	3

Table 4. 2 Mass spectrometry results from CC3::BirA*::HA::MAO

Unique peptide count organized in the descending order of the difference in number of peptides from CC1+2::BirA*::HA::MAO minus the number of peptides in the negative control BirA*::HA::MAO. The table shows the hits where the difference was 3 or greater.

Plasmid name	Vector backbone	Description
pET50	pEGFP-N1	CCCP1::GFP full length, rat cDNA
pET159	pEGFP-N1	CCCP1(1-743)::GFP or CC1+2::GFP
pJC218	pEGFP-N1	CCCP1(750-922)::GFP or CC3::GFP
pJC215	pEGFP-N1	CCCP1(323-922)::GFP or CC2+3::GFP
		VPS50::Myc13, a gift from Juan Bonifacino
		VPS51::Myc13, a gift from Juan Bonifacino
pJC207	pEGFP-N1	GFP::RAB5A, PCR amplified from 832/13 cDNA library
pJC205	pEGFP-N1	GFP::RAB4A, PCR amplified from 832/13 cDNA library
pJC208	pEGFP-N1	GFP::RAB7, PCR amplified from 832/13 cDNA library
		ANF::GFP, a gift from Cedric Asensio
pET55	pEGFP-N1	GFP::RAB2A, PCR amplified from 832/13 cDNA library
pET54	pEGFP-N1	GFP::RAB2B, PCR amplified from 832/13 cDNA library
pJC239	pCMV-Myc	Myc::CCCP1
pJC268	pCDNA3.1	CCCP1::HA::MAO
pJC271	pCDNA3.1	CCCP1(750-922)::HA::MAO
pJC272	pCDNA3.1	CCCP1(1-749)::HA::MAO
pJC280	pCDNA3.1	CCCP1(759-922)::BirA*::HA::MAO
pJC281	pCDNA3.1	CCCP1(1-749)::BirA*::HA::MAO
pJJS112	pCDNA3.1	BirA*::HA::MAO, a gift from Sean Munro
pJC279	pEGFP-N1	CD-MPR::GFP, PCR amplified from 832/13 cDNA library
pJC282	pEGFP-N1	ST6GAL1::GFP, PCR amplified from 832/13 cDNA library

Table 4. 3 Plasmid list

Antibody target	Manufacturer and catalog number	Notes
CCCP1	Novus #NBP1-90440	Rabbit polyclonal, 1:150 for IF and 1:1,000 for WB
TGN38	Sigma #T9826	Rabbit polyclonal, 1:350 for IF
EEA1	BD Biosciences #610456	Mouse monoclonal, 1:100 for IF
GM130	BD Biosciences #610822	Mouse monoclonal, 1:100 for IF, but works at 1:300
ERGIC53	Santa Cruz #sc-398893	Mouse monoclonal, 1:50 for IF
LAMP-1	DHSB	Mouse monoclonal, 1:50 for IF
GFP	Santa Cruz #sc-9996	Mouse monoclonal, 1:200 to 1:400 for IF, 1:1,000 for WB
GFP	Santa Cruz #sc-8334	Rabbit polyclonal, 1:200 to 1:400 for IF, 1:1,000 for WB
Insulin	Sigma #I2018	Mouse monoclonal, 1:400 for IF
Proinsulin	Abcam #ab8301	Mouse monoclonal, 1:200 for IF
Syntaxin 6	Abcam #ab12370	Mouse monoclonal, 1:100 for IF
Vti1a	Santa Cruz #sc-136117	Mouse monoclonal, 1:100 for IF
TGN38	Novus #NB300-575S	Mouse monoclonal, 1:500 for IF
CgA	Santa Cruz #sc-393941	Mouse monoclonal, 1:200 for IF
Myc	Santa Cruz sc-40	Mouse monoclonal, 1:200 for IF, 1:1,000 for WB
Rab2	Santa Cruz	Rabbit polyclonal, 1:200-1:500 for WB
6xHis	Fisher	?
GFP	Roche #11814460001	Mouse monoclonal, 1:1,000 for WB
Beta-Tubulin	DHSB E7	Mouse monoclonal, 1:1,000 for WB
Beta-Tubulin	ThermoFisher , BT7R, #MA5-16308	Mouse monoclonal, 1:1,000 for WB
HA	Roche #11867423001	Rat monoclonal, 1:150 for IF and 1:1,000 for WB
CPD	Lloyd Fricker	Raised to CPD cytosolic tail, rabbit polyclonal, 1:200 for IF and 1:1,000 for WB
VPS50	Sigma HPA026679	Rabbit polyclonal, 1:100 for IF and 1:1,000 for WB
PCSK1 (PC1/3)	Sigma SAB1100415	Rabbit polyclonal, 1:1,000 for WB

Table 4. 4 Primary antibodies list

Antibody target	Manufacturer and catalog number	Notes
Anti-Mouse Alexa488	Jackson immunoresearch #115-545-146	1,1000 for IF
Anti-Mouse Rhodamine Rex-X	Jackson immunoresearch #715-295-150	1,1000 for IF
Anti-Rabbit Alexa488	Jackson immunoresearch	1,1000 for IF, (1:100 for STED microscopy)
Anti-Rabbit Rhodamine TRITC	Jackson immunoresearch #111-025-144	1,1000 for IF
Anti-Rat Dyligth550	ThermoFisher #SA5-10027	Highly cross-adsorbed , used at 1:200 to 1:500
Anti-Rabbit Atto647	A gift from Joshua C. Vaughan's lab	1:200 for IF
Anti-Mouse Dylight488	ThermoFisher #SA5-10166	Highly cross-adsorbed , used at 1:200 to 1:500
Anti-Mouse Alexa555	A gift from Joshua C. Vaughan's lab	Used at 1:100 for STED microscopy
Goat anti-Rabbit Alexa680	Jackson immunoresearch #115-625-144	1:20,000 for western
Goat anti-Mouse Alexa680	Jackson immunoresearch #115-625-166	1:20,000 for western
Donkey anti-Mouse Alexa790	Jackson immunoresearch #715-655-150	1:20,000 for western
Alexa790 Streptavidin	Jackson immunoresearch #016-650-084	1:10,000 for western

Table 4. 5 Secondary antibodies list

Chapter 5. GENERAL CONCLUSION

The mechanisms of cargo sorting to the regulated secretory pathway are largely unknown. Sorting has been proposed to occur at the TGN while dense-core vesicles (DCVs) bud off ("sorting by entry" model), but also at post-Golgi steps, where DCV cargo is retained into immature DCVs (iDCVs) while proteins not destined to the regulated secretory are removed ("sorting by retention" model). Our lack of knowledge is largely due to the lack of proteins known to work in these processes. Screens in C. elegans for DCV function have identified the small G protein RAB2, its effector the coiled-coil containing protein 1 (CCCP1), the endosome associated recycling protein (EARP) complex, and the EARP interacting protein 1 (EIPR1) (Ailion et al., 2014; Edwards et al., 2009; Sumakovic et al., 2009; Topalidou et al., 2016).

In my thesis work, I have contributed to several projects that characterize the role and molecular functions of these novel proteins. The main finding of my work has been that in mammalian insulinoma 832/13 cells, CCCP1 and EIPR1 are both required for sorting cargo into DCVs at the Golgi, as well as to the removal of cargo not destined to the regulated secretory pathway during a post-Golgi step. Moreover, I have contributed to critical cell biological, biochemical and biophysical characterization of these proteins to gain insight into their interactions, subcellular localizations, and molecular functions.

5.1 CCCP1, EIPR1, AND EARP ARE NEW REGULATORS OF CARGO SORTING TO DCVS

CCCP1, EIPR1 and EARP were known to regulate the sorting of cargo to DCVs in C. elegans neurons. The work I report here defines their roles in the insulin secreting beta-cell line

832/13. In the absence of EIPR1 and of CCCP1, insulin is aberrantly retained at a late Golgi compartment. Furthermore, Carboxypeptidase D (CPD), a cargo present in immature DCVs (iDCVs) but absent from mature DCVs (mDCVs) is aberrantly retained in mDCVs in *Cccp1KO* and *Eipr1KO* cells. These results suggest that CCCP1 is important for both sorting DCV cargo into DCVs, and to promoting cargo removal from iDCVs. Other cargo such as the cation-dependent mannose-6-phosphate receptor (CD-MPR) are known to follow a removal route. Interestingly, CCCP1 and EIPR1 have no effect on the removal of CD-MPR. Thus, CCCP1 is required specifically to remove CPD, likely via a novel removal pathway. I find that these proteins localize near the TGN of 832/13 cells, where the early stages of DCV biogenesis take place. Together, these functional and localization studies suggest that CCCP1 and EIPR1 are required to (1) sort luminal cargo into DCVs as they bud off TGN membranes, and (2) remove proteins not destined to mature DCVs in a post-TGN step.

5.2 MOLECULAR FUNCTIONS OF EIPR1 AND EARP

EIPR1 is a WD40 domain containing protein of unknown function, originally discovered in C. elegans for its DCV function phenotypes. I have contributed to work showing that EIPR1 interacts with the EARP complex (Topalidou et al., 2016). A parallel high-throughput study has shown that EIPR1 and EARP form a stable complex of 1:1 stoichiometry (Hein et al., 2015). EARP and EIPR1 were found to localize to recycling endosomes to regulate endocytic recycling of transferrin (Gershlick et al., 2016; Schindler et al., 2015). EARP and EIPR1 were the first recycling endosome-localized proteins discovered to function in a DCV biogenesis pathway, raising the fascinating possibility that endosomal recycling and the regulated secretory pathway are connected. Here, I show that EARP actually localizes to at least two pools, one at recycling

endosomes and another distinct one at CCCP1 positive compartments near TGN/iDCVs markers. It is unknown whether these two pools represent two independent functions of EARP (endocytic recycling for the endosomal pool, and DCV function for the CCCP1 positive pool) or these two pools are connected, such that both are relevant for DCV function.

What is the molecular function of EIPR1? EARP was proposed to act as a tethering complex but EIPR1's molecular function was unknown (Schindler et al., 2015). I have contributed to work showing that the absence of EIPR1 results in decreased levels of EARP complex subunits VPS50 and VPS51 suggesting that EIPR1 is needed for the stability of the EARP complex. The data suggest that EIPR1 is not critical for the EARP complex subunits to assemble into a complex, but is instead required for the proper localization of the EARP complex to membrane compartments, as well as its association with them. Thus, one of EIPR1's functions is to act as a localization factor for EARP.

5.3 MOLECULAR FUNCTIONS OF CCCP1

CCCP1 is a novel conserved protein discovered for its DCV function phenotypes in C. elegans. It is predicted to contain coiled-coil domains over most of its length. Here, I present a structure-function analysis on CCCP1 and have determined independent functions for the C-terminal CC3 domain and for the middle CC2 domain of the protein.

(1) The C-terminal CC3 domain is both necessary and sufficient for CCCP1's localization to membranes near TGN/iDCV markers and binding to active RAB2. Often Rab effectors are recruited to membranes via their interaction with activated Rabs. However, RAB2 is not required for CCCP1's localization. How does CCCP1 associate with TGN/iDCV membranes? CCCP1 could be recruited to membranes via an additional protein, or it could bind directly to membranes.

I found that CC3 is both necessary and sufficient to bind directly to synthetic membranes in vitro, raising the possibility that CC3 is a novel membrane interaction domain. The identity of the membranes bound by CC3 is unknown. CCCP1 localizes near TGN and iDCV markers. Super-resolution microscopy shows that it binds to membranes that surround proinsulin, and proximity biotinylation suggests that it is in close proximity to CPD, a protein that cycles through TGN, iDCVs, endosomes and the plasma membrane. Together, these data suggest that via its C-terminal CC3 domain, CCCP1 localizes to iDCVs, to subdomains of the TGN positive for CPD and iDCV cargo, or to both.

(2) The middle coiled-coil domain of CCCP1 (CC2) controls the localization of the EARP complex. I find that CCCP1 overexpression recruits VPS50 and displaces it from its recycling endosome pool. Moreover, relocation of CCCP1 to the mitochondria relocates EARP complex subunits to the mitochondria. The nature of the interaction between CCCP1 and EARP is unknown, but it requires EIPR1. We couldn't detect any physical interactions between CCCP1 and EIPR1 or EARP subunits, suggesting that CCCP1 might recruit EARP-positive membranes in a manner dependent on EIPR1. Consistent with this model is the finding that EIPR1 is important for EARP localization to membranes.

What is the molecular function of CCCP1? My cell biological, biochemical, and biophysical work suggest that CCCP1 is a member of the golgin family, a group of proteins that function as tethering factors between membranes before fusion. We propose that CCCP1's CC3 domain localizes CCCP1 to CPD-positive TGN or iDCV membranes while its CC2 domain recruits the EARP positive membranes via EIPR1. Why might a golgin be important in DCV biogenesis? There are several steps in DCV maturation that involve membrane fusion reactions that may require tethering molecules. One is the homotypic fusion of iDCVs. Another possibility

is the recycling of iDCV or plasma membrane proteins that are needed for the formation of new DCVs. One can imagine that yet unknown sorting receptors need to be retrieved. Another example is the SNARE Syntaxin 6, required for homotypic fusion of iDCVs and removed from iDCV during the maturation process. Such a recycling route has been observed using the DCV specific protein phogrin as a model cargo (Vo et al., 2004; Wasmeier et al., 2005). One possibility is that CCCP-1 interacts via CC2 with EARP positive transport vesicles to mediate the tethering of endosomally-derived vesicles that contain DCV cargo or recycled sorting factors.

5.4 FUTURE WORK

What are the molecular pathways that sort into DCVs, remove CPD from iDCVs and how do CCCP1, EIPR1 and EARP contribute to these pathways? To understand the pathway of DCV biogenesis, it is critical to understand at what points along the pathway CCCP1, EIPR1, and EARP act, as well as to discover new interactors and define their molecular functions.

I propose to characterize further the phenotypes caused by the absence of CCCP1 and EIPR1 in 832/13 cells by electron microscopy. Work in *C. elegans* has shown that in mutants of *rab-2* and its effectors, normal DCVs in number and morphology are generated. A limitation of the *C. elegans* work is that maturation status of DCVs was not investigated. Using 832/13 cells, it is critical to carry out the same study, and investigate the number, size, and morphology of mature DCVs-- but also to characterize immature DCVs.

One of our working hypotheses is that CCCP1, EIPR1, and EARP are required to recycle DCV cargo back to the TGN to be used for a new round of DCV biogenesis. A simple way to test this hypothesis is to chase the recycling of phogrin using an antibody to its luminal domain. If

CCCP1 and EIPR1 are needed for phogrin's recycling, we expect it to be impaired in *Cccp1KO* and *Eipr1KO* cells.

To gain insight into the molecular function of CCCP1, EIPR1, and EARP, it is critical to discover new interactors and to investigate the nature of the membranes with which they associate. I propose to improve the BioID screen. I propose to image cells that express my (mitochondria-relocated) proteins of interest by electron microscopy (EM) studies to visualize the nature of the membranes that relocated.

Live imaging is a critical tool to map intracellular trafficking pathways. To date, no precise in vivo live imaging studies observing DCV trafficking have been carried out. Observation of both the anterograde route (TGN exit of DCV cargo, removal of CPD, transport to release sites) and the retrograde route (protein recycling following DCV release) would inform us of pathways of DCV biogenesis. Observations of the point at which anterograde or retrograde DCV cargo transit through CCCP1 or EARP positive compartments would inform us of their functions.

BIBLIOGRAPHY

Ahras, M., Otto, G.P., and Tooze, S.A. (2006). Synaptotagmin IV is necessary for the maturation of secretory granules in PC12 cells. J Cell Biol *173*, 241–251.

Ailion, M., and Thomas, J.H. (2003). Isolation and Characterization of High-Temperature-Induced Dauer Formation Mutants in Caenorhabditis elegans. Genetics *165*, 127–144.

Ailion, M., Hannemann, M., Dalton, S., Pappas, A., Watanabe, S., Hegermann, J., Liu, Q., Han, H.-F., Gu, M., Goulding, M.Q., et al. (2014). Two Rab2 Interactors Regulate Dense-Core Vesicle Maturation. Neuron *82*, 167–180.

Antonny, B., Beraud-Dufour, S., Chardin, P., and Chabre, M. (1997). N-terminal hydrophobic residues of the G-protein ADP-ribosylation factor-1 insert into membrane phospholipids upon GDP to GTP exchange. Biochemistry (Mosc.) *36*, 4675–4684.

Arvan, P., and Castle, D. (1998). Sorting and storage during secretory granule biogenesis: looking backward and looking forward. Biochem. J. *332*, 593–610.

Arvan, P., and Halban, P.A. (2004). Sorting Ourselves Out: Seeking Consensus on Trafficking in the Beta-Cell. Traffic *5*, 53–61.

Asensio, C.S., Sirkis, D.W., and Edwards, R.H. (2010). RNAi screen identifies a role for adaptor protein AP-3 in sorting to the regulated secretory pathway. J. Cell Biol. *191*, 1173–1187.

Asensio, C.S., Sirkis, D.W., Maas Jr., J.W., Egami, K., To, T.-L., Brodsky, F.M., Shu, X., Cheng, Y., and Edwards, R.H. (2013). Self-Assembly of VPS41 Promotes Sorting Required for Biogenesis of the Regulated Secretory Pathway. Dev. Cell *27*, 425–437.

Austin, C., Hinners, I., and Tooze, S.A. (2000). Direct and GTP-dependent Interaction of ADP-ribosylation Factor 1 with Clathrin Adaptor Protein AP-1 on Immature Secretory Granules. J. Biol. Chem. *275*, 21862–21869.

Bäck, N., Rajagopal, C., Mains, R.E., and Eipper, B.A. (2010). Secretory Granule Membrane Protein Recycles through Multivesicular Bodies. Traffic *11*, 972–986.

Bigay, J., Casella, J.-F., Drin, G., Mesmin, B., and Antonny, B. (2005). ArfGAP1 responds to membrane curvature through the folding of a lipid packing sensor motif. EMBO J. *24*, 2244–2253.

Bonnemaison, M., Bäck, N., Lin, Y., Bonifacino, J.S., Mains, R., and Eipper, B. (2014). AP-1A Controls Secretory Granule Biogenesis and Trafficking of Membrane Secretory Granule Proteins. Traffic *15*, 1099–1121.

Borgonovo, B., Ouwendijk, J., and Solimena, M. (2006). Biogenesis of secretory granules. Curr. Opin. Cell Biol. *18*, 365–370.

Brenner, S. (1974). The Genetics of Caenorhabditis Elegans. Genetics *77*, 71–94.

Briguglio, J.S., Kumar, S., and Turkewitz, A.P. (2013). Lysosomal sorting receptors are essential for secretory granule biogenesis in Tetrahymena. J. Cell Biol. *203*, 537–550.

Brown, F.C., Schindelhaim, C.H., and Pfeffer, S.R. (2011). GCC185 plays independent roles in Golgi structure maintenance and AP-1–mediated vesicle tethering. J. Cell Biol. *194*, 779–787.

Buffa, L., Fuchs, E., Pietropaolo, M., Barr, F., and Solimena, M. (2008). ICA69 is a novel Rab2 effector regulating ER–Golgi trafficking in insulinoma cells. Eur. J. Cell Biol. *87*, 197–209.

Burgess, J., Jauregui, M., Tan, J., Rollins, J., Lallet, S., Leventis, P.A., Boulianne, G.L., Chang, H.C., Borgne, R.L., Krämer, H., et al. (2011). AP-1 and clathrin are essential for secretory granule biogenesis in Drosophila. Mol. Biol. Cell *22*, 2094–2105.

Cao, M., Mao, Z., Kam, C., Xiao, N., Cao, X., Shen, C., Cheng, K.K.Y., Xu, A., Lee, K.-M., Jiang, L., et al. (2013). PICK1 and ICA69 Control Insulin Granule Trafficking and Their Deficiencies Lead to Impaired Glucose Tolerance. PLoS Biol *11*, e1001541.

Caro, L.G., and Palade, G.E. (1964). PROTEIN SYNTHESIS, STORAGE, AND DISCHARGE IN THE PANCREATIC EXOCRINE CELL. J. Cell Biol. *20*, 473–495.

Cattin-Ortolá, J., Topalidou, I., Dosey, A., Merz, A.J., and Ailion, M. (2017). The dense-core vesicle maturation protein CCCP-1 binds RAB-2 and membranes through its C-terminal domain. Traffic *18*, 720–732.

Chanat, E., and Huttner, W.B. (1991). Milieu-induced, selective aggregation of regulated secretory proteins in the trans-Golgi network. J. Cell Biol. *115*, 1505–1519.

Cheung, P.P., Limouse, C., Mabuchi, H., and Pfeffer, S.R. (2015). Protein flexibility is required for vesicle tethering at the Golgi. ELife *4*.

Cheviet, S., Coppola, T., Haynes, L.P., Burgoyne, R.D., and Regazzi, R. (2004). The Rab-Binding Protein Noc2 Is Associated with Insulin-Containing Secretory Granules and Is Essential for Pancreatic β-Cell Exocytosis. Mol. Endocrinol. *18*, 117–126.

Conibear, E., Stevens, T.H., and Kaiser, C. (2000). Vps52p, Vps53p, and Vps54p Form a Novel Multisubunit Complex Required for Protein Sorting at the Yeast Late Golgi. Mol. Biol. Cell *11*, 305–323.

Conibear, E., Cleck, J.N., and Stevens, T.H. (2003). Vps51p mediates the association of the GARP (Vps52/53/54) complex with the late Golgi t-SNARE Tlg1p. Mol. Biol. Cell *14*, 1610–1623.

Csizmadia, T., Lőrincz, P., Hegedűs, K., Széplaki, S., Lőw, P., and Juhász, G. (2018). Molecular mechanisms of developmentally programmed crinophagy in Drosophila. J Cell Biol *217*, 361–374.

Davidson, H.W. (2004). (Pro)Insulin processing. Cell Biochem. Biophys. *40*, 143–157.

Dikeakos, J.D., and Reudelhuber, T.L. (2007). Sending proteins to dense core secretory granules: still a lot to sort out. J. Cell Biol.

Dikeakos, J.D., Lello, P.D., Lacombe, M.-J., Ghirlando, R., Legault, P., Reudelhuber, T.L., and Omichinski, J.G. (2009). Functional and structural characterization of a dense core secretory granule sorting domain from the PC1/3 protease. Proc. Natl. Acad. Sci. *106*, 7408–7413.

Dittie, A.S., Hajibagheri, N., and Tooze, S.A. (1996). The AP-1 adaptor complex binds to immature secretory granules from PC12 cells, and is regulated by ADP-ribosylation factor. J. Cell Biol. *132*, 523–536.

Dittié, A.S., Thomas, L., Thomas, G., and Tooze, S.A. (1997). Interaction of furin in immature secretory granules from neuroendocrine cells with the AP-1 adaptor complex is modulated by casein kinase II phosphorylation. EMBO J. *16*, 4859–4870.

Dittie, A.S., Klumperman, J., and Tooze, S.A. (1999). Differential distribution of mannose-6-phosphate receptors and furin in immature secretory granules. J Cell Sci *112*, 3955–3966.

Drin, G., and Antonny, B. (2010). Amphipathic helices and membrane curvature. FEBS Lett. *584*, 1840–1847.

Drin, G., Casella, J.-F., Gautier, R., Boehmer, T., Schwartz, T.U., and Antonny, B. (2007). A general amphipathic α-helical motif for sensing membrane curvature. Nat. Struct. Mol. Biol. *14*, 138–146.

Du, W., Zhou, M., Zhao, W., Cheng, D., Wang, L., Lu, J., Song, E., Feng, W., Xue, Y., Xu, P., et al. (2016). HID-1 is required for homotypic fusion of immature secretory granules during maturation. ELife *5*, e18134.

Edwards, S.L., Charlie, N.K., Richmond, J.E., Hegermann, J., Eimer, S., and Miller, K.G. (2009). Impaired dense core vesicle maturation in Caenorhabditis elegans mutants lacking Rab2. J. Cell Biol. *186*, 881–895.

Feng, L., and Arvan, P. (2003). The Trafficking of α1-Antitrypsin, a Post-Golgi Secretory Pathway Marker, in INS-1 Pancreatic Beta Cells. J. Biol. Chem. *278*, 31486–31494.

Fricker, L.D. (2013). Chapter 235 - Carboxypeptidases E and D. In Handbook of Biologically Active Peptides (Second Edition), A.J. Kastin, ed. (Boston: Academic Press), pp. 1715–1720.

Frøkjær-Jensen, C., Davis, M.W., Hopkins, C.E., Newman, B., Thummel, J.M., Olesen, S.-P., Grunnet, M., and Jorgensen, E.M. (2008). Single copy insertion of transgenes in C. elegans. Nat. Genet. *40*, 1375–1383.

Frøkjær-Jensen, C., Davis, M.W., Ailion, M., and Jorgensen, E.M. (2012). Improved Mos1-mediated transgenesis in C. elegans. Nat. Methods *9*, 117–118.

Fukuda, M. (2008). Regulation of secretory vesicle traffic by Rab small GTPases. Cell. Mol. Life Sci. CMLS *65*, 2801–2813.

Gautier, R., Douguet, D., Antonny, B., and Drin, G. (2008). HELIQUEST: a web server to screen sequences with specific α-helical properties. Bioinformatics *24*, 2101–2102.

Gehart, H., Goginashvili, A., Beck, R., Morvan, J., Erbs, E., Formentini, I., De Matteis, M.A., Schwab, Y., Wieland, F.T., and Ricci, R. (2012). The BAR Domain Protein Arfaptin-1 Controls Secretory Granule Biogenesis at the trans-Golgi Network. Dev. Cell *23*, 756–768.

Gershlick, D.C., Schindler, C., Chen, Y., and Bonifacino, J.S. (2016). TSSC1 is novel component of the endosomal retrieval machinery. Mol. Biol. Cell *27*, 2867–2878.

Ghosh, P., Dahms, N.M., and Kornfeld, S. (2003). Mannose 6-phosphate receptors: new twists in the tale. Nat. Rev. Mol. Cell Biol. *4*, nrm1050.

Gibson, D.G., Young, L., Chuang, R.-Y., Venter, J.C., Hutchison, C.A., and Smith, H.O. (2009). Enzymatic assembly of DNA molecules up to several hundred kilobases. Nat. Methods *6*, 343–345.

Gillingham, A.K., and Munro, S. (2003). Long coiled-coil proteins and membrane traffic. Biochim. Biophys. Acta BBA - Mol. Cell Res. *1641*, 71–85.

Gillingham, A.K., and Munro, S. (2016). Finding the Golgi: Golgin Coiled-Coil Proteins Show the Way. Trends Cell Biol. *0*.

Gillingham, A.K., Sinka, R., Torres, I.L., Lilley, K.S., and Munro, S. (2014). Toward a Comprehensive Map of the Effectors of Rab GTPases. Dev. Cell *31*, 358–373.

Glombik, M.M., Krömer, A., Salm, T., Huttner, W.B., and Gerdes, H.-H. (1999). The disulfide-bonded loop of chromogranin B mediates membrane binding and directs sorting from the trans-Golgi network to secretory granules. EMBO J. *18*, 1059–1070.

Gondré-Lewis, M.C., Park, J.J., and Loh, Y.P. (2012). Cellular mechanisms for the biogenesis and transport of synaptic and dense-core vesicles. Int. Rev. Cell Mol. Biol. *299*, 27–115.

Griffiths, G., and Simons, K. (1986). The trans Golgi network: sorting at the exit site of the Golgi complex. Science *234*, 438–443.

Hammarlund, M., Watanabe, S., Schuske, K., and Jorgensen, E.M. (2008). CAPS and syntaxin dock dense core vesicles to the plasma membrane in neurons. J Cell Biol *180*, 483–491.

Hannemann, M., Sasidharan, N., Hegermann, J., Kutscher, L.M., Koenig, S., and Eimer, S. (2012). TBC-8, a Putative RAB-2 GAP, Regulates Dense Core Vesicle Maturation in Caenorhabditis elegans. PLoS Genet *8*, e1002722.

Hao, Z., Wei, L., Feng, Y., Chen, X., Du, W., Ma, J., Zhou, Z., Chen, L., and Li, W. (2015). Impaired maturation of large dense-core vesicles in muted-deficient adrenal chromaffin cells. J. Cell Sci. *128*, 1365–1374.

Hein, M.Y., Hubner, N.C., Poser, I., Cox, J., Nagaraj, N., Toyoda, Y., Gak, I.A., Weisswange, I., Mansfeld, J., Buchholz, F., et al. (2015). A Human Interactome in Three Quantitative Dimensions Organized by Stoichiometries and Abundances. Cell *163*, 712–723.

Hirst, J., Borner, G.H.H., Antrobus, R., Peden, A.A., Hodson, N.A., Sahlender, D.A., and Robinson, M.S. (2012). Distinct and Overlapping Roles for AP-1 and GGAs Revealed by the "Knocksideways" System. Curr. Biol. *22*, 1711–1716.

Hohmeier, H.E., Mulder, H., Chen, G., Henkel-Rieger, R., Prentki, M., and Newgard, C.B. (2000). Isolation of INS-1-derived cell lines with robust ATP-sensitive K+ channel-dependent and -independent glucose-stimulated insulin secretion. Diabetes *49*, 424–430.

Holst, B., Madsen, K.L., Jansen, A.M., Jin, C., Rickhag, M., Lund, V.K., Jensen, M., Bhatia, V., Sørensen, G., Madsen, A.N., et al. (2013). PICK1 Deficiency Impairs Secretory Vesicle Biogenesis and Leads to Growth Retardation and Decreased Glucose Tolerance. PLoS Biol *11*, e1001542.

Huang, X.F., and Arvan, P. (1994). Formation of the insulin-containing secretory granule core occurs within immature beta-granules. J. Biol. Chem. *269*, 20838–20844.

Hutton, J.C. (1994). Insulin secretory granule biogenesis and the proinsulin-processing endopeptidases. Diabetologia *37 Suppl 2*, S48-56.

Ishida, R., Yamamoto, A., Nakayama, K., Sohda, M., Misumi, Y., Yasunaga, T., and Nakamura, N. (2015). GM130 is a parallel tetramer with a flexible rod-like structure and N-terminally open (Y-shaped) and closed (I-shaped) conformations. FEBS J. *282*, 2232–2244.

Johnson, K.F., and Kornfeld, S. (1992). A His-Leu-Leu sequence near the carboxyl terminus of the cytoplasmic domain of the cation-dependent mannose 6-phosphate receptor is necessary for the lysosomal enzyme sorting function. J. Biol. Chem. *267*, 17110–17115.

Kakhlon, O., Sakya, P., Larijani, B., Watson, R., and Tooze, S.A. (2006). GGA function is required for maturation of neuroendocrine secretory granules. EMBO J. *25*, 1590–1602.

Kebede, M.A., Oler, A.T., Gregg, T., Balloon, A.J., Johnson, A., Mitok, K., Rabaglia, M., Schueler, K., Stapleton, D., Thorstenson, C., et al. (2014). SORCS1 is necessary for normal insulin secretory granule biogenesis in metabolically stressed β cells. J. Clin. Invest. *124*, 4240–4256.

Kim, T., Gondré-Lewis, M.C., Arnaoutova, I., and Loh, Y.P. (2006). Dense-Core Secretory Granule Biogenesis. Physiology *21*, 124–133.

Kirchhausen, T., Bonifacinot, J.S., and RiezmanS, H. Linking cargo to vesicle formation: receptor tail interactions with coat proteins. 8.

Klausner, R.D., Donaldson, J.G., and Lippincott-Schwartz, J. (1992). Brefeldin A: insights into the control of membrane traffic and organelle structure. J. Cell Biol. *116*, 1071–1080.

Klumperman, J., Kuliawat, R., Griffith, J.M., Geuze, H.J., and Arvan, P. (1998). Mannose 6–Phosphate Receptors Are Sorted from Immature Secretory Granules via Adaptor Protein AP-1, Clathrin, and Syntaxin 6–positive Vesicles. J. Cell Biol. *141*, 359–371.

Kögel, T., Rudolf, R., Hodneland, E., Copier, J., Regazzi, R., Tooze, S.A., and Gerdes, H.-H. (2013). Rab3D Is Critical for Secretory Granule Maturation in PC12 Cells. PLoS ONE *8*, e57321.

Kögel Tanja, Rudolf Rüdiger, Hodneland Erlend, Hellwig Andrea, Kuznetsov Sergei A., Seiler Florian, Söllner Thomas H., Barroso João, and Gerdes Hans-Hermann (2010). Distinct Roles of Myosin Va in Membrane Remodeling and Exocytosis of Secretory Granules. Traffic *11*, 637–650.

Kuroki, K., Eng, F., Ishikawa, T., Turck, C., Harada, F., and Ganem, D. (1995). gp180, a host cell glycoprotein that binds duck hepatitis B virus particles, is encoded by a member of the carboxypeptidase gene family. J. Biol. Chem. *270*, 15022–15028.

Li, H., Waites, C.L., Staal, R.G., Dobryy, Y., Park, J., Sulzer, D.L., and Edwards, R.H. (2005). Sorting of Vesicular Monoamine Transporter 2 to the Regulated Secretory Pathway Confers the Somatodendritic Exocytosis of Monoamines. Neuron *48*, 619–633.

Lippincott-Schwartz, J., Yuan, L., Tipper, C., Amherdt, M., Orci, L., and Klausner, R.D. (1991). Brefeldin A's effects on endosomes, lysosomes, and the TGN suggest a general mechanism for regulating organelle structure and membrane traffic. Cell *67*, 601–616.

Lőrincz, P., Tóth, S., Benkő, P., Lakatos, Z., Boda, A., Glatz, G., Zobel, M., Bisi, S., Hegedűs, K., Takáts, S., et al. (2017). Rab2 promotes autophagic and endocytic lysosomal degradation. J Cell Biol *216*, 1937–1947.

Matsunaga, K., Taoka, M., Isobe, T., and Izumi, T. (2017). Rab2a and Rab27a cooperatively regulate the transition from granule maturation to exocytosis through the dual effector Noc2. J Cell Sci *130*, 541–550.

Mello, C.C., Kramer, J.M., Stinchcomb, D., and Ambros, V. (1991). Efficient gene transfer in C.elegans: extrachromosomal maintenance and integration of transforming sequences. EMBO J. *10*, 3959–3970.

Mesa, R., Luo, S., Hoover, C.M., Miller, K., Minniti, A., Inestrosa, N., and Nonet, M.L. (2011). HID-1, a New Component of the Peptidergic Signaling Pathway. Genetics *187*, 467–483.

Miller, M.B., Vishwanatha, K.S., Mains, R.E., and Eipper, B.A. (2015). An N-terminal Amphipathic Helix Binds Phosphoinositides and Enhances Kalirin Sec14 Domain-mediated Membrane Interactions. J. Biol. Chem. *290*, 13541–13555.

Molinete, M., Dupuis, S., Brodsky, F.M., and Halban, P.A. (2001). Role of clathrin in the regulated secretory pathway of pancreaticβ -cells. J. Cell Sci. *114*, 3059–3066.

Monies, D., Abouelhoda, M., AlSayed, M., Alhassnan, Z., Alotaibi, M., Kayyali, H., Al-Owain, M., Shah, A., Rahbeeni, Z., Al-Muhaizea, M.A., et al. (2017). The landscape of genetic diseases in Saudi Arabia based on the first 1000 diagnostic panels and exomes. Hum. Genet. 1–19.

Morvan, J., and Tooze, S.A. (2008). Discovery and progress in our understanding of the regulated secretory pathway in neuroendocrine cells. Histochem. Cell Biol. *129*, 243–252.

Munro, S., and Nichols, B.J. (1999). The GRIP domain – a novel Golgi-targeting domain found in several coiled-coil proteins. Curr. Biol. *9*, 377–380.

Murray, D.H., Jahnel, M., Lauer, J., Avellaneda, M.J., Brouilly, N., Cezanne, A., Morales-Navarrete, H., Perini, E.D., Ferguson, C., Lupas, A.N., et al. (2016). An endosomal tether undergoes an entropic collapse to bring vesicles together. Nature *537*, 107–111.

Paquin, N., Murata, Y., Froehlich, A., Omura, D.T., Ailion, M., Pender, C.L., Constantine-Paton, M., and Horvitz, H.R. (2016). The Conserved VPS-50 Protein Functions in Dense-Core Vesicle Maturation and Acidification and Controls Animal Behavior. Curr. Biol. *26*, 862–871.

Pérez-Victoria, F.J., and Bonifacino, J.S. (2009). Dual Roles of the Mammalian GARP Complex in Tethering and SNARE Complex Assembly at the trans-Golgi Network. Mol. Cell. Biol. *29*, 5251–5263.

Pérez-Victoria, F.J., Mardones, G.A., and Bonifacino, J.S. (2008). Requirement of the Human GARP Complex for Mannose 6-phosphate-receptor-dependent Sorting of Cathepsin D to Lysosomes. Mol. Biol. Cell *19*, 2350–2362.

Pérez-Victoria, F.J., Schindler, C., Magadán, J.G., Mardones, G.A., Delevoye, C., Romao, M., Raposo, G., and Bonifacino, J.S. (2010). Ang2/Fat-Free Is a Conserved Subunit of the Golgi-associated Retrograde Protein Complex. Mol. Biol. Cell *21*, 3386–3395.

Pinheiro, P.S., Jansen, A.M., Wit, H. de, Tawfik, B., Madsen, K.L., Verhage, M., Gether, U., and Sørensen, J.B. (2014). The BAR Domain Protein PICK1 Controls Vesicle Number and Size in Adrenal Chromaffin Cells. J. Neurosci. *34*, 10688–10700.

Ran, F.A., Hsu, P.D., Wright, J., Agarwala, V., Scott, D.A., and Zhang, F. (2013). Genome engineering using the CRISPR-Cas9 system. Nat. Protoc. *8*, 2281–2308.

Robinson, M.S. (2004). Adaptable adaptors for coated vesicles. Trends Cell Biol. *14*, 167–174.

Roth, J., Taatjes, D.J., Lucocq, J.M., Weinstein, J., and Paulson, J.C. (1985). Demonstration of an extensive trans-tubular network continuous with the Golgi apparatus stack that may function in glycosylation. Cell *43*, 287–295.

Roux, K.J., Kim, D.I., Raida, M., and Burke, B. (2012). A promiscuous biotin ligase fusion protein identifies proximal and interacting proteins in mammalian cells. J Cell Biol *196*, 801–810.

Sahu, B.S., Manna, P.T., Edgar, J.R., Antrobus, R., Mahata, S.K., Bartolomucci, A., Borner, G.H.H., and Robinson, M.S. (2017). Role of clathrin in dense core vesicle biogenesis. Mol. Biol. Cell *28*, 2676–2685.

Sapperstein, S.K., Walter, D.M., Grosvenor, A.R., Heuser, J.E., and Waters, M.G. (1995). p115 is a general vesicular transport factor related to the yeast endoplasmic reticulum to Golgi transport factor Uso1p. Proc. Natl. Acad. Sci. *92*, 522–526.

Sasidharan, N., Sumakovic, M., Hannemann, M., Hegermann, J., Liewald, J.F., Olendrowitz, C., Koenig, S., Grant, B.D., Rizzoli, S.O., Gottschalk, A., et al. (2012). RAB-5 and RAB-10 cooperate to regulate neuropeptide release in Caenorhabditis elegans. Proc. Natl. Acad. Sci. *109*, 18944–18949.

Schindler, C., Chen, Y., Pu, J., Guo, X., and Bonifacino, J.S. (2015). EARP is a multisubunit tethering complex involved in endocytic recycling. Nat. Cell Biol. *17*, 639–650.

Sheffield, P., Garrard, S., and Derewenda, Z. (1999). Overcoming Expression and Purification Problems of RhoGDI Using a Family of "Parallel" Expression Vectors. Protein Expr. Purif. *15*, 34–39.

Shin, J.J.H., Gillingham, A.K., Begum, F., Chadwick, J., and Munro, S. (2017). TBC1D23 is a bridging factor for endosomal vesicle capture by golgins at the *trans*-Golgi. Nat. Cell Biol. ncb3627.

Stenmark, H. (2009). Rab GTPases as coordinators of vesicle traffic. Nat. Rev. Mol. Cell Biol. *10*, 513–525.

Sumakovic, M., Hegermann, J., Luo, L., Husson, S.J., Schwarze, K., Olendrowitz, C., Schoofs, L., Richmond, J., and Eimer, S. (2009). UNC-108/RAB-2 and its effector RIC-19 are involved in dense core vesicle maturation in Caenorhabditis elegans. J. Cell Biol. *186*, 897–914.

Sztul, E., and Lupashin, V. (2009). Role of vesicle tethering factors in the ER-Golgi membrane traffic. FEBS Lett. *583*, 3770–3783.

Tooze, S.A., Martens, G.J., and Huttner, W.B. (2001). Secretory granule biogenesis: rafting to the SNARE. Trends Cell Biol. *11*, 116–122.

Topalidou, I., Cattin-Ortolá, J., Pappas, A.L., Cooper, K., Merrihew, G.E., MacCoss, M.J., and Ailion, M. (2016). The EARP Complex and Its Interactor EIPR-1 Are Required for Cargo Sorting to Dense-Core Vesicles. PLOS Genet. *12*, e1006074.

Torii, S., Saito, N., Kawano, A., Zhao, S., Izumi, T., and Takeuchi, T. (2005). Cytoplasmic Transport Signal is Involved in Phogrin Targeting and Localization to Secretory Granules. Traffic *6*, 1213–1224.

Torres, I.L., Rosa-Ferreira, C., and Munro, S. (2014). The Arf family G protein Arl1 is required for secretory granule biogenesis in Drosophila. J. Cell Sci. *127*, 2151–2160.

Tropea, J.E., Cherry, S., and Waugh, D.S. (2009). Expression and Purification of Soluble His6-Tagged TEV Protease. In High Throughput Protein Expression and Purification, (Humana Press), pp. 297–307.

Urbé, S., Page, L.J., and Tooze, S.A. (1998). Homotypic Fusion of Immature Secretory Granules during Maturation in a Cell-free Assay. J Cell Biol *143*, 1831–1844.

Varlamov, O., and Fricker, L.D. (1998). Intracellular trafficking of metallocarboxypeptidase D in AtT-20 cells: localization to the trans-Golgi network and recycling from the cell surface. J. Cell Sci. *111*, 877–885.

Varlamov, O., Eng, F.J., Novikova, E.G., and Fricker, L.D. (1999a). Localization of Metallocarboxypeptidase D in AtT-20 Cells POTENTIAL ROLE IN PROHORMONE PROCESSING. J. Biol. Chem. *274*, 14759–14767.

Varlamov, O., Wu, F., Shields, D., and Fricker, L.D. (1999b). Biosynthesis and Packaging of Carboxypeptidase D into Nascent Secretory Vesicles in Pituitary Cell Lines. J. Biol. Chem. *274*, 14040–14045.

Vo, Y.P., Hutton, J.C., and Angleson, J.K. (2004). Recycling of the dense-core vesicle membrane protein phogrin in Min6 β-cells. Biochem. Biophys. Res. Commun. *324*, 1004–1010.

Waites, C.L., Mehta, A., Tan, P.K., Thomas, G., Edwards, R.H., and Krantz, D.E. (2001). An Acidic Motif Retains Vesicular Monoamine Transporter 2 on Large Dense Core Vesicles. J. Cell Biol. *152*, 1159–1168.

Walter, A.M., Kurps, J., Wit, H. de, Schöning, S., Toft-Bertelsen, T.L., Lauks, J., Ziomkiewicz, I., Weiss, A.N., Schulz, A., Mollard, G.F. von, et al. (2014). The SNARE protein vti1a functions in dense-core vesicle biogenesis. EMBO J. *33*, 1681–1697.

Wasmeier, C., Burgos, P.V., Trudeau, T., Davidson, H.W., and Hutton, J.C. (2005). An Extended Tyrosine-Targeting Motif for Endocytosis and Recycling of the Dense-Core Vesicle Membrane Protein Phogrin. Traffic *6*.

Wendler, F., Page, L., Urbé, S., and Tooze, S.A. (2001). Homotypic Fusion of Immature Secretory Granules During Maturation Requires Syntaxin 6. Mol. Biol. Cell *12*, 1699–1709.

Witkos, T.M., and Lowe, M. (2016). The Golgin Family of Coiled-Coil Tethering Proteins. Front. Cell Dev. Biol. *3*.

Wong, M., and Munro, S. (2014). The specificity of vesicle traffic to the Golgi is encoded in the golgin coiled-coil proteins. Science *346*, 1256898–1256898.

Xin, X., Varlamov, O., Day, R., Dong, W., Bridgett, M.M., Leiter, E.H., and Fricker, L.D. (1997). Cloning and Sequence Analysis of cDNA Encoding Rat Carboxypeptidase D. DNA Cell Biol. *16*, 897–909.

Yi, Z., Yokota, H., Torii, S., Aoki, T., Hosaka, M., Zhao, S., Takata, K., Takeuchi, T., and Izumi, T. (2002). The Rab27a/granuphilin complex regulates the exocytosis of insulin-containing dense-core granules. Mol. Cell. Biol. *22*, 1858–1867.

Yin, J., Huang, Y., Guo, P., Hu, S., Yoshina, S., Xuan, N., Gan, Q., Mitani, S., Yang, C., and Wang, X. (2017). GOP-1 promotes apoptotic cell degradation by activating the small GTPase Rab2 in C. elegans. J Cell Biol jcb.201610001.

Yu, I.-M., and Hughson, F.M. (2010). Tethering factors as organizers of intracellular vesicular traffic. Annu. Rev. Cell Dev. Biol. *26*, 137–156.

Yu, Y., Wang, L., Jiu, Y., Zhan, Y., Liu, L., Xia, Z., Song, E., Xu, P., and Xu, T. (2011). HID-1 is a novel player in the regulation of neuropeptide sorting. Biochem. J. *434*, 383–390.

Zhang, X., Jiang, S., Mitok, K.A., Li, L., Attie, A.D., and Martin, T.F.J. (2017). BAIAP3, a C2 domain–containing Munc13 protein, controls the fate of dense-core vesicles in neuroendocrine cells. J Cell Biol *216*, 2151–2166.

APPENDIX A

Alignment of the CCCP-1 protein. Alignment of CCCP-1 proteins from *Capsaspora owczarzaki* (Capsaspora, CAOG_00459, accession # XP_004365330.2), *Monosiga brevicollis* (Choano, hypothetical protein, accession # XP_001745351.1), *Drosophila melanogaster* (Fly, golgin 104, accession # NP_648879.1), *Takifugu rubripes* (Fugu, Ccdc186, XP_011604585.1), *Homo sapiens* (Human, Ccdc186, accession # AAI03500.1), *Hydra vulgaris* (Hydra, Ccdc186-like, XP_012558241.1), *Rattus norvegicus* (Rat, Ccdc186, accession # KX954625), *Amphimedon queenslandica* (Sponge, Ccdc186-like, XP_011409991.1), *C. elegans* (Worm, CCCP-1b, accession # NP_499628.1). Identical residues are shaded in black and similar residues are shaded in grey. Alignment was made with T-Coffee[1], http://www.ebi.ac.uk/Tools/msa/tcoffee/, using default parameters and exhibited with BoxShade 3.21 (http://embnet.vital-it.ch/software/BOX_form.html). The coiled-coil domains of the worm protein (from SMART[2], http://smart.embl-heidelberg.de) are marked with blue bars. The CC3 domain of worm CCCP-1 is marked with a red bar. The presence of potential amphipathic helices in the CC3 domain was determined using the following settings in HeliQuest[3] (http://heliquest.ipmc.cnrs.fr): Helix type: α, window size: 18 amino acids, Hydrophobic moment (μH) peaks above 0.35. The predicted helices with a patch of five or more hydrophobic amino acids are numbered 1, 2 and 3. In the human ortholog, the region of helices #1 and #2 is still predicted to form amphipathic helices, but the region of helix #3 is not predicted to form an amphipathic helix.

1. Notredame C, Higgins DG, Heringa J. T-Coffee: A novel method for fast and accurate multiple sequence alignment. J Mol Biol. 2000;302(1):205-217.

2. Schultz J, Milpetz F, Bork P, Ponting CP. SMART, a simple modular architecture research tool: Identification of signaling domains. Proc Natl Acad Sci. 1998;95(11):5857-5864.

3. Gautier R, Douguet D, Antonny B, Drin G. HELIQUEST: a web server to screen sequences with specific α-helical properties. Bioinformatics. 2008;24(18):2101-2102.

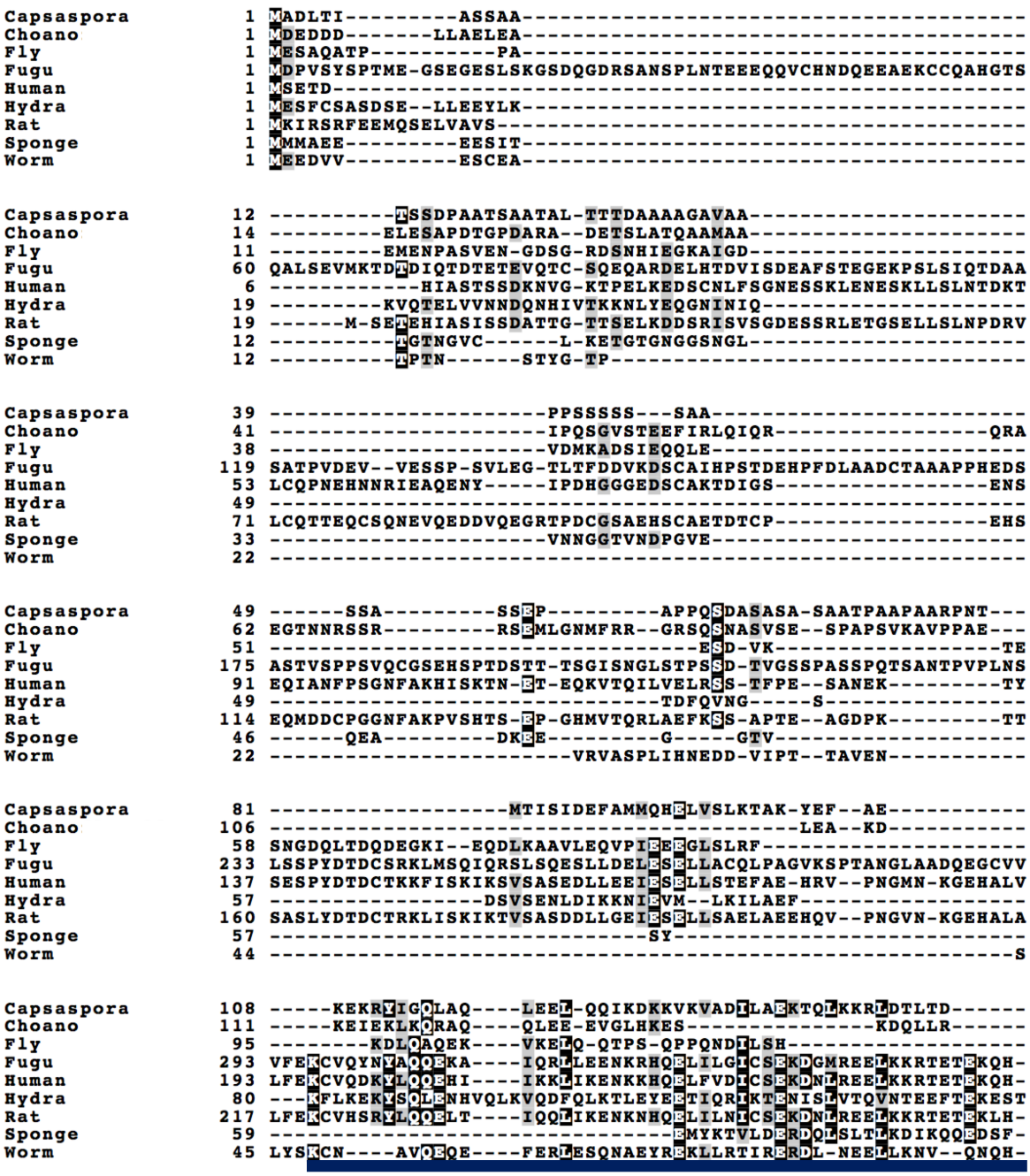

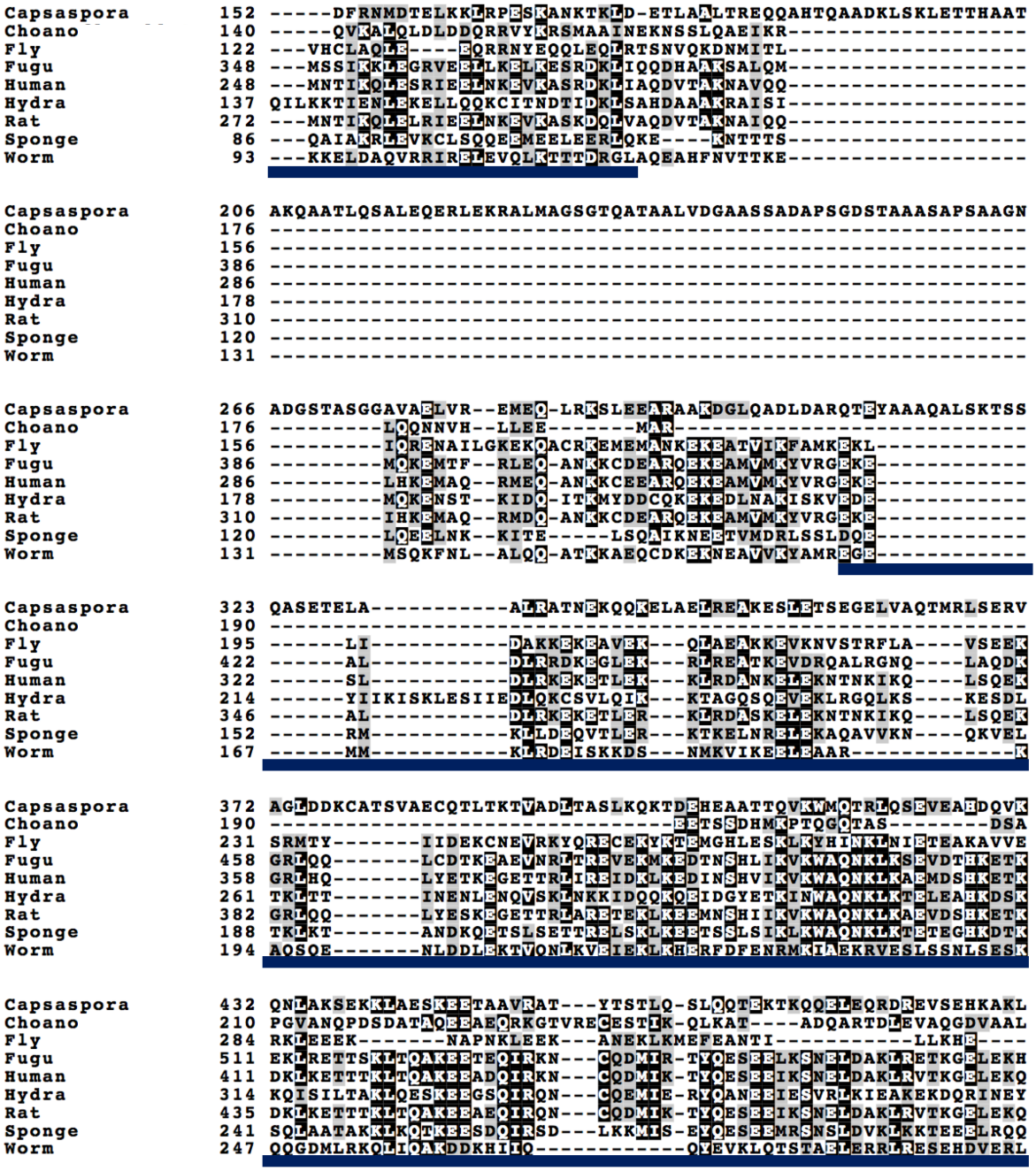
Capsaspora 152 -----DFRNMDTELKKLRPESKANKTKLD-ETLAALTREQQAHTQAADKLSKLETTHAAT
Choano 140 -----QVKALQLDLDDQRRVYKRSMAAINEKNSSLQAEIKR----------
Fly 122 ---VHCLAQLE----EQRRNYEQQLEQLRTSNVQKDNMITL----------
Fugu 348 ---MSSIKKLEGRVESLLKELKESRDKLIQQDHAAKSALQM----------
Human 248 ---MNTIKQLESRIEELNKEVKASRDKLIAQDVTAKNAVQQ----------
Hydra 137 QILKKTIENLEKELLQQKCITNDTIDKLSAHDAAAKRAISI----------
Rat 272 ---MNTIKQLELRIEELNKEVKASKDQLVAQDVTAKNAIQQ----------
Sponge 86 ---QAIAKRLEVKCLSQQEEMEELEERLQKE----KNTTTS----------
Worm 93 ---KKELDAQVRRIRELEVQLKTTTDRGLAQEAHFNVTTKE----------
Capsaspora 206 AKQAATLQSALEQERLEKRALMAGSGTQATAALVDGAASSADAPSGDSTAAASAPSAAGN
Choano 176 ----------
Fly 156 ----------
Fugu 386 ----------
Human 286 ----------
Hydra 178 ----------
Rat 310 ----------
Sponge 120 ----------
Worm 131 ----------
Capsaspora 266 ADGSTASGGAVAELVR--EMEQ-LRKSLEEARAAKDGLQADLDARQTEYAAAQALSKTSS
Choano 176 ---------LQQNNVH--LLEE-------MAR----------
Fly 156 ---------IQRENAILGKEKQACRKEMEMANKEKEATVIKFAMKEKL----------
Fugu 386 ---------MQKEMTF--RLEQ-ANKKCDEARQEKEAMVMKYVRGEKE----------
Human 286 ---------LHKEMAQ--RMEQ-ANKKCEEARQEKEAMVMKYVRGEKE----------
Hydra 178 ---------MQKENST--KIDQ-ITKMYDDCQKEKEDLNAKISKVEDE----------
Rat 310 ---------IHKEMAQ--RMDQ-ANKKCDEARQEKEAMVMKYVRGEKE----------
Sponge 120 ---------LQEELNK--KITE-----LSQAIKNEETVMDRLSSLDQE----------
Worm 131 ---------MSQKFNL--ALQQ-ATKKAEQCDKEKNEAVVKYAMREGE----------
Capsaspora 323 QASETELA-----------ALRATNEKQQKELAELREAKESLETSEGELVAQTMRLSERV
Choano 190 ----------
Fly 195 ------LI----------DAKKEKEAVEK---QLAEAKKEVKNVSTRFLA----VSEEK
Fugu 422 ------AL----------DLRRDKEGLEK---RLREATKEVDRQALRGNQ----LAQDK
Human 322 ------SL----------DLRKEKETLEK---KLRDANKELEKNTNKIKQ----LSQEK
Hydra 214 ------YIIKISKLESIIEDLQKCSVLQIK---KTAGQSQEVEKLRGQLKS----KESDL
Rat 346 ------AL----------DLRKEKETLER---KLRDASKELEKNTNKIKQ----LSQEK
Sponge 152 ------RM----------KLLDEQVTLER---KTKELNRELEKAQAVVKN----QKVEL
Worm 167 ------MM----------KLRDEISKKDS---NMKVIKELEAAR----------K
Capsaspora 372 AGLDDKCATSVAECQTLTKTVADLTASLKQKTDEHEAATTQVKWMQTRLQSEVEAHDQVK
Choano 190 ----------EETSSDHMKPTQGQTAS--------DSA
Fly 231 SRMTY-------IIDEKCNEVRKYQRECEKYKTEMGHLESKLKYHINKLNIETEAKAVVE
Fugu 458 GRLQQ-------LCDTKEAEVNRLTREVEKMKEDTNSHLIKVKWAQNKLKSEVDTHKETK
Human 358 GRLHQ-------LYETKEGETTRLIREIDKLKEDINSHVIKVKWAQNKLKAEMDSHKETK
Hydra 261 TKLTT-------INENLENQVSKLNKKIDQQKQEIDGYETKINWAQNKLKTELEAHKDSK
Rat 382 GRLQQ-------LYESKEGETTRLARETEKLKEEMNSHIIKVKWAQNKLKAEVDSHKETK
Sponge 188 TKLKT-------ANDKQETSLSETTRELSKLKEETSSLSIKLKWAQNKLKTETEGHKDTK
Worm 194 AQSQE-------NLDDLEKTVQNLKVEIEKLKHERFDFENRMKIAEKRVESLSSNLSESK
Capsaspora 432 QNLAKSEKKLAESKEETAAVRAT---YTSTLQ-SLQQTEKTKQQELEQRDREVSEHKAKL
Choano 210 PGVANQPDSDATAQEEAEQRKGTVRECESTIK-QLKAT----ADQARTDLEVAQGDVAAL
Fly 284 RKLEEEK-------NAPNKLEEK---ANEKLKMEFEANTI----------LLKHE----
Fugu 511 EKLRETTSKLTQAKEETEQIRKN---CQDMIR-TYQESEELKSNELDAKLRETKGELEKH
Human 411 DKLKETTTKLTQAKEEADQIRKN---CQDMIK-TYQESEEIKSNELDAKLRVTKGELEKQ
Hydra 314 KQISILTAKLQESKEEGSQIRQN---CQEMIE-RYQANEEIESVRLKIEAKEKDQRINEY
Rat 435 DKLKETTTKLTQAKEEAEQIRQN---CQDMIK-TYQESEEIKSNELDAKLRVTKGELEKQ
Sponge 241 SQLAATAKKLKQTKEESDQIRSD---LKKMIS-EYQESEEMRSNSLDVKLKKTEEELRQQ
Worm 247 QQGDMLRKQLIQAKDDKHIIQ----------QYEVKLQTSTAELERRLRESEHDVERL

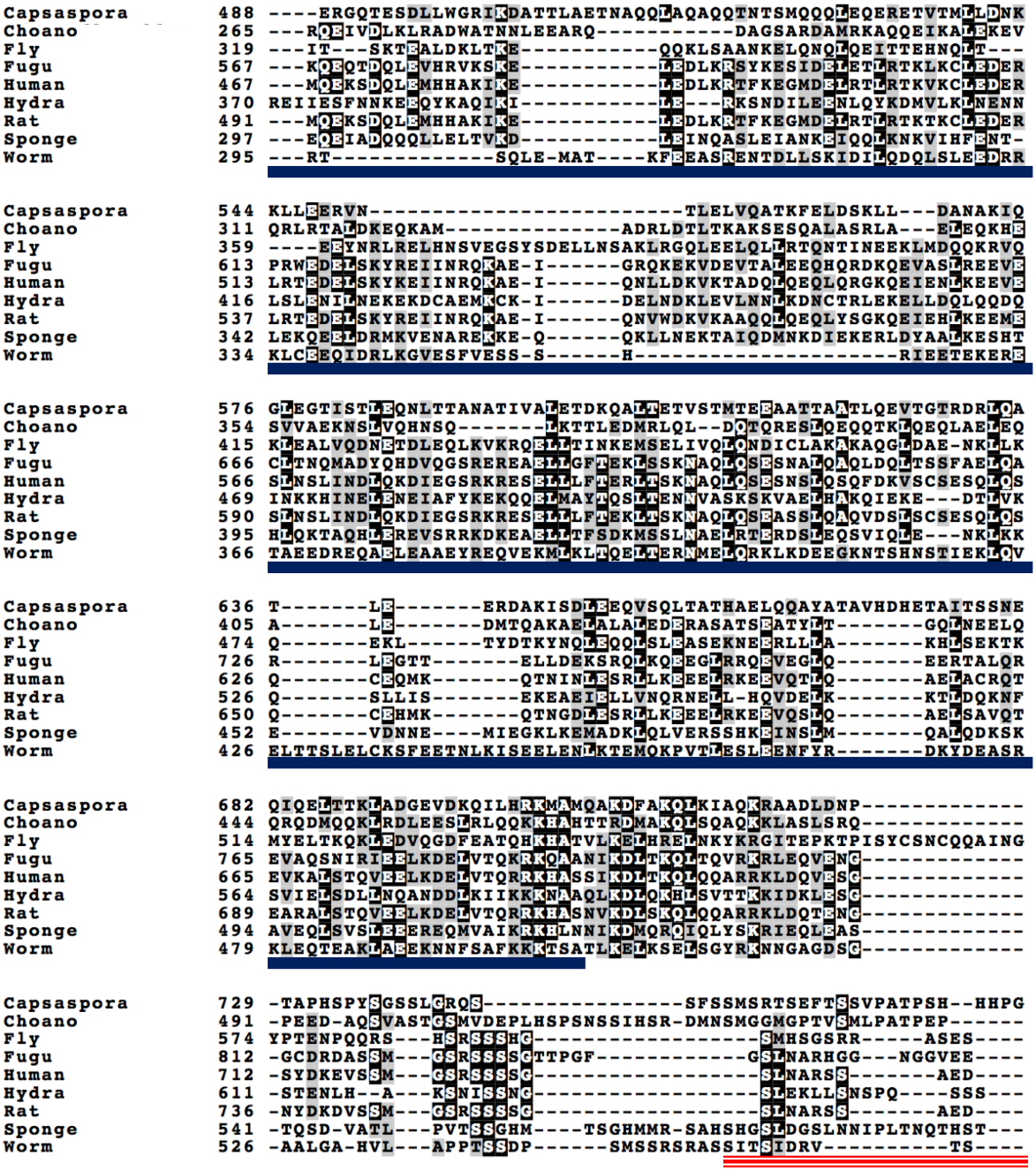
Capsaspora 488 ----ERGQTESDLLWGRIKDATTLAETNAQQLAQAQQTNTSMQQQLEQERETVTMLLDNK
Choano 265 ---RQEIVDLKLRADWATNNLEEARQ----------DAGSARDAMRKAQQEIKALEKEV
Fly 319 ---IT---SKTEALDKLTKE----------QQKLSAANKELQNQLQEITTEHNQLT---
Fugu 567 ---KQEQTDQLEVHRVKSKE----------LEDLKRSYKESIDELETLRTKLKCLEDER
Human 467 ---MQEKSDQLEMHHAKIKE----------LEDLKRTFKEGMDELRTLRTKVKCLEDER
Hydra 370 REIIESFNNKEEQYKAQIKI----------LE---RKSNDILENLQYKDMVLKLNENN
Rat 491 ---MQEKSDQLEMHHAKIKE----------LEDLKRTFKEGMDELRTLRTKTKCLEDER
Sponge 297 ---EQEIADQQQLLELTVKD----------LEINQASLEIANKEIQQLKNKVIHFENT-
Worm 295 ---RT----------SQLE-MAT----KFEEASRENTDLLSKIDILQDQLSLEEDRR
Capsaspora 544 KLLEERVN----------TLELVQATKFELDSKLL---DANAKIQ
Choano 311 QRLRTALDKEQKAM----------ADRLDTLTKAKSESQALASRLA---ELEQKHE
Fly 359 ----ESYNRLRELHNSVEGSYSDELLNSAKLRGQLEELQLLRTQNTINEEKLMDQQKRVQ
Fugu 613 PRWEDELSKYREIINRQKAE-I------GRQKEKVDEVTALEEQHQRDKQEVASLREEVE
Human 513 LRTEDELSKYKEIINRQKAE-I------QNLLDKVKTADQLQEQLQRGKQEIENLKEEVE
Hydra 416 LSLENILNEKEKDCAEMKCK-I------DELNDKLEVLNNLKDNCTRLEKELLDQLQQDQ
Rat 537 LRTEDELSKYREIINRQKAE-I------QNVWDKVKAAQQLQEQLYSGKQEIEHLKEEME
Sponge 342 LEKQEELDRMKVENARERKE-Q------QKLLNEKTAIQDMNKDIEKERLDYAALKESHT
Worm 334 KLCEEQIDRLKGVESFVESS-S------H----------RIEETEKERE
Capsaspora 576 GLEGTISTLEQNLTTANATIVALETDKQALTETVSTMTEEAATTAATLQEVTGTRDRLQA
Choano 354 SVVAEKNSLVQHNSQ-------LKTTLEDMRLQL--DQTQRESLQEQQTKLQEQLAELEQ
Fly 415 KLEALVQDNETDLEQLKVKRQELLTINKEMSELIVQLQNDICLAKAKAQGLDAE-NKLLK
Fugu 666 CLTNQMADYQHDVQGSREREAELLGFTEKLSSKNAQLQSESSNALQAQLDQLTSSFAELQA
Human 566 SLNSLINDLQKDIEGSRKRESELLLFTERLTSKNAQLQSESSNSLQSQFDKVSCSESQLQS
Hydra 469 INKKHINELENEIAFYKEKQQELMAYTQSLTENNVASKSKVAELHAKQIEKE---DTLVK
Rat 590 SLNSLINDLQKDIEGSRKRESELLLFTEKLTSKNAQLQSEASSLQAQVDSLSCSESQLQS
Sponge 395 HLQKTAQHLEREVSRRKDKEAELLTFSDKMSSLNAELRTERDSLEQSVIQLE---NKLKK
Worm 366 TAEEDREQAELEAAEYREQVEKMLKLTQELTERNMELQRKLKDEEGKNTSHNSTIEKLQV
Capsaspora 636 T-------LE-------ERDAKISDLEEQVSQLTATHAELQQAYATAVHDHETAITSSNE
Choano 405 A-------LE-------DMTQAKAELALALEDERASATSEATYLT-------GQLNEELQ
Fly 474 Q-------EKL------TYDTKYNQLEQQLSLEASEKNESRLLLA-------KHLSEKTK
Fugu 726 R-------LEGTT-------ELLDEKSRQLKQEEGLRRQEVEGLQ-------EERTALQR
Human 626 Q-------CEQMK-------QTNINLESRLLKEEELRKESVQTLQ-------AELACRQT
Hydra 526 Q-------SLLIS-------EKEAEIELLVNQRNELL-HQVDELK-------KTLDQKNF
Rat 650 Q-------CEHMK-------QTNGDLESRLLKEEELRKESVQSLQ-------AELSAVQT
Sponge 452 E-------VDNNE----MIEGKLKEMADKLQLVERSSHKEINSLM-------QALQDKSK
Worm 426 ELTTSLELCKSFEETNLKISEELENLKTEMQKPVTLESLEENFYR-------DKYDEASR
Capsaspora 682 QIQELTTKLADGEVDKQILHRKMAMQAKDFAKQLKIAQKRAADLDNP----------
Choano 444 QRQDMQQKLRDLEESLRLQQKKHAHTTRDMAKQLSQAQKKLASLSRQ----------
Fly 514 MYELTKQKLEDVQGDFEATQHKHATVLKELHRELNKYKRGITEPKTPISYCSNCQQAING
Fugu 765 EVAQSNIRIEELKDELVTQKRKQAANIKDLTKQLTQVRKRLEQVENG----------
Human 665 EVKALSTQVEELKDELVTQRRKHASSIKDLTKQLQQARRKLDQVESG----------
Hydra 564 SVIELSDLLNQANDDLKIIKKKNAAQLKDLQKHLSVTTKKIDKLESG----------
Rat 689 EARALSTQVEELKDELVTQRRKHASNVKDLSKQLQQARRKLDQTENG----------
Sponge 494 AVEQLSVSLEEEREQMVAIKRKHLNNIKDMQRQIQLYSKRIEQLEAS----------
Worm 479 KLEQTEAKLAEEKNNFSAFKKKTSATLKELKSELSGYRKNNGAGDSG----------
Capsaspora 729 -TAPHSPYSGSSLGRQS----------SFSSMSRTSEFTSSVPATPSH--HHPG
Choano 491 -PEED-AQSVASTGSMVDEPLHSPSNSSIHSR-DMNSMGGMGPTVSMLPATPEP------
Fly 574 YPTENPQQRS---HSRSSSHG----------SMHSGSRR-----ASES----
Fugu 812 -GCDRDASSM---GSRSSSSGTTPGF----------GSLNARHGG---NGGVEE----
Human 712 -SYDKEVSSM---GSRSSSSG----------SLNARSS-------AED----
Hydra 611 -STENLH--A---KSNISSNG----------SLEKLLSNSPQ----SSS---
Rat 736 -NYDKDVSSM---GSRSSSSG----------SLNARSS-------AED----
Sponge 541 -TQSD-VATL---PVTSSGHM----TSGHMMR-SAHSHGSLDGSLNNIPLTNQTHST---
Worm 526 -AALGA-HVL---APPTSSDP------SMSSRSRASSITSIDRV----------TS----

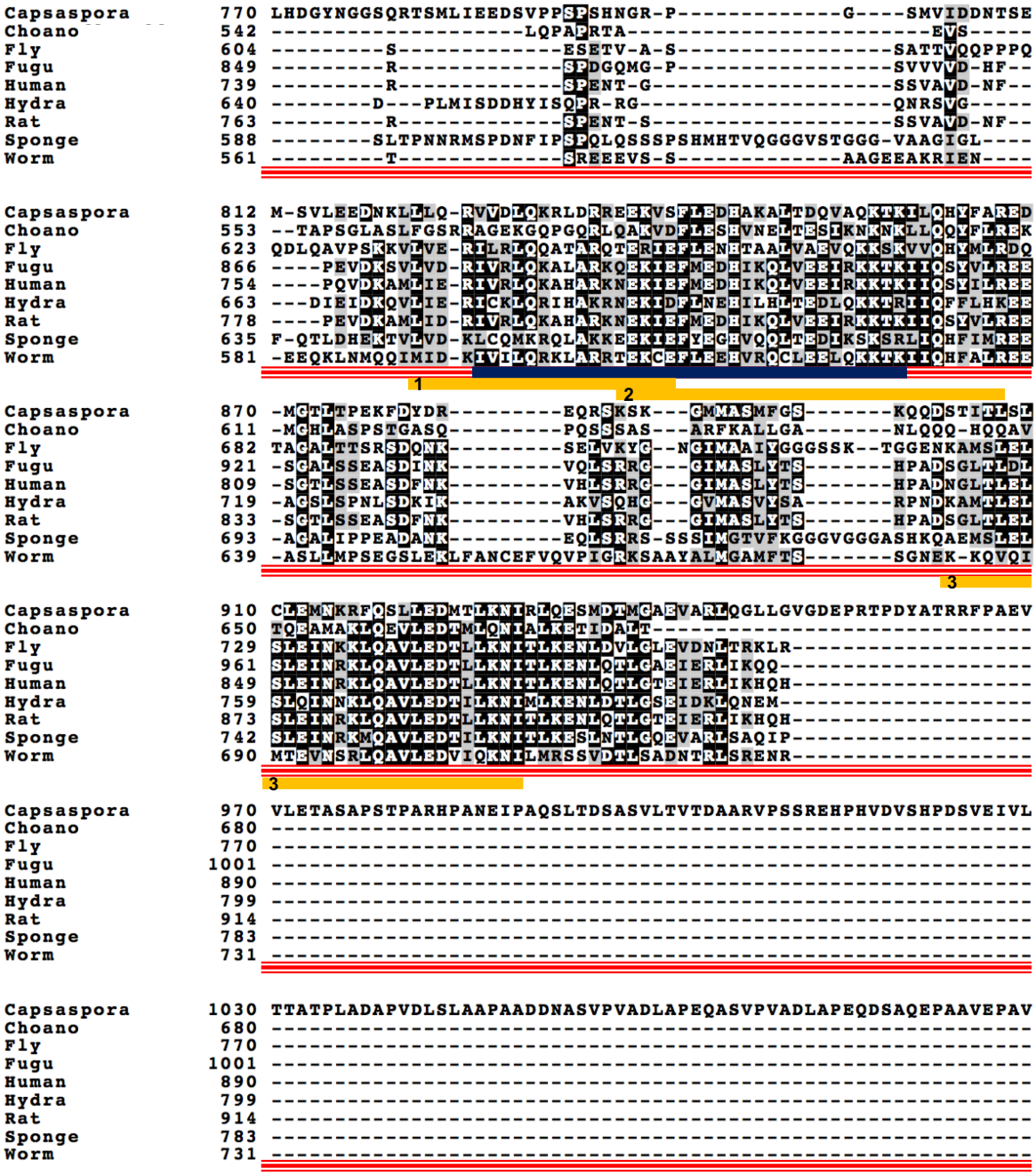
Capsaspora 770 LHDGYNGGSQRTSMLIEEDSVPPSPSHNGR-P----------G----SMVIDDNTSE
Choano 542 ----------LQPAPRTA----------EVS-----
Fly 604 ---------S----------ESETV-A-S----------SATTVQQPPPQ
Fugu 849 ---------R----------SPDGQMG-P----------SVVVVD-HF--
Human 739 ---------R----------SPENT-G----------SSVAVD-NF--
Hydra 640 --------D---PLMISDDHYISQPR-RG----------QNRSVG-----
Rat 763 ---------R----------SPENT-S----------SSVAVD-NF--
Sponge 588 --------SLTPNNRMSPDNFIPSPQLQSSSPSHMHTVQGGGVSTGGG-VAAGIGL----
Worm 561 ---------T----------SREEEVS-S----------AAGEEAKRIEN----
Capsaspora 812 M-SVLEEDNKLLLQ-RVVDLQKRLDRREEKVSFLEDHAKALTDQVAQKTKILQHYFAREDE
Choano 553 --TAPSGLASLFGSRRAGEKGQPGQRLQAKVDFLESHVNELTESIKNKNKLLQQYFLREKE
Fly 623 QDLQAVPSKKVLVE-RILRLQQATARQTERIEFLENHTAALVAEVQKKSKVVQHYMLRDQE
Fugu 866 ----PEVDKSVLVD-RIVRLQKALARKQEKIEFMEDHIKQLVEEIRKKTKIIQSYVLREEE
Human 754 ----PQVDKAMLIE-RIVRLQKAHARKNEKIEFMEDHIKQLVEEIRKKTKIIQSYILREEE
Hydra 663 ---DIEIDKQVLIE-RICKLQRIHAKRNEKIDFLNEHILHLTEDLQKKTRIIQFFLHKEE
Rat 778 ----PEVDKAMLID-RIVRLQKAHARKNEKIEFMEDHIKQLVEEIRKKTKIIQSYVLREE
Sponge 635 F-QTLDHEKTVLVD-KLCQMKRQLAKKEEKIEFYEGHVQQLTEDIKSKSRLIQHFIMREEE
Worm 581 -EEQKLNMQQIMID-KIVILQRKLARRTEKCEFLEEHVRQCLEELQKKTKIIQHFALREEE
1
2
Capsaspora 870 -MGTLTPEKFDYDR----------EQRSKSK---GMMASMFGS-------KQQDSTITLSL
Choano 611 -MGHLASPSTGASQ----------PQSSSAS---ARFKALLGA-------NLQQQ-HQQAV
Fly 682 TAGALTTSRSDQNK----------SELVKYG--NGIMAAIYGGGSSK--TGGENKAMSLEL
Fugu 921 -SGALSSEASDINK----------VQLSRRG---GIMASLYTS-------HPADSGLTLDL
Human 809 -SGTLSSEASDFNK----------VHLSRRG---GIMASLYTS-------HPADNGLTLEL
Hydra 719 -AGSLSPNLSDKIK----------AKVSQHG---GVMASVYSA-------RPNDKAMTLEL
Rat 833 -SGTLSSEASDFNK----------VHLSRRG---GIMASLYTS-------HPADSGLTLEL
Sponge 693 -AGALIPPEADANK----------EQLSRRS-SSSIMGTVFKGGGVGGGASHKQAEMSLEL
Worm 639 -ASLLMPSEGSLEKLFANCEFVQVPIGRKSAAYALMGAMFTS-------SGNEK-KQVQI
3
Capsaspora 910 CLEMNKRFQSLLEDMTLKNIRLQESMDTMGAEVARLQGLLGVGDEPRTPDYATRRFPAEV
Choano 650 TQEAMAKLQEVLEDTMLQNIALKETIDALT----------
Fly 729 SLEINKKLQAVLEDTLLKNITLKENLDVLGLEVDNLTRKLR----------
Fugu 961 SLEINRKLQAVLEDTLLKNITLKENLQTLGAEIERLIKQQ----------
Human 849 SLEINRKLQAVLEDTLLKNITLKENLQTLGTEIERLIKHQH----------
Hydra 759 SLQINNKLQAVLEDTILKNIMLKENLDTLGSEIDKLQNEM----------
Rat 873 SLEINRKLQAVLEDTLLKNITLKENLQTLGTEIERLIKHQH----------
Sponge 742 SLEINRKMQAVLEDTILKNITLKESLNTLGQEVARLSAQIP----------
Worm 690 MTEVNSRLQAVLEDVIQKNILMRSSVDTLSADNTRLSRENR----------
3
Capsaspora 970 VLETASAPSTPARHPANEIPAQSLTDSASVLTVTDAARVPSSREHPHVDVSHPDSVEIVL
Choano 680 ----------
Fly 770 ----------
Fugu 1001 ----------
Human 890 ----------
Hydra 799 ----------
Rat 914 ----------
Sponge 783 ----------
Worm 731 ----------
Capsaspora 1030 TTATPLADAPVDLSLAAPAADDNASVPVADLAPEQASVPVADLAPEQDSAQEPAAVEPAV
Choano 680 ----------
Fly 770 ----------
Fugu 1001 ----------
Human 890 ----------
Hydra 799 ----------
Rat 914 ----------
Sponge 783 ----------
Worm 731 ----------


Capsaspora 1090 AEQAPVEQAPVEPAAVEPAAVEPAAAAPEPAAAAEQPAPVEAPALESSPAEDQPIQQADA
Choanoflagellat 680
Fly 770
Fugu 1001
Human 890
Hydra 799
Rat 914
Sponge 783
Worm 731
Capsaspora 1150 PEIAPDSTIAAEPLPEQASDEAQPDANPVTDAAAESAPLPDAVPAEETTPDVPSQDE---
Choanoflagellat 680
Fly 770 -SL---
Fugu 1001
Human 890 -EL---
Hydra 799
Rat 914 -EL---
Sponge 783 -K---
Worm 731 -LLSLS
Capsaspora 1207 -ASEDSLL
Choanoflagellat 680 ------KA
Fly 772 ---EGSCK
Fugu 1001 ------RS
Human 892 -EQRTKKT
Hydra 799 ---RSSKK
Rat 916 -EQRTKKA
Sponge 784 -NTSTSNR
Worm 736 QVRTTQDN
CC3 fragment
Predicted Coiled-Coil domains
Predicted Amphipathic helix

VITA

Jerome Cattin went to the engineering college ESCPE Lyon, where he graduated in 2012 with an M.S. in Chemical Engineering. He did his Master's thesis research at the University of California, Berkeley, where he spent two years in the laboratory of Judith P. Klinman. Jerome joined the Biochemstry PhD program at the University of Washington in 2012.